Optogenetic control of cell migration polarity through the RhoA pathway

Jean de Seze

PSL
UNIVERSITÉ PARIS

THÈSE DE DOCTORAT

DE L'UNIVERSITÉ PSL

Préparée à l'Institut Curie, UMR 168

Contrôle optogénétique de la polarité de la migration cellulaire par la voie de signalisation RhoA

Optogenetic control of cell migration polarity through the RhoA pathway

Soutenue par

Jean DE SEZE

Le 10 octobre 2023

École doctorale n°564

Physique en Ile-de-France

Spécialité

Physique

Composition du jury :

Ana-Maria LENNON-DUMENIL Dr., Insitut Curie	*Présidente*
Olivier DESTAING Dr., Université de Grenoble Alpes	*Rapporteur*
Olivier PERTZ Prof. Dr., University of Bern	*Rapporteur*
Jihye SEONG Dr., Korea Institute of Science and Technology	*Examinatrice*
Mathieu COPPEY Dr., Institut Curie	*Directeur de thèse*
Fanny JAULIN Dr., Institut Gustave Roussy	*Co-directrice de thèse*

institut Curie | PSL

Acknowledgements

En premier lieu, j'aimerais remercier Mathieu, qui m'a supervisé et soutenu pendant ces années de thèse. Merci Mathieu pour ta joie, ton enthousiasme communicatif, toutes les discussions scientifiques qui partent dans tous les sens, toutes les discussions non scientifiques sur la vie, la crise écologique, l'existence de Dieu ... Merci pour ton soutien et ta disponibilité, qui m'ont permis de grandir et me former, aussi bien scientifiquement qu'humainement, pendant ces années de thèse.

Un grand merci aussi à Fanny, qui m'a cosupervisé pendant cette thèse sur le projet collamoeboid. Merci de m'avoir fait découvrir ce projet en collaboration avec des acteurs très différents, de toujours avoir été de bon conseil et exigeante avec moi, tout en me faisant confiance et en partageant tes encouragements et ton enthousiasme pendant les comités de thèse.

Thank you to the other members of my thesis advisory comittee, Ana-Maria and Wolfgang, for these long and helpful moments you took to help me progressing in my PhD projects.

I also thank Olivier Pertz and Olivier Destaing, for kindly accepting to review my thesis, as well as Jihye Seong and Ana-Maria Lennon-Duménil for being members of my PhD thesis jury.

J'aimerais également remercier l'Ecole Polytechnique pour la bourse AMX m'ayant permis de réaliser ma thèse, la fondation ARC pour le financement de ma quatrième année, ainsi que le Labex Cell(n)Scale pour le financement des différentes conférences auxquelles j'ai participé.

Un remerciement spécial à tous ceux avec qui j'ai pu travailler tout au long de ma thèse, qui ont enrichi et surtout permis ce travail. Je pense aux membres de BMBC avec qui j'ai pu travailler, Fahima, Aude, Laurence, Fanny et Benoit, ainsi qu'à tous les différents stagiaires qui ont travaillé avec moi sur ce projet: Guilhem, Ajmal, Romain, Joséphine. Je pense aussi à tous les collaborateurs du projet collamoeboid que j'ai côtoyés: Diane-Laure et Emmanuel tout d'abord, ainsi que Matthieu, Raphaël, Ananyo, Li, et Emilie.

Un grand grand merci aussi à l'équipe LOCCO, qui a changé en composition pendant toutes ces années, mais pas dans son état d'esprit. Merci pour l'accueil chaleureux, pour tous les bons moments passés ensemble dans et hors du labo, merci pour les retraites d'équipe inoubliables et toute votre aide et votre soutien, scientifique et humain. Merci Kotryna de m'avoir formé au labo avec joie et enthousiasme, merci Lorena pour tes encouragements de tous les jours et la relecture de ce manuscrit, merci à Elie,

Alicia, Laura, Tommaso, Thomas, Mirna, Bassam, Yasmina, Manuel, Andrea, ainsi que tous ceux, stagiaires et alternants, qui ont passé quelques mois ici. Un merci tout particulier à mes deux voisines de ces deux dernières années, Louise et Maud, pour leur soutien indéfectible, leur bonne humeur et toutes les discussions qu'on a pu avoir ensemble.

Merci à tous les membres du labo, pour toutes les interactions et discussions, scientifiques ou non, tout au long de ma thèse. Un merci particulier à Caroline, avec qui nous avons passé tant de temps pour le Green Physics Lab, pour évaluer notre empreinte carbone et lancer une dynamique dans le laboratoire: merci pour ton enthousiasme et ta volonté d'avancer. Merci aussi à tous les membres du Green Physics Lab pour le travail accompli, les encouragements et tout le temps passé ensemble !

Merci aussi à tous mes bons amis, qui ont toujours été là et qui m'apportent tant. Merci à mes frérots de Bordeaux, à mes témoins Matthieu, Pierre et Ambroise, à Ophélie, à tous mes bons amis du lycée et de la communauté, mes amis d'école et de la Kès, ainsi que ceux qui ont partagé avec moi la joie et les douleurs de la thèse - Ludovic, Diane-Laure, Lucas, Julienne, JB et Cécile.

Enfin, merci à ma grande famille, mes frères et sœurs et parents, qui sont pour moi source de paix et de joie. Merci de m'avoir toujours encouragé, de vous être intéressés à mon travail et de m'avoir permis de devenir qui je suis. Merci également à toute ma belle-famille que j'ai la joie d'apprendre à connaître petit à petit. Un grand merci pardessus tout à Alix, qui est devenue ma femme pendant cette thèse, et qui m'a toujours soutenu avec tendresse malgré mes hauts et bas et mes questions existentielles à tout bout de champ. Merci enfin à ce petit être qui commence sa vie en toi, et merci à Celui qui nous donne la vie, en qui je trouve ma joie.

Abstract

Cells sense external chemical or physical signals, interpret them using their protein network and modify their behavior accordingly. A better understanding of living systems involves deciphering how biochemical signals are transmitted within the cell, leading to specific phenotypic responses. Among all cellular processes, cell migration is fascinating because it reveals the ability of cells to act as individual or collective units, which polarize by themselves and have their own independence.

Rho-GTPases play a key role in mammalian cell migration: they are proteins often regarded as controllers of the cellular cytoskeleton, and therefore responsible for morphological changes caused by filaments and motors such as actin and myosin. To probe the protein network and study causal links on cellular or multicellular behavior, optogenetics is a great tool that enables precise spatio-temporal control of Rho-GTPase activity.

This PhD manuscript addresses the question of the control of single and multicellular migration by Rho-GTPases, using optogenetics in two different model systems.

The first project focuses on the migration and polarization of single cells following membrane recruitment of a RhoA activator (a GEF domain). Using optogenetics, I discovered that a GEF domain is capable of triggering two opposite phenotypic responses in the same cell line: protrusion or retraction. Characterization of the phenotypes showed that the choice is dictated by the concentration of optogenetic activator present in the cell prior to activation. I described the consequences of this change in concentration on the signalling pathways involved, and developed a model that summarizes the main results with few parameters. Thanks to it, I was able to control the two opposite effects of this protein in the same cell. This project reveals and explains a clear example of cellular signal multiplexing, i.e. the ability of a signaling pathway to have multiple functions, here in the same cellular context and on a minute scale.

The second project was carried out in collaboration with Fanny Jaulin's team at the Institut Gustave Roussy. It aimed to understand a new mode of collective migration discovered by them in the initiation of colorectal cancer metastases. This migration of epithelial clusters of tens to hundreds of cells relies on unique properties: absence of focal adhesions to the substrate, confined environment, and high contractility. This mode of collective migration is reminiscent of single cell amoeboid migration. Using optogenetic tools developed in our laboratory and microfluidic channels, I designed and carried out experiments to understand the role of Rho-GTPases in the polarity and migration of these multicellular spheres. My main finding is that a contractility imbalance triggered by the RhoA protein is sufficient to control the polarity and movement of the cell group.

Overall, my PhD has provided insight into how the RhoA signaling pathway acts to establish polarity in cell migration: I examined it at the single-cell level, revealing a unique example of multifunctionality of a protein, as well as at the collective level, dissecting a novel mode of collective cancer cell migration.

Résumé

Les cellules perçoivent des signaux chimiques ou physiques externes, les interprètent à l'aide de leur réseau de protéines et modifient leur comportement en conséquence. Mieux comprendre les systèmes vivants passe par le décryptage des signaux biochimiques à l'intérieur de la cellule, qui sont responsables de réponses phénotypiques spécifiques. Parmi tous les processus cellulaires, la migration cellulaire est fascinante car elle révèle la capacité des cellules à agir comme des unités individuelles ou collectives, qui se polarisent par elles-mêmes et ont leur propre indépendance.

Les Rho-GTPases jouent un rôle clé dans la migration des cellules de mammifères : ce sont des protéines souvent considérées comme des contrôleurs du cytosquelette cellulaire, et donc responsables des changements morphologiques provoqués par les filaments et les moteurs tels que l'actine et la myosine. Pour sonder le réseau de protéines et étudier les liens de cause à effet sur le comportement cellulaire ou multicellulaire, l'optogénétique est un outil formidable qui permet un contrôle spatio-temporel précis de l'activité des Rho-GTPases.

Ce manuscrit aborde la question du contrôle de la migration cellulaire et multicellulaire par les Rho-GTPases à travers deux systèmes modèles différents, grâce à l'optogénétique.

Le premier projet porte sur la migration et la polarisation de cellules individuelles après le recrutement membranaire d'un activateur de la protéine RhoA (un domaine GEF). En utilisant l'optogénétique, j'ai découvert qu'un domaine GEF est capable de déclencher deux réponses phénotypiques opposées dans la même lignée cellulaire : une protrusion ou une rétraction. La caractérisation des phénotypes a permis de montrer que le choix est dicté par la concentration de l'activateur optogénétique présent dans la cellule avant l'activation. J'ai décrit la conséquence de ce changement de concentration sur les voies de signalisation impliquées et j'ai développé un modèle qui récapitule les principaux résultats avec peu de paramètres. Grâce à lui, j'ai pu contrôler les deux effets opposés de cette protéine dans la même cellule. Ce projet révèle et explique un exemple clair de multiplexage des signaux cellulaires, à savoir la capacité d'une voie de signalisation à avoir plusieurs fonctions, ici dans le même contexte cellulaire et à l'échelle de la minute.

Le second projet a été réalisé en collaboration avec l'équipe de Fanny Jaulin de l'Institut Gustave Roussy. Il visait à comprendre un nouveau mode de migration collective découvert par eux dans l'initiation des métastases du cancer colorectal. Cette migration d'amas épithéliaux de dizaines à centaines de cellules repose sur des propriétés uniques : absence d'adhésions focales sur le substrat, environnement confiné, et forte contractilité. Ce mode de migration collective rappelle la migration amiboïde d'une seule cellule. En utilisant des outils optogénétiques développés dans notre laboratoire et des canaux microfluidiques, j'ai conçu et réalisé des expériences pour comprendre le rôle des Rho-GTPases dans la polarité et la migration de ces sphères multicellulaires. Mon principal résultat est qu'un déséquilibre de contractilité déclenché par la protéine RhoA est suffisant pour contrôler la polarité et le mouvement du groupe de cellules.

Dans l'ensemble, mon doctorat a permis de comprendre comment la voie de signalisation RhoA agit pour établir une polarité dans la migration cellulaire : je l'ai examinée au niveau de la cellule unique, révélant un exemple unique de multifonctionnalité d'une protéine, ainsi qu'au niveau collectif, disséquant un nouveau mode de migration collective des cellules cancéreuses.

Contents

List of Figures

Abbreviations

- **10x,20x,60x**: magnified 10,20 or 60 times.
- **Arp2/3**: Actin-Related Proteins 2/3.
- **AsLOV2**: *Avena sativa* light-oxygen-voltage-sensing domain 2.
- **ATP**: Adenosine triphosphate.
- **Cdc42**: Cell division control protein 42.
- **CDC42-PAR3-PAR6-aPKC**: Cell division control protein 42; Partitioning defective 3; Partitioning defective 6, Atypical protein kinase C.
- **Cry2/CIBN**: Cryptochrome2/CIB N-terminal.
- **DH-PH domain**: Dbl homology-pleckstrin homology domain.
- **DH domain**: Dbl homology domain.
- **DIC**: Differential Interference Contrast.
- **DMD**: Digital Micromirror Device.
- **DMEM**: Dulbecco's Modified Eagle Medium.
- **DMSO**: Dimethylsulfoxyde.
- **DNA**: Deoxyribonucleic acid.
- **DOCK**: Dedicator of cytokinesis.
- **ELC**: Essential light chains.
- **ER**: Endoplasmic reticulum.
- **ERK**: Extracellular signal-regulated kinases.
- **EMT**: Epithelial-to-mesenchymal transition..
- **FRET**: Förster resonance energy transfer.
- **FP**: Fluorescence protein.
- **GAP**: GTPase activating protein.
- **GDI**: GDP Dissociation Inhibitor.
- **GDP**: Guanosine diphosphate.

- **GEF**: Guanine nucleotide exchange factor.
- **GFP**: Green fluorescent protein.
- **GTP**: Guanosine triphosphate.
- **GTPase**: Enzyme hydrolyzing GTP.
- **GUI**: Graphical user interface.
- **HEK**: Human embryonic kidney.
- **HILO**: Highly inclined and laminated optical sheet.
- **iLID**: improved light-induced dimer.
- **iRFP**: near-infrared red fluorescent protein.
- **LARG**: Leukemia-associated Rho guanine nucleotide exchange factor
- **LED**: Light Emitting Diode
- **LOV**: Light-oxygen-voltage-sensitive domain.
- **LR**: Leucine rich.
- **mDia1**: mouse Diaphanous-related formin-1.
- **MLC**: Myosin-II light chain.
- **MLC**: Myosin-II regulatory light chain.
- **MSD**: Mean square displacement.
- **MTOC**: Microtubule organizing center.
- **MT**: Microtubule
- **myr**: myristoylated.
- **NLS**: Nuclear localization signal.
- **NPF**: Nucleation promoting factor.
- **PBD**: PAK-binding domain.
- **PBS**: Phosphate-buffered saline.
- **PDGF**: Platelet-Derived Growth Factor
- **PRG**: PDZ-RhoGEF.
- **PhyB/PIF**: PhytochromeB/Phytochrome-interacting protein.
- **PH domain**: Pleckstrin homology domain.
- **PI(3,4,5)P_3 or PIP$_3$**: Phosphatidylinositol (3,4,5)-trisphosphate.
- **PI(4,5)P_2 or PIP$_2$**: Phosphatidylinositol (4,5)-diphosphate.
- **PI3K**: Phosphoinositide 3-kinase.

- **PLL-g-PEG**: Poly(L-lysine)-graft-poly(ethylene glycol).
- **PM**: Plasma membrane.
- **Rac1**: Ras-related C3 botulinum toxin substrate 1.
- **Ras**: Rat sarcoma related.
- **RBD**: PhoA-binding domain
- **RGS**: Regulator of G-protein signaling.
- **Rho**: Ras homolog.
- **RhoA**: Ras homolog family member A
- **RLC** : Regulatory light chain
- **ROCK**: Rho-associated protein kinase.
- **RPA**: Robust Perfect Adaptation
- **RPE1**: Retinal pigmented epithelium 1.
- **RTK**: Receptor Tyrosine Kinase.
- **siRNA**: Small interfering RNA.
- **SspB**: Stringent starvation protein B.
- **sem**: standard error of the mean
- **std**: standard deviation
- **TIRF**: Total Internal Reflection Fluorescence.
- **TULIP**: Tunable, light-controlled interacting protein.
- **UV**: Ultraviolet light.
- **WASP**: Wiskott–Aldrich Syndrome protein.
- **WAVE**: WASP-family verprolin-homologous protein.
- **WT**: Wild-type
- **ZF**: Zinc finger-like binding domain.

Chapter 1

Introduction

During my PhD, I had the opportunity to work on two different projects. The first one dealt with single cell behavior and was entirely carried out in Mathieu Coppey's team at the Institut Curie (see chapter 2). The second one, which was part of a collaboration led by Fanny Jaulin's team at the Institut Gustave Roussy, studied the collective movement of cancer cells (see chapter 3).

Despite their differences, these two projects are related in the way I look at cell biology, ask questions, and design experiments. In both cases, I studied cells in a laboratory under a microscope, as much as possible in a controlled environment. In both cases, I used live microscopy and image analysis as the main tools for my experiments. In both cases, I examined cell signalling at the level of one protein pathway, the RhoA pathway, using optogenetics, a technique that has long been used in our team. In both cases, the main cellular response to our perturbations was a cellular displacement, both at the single cell level and at the multicellular level. In both cases, we eventually created a physical model of the cellular system we were studying.

To better understand the results and the discussion, I will introduce some important concepts of cell biology with different degrees of detail. First, to avoid an unrealistic, static picture of the current state of scientific knowledge, I have started my introduction with a historical section. In it, I will attempt to summarize the techniques and concepts that have slowly evolved over the years and that have enabled me to conduct my research, but that have also discretely pushed me toward a particular view of cells, cellular processes, and cellular signalling networks. Second, I will try to give some intuition of the timescales involved in cell biology processes so that we can enter this very different nano- to microscopic world. Third, I will give an introduction to intracellular signalling: How does a cell process signals and compute responses? What tools do we have to detect these signals, and how can we interrogate them with optogenetics? Fourth, since both of my projects deal with cell movement, I will introduce eukaryotic cell migration both at the single and multicellular level. This is a huge area of research, and I will try to go through the main concepts of cell deformation and polarity, as well as the main different types of migration that have been described so far. Finally, I will detail the role of one particular protein, the protein RhoA. This protein can be used as an example of the complexity of cell signalling. It plays a key role in cell migration and its entire signalling pathway will be an important part of the results of my PhD thesis.

1.1 Some historical facts of mammalian cell biology - what principles guide our knowledge?

The discoveries of the last three hundred years have completely changed our view of living organisms, and the field of what we now call cell biology is now so diverse that it would be pointless to attempt to write a single history of it. I will therefore attempt to point out some specific findings that I believe are particularly important for understanding my research and the field, as well as some key concepts that guide our conception of living matter. I realize that all of these historical facts mentioned here are controversial and each of them could be the subject of a separate thesis, but I think that they are nevertheless part of the general knowledge that drives our research and are therefore worth mentioning.

Three historical findings will be mentioned here, which I have chosen because of their relevance to the way I have been taught about cells and living systems. First, I will discuss the emergence of cell theory, which has given so much importance to the cell as the fundamental unit of life. Next, I will examine the concept of central dogma and its impact on our understanding of proteins and the central role of the nucleus. Finally, I will discuss recent concepts of cell signalling networks that illuminate our evolving understanding of the computational capacities of proteins and the decision-making processes in cells.

1.1.1 Cell theory

Nowadays, cell biology is a fundamental research field whose concepts and discoveries are used in many other areas of biology: Developmental Biology, Immunology, Evolution and Medicine for example. Why does looking at the cellular level help us understand completely different processes that occur on completely different time and length scales? Mostly because of the cell theory, which we all know as a fundamental property of living systems. This cell theory can be stated as follows: "all plants and animals are made of cells, cells possess all the attributes of life (assimilation, growth, reproduction), and all cells arise from division of preexisting cells" [Sapp, 2003].

Cells were first described in plants by Robert Hooke in 1665 [Hooke, 1665] to refer to the small compartments that made them up and that were observed thanks to advances in light microscopes. Two centuries later, in 1824, Henri Ductrochet described the same type of compartments in animal tissue [Dutrochet, 1824], at a time when scientists were searching for fundamental properties of living systems. In this context, Mathias Jacob Schleiden proposed that these cells have their own autonomy, ”a double life, one completely autonomous life relative to its own development and another, mediated, as an integrated part of the plant. ” (translated by me, [Vignais, 2001, Schleiden, 1838]).

Theodor Schwann is usually considered as the true father of the cell theory, which he developed in 1839 after a discussion with Schneiden. In his book [Schwann, 1839] he postulated that the cell is the basic unit of both vegetal and animal living systems, and described the similarities in cellular unit among different species, both plants and animals (Figure 1.1). A few years later, Robert Remak and then Rudolf Virchow refuted the spontaneous cell formation that Schwann believed in and proposed that every cell arises from another cell [Virchow, 1855], completing the few principles of cell theory. R. Virchow then advanced the idea that diseases may stem from problems at the cellular level and that basic research on the functioning of cells should predominate

in order to understand pathologies. By the end of the 19th century, cell theory is widely accepted among scientists, and the cell is recognized as the principal structural and functional unit of all living tissues [Vignais, 2001].

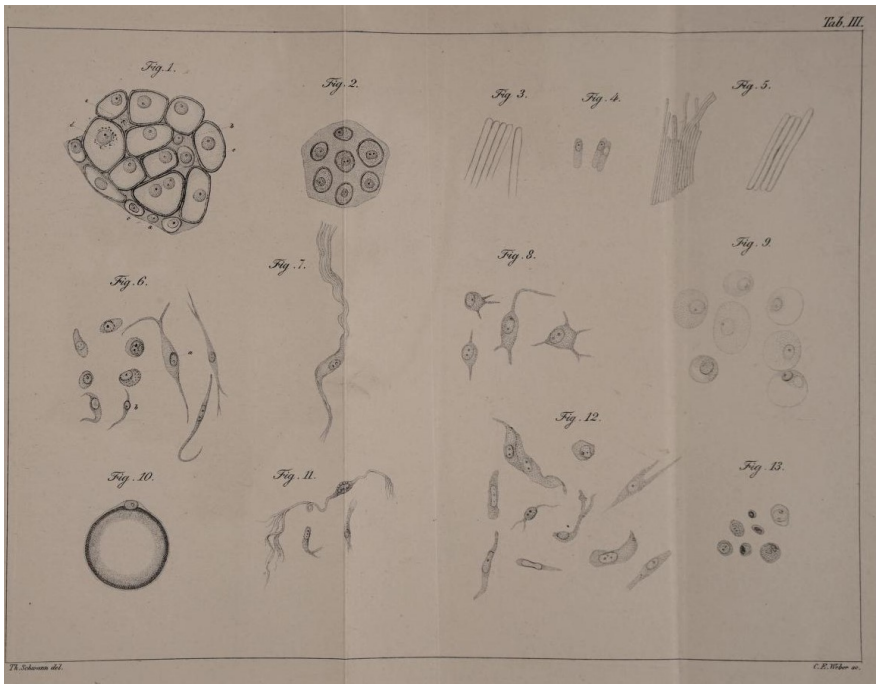

Figure 1.1: Some cells of different species drawn by Schwann in his book stating cell theory. Dozens of drawings are present to show similarities in diversity. Taken from [Schwann, 1839].

Interestingly, this cell theory was part of a program aimed at establishing "biological laws" to elevate botany and zoology to the status of a truly scientific discipline. In particular, Schwann wanted to "identify specific material agents that exert specific life forces." [Parnes, 2000]. The goal was to find laws that did not rely on a life force but had to be conceived in terms of specific agencies - with cells being the agents [Parnes, 2000]. This notion of the cell as the basic unit of life, which we must study if we are to understand what life is, has persisted to this day. Erwin Schroedinger's famous book, *What is Life*, which sparked the interest of physicists in biology, is subtitled 'The Physical Aspect of the Living Cell," showing that he considered the cell the key to unlocking the secrets of life. Scientists in the field of abiogenesis (the study of the origin of life) usually consider the cell as the smallest living system [Caliari et al., 2021]. Our interest in looking at individual cells is based on the belief that by looking at cells we can get a glimpse of life as a whole.

1.1.2 Central dogma

At the same time that cell theory was being developed, advances in chemistry were making possible the dissection of elementary molecules of living systems. In 1839, Gerrit Mulder showed that blood fibrin, blood serum albumines and eggs had the same atomic composition, with carbon, hydrogen, nytrogen, and oxygen in almost equal proportions (with some traces of sulfur and phosphorus). This led to the first proposal of the term protein to designate these molecules of living systems [Mulder, 1839]. The decomposition of these proteins revealed simple structures with one carboxylic group,

named amino acids, which were isolated and characterized in the second half of the 19^{th} century (for 13 of them) and in the first half of the 20^{th} century (for the other 7). Scientists looked for order and periodicity in protein sequences, until 1953 and the discovery of the 'disordered' insulin sequence.

In the same second half of 19^{th} century, Johann Friedrich Miescher and then Felix Hoppe-Seyler showed the different chemical nature of the nuclear content and called it nucleins, and Albrecht Kossel and his group revealed the composition of the nucleic acids that make up DNA (deoxyribonucleic acid). The informative role of DNA would emerge much later. The connection between Mendel's main laws of heredity [Mendel, 1865] and proteins and metabolism is described by Beadle and Tatum in 1941 [Beadle and Tatum, 1941]. Heredity was thought to originate from proteins themselves and DNA was thought to be a periodic molecule. In 1944, Avery *et al.* first demonstrated that DNA alone was capable of transforming bacteria and giving them new metabolism [Avery et al., 1944], but it took several more years to conclude that DNA was the carrier of information. In 1953, Watson and Crick postulated the double helix model of DNA, while Franklin and Gosling published some X-ray images of one form of DNA. Watson and Crick suggest that base pairing of the DNA structure could be the basis of DNA copying mechanisms.

In the decade following this discovery, the role of ribonucleic acid (RNA) as a messenger from DNA to proteins is proposed and proven [Jacob and Monod, 1961, Gros et al., 1961, Brenner et al., 1961], and the genetic code is fully decoded in 1966. These discoveries led to what is now called the central dogma of molecular biology, first proposed by Crick in 1957 (and largely speculative at that time), which asserts that information flows from DNA to RNA to proteins [CRICK, 1958, Crick and Francis, 1970] (see 1.2) and that proteins do not rewrite DNA sequences.

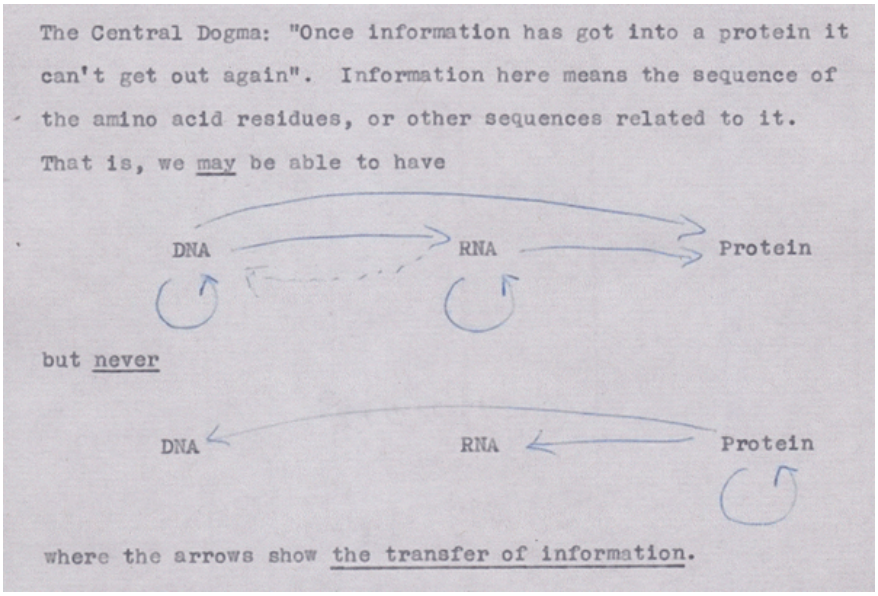

Figure 1.2: Central dogma as drawn by Crick, from an unpublished 1956 note. Taken from [Cobb, 2017].

Although there are exceptions to these information transfers [Koonin, 2012], the central dogma of molecular biology is still relevant and shapes the way we view living cells. Most importantly, it leads us to think of DNA as the sole carrier of heredity, which is more and more subject to debate [Noble, 2018], and to view the nucleus as the brain of the cell, from which all information emanates and to which it is transmitted. This

also has implications for the way we represent the signalling networks that generally lead from the outer membrane to the nucleus, with the cellular response taking the reverse path.

1.1.3 Cell signalling networks

The discovery of proteins as essential components of every living cell has led to a progressive understanding of their various roles. By the end of the 19th century, enzymes were known for catalyzing chemical reactions, and their specificity for one substrate was proposed by Emil Fischer in 1894 [Fischer, 1894]. However, the proteic nature of enzymes was not demonstrated until 1926 by James Sumner [Sumner, 1926]. Until 1950, most proteins were considered important for metabolic reactions or as structural components of the cell. In the 1950s, the concept of cellular signal transduction emerged with two discoveries. First, it was shown that phosphorylation can reversibly alter the activity of an enzyme [Krebs and Fischer, 1956, Krebs and Beavo, 1979]. Second, it was demonstrated that cyclic adenosine monophosphate (cAMP) is accumulated by adrenaline and further triggers the activity of an enzyme, glycogen phosphorylase [Sutherland and Rall, 1957]. The concept of 'second messenger', whose sole function was to transmit information, was born [Hunter, 2000]. The discovery of other receptors and proteins such as G-proteins followed [Nair et al., 2019] and led to the beginning of the field of 'signal transduction' (although the term was not used until the 1970s [Nair et al., 2019]).

Martin Rodbell is often credited with the idea of signalling cascade, in which some proteins act as transducers or amplifiers, with his discriminator-transducer-amplifier model [Birnbaumer, 2007] (Figure 1.3). The simple scheme shows an external signal such as a hormone being 'sensed' by the discriminator (specific to that hormone). The signal must be transmitted across the membrane. This task is performed by the transducer, which is often a transmembrane protein. The signal is further amplified by amplifying proteins such as cAMP and leads to specific cell responses. This has led scientists to speak of signals that must be transmitted from the environment and trigger a specific response from the cell after a series of biochemical reactions. Terms coming from engineering started to be used at that time, such as computation, transfer and processing of information, biomolecular circuits, information storage, inputs and outputs. This was formalized a few years later by Dennis Bray in 1995 in his review paper *Protein molecules as computational elements in living cells* [Bray, 1995]? This helped to establish the field of Systems Biology, which has developed in all areas of biology, using knowledge from engineering and physics [Alon, 2020]. Some principles of biochemical circuits and information processing in cells are discussed in 1.3.1.

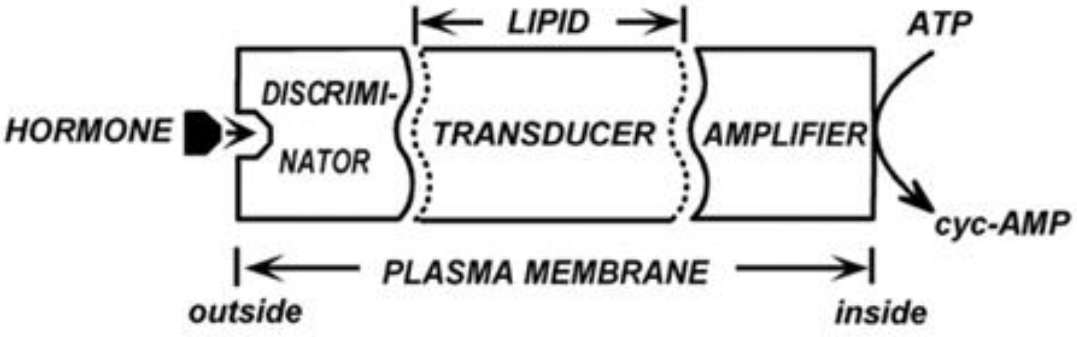

Figure 1.3: Discriminator-Transducer-Amplifier model proposed by Rodbell in a conference in 1970 [Rodbell, 1970]. Cell receptors are the discriminators that receive external signals and transmit the information across the cell membrane via the transducers. The signal is further amplified through amplifiers that relay signals within or across the cells. Taken from [Birnbaumer, 2007].

1.2 Timescales in cell biology

Now that we have seen some key concepts that still drive our understanding and questions in biological research, it is time to enter the cellular world, which requires a profound change in perspective. Indeed, because of the micrometer scale of mammalian cells, a lot of our intuitions regarding size, movement, diffusion and chemical reactions must be revised. Cells are not static matter: they are constantly producing new proteins, changing expression levels, adapting to their environment, and changing their mitotic stages. It is therefore important to consider the timescales of these various processes to get an idea of what is at play in each experiment (Figure 1.4).

I will first describe the biochemical reactions, happening often at the subsecond timescale, then move on to diffusion, cell shape changes and migration, protein synthesis and then cell division, which are processes happening at longer and longer timescales, with obviously a lot of overlaps.

Most of this chapter is inspired by and taken from the book *Cell biology by the Numbers* [Milo and Phillips, 2015], whose authors have done a tremendous job of compiling and calculating key orders of magnitude in cell biology.

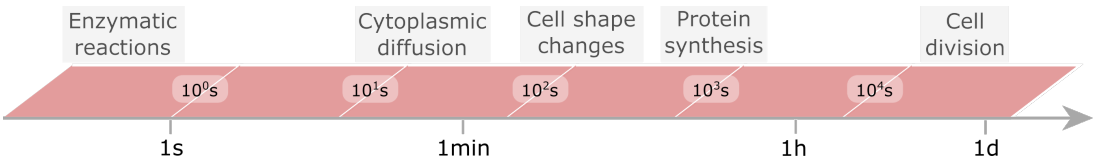

Figure 1.4: Timescales in cell biology. Adapted from [Milo and Phillips, 2015].

1.2.1 Biochemical reactions

Biochemical reactions can have very different timescales depending on the affinity between the different binding partners, and mostly rely on the processing speed of the enzymes involved in the reactions. Enzymes are needed to increase reaction rates, sometimes by tens of orders of magnitude in low spontaneous reactions. These enzymatic reactions are described by two numbers, k_{cat}, which represents the maximum

reaction rate (when the substrate is at high concentration), and K_M, which is the concentration at half-maximum rate (Figure 1.5).

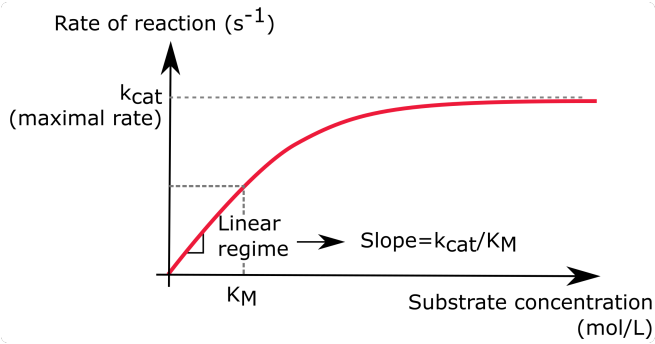

Figure 1.5: The characteristic dependence of enzyme catalysis rate on substrate concentration, with defining effective parameters such as kcat, K_M and their ratio. Adapted from [Milo and Phillips, 2015].

These numbers highly depend on the enzyme-substrate pair, but a sense of the characteristic rates can be given by their median. The median k_{cat} is around $10s^{-1}$, i.e., ten reactions per second per enzyme at maximum rate, with extreme values going from $10^{-2}s^{-1}$ to $10^{5}s^{-1}$. Median K_M is about 100µM, well above individual concentrations of most of the proteins in mammalian cells [Bar-Even et al., 2011]. It implies that most enzymatic reactions in a cell are theoretically in the linear regime, i.e., proportional to the local concentrations of both the enzyme and the substrate, with a proportionality rate factor k_{cat}/K_M, which median value is $10^5 s^{-1} M^{-1}$.

An approximation of the residence time, which indicates how long an enzyme and its substrate remain bound to each other, can be calculated from K_M and the diffusion-limited *on* rate (assuming that every encounter results in an interaction). This leads to a timescale of $\sim 1s$ for extremely strong enzyme-substrate binders, and up to five orders of magnitude less for others.

Overall, most biochemical reactions can be considered happening at the second timescale or much below if both binding partners are present in the cytoplasm, like in a solution. Equilibrium will be reached much faster than processes such as diffusion at the membrane, sequestration by another binder >10s,... As these processes happen at longer timescales, they will be the limiting ones for most reactions to happen.

1.2.2 Diffusion

Diffusion within the cytoplasm is the main driver of protein encounters leading to biochemical reactions. Diffusion of one molecule is best described by the diffusion coefficient D, higher D indicating a higher rate of jiggling around. One time scale τ can be derived from this coefficient and the characteristic length l of the process $\tau = l^2/D$. In the cytoplasm, a monomeric protein with few interactions has a diffusion coefficient of the order of $\sim 10\mu m^2/s$ [Etoc et al., 2018], with the diffusion coefficient being lower if the protein is larger or has more interactions. For such a monomeric protein with few interactions to cross an adherent cell (about 10 µm in diameter), the typical timescale for diffusion would be ∼10s.

At membranes, lateral protein diffusion (for a protein with little interactions with other membrane proteins) is two orders of magnitude smaller, namely $\sim 0.1\mu m^2/s$ [Jacobson et al., 1984, Valon et al., 2015], due to the 2D property of the membrane.

Crossing the adherent cell by only diffusing at the plasma membrane would then take 1000s. Other diffusion timescales for displacement over a few micrometers are shown on Figure 1.6.

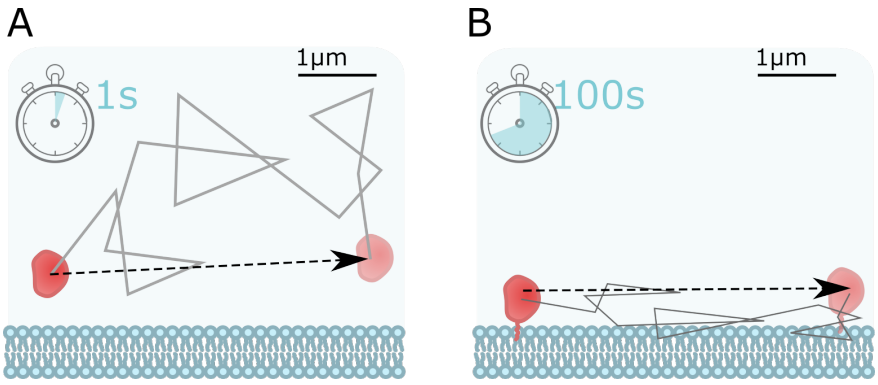

Figure 1.6: Diffusion timescales of a cytoplasmic or membrane bound protein. (A) A soluble protein needs 1s to move a few micrometers only by diffusion. (B) A membrane-bound protein needs 100s to move a few micrometers only by diffusion

As a consequence of this difference between membrane and cytosolic diffusion, signalling and chemical reactions speed will largely vary depending on the cytoplasmic or membrane-bound nature of the protein considered. This will be of particular importance for proteins that constantly switch between membrane and cytosolic localization, as we will see for the specific case or RhoA (see 1.5).

1.2.3 Cell shape changes and migration

Since most of my thesis has been dealing with cell movements, it is critical to get an understanding of the constraints that exist at the cellular scale. To have an intuition of how an object moves in a fluid, one has to consider Reynold's number, which is the ratio between inertial forces and viscous forces. As described in the famous 1976 lecture by Adward Mills Purcell [Purcell, 1977], the Reynold's number for a man swimming in water might be 10^4, while a cell of a few tens of micrometers migrating at a few micrometers per minutes might move at a Reynold's number on the order of 10^{-5}. This means that on the cellular scale, inertia is absolutely irrelevant, and cell must constantly generate forces (and thus spend energy) in order to actively move forward.

When cells do migrate, they need to change shape and usually have a protruding front and a retracting rear (see 1.4 for more details). These cell deformations due to the cytoskeleton happen usually at the minute timescale, sometimes less for fast migrating cells.

Most cells in our body do not move actively, and those that do move reach very different speeds depending on their type (Figure 1.7). Human neutrophils can typically reach 20 µm/min (∼ 2 body length/min) [Hoang et al., 2013], while the single cells I studied in my thesis have a mean speed of around 20µm/h (∼ 1 body length/h) [Vaidžiulytė et al., 2022]. At the collective scale, speed can be one order of magnitude slower (1-5µm/h), as we will see in 1.4.4.

As a consequence of all of these timescales, looking at significative cell movement requires an observation time frame that depends on the cell type, and whether we look at membrane displacement (seconds to minutes) or significative migration over many body lengths (minutes to hours). However, in most cases, timescales are usually bigger

than the time frame of the biochemical reactions and cytosolic diffusion we discussed above.

Ciliate Paramecium tetraurelia	100–1000 µm/s	1-5 bl/sec	108087, ciliated, assuming 200 µm cell length
Tetrahymena thermophila	200–400 µm/s	4–8 bl/sec	111429, 111435, 111436, ciliated
Gyrodinium dorsum	300 µm/s	10 bl/sec	111432, flagellated
green algae *Chlamydomonas Reinhardtii*	50–150 µm/s	5–15 bl/sec	108086, 111430
fish keratocytes - wound healing fibroblasts of the cornea	10–50 µm/min	0.7-3 bl/min	106807, 106817
Amoeba Dictyostelium discoideum	10 µm/min	≈1 bl/min	106825
human neutrophil	9 µm/min	≈1 bl/min	106809
glioma cells	50 µm/hour	4 bl/hour	106810
mouse fibroblastoid L929 cells	30 µm/hour	2 bl/hour	106808
human H69 small cell lung cancer cell	16 µm/hour	1 bl/hour	106815

Figure 1.7: Average cell speed for different eukaryotes in µm and body length per time unit. Adapted from [Milo and Phillips, 2015].

1.2.4 Protein synthesis

Most of the signal transmission within the biochemical network is carried out by proteins, as well as most of the shape changes. They are constantly produced through the two well known mechanisms of transcriptions and translations.

How fast is a protein synthesized in a mammalian cell? Rates have been measured in different cell types, both for transcription and translation. In Hela cells, a method developed by Fuchs et al. [Fuchs et al., 2014] gave a transcription elongation rate of 2 to 6 kb/min, while translation rates have been estimated at 30 to 600aa/min [Siwiak and Zielenkiewicz, 2013]. This would mean that approximately one minute is necessary for synthesizing a protein of 1kb. However, it seems that in most cases, RNA splicing is the key limiting step for full protein synthesis, ranging from 5 to 10 minutes [Singh and Padgett, 2009]. Protein folding should not be limiting [Naganathan and Muñoz, 2005], but other steps such as maturation can be required for the protein to be fully functional. This is especially the case for fluorescent proteins, that have a wide variety of maturation time, ranging from minute to hour timescale [Iizuka et al., 2011].

As a result, after applying any perturbation to the cell, the response in terms of changes in protein content takes at least 10 minutes, and is often considered as being significative at the hour timescale. Compared with cell movement, this means that first cellular displacement happens without involving proteomic changes, but can have an impact when looking at long-term migration.

1.2.5 Cell division

Mammalian cell division constantly occurs for the cell lines used in the labs, that have been selected and sometimes genetically modified for their ability to proliferate without differentiating. For the most known Hela cells, this division occurs every 20 hours, with most of its time spent in G1 and S phase (growing and duplicating its DNA) [Hahn et al., 2009]. This will be a good order of magnitude for all the cells used during the experiments described here. This means that there is no need to take it into account for experiments that last below one hour, but that it starts being an important parameter when reaching the hours timescale.

1.3 Cell signalling

These different timescales gave us an overview of the speed of the processes happening at the cellular level, in order to have a better intuition of the cellular world. In this section, I will focus on one of the key property of cellular systems: their ability to integrate signals that come from their environment, process them and respond accordingly.

A single mammalian cell has the ability to sense the environment through its outer boundary, the plasma membrane; it then transduces the signal along its internal signalling network; internal computation leads to cell response at different timescales, ranging from immediate change in membrane potentials (ms), to protein activation (seconds), cell shape changes (minutes), or durable changes in protein expression (hours).

I will first detail the different mechanisms by which a signal is transmitted and give a glimpse of the complexity of signalling networks. I will then turn to biosensors that are developed to follow intracellular signalling in space and time (output), and look at optogenetics, which proposes a unique way of probing intracellular signalling networks (input).

1.3.1 How do cells process signals?

The plasma membrane is the outer boundary of the cell, containing a lot of transmembrane proteins that are incorporated into it. All signals integrated by the cell, chemical, mechanical or event electrical, have to be transmitted across this barrier. For biochemical signals such as chemokines present in the environment, cells have transmembrane receptors that will change conformation upon binding and trigger a signalling cascade. This cascade of reactions, called intracellular signal transduction, can be of different nature : post-translational modifications like phosphorylation -which is one of the most common signal transmission event-, displacement of one protein, change of conformation, complex formation... It has been a particularly important area of research in cancer where most tumors arise as a consequence of genetic alterations to cellular genes that lead to failures in signal transduction and tumorigenic behaviors [Sever and Brugge, 2015].

Signal transduction has first been seen as linear pathways where one specific input would trigger a defined signalling cascade that will lead to one specific response [Kestler et al., 2008]. However, new data has led to a change in point of view: one signalling pathway cannot be considered outside of its network, with hundreds of interactions and feedbacks at all the different layers (see Figure 1.8). There has been tremendous work to model these networks mathematically, to translate all these biological interactions into simple nodes of a complex network that would give us a global picture of cell transduction pathways [Janes and Yaffe, 2006, Cirit and Haugh, 2011, Kolch et al., 2015].

Signal transduction can be separated into two intertwined networks based on the timescales involved:

- **Protein-protein interaction network:** it concerns all the biochemical reactions that happen without any change in the protein content, i.e., without intervention of the transcription-translation machinery. As stated previously in 1.2.1, these biochemical reactions occur at the subsecond to second timescale, as they are mainly enzymatic reactions or phosphorylation events, driven by diffusion in

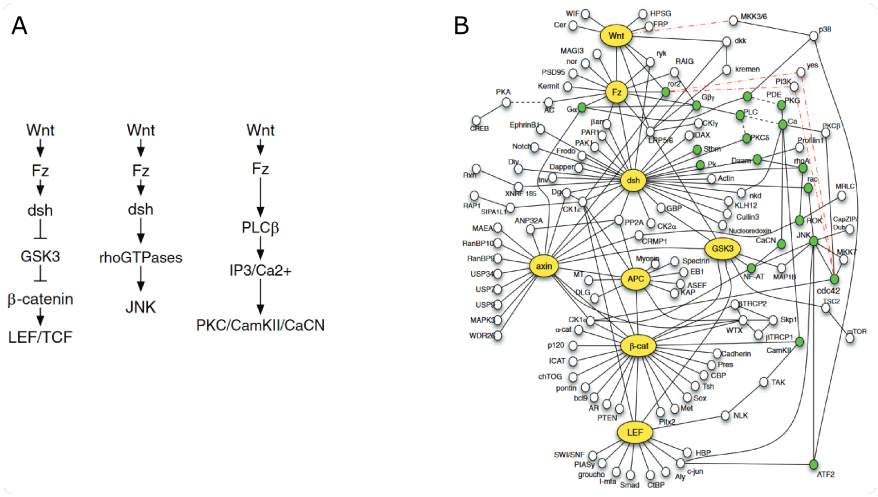

Figure 1.8: Signal transduction network of Wnt pathway seen as three linear cascades corresponding to the three functions of the pathway (A), or as a complex undirected interaction network (B). Yellow circles indicate the originally identified mediators of Wnt signalling, which represent hubs as they have many interaction partners. Green circles indicate proteins that were originally reported to be mediators of non-canonical Wnt signalling branches. Taken from [Kestler et al., 2008].

the cytoplasm. Reactions can occur within the cytoplasm, at the plasma membrane, or in any other compartment. A biochemical reaction cascade can lead to two non-mutually exclusive outputs. One output will be a 'fast' response of the cell, with a few seconds to a few minutes of immediate reaction to the external signal. This reaction can be a change in cell shape [Martin et al., 2016], movement of the cell in one direction (to follow a chemotactic cue for example [Wu, 2005]), transmission of information to another cell by cleavage of a receptor [Hino et al., 2020], or change in organelle positioning [Vaidžiulytė et al., 2022]. The second output can be the activation (by phosphorylation, for example) of a transcription factor that triggers the entire transcription-translation machinery and changes the protein content. This output will occur on much longer timescales (tens of minutes to hours) and will lead to the second network described below.

- **Transcription network:** it refers to the network that allows the cell to adapt its protein synthesis (and, therefore, concentration) in response to signalling events. As just recalled, these changes occur at much longer timescales than protein-protein interaction networks. Thus, the activity levels within the protein-protein interaction network can be considered at steady state within the equations that describe network dynamics on the timescale of changes in the protein level [Alon, 2020]. This transcription network was first studied in detail in *E. coli* , but new techniques (transcriptomics, proteomics, etc.) now provide a more detailed picture of this network in mammalian cells.

Key properties of these networks can be studied by comparing them to randomly generated networks with different rules [Alon, 2020]. Interestingly, some patterns of nodes and links happen much more often in biochemical networks than in randomized ones. This means than these patterns have been selected by evolution because of their usefulness, and can be considered as building blocks of the whole network. These patterns, called network motifs, can be studied independently, and display key properties such as robustness, adaptation, and sometimes optimality, which are properties needed

for life to perform so efficiently in an environment with strong thermal noise. I will describe briefly these properties, but refer to the excellent book from Uri Alon [Alon, 2020] for more exhaustive study of these motifs.

Robustness: "This principle states that biological systems have special designs that make their essential function work precisely despite naturally occurring noise." [Alon, 2020] This property is key, as thermal noise is strong at the cell level - the thermal energy k_BT (k_B being Boltzmann constant and T the temperature) is on the order of magnitude of most protein-protein interaction - and cell to cell variability can be quite important - often tens of percent of the protein concentration level [Mahdessian et al., 2021]. Another source of uncertainty is due to the multiplicity of interactions of each protein, which require proofreading processes. Motifs found commonly in the biochemical networks can answer to this property of robustness, such as kinetic proofreading, or the use of two-components systems, which I will describe here as an example. Two-components systems are network motifs that rely on bifunctional components -proteins that have two opposite effects on one pathway, both activating and inhibiting. An example of such a two-components system with a bifunctional component is shown on 1.9. In this example, protein X acts both as a phosphatase when not phosphorylated (X_0), and a kinase when phosphorylated (X_p). As both processes are proportional to the concentrations of X and Y, one can show that they cancel out when calculating the output, which then only depend on the input S and the different reaction rates.

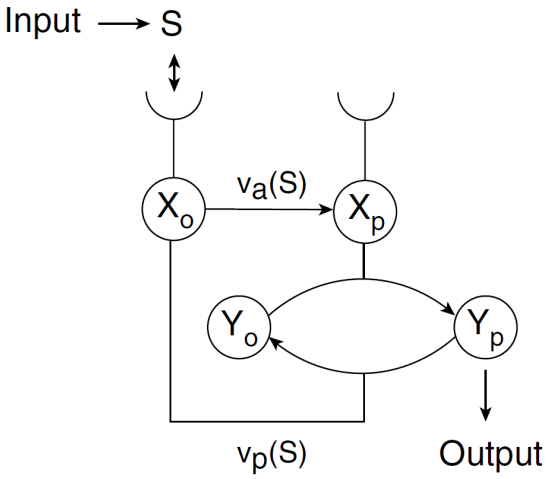

Figure 1.9: Bifunctional component. Component X acts both as a phosphatase when not phosphorylated (X_0), and a kinase when phosphorylated (X_p). This enables the robustness of the output, which is independent of the concentrations of X and Y, and only dependent on the input S. Taken from [Alon, 2020].

Adaptation: adaptation refers to a network motif where the steady-state of an output is independent of the level of the input. An example of adaptation is shown on Figure 1.10: when changing the input S, the output X^* will first change due to the changes of the input, but will then come back to its initial steady state. Robust Perfect Adaptation (RPA) refers to an adaptative network that is also robust -it is resilient to perturbations such as changes in protein levels [Khammash, 2021]. Recently, it was mathematically proven that a single fundamental biomolecular controller topology could achieve integral feedback -a strategy that performs mathematical integration to achieve structurally robust regulation- and achieve robust perfect adaptation. This kind of network topology is found in many different biological systems, ranging from

calcium homeostasis to bacterial chemotaxis [Khammash, 2021].

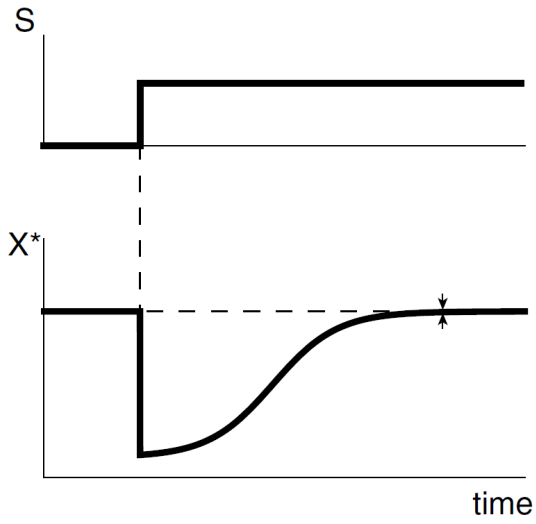

Figure 1.10: Adaptation. Changing the input S will first have an effect on the output X^*. After some time, it will adapt and come back to its initial steady state. Taken from [Alon, 2020].

Optimality: "Optimality theory is based on the ability of natural selection to maximize fitness, and hence to converge on particular circuit designs and parameter values in a given environment." [Alon, 2020] Biological circuits are optimized to a certain extent, as a lot of mutations lead to defects, sometimes death or much worse performances. All the more so, the recurrence of certain motifs is probably due to better functioning of this kind of network, as optimization is a consequence of evolution and natural selection. Optimality is not achieved for only one function, as multiple functions must be carried on by the cell simultaneously, but looking at optimal motifs can help us understand biological networks and their evolution. Usually, optimality will be described and reached when the constraints of the environment are clear, and a specific property, such as growth, has to be optimized. [Alon, 2020] Optimality has been studied a lot in bacteria, for example considering benefits and burdens of some protein expression and how the cell reaches optimal or suboptimal growth [Dekel and Alon, 2005, Towbin et al., 2017]. In a natural environment, constraints are multiple and leads to trade-offs to both perform multiple functions and adapt to changes in environment [Poelwijk et al., 2011]. Although done in bacteria, optimality can help us understand why some motifs are more prone to be selected [Dekel et al., 2005] when they have direct impacts on the cell metabolism.

These properties of signalling networks are global and not always applicable to the study and modeling of a specific set of proteins. However, they help putting some constraints on the way we model and fit the study of specific interactions into a global view.

In the study of protein-protein interaction networks, there is always a trade-off between the molecular details of each protein-protein interaction or protein conformational changes, and staying with a global picture of how the interactions lead to very robust systems that can perform extremely complex behaviors. It requires combining large-scale studies with high-throughput data, as well as structural studies of protein conformations and protein-protein interactions. It also calls for single cell experiments with a well-resolved temporal and spatial dissection of molecular pathways, if we want

to better understand protein-protein interaction networks in action. Indeed, both high-throughput experiments and structural studies often lack the time dimension specific to protein-protein interaction networks. To reach these timescales and get an understanding of the dynamic of these signalling networks, one powerful tool is the use of fluorescent microscopy, combined with a set of tools that I will introduce in the next sections.

1.3.2 Fluorescent biosensors to monitor cell signalling in space and time

The complexity of signalling networks described in the previous paragraph calls for a development of tools that will efficiently report the activity of proteins of interest. A lot of discoveries have been done through biochemistry techniques such as immunoprecipitations, where specific antibodies against the desired protein are used [Corthell, 2014]. These biochemistry techniques have been ingeniously used to reveal protein-protein interactions, protein activities, changes in gene expression, etc... They have been combined with immunofluorescence, where cells can be observed at the single cell level, and proteins of interest can be marked by specific antibodies. However, these widely used techniques do not reach the spatiotemporal scale of the cellular transduction network, where signals are spatially localized and happen at the seconds timescale.

The first cloning of Green Fluorescent protein [Prasher et al., 1992] has been a revolution for live-cell imaging of intracellular signalling networks. Firstly, it has enabled the tagging of proteins, to monitor their localization in space and time during different cellular processes and perturbations. Furthermore, it has enabled the development of genetically encoded biosensors, with an infinite range of combinations for rapid and efficient monitoring of cellular activities [Snapp, 2009, Pendin et al., 2017]. Other types of biosensors, chemically synthesized (organic dyes) and uptaken by the cell, have been rapidly developing at the same time. The common feature between these biosensors is that the desired signal should trigger a change in the fluorescence level of the fluorophore. Extensive descriptions of genetically encoded biosensors or organic dyes can be found in [Kim et al., 2021] and [Pendin et al., 2017], and I will here only recall three main strategies used to monitor signaling activities.

Translocation biosensors: These biosensors rely on the fact that protein localization can change upon activation/deactivation of a specific pathway. The fluorophore is linked to a protein, or a part of a protein, that will translocate when a specific signalling event takes place.

As an example, this strategy has been used to look at the activity of Rho-GTPases, which is a family of small signalling proteins involved in many cellular processes (see 1.4.2.1 for more details) that constantly switch between an active state (GTP) at the membrane and an inactive state (GDP). Biosensors to monitor Rho-GTPases activity are constantly improved [Mahlandt et al., 2021, Mahlandt et al., 2023, Nanda et al., 2023]: they use specific protein fragments that bind to Rho-GTPases only when they are in an active state. The signal can then be measured by looking at the changes of fluorescence intensity along time. (see Figure 1.11)

Another example has been recently widely used to monitor ERK activity, a kinase translocation reporter [de la Cova et al., 2017, Goglia et al., 2020, Ender et al., 2022]. ERK, when phosphorylated, translocates into the nucleus. The biosensor is a substrate

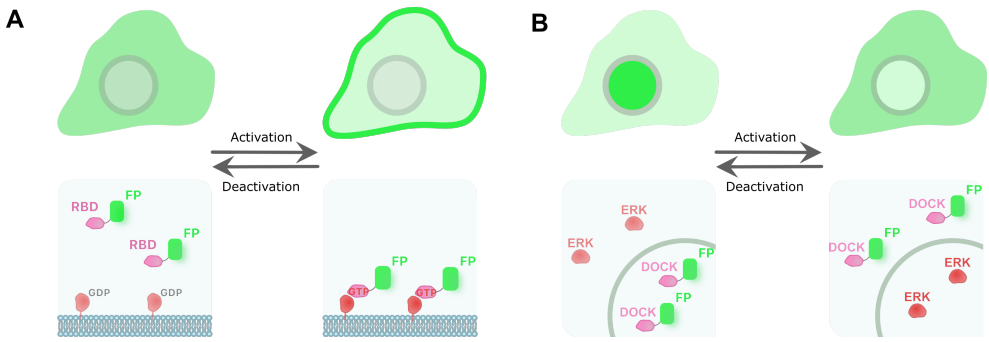

Figure 1.11: Translocation biosensors cartoon. (A) Translocation biosensor for RhoGTPases. When the RhoGTPase is active (in GTP state, dark red) the RhoGTPase binding domain (RBD in pink) will come and bind to it, changing the localization of the fluorescent protein (FP, in green). (B) Kinase translocation reporter, to measure ERK activity. When ERK (in red) is phosphorylated, it translocates to the nucleus, binds on the docking site (DOCK in pink), phosphorylates the nuclear importer and/or exporter, leading to the export of the biosensor out of the nucleus.

of ERK, that will be exported out of the nucleus when phosphorylated by ERK. (see Figure 1.11).

Translocation biosensors have many advantages: they are usually easy to use in single cells and require only one wavelength, contrary to the FRET biosensors we will discuss below. The fidelity of the temporal signal will depend on the binding dynamic of the biosensor - mainly its rate of unbinding k_{off} - which has to be taken into account but can be less that a few seconds. However, as they are effectors to the protein of interest, they can lead to dominant-negative effect. Moreover, cell-cell comparison can be hard, as their translocation can depend on the expression level.

FRET biosensors: FRET (Förster Resonance Energy Transfer) biosensors rely on a specific property of two fluorescent proteins - a donor and an acceptor - when the emission spectrum of the donor overlaps the excitation spectrum of the acceptor. In this case, an energy transfer can happen between the donor and the acceptor, when both molecules are at very close proximity (<10nm). This energy transfer can be measured by exciting the donor and looking at the emission of both the donor and acceptor.

As signal transmission depends on direct interaction between proteins, FRET biosensors have been widely used to assess signal transduction. Efficiency of the FRET biosensor depends on the distance, but also the orientation and the different properties of the fluorophores, which calls for optimization steps [Shrestha et al., 2015]. Different strategies can be used for the design of FRET biosensors (we show two of them in Figure 1.12), and each of them comes with its own experimental constraints.

There are many advantages to FRET biosensors. One is that they are very sensitive to distance, which means that they reveal direct interactions much below the resolution limit of the microscope. Moreover, for intramolecular FRET biosensors (see Figure 1.12 (B)), a cell-cell comparison is much easier and can be done at high throughput [Müller et al., 2020], because of the one-to-one ratio between donor and acceptor. One of the main drawbacks is that two colors are used, therefore few fluorescent channels are left for looking at other features of the cell.

Ligand binding biosensors: A third important class of biosensors uses changes in fluorophore spectral properties upon changes in conformation, or electronic distribu-

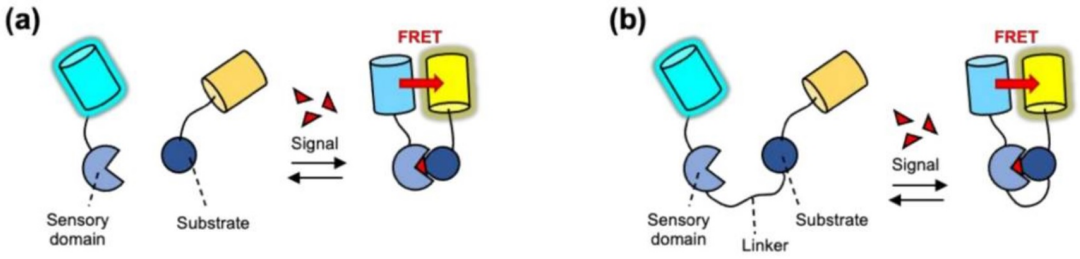

Figure 1.12: Two different designs of FRET biosensors.(A) Intermolecular FRET biosensor. Each fluorophore is on a different protein, and FRET happens when there is direct interaction. (B) Intramolecular FRET biosensor. The change in protein conformation triggers FRET. Taken from [Kim et al., 2021].

tion. This class of biosensors includes biosensors with direct or indirect ligand binding (Figure 1.13,(A) and (B)), and are very often used to probe for changes in ion concentrations. It also includes chemoluminescence, when binding of the ligand enables photon emission [Pendin et al., 2017] (Figure 1.13(C)).

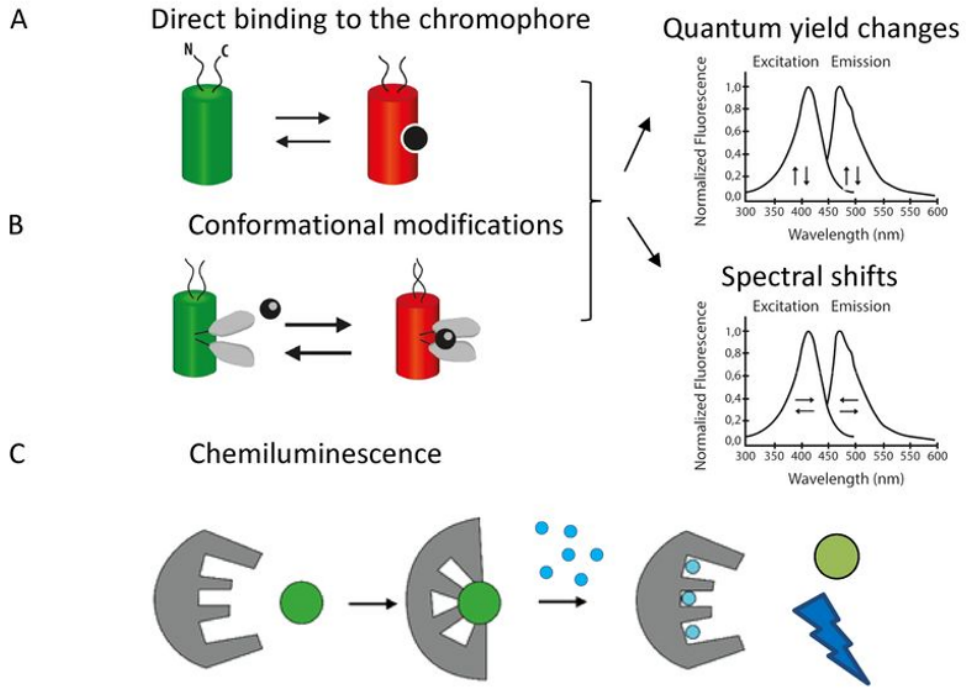

Figure 1.13: Three different types of ligand binding biosensors.(A) Direct binding without any modification of the fluorophore (often an organic dye). (B) Conformational modifications by adding a sensing domain (often genetically encoded). (C) Chemiluminescence where fluorescence happens only in presence of the ligand. Taken from [Pendin et al., 2017].

The toolbox of fluorescent biosensors continuously increases, as well as the number of strategies to increase fidelity. All in all, fluorescent biosensors are powerful tools to probe signalling events in space and time, but have to be used carefully. Indeed, they usually require overexpression of either one of the proteins of interest, or one of its ligands. Thus, they are never neutral and can always lead to artefactual results, due to cell adaptation or dominant negative effects. Their second main drawback is

the limitation in the multiplexing capacities, which is usually limited to four different colors [Welch et al., 2011]. A strategy to overcome this limitation can be computational multiplexing where the network dynamic is reconstructed from pairs of biosensors and correlation between time series [Welch et al., 2011]. Another recent strategy uses cellular barcoding in order to have multiple biosensors in the same cell population, where a specific biosensor can be identified in a single cell thanks to the barcoding system [Yang et al., 2021].

Despite these limitations, fluorescent biosensors are great outputs to study signalling pathways in space and time, with often subcellular resolution in space and seconds to minutes resolution in time. They call for techniques that can serve as inputs matching these spatial and temporal scales. Drug addition, for example, can be quite precise in time (a few seconds for the mixing drug to reach the membrane + uptaking time that will depend on the drug) but lacks spatial precision. Optogenetics, as we will see with the next section, will offer the input counterpart to fluorescent biosensors, with unmatched spatiotemporal precision thanks to the use of light as the input.

1.3.3 Optogenetics to perturb in space and time

Optogenetics refers to techniques involving any genetically encoded protein system designed to perform a specific light-mediated task [Wittmann et al., 2020]. It was first used in neuroscience to trigger membrane depolarization, and, thus, neuronal spikes upon light stimulation [Boyden et al., 2005]. Subsequently, it was extended to virtually all areas of cell biology thanks to its versatility and its combination with fluorescence microscopy.

Optogenetic techniques use proteins that change their conformation in response to light and modify them to regulate various signalling activities in living cells. Thanks to the continuous improvements of optogentic systems, a lot of different approaches have been used to control protein activity, protein localization, heterodimerization or homodimerization, formation of higher order structures... (see Figure 1.14) Four main light-sensitive systems have been used, with advantages and disadvantages. Cryptochromes [Liu et al., 2008], light-oxygen-voltage (LOV) [Christie et al., 1999], and phytocromes [Ni et al., 1999] are derived from plants, while Dronpa protein [Zhou et al., 2012] was isolated from the coral Pectiniidae. Here I will describe cryptochromes and LOV domains that are most commonly used in mammalian cells.

Cyptochrome 2 (CRY2) protein : this protein from *A.thaliana* is sensitive to blue light, with an absorption spectrum ranging from 300 to 500nm [Li et al., 2011]. Its conformational change upon light exposure leads to two different effects: it homo-oligomerizes and binds to its binding partner, CIBI (cryptochrome-interacting basic helix-loop-helix 1), both within seconds. Both processes are reversible in the dark with a half life of 5 minutes [Kennedy et al., 2010, Valon et al., 2015]. It has been widely used for both of its properties, inducing oligomerization of a protein of interest at the membrane [Kim et al., 2016] or in the cytoplasm [Bugaj et al., 2013, Park et al., 2017], or to recruit a protein of interest to the membrane [Valon et al., 2015, de Beco et al., 2018]. Interestingly, using these different strategies with the same protein does not necessarily give the same cellular output [Kerjouan et al., 2021]. Different mutated versions exist that increase or decrease its homo-oligomerization properties [Duan et al., 2017], and it has also been used to create higher order structures like liquid droplets [Shin et al.,

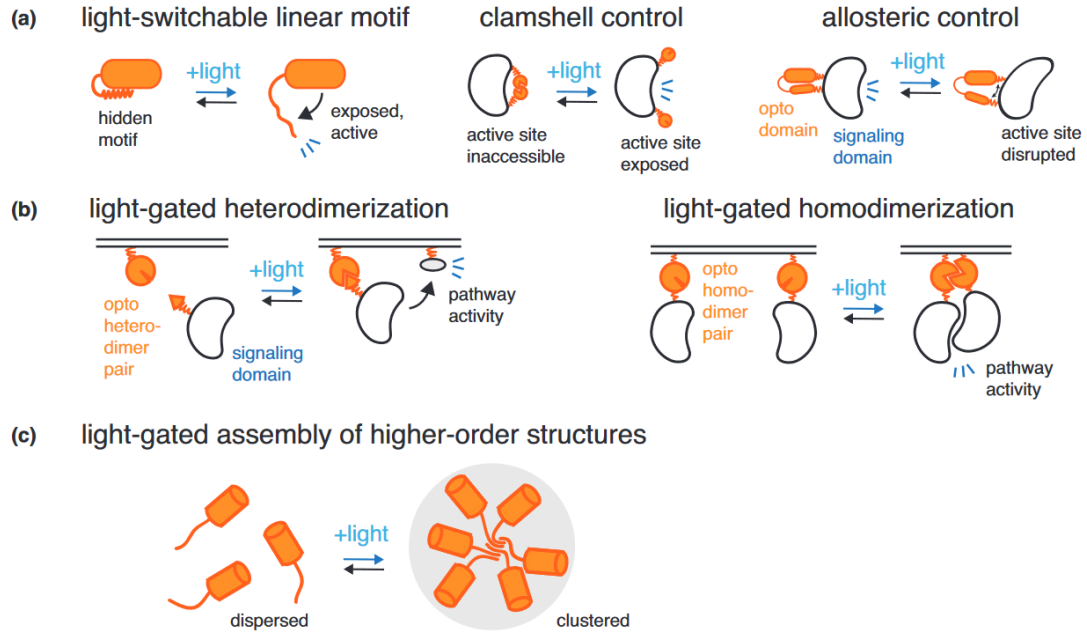

Figure 1.14: Optogenetic approaches to trigger intracellular signalling. (a) Single protein activity is controlled by caging/uncaging (left), occlusing/exposing the active site (middle) or altering the active site (right) (b) Light-dependent heterodimerization partners to control subcellular localization (left) or homodimerization partners (right). (c) Light-dependent oligomerization or higher order structures formation.Taken from [Goglia and Toettcher, 2019].

2017].

Light-oxygen-voltage : LOV domains from various organisms have been used as optogenetic tools. They are also sensitive to blue light, in the same spectral range as CRY2, roughly from 300 to 500nm [Christie et al., 2002]. They use the ubiquitously expressed (in human) endogenous flavin as a chromophore. LOV domains have been used in all strategies described in Figure 1.14 thanks to their number and versatility. One of the main development has been the engineering of improved light-induced dimer (iLID) [Guntas et al., 2015] that binds under light to its natural binding partner SspB. iLID and SspB have been further engineered in order to span different dynamic ranges in terms of affinities in the dark and in the light, as described in Figure 1.15 [Zimmerman et al., 2016], but also very different binding times (going from seconds to tens of minutes). They are much smaller than CRY2 dimerization systems, AsLOV2 being 16 kDa and SspB 13 kDa, while Cry2 has a size of 57 kDa and CIBN 20 kDa [Wittmann et al., 2020].

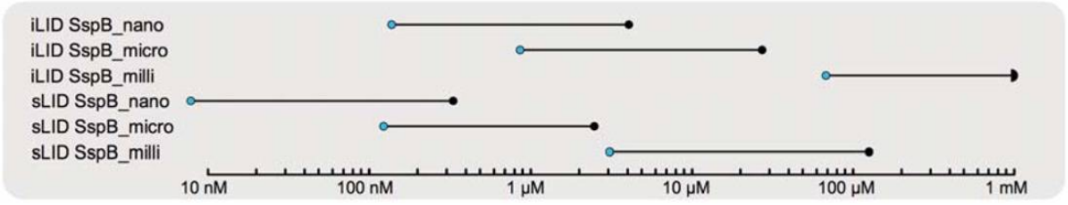

Figure 1.15: Dynamic range of each pair of iLID-SspB optogenetic dimers comprising all mutants. For each pair, black dots denote the dark state affinity, blue dots denote the lit state affinity. Taken from [Zimmerman et al., 2016].

Optogenetic tools offer a lot of versatility, and virtually all cellular processes can be targeted. The number of optogenetic tools developed for cell biology is continuously increasing. Its main advantage relies in the use of light, which offers great spatiotemporal precision and control. Thanks to its subcellular precision and very high temporal resolution, and the possibility to target almost any node in the signalling network, it offers a way to distinguish correlation from causality, by triggering a precise signalling event at a definite space and time.

It also comes with its limitation. First one is the use of light which leads to several issues. Light cannot be used in deep tissues, making it difficult to use *in vivo*. This can be partially overcome thanks to two-photon microscopy that enable much deeper activation [Oron et al., 2012]. Second issue due to light is the limitation in number of fluorescent proteins that can be monitored while performing optogenetic activations. Indeed, both CRY2 and iLID presented above are activated in standard blue or violet channels, preventing the usage of commonly used fluorescent proteins such as GFP and YFP. In optogenetic live experiments with these tools, one has two remaining channels for standard fluorescence microscopy, red (such as mCherry or RFP) and infrared (such as iRFP). This makes the use of biosensors such as FRET biosensors quite challenging, even if it was recently done with the help of the Dronpa protein [Ju et al., 2022]. Another drawback due to light: most of the common optogenetic tools such as iLID and CRY2 require blue light, which can also damage the cells. However, the optogenetic activation generally requires much less light than the light required for the excitation of low wavelength fluorophores for fluorescent microscopy. Last issue due to the use of light sensitive proteins is experimental. As ambient light can activate the optogenetic tool, all experiments must be performed in the dark, which can sometimes be challenging. Also, residual light will always trigger some leakage that can have some impact but be difficult to quantify [Valon et al., 2017].

A second challenge comes from the nature of the optogenetic changes. Optogenetic tools have their own behavior that do not necessarily match the one of the biological processes we want to look at. As stated above, for instance, CRY2 dimerizes with CIBN but also homoligomerizes. It has an interaction time of a couple of minutes, which can be far more than the endogenous biological process. iLID and SspB have shorter interactions, but they may not match the ones *in vivo* as well.

A third challenge relies in the choice of the protein that will trigger the input. This protein must be designed to be as inactive as possible in the dark, and active in the light, which can be sometimes challenging [Valon et al., 2017]. It implies removing most of the regulatory parts, which necessarily will change the way the signal will be transmitted upon activation.

Despite all these limitations, optogenetics, combined with fluorescent biosensors, provides a precise and useful way to interrogate cell signalling at the single cell level in space and time [Toettcher et al., 2013], and to get insights into the complexity of signalling networks, feedback loops and causality [Kowalczyk et al., 2022]. It is now used in developmental biology in multiple model systems such as drosophila, *C.Elegans* or zebrafish [Krueger et al., 2019], and has even started to develop for therapeutic applications [Bansal et al., 2022].

1.4 Single and collective eukaryotic cell migration

The signalling events presented in the previous section are the basis for the cell to integrate external signals and perform complex functions such as growth, differentiation

or migration. During my PhD, I focused on cell movement, which requires very complex structures and coordination within the cell, and reveals one part of the complexity of life.

Most cells in our body are embedded in tissues and do not migrate, yet cell migration is a crucial biological process. It is strongly involved in embryonic development, as well as in our adult immunitary response and tissue homeostasis [Lauffenburger and Horwitz, 1996]. Cell migration can also be strongly deregulated, as in the case of cancer dissemination, when some cells from a primary tumor start escaping to form metastases. This last process is a key aspect in cancer mortality, which remains the second cause of death worldwide [Sung et al., 2021]. Understanding the fundamental biological and physical processes that regulate cancer cell invasion is therefore one of the key challenges of today's cancer research.

Mammalian cell migration complexity is immense and beyond the scope of this introduction. Thus, I will first detail the main principles and components triggering cell deformation (1.4.1), a first step requirement for migration. I will then explain how these deformations can lead to effective cell body displacement by initiating a global polarity (1.4.2), and will end by describing the main known modes of single and collective cell migration (1.4.3,1.4.4).

1.4.1 Cell deformation

Cell deformation requires the deformation of its outer boundary, the plasma membrane (1.4.1.1). This can be achieved thanks to the forces exerted by the cytoskeleton, and especially the actomyosin network that constantly gives the cell its shape (1.4.1.2). For this deformation to lead to effective movement, forces must be transmitted to the substrate either through specific adhesions that anchor the cell, or through non specific interactions that will transmit forces through friction (1.4.1.3).

1.4.1.1 Plasma membrane

Mammalian cells are delimited from their environment by their plasma membrane, the basic structure of which is a phospholipid bilayer [Cooper, 2000]. This bilayer acts as a barrier between the two aqueous compartments inside and outside of the cell, but is also a key component of most signalling pathways, serving as an integrator to the extracellular environment, as well as a platform for information to be transmitted [Grecco et al., 2011].

A simple homogeneous lipid bilayer in an aqueous environment minimizes its energy by minimizing its surface to volume ratio and thus has a spherical shape. To deviate from this shape, the plasma membrane can be strongly deformed by various means. The intrinsic composition of the plasma membrane, either lipid or protein content, can lead to membrane deformation. Extrinsic mechanisms include binding of asymmetric proteins, formation of protein scaffolds, forces exerted by the cytoskeleton [Jarsch et al., 2016] (Figure 1.16) or hydrostatic pressure. We will focus here on the forces exerted by the cytoskeleton, which are the main active processes for membrane deformation and body displacement during cell migration.

1.4.1.2 Actomyosin network

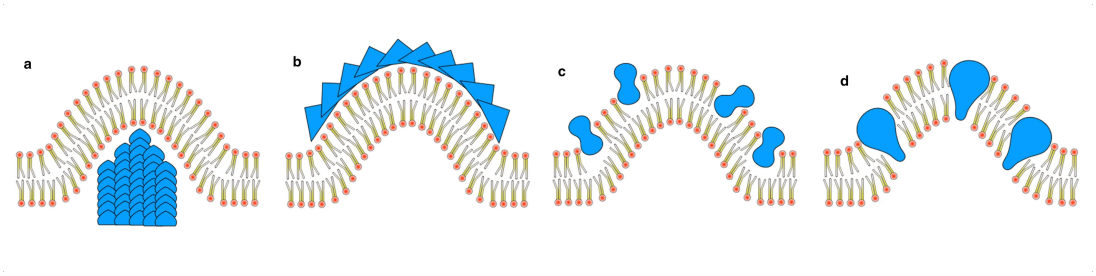

Figure 1.16: Mechanisms of membrane deformation. (a) External pushing or pulling forces, like the cytoskeleton represented here. (b) Protein supramolecular scaffolding. (c) Asymmetric composition of the lipid bilayer. (d) Transmembrane protein with wedged shapes. Adapted from [Royes et al., 2020].

The cytoskeleton consists of three types of filamentous structures: microtubules, actin filaments, and intermediate filaments. While they all contribute to the maintenance of cell shape and structure, the actin network is known to be crucial for almost all types of cell migration. Coupled with the myosin motors, they form the actomyosin network, and are the main force generator for powering cell migration [Mitchison and Cramer, 1996].

Actin : Composed of 42 kDa actin monomers, actin can polymerize and form linear filaments called F-actin. F-actin filaments are polar in nature and polymerize at different speeds at their two ends. The barbed end polymerizes faster than the pointed end [Pollard, 1986]. New polymers are added in complex with ATP and begin to hydrolyze after incorporation. Once ATP hydrolysis is complete and the phosphate group dissociates, the actin monomer can also detach. The combined effects of polymerization and detachment at the two opposite ends, called actin treadmilling [Rzadzinska et al., 2004], results in a net displacement of the actin filament (Figure 1.17).

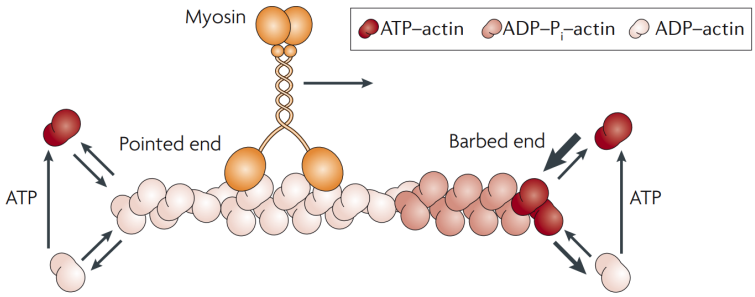

Figure 1.17: Actin filaments properties. Actin subunits are oriented in the same direction, which results in a polarized filament. Myosins move in a unidirectional manner along the filament surface. Both ends exhibit different monomer association and dissociation rates. Taken from [Li and Gundersen, 2008].

Filament formation is a slow process, also prevented by some proteins such as profilin than binds to unpolymerized actin. Therefore, actin nucleators are required to start actin polymerization. Arp2/3 and the formins are the two main types of actin nucleators, a process that can be favored by different nucleation-promoting factors, such as WASP and WAVE [Campellone and Welch, 2010]. Polymerizing filaments are stopped either by a physical barrier or capping proteins.

Myosin : Non-muscle myosin II is the most abundant motor protein that binds

on actin filaments and produces forces. It is composed of three pairs of peptides: two heavy chains of 230kDa, two regulatory light chains (RLCs) of 20kDa that regulate myosin activity, and two essential light chains (ELCs) that stabilize the heavy chain structure [Vicente-Manzanares et al., 2009]. The two globular head domains contain a binding site for both ATP and actin, while rod-shaped domains can assemble to form bipolar filaments (Figure 1.18), which tends to promote actin filament alignment and bundle structure formation.

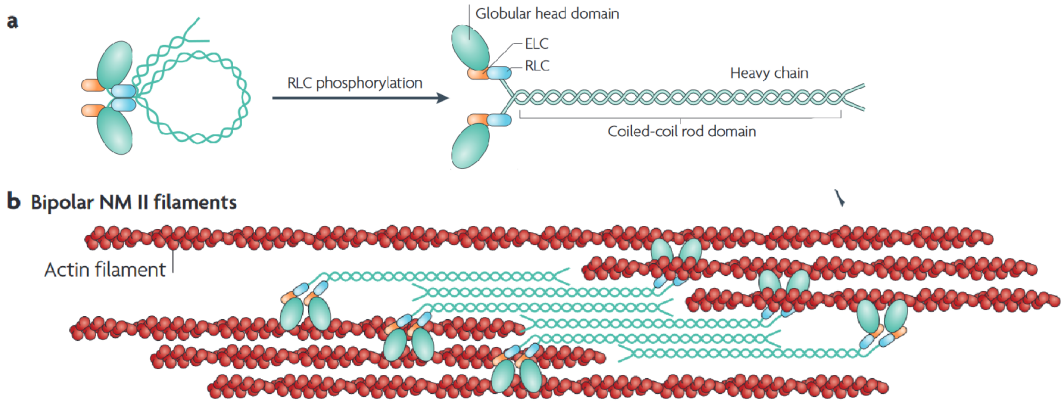

Figure 1.18: Structure of non-muscle myosin II. (a) In the absence of RLC phosphorylation, non-muscle myosin II forms a compact molecule through a head to tail interaction. The essential light chains (ELCs) and the regulatory light chains (RLCs) bind to the heavy chains at the lever arms that link the head and rod domains. (b) Non-muscle myosin II molecules assemble into bipolar filaments through interactions between their rod domains, moving actin filaments in an anti-parallel manner, promoting structures such as stress fibers. Adapted from [Vicente-Manzanares et al., 2009].

Adding to actin and myosin, different types of crosslinkers can bind actin filaments together, which can lead to very different types of structures. The most common ones are described in Figure 1.19. These structures are responsible for most of the mechanical cellular forces, and can be both pulling or pushing forces, applied on the environment or on the cell, as we will see in the case of cell migration (see 1.4.3).

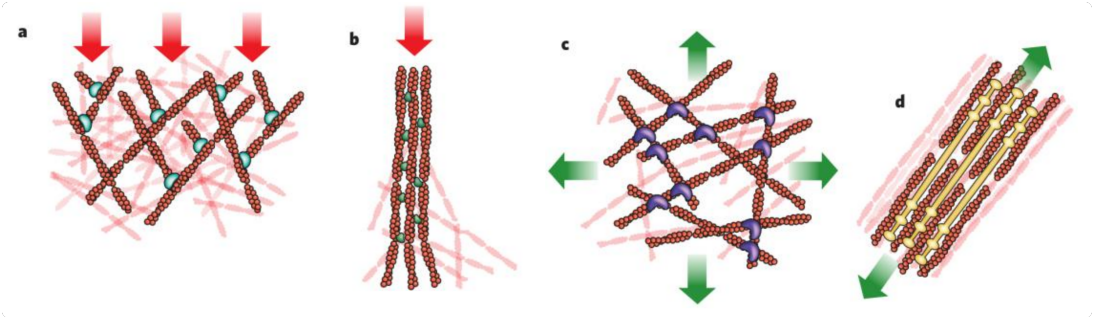

Figure 1.19: Four actin structures generated by actin filaments and the stresses typically encountered by these structures (red arrows, compression; green arrows, tension). a, Branched actin-filament networks push against the plasma membrane and external barriers, thereby encountering an inward force of compression. (b) Filaments bundled into filopodia also generate protrusive forces as they extend from the cell body, encountering similar compressive force. (c) Cortical networks (that is, non-aligned networks) form below the plasma membrane and carry tension loads in multiple directions. (d) Stress fibers form from bundled actin filaments, shown here associated with filaments of myosin, and generate tension against cell adhesions to the extracellular matrix. Adapted from [Fletcher and Mullins, 2010].

1.4.1.3 Adhesions

To deform and then migrate, cells need to transmit forces to their substrate. This will be mostly done through specialized transmembrane proteins, which will anchor them and make them adhere to the substrate. Cell adhesion molecules can be divided into four classes: cadherins, integrins, selectins and immunoglobulins [Janiszewska et al., 2020]. They have the role of maintaining cell-cell contact and attachment to the extracellular matrix, but also have a function in signalling. The two major groups are cadherins, which are responsible for maintaining cell-cell contact, and integrins, which are essentially involved in cellular adhesion to the substrate.

Integrin is a 24 members protein family, with large multidomain extracellular portions and small cytoplasmic tails [Gahmberg et al., 2019]. Integrin adhesions are huge complexes that are dynamic in time. When the cell moves, they matures in a sequence from nascent adhesions to focal complexes, focal adhesions, fibrillar adhesions and can be disassembled [Vicente-Manzanares and Horwitz, 2011]. When a nascent adhesion starts maturing, its intracellular part binds the actomyosin networks through proteins like vinculin and recruit a large number of proteins, while the transmembrane integrins stays bound to the extracellular matrix. Beyond its anchoring role, focal adhesions also play a role in mechanotransduction and serves as a signalling platform [Huveneers and Danen, 2009] for many signalling molecules (Figure 1.20).

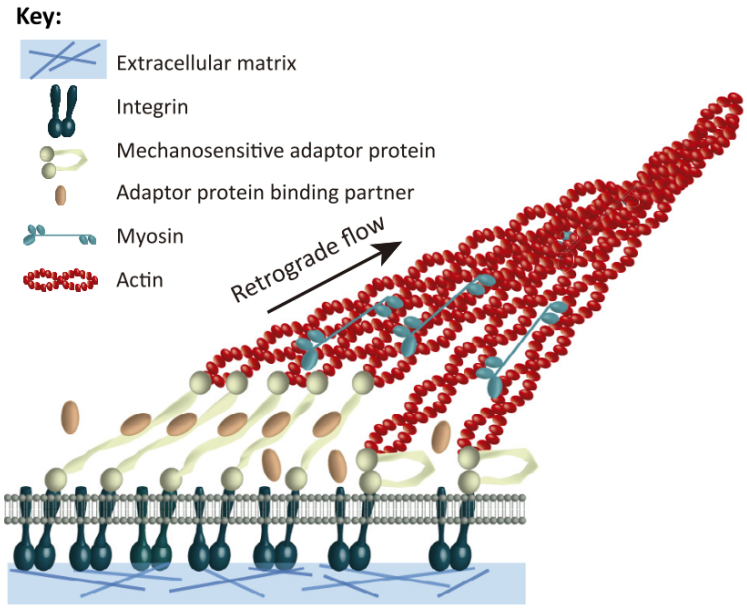

Figure 1.20: Connection between the Extracellular Matrix, Integrins, Mechanosensitive Adaptor Proteins, and Actin. As myosin pulls on actin filaments, force is transmitted to the different elements, leading to conformational changes in adaptor proteins and affecting unbinding events. Taken from [Elosegui-Artola et al., 2018].

Other types of interactions exist in low adhesion environments that are not specifically adhesions. These non-specific interactions are known for being able to transmit forces by friction in the amoeboid mode of migration (see 1.4.3.2), and do not seem to rely on one specific protein [Bodor et al., 2020].

1.4.2 Front-Back polarity in cell migration

Movement requires deformation of the cell thanks to forces exerted by the actomyosin network, as well as transmission of the forces to the substrate through adhesion or friction. However, to have a net cell displacement, cell must also effectively polarize, so that this deformation and displacement of the cell occurs in one specific direction. Cells can polarize due to the presence of asymmetric external cues that can be of very different nature: diffusible molecules (chemotaxis), substrate-bound molecules (haptotaxis), substrate stiffness (durotaxis), geometrical features (topotaxis), hydraulic pressure (barotaxis) and in electric fields (galvanotaxis) [Lennon-Duménil and Moreau, 2021, SenGupta et al., 2021]. Some cells can also spontaneously polarize, leading to effective random migration [Martin, 2015]. In both cases, persistent migration over long time scales (many times the body length displacement) will require intracellular reorganization at different levels: protein concentration or activity, organelles, and cell shape. These different polarity levels cannot be considered as a linear sequence in time: it is now clear that cell migration polarity emerges from the interaction between these different cellular properties [Vaidžiulyte et al., 2019].

I will detail here three levels of polarity: the polarity of proteins activities, focusing on the Rho-GTPases family, the polarity of the actin cytoskeleton, and polarity of organelle positioning.

1.4.2.1 Protein activity polarity - RhoGTPases

The asymmetric distribution of protein concentration and/or activity is one of the most studied aspect of cell polarity. Some broadly conserved polarity complexes such as partition defective PAR (CDC42–PAR3–PAR6–aPKC) are considered as polarity initiators for cell division when tethered at the plasma membrane [Peglion and Goehring, 2019]. Maintenance of this polarity is dynamic, which enables flexible and rapid cellular adjustments to external changes.

In cell migration, this dynamic maintenance is notably achieved by a well-studied protein family, the Rho-GTPases. It is a family of small (∼21 kDa) proteins, which belong to Ras superfamily [Wennerberg et al., 2005] and are molecular switches: they constantly shift between an inactive GDP-bound state and an active GTP-bound state [Etienne-Manneville and Hall, 2002]. They are known for playing an important role as remodelers of the actin cytoskeleton, thus being key controllers of cell migration [Raftopoulou and Hall, 2004]. Of the 20 Rho-GTPases that comprise the human family, three are more studied for their abundance and role in a broad range of cellular processes: Rac1, RhoA and Cdc42 [Ridley, 2015].

As both exchange from GTP to GDP and from GDP to GTP are slow processes, RhoGTPases are regulated by proteins that promote their switches: GEFs (guanine nucleotide exchange factors) and GAPs (GTPase-activating proteins). Rac1, RhoA and Cdc42 have lipid moieties, which give them an affinity for the plasma membrane but can be hidden by GDIs (Guanosine nucleotide dissociation inhibitors) [Etienne-Manneville and Hall, 2002]. RhoGTPases are classically thought to be activated and inactivated by GEFs and GAPs at the membrane, where they can bind to different effectors, while GDIs sequester inactive RhoGTPases in the cytosol. Recently, Golding et al. challenged this view, showing that active RhoGTPases can also be extracted from the membrane by GDIs, which complexified the picture [Golding et al., 2019](Figure 1.21). Moreover, regulation can vary from one GTPase to the other, as we will see for

the specific example of RhoA in 1.5.

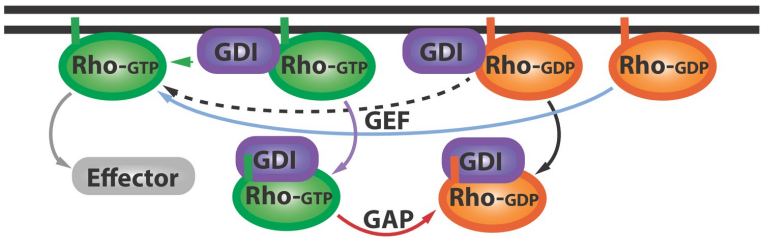

Figure 1.21: Rho GTPases cycles adapted from [Golding et al., 2019]. The inactive Rho-GDP form is activated (blue arrow) by GEFs (not shown), and the active form can activate (grey arrow) various downstream effector proteins (grey). GDIs can bind both inactive Rho-GDP (black arrow) and active Rho-GTP (purple arrow) forms and extract them from the membrane. GAPs help convert these active GDI-Rho-GTP complexes into inactive GDI-Rho-GDP complexes (red arrow): this can happen at the membrane or in the cytoplasm. There is uncertainty on the ability of Rho-GTP to escape from the GDI-Rho-GTP complex (green arrow). Taken from [Perry and Maddox, 2019].

The crosstalks between the main Rho-GTPases have also been subject to debate. A mutual antagonism between Rac1 and RhoA has been documented in a lot of different biological systems [Parri and Chiarugi, 2010], but the potential interactions between them is still very much context-dependent, as can be seen when looking at crosstalks described in the literature (see Figure 1.22). A tremendous work has been done recently to look in an exhaustive manner at all the interactions between 141 GEFs and GAPs, looking at their effect on the main GTPases, their interactions, as well as their spatial distribution in the cell [Müller et al., 2020]. Among other things, it revealed the complexity of this network, the number of potential crosstalks at the GEFs and GAPs level, and the fact that GAPs tend to be less specific than GEFs, a potential mechanism for confining RhoGTPases activity.

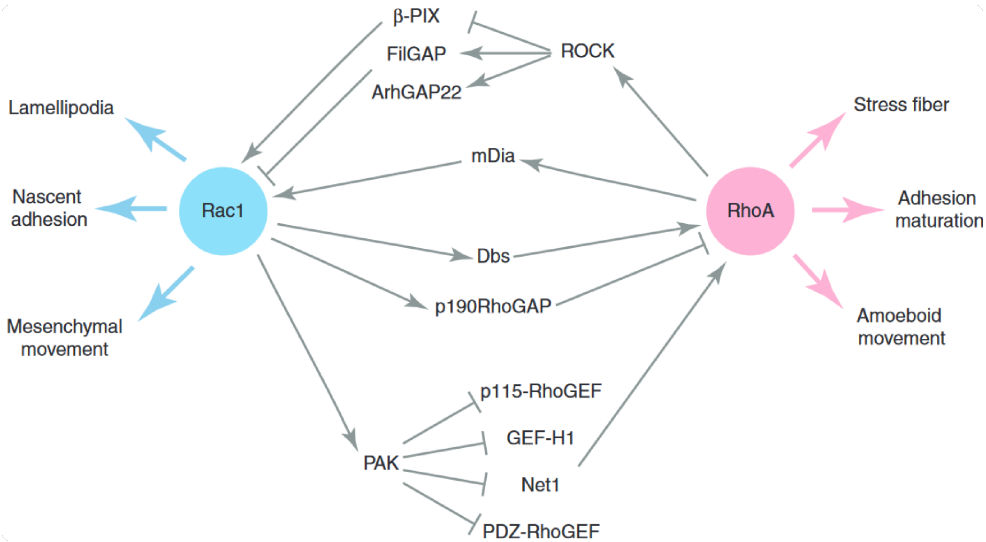

Figure 1.22: Example of crosstalks between two GTPases. Here positive and negative crosstalks between Rac1 and RhoA are shown, with known intermediate proteins. Taken from [Guilluy et al., 2011].

Last but not least, our understanding of their role in cell migration has complexified over the past twenty years. In the classical view, each of the main GTPase (Rac1,

Cdc42 and RhoA) had a distinct role in regulating actin remodeling and was responsible for one type of structure. Rac1 would promote branched actin and the formation of lamellipodia [Ridley et al., 1992], Cdc42 would initiate bundled actin and trigger filopodia [Nobes and Hall, 1995] and RhoA would be responsible for stress fibers formation and contractility [Ridley and Hall, 1992]. In cell migration, actin polymerization often happens at the front in order to push the membrane, while retraction of the rear requires stress fibers to be formed and contractility to occur. This leads to the canonical image where Rac1 and Cdc42 are most active at the front of migrating cells, while RhoA is restricted to the rear [Etienne-Manneville and Hall, 2002]. However, as we will discuss for RhoA later (see 1.5), the spatiotemporal mapping of RhoGTPases activity has shed light on a much more complex dynamic, especially in protruding cells where RhoA, Rac1 and Cdc42 are all activated with spatiotemporal coordination [MacHacek et al., 2009, Martin et al., 2016].

Rho-GTPases are only one part of the complex signalling processes defining the front and the rear of a migrating cell. These signals modify the mechanical processes happening at the front and at the back, which trigger a net displacement of the cell. Consequently, polarity at the level of protein activities, especially Rho-GTPases, has influence on the polarization of the actomyosin network.

1.4.2.2 Actomyosin polarity

For a cell to migrate efficiently, two different mechanisms must occur at the front and at the rear that both require the actomyosin network. At the front, the membrane needs to go forward, making a protrusion. Different types of protrusions have been described, which depend on the cell type, the environment and the state of contractility of the cell [Bodor et al., 2020] (see Figure 1.23). The most studied protrusions, lamellipodia and filopodia, are actin-driven, which means that they require actin polymerization to actively push the membrane. They are the predominant protrusion type on 2D substrates -but happen also in 3D environments-, are particularly thin (200nm), and can be combined together [Rottner and Schaks, 2019]. Both lamellipodia (sheet-like) and filopodia (finger-like) are probing the surface and drive path finding in the front of migrating cells [Leithner et al., 2016]. In contrast, blebs and lobopodia (see Figure 1.23) are mostly pressure-driven and occur preferentially in 3D environments. They initially expand as actin-free spherical bulges where the actin cortex reassembles afterwards [Paluch and Raz, 2013]. It has been shown recently that in both types of protrusions, the first step is actin-membrane detachment [Welf et al., 2020]. They are also not mutually exclusive, but all result in a net displacement of the membrane at the front of a polarized cell.

At the other side, the cell rear must detach from the substrate and retract in order for the whole cell body to move forward. This is most often driven by non muscle myosin II that cross-links actin stress fibers and triggers detachment from the substrate [Vicente-Manzanares et al., 2009], even if some other mechanisms have been proposed that do not rely directly on myosin II activation [Cramer, 2013].

How are the front and the back coordinated? It seems that coupling between back and front is very context dependent. In some cases, membrane tension seems to be a key parameter for front-back coupling [Hetmanski et al., 2019, Belly et al., 2022]. In neutrophils, mysosin II localization has been shown as the effective coupling parameter [Tsai et al., 2019], while some other groups have proposed that it happens at the level of RhoGTPases [Bolado-Carrancio et al., 2020]. These mechanisms are not mutually exclusive, as they can happen at different timescales.

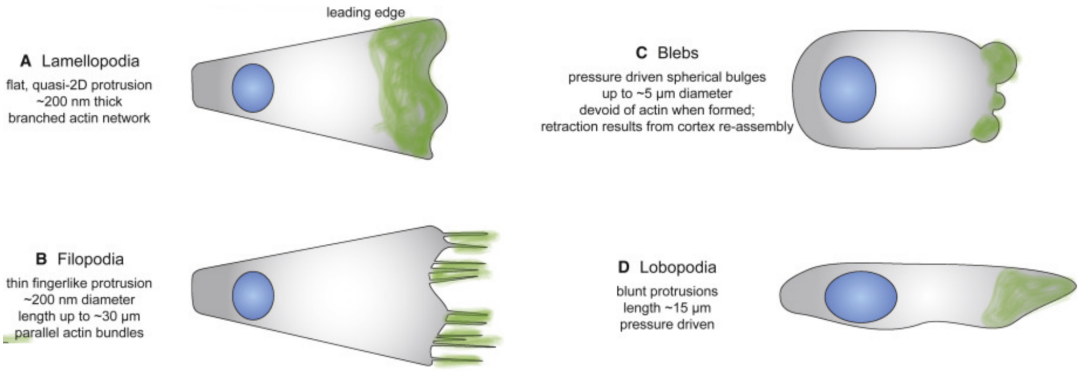

Figure 1.23: Protrusions types in migrating cells. Four types are shown (highlighted in green):(A) Lamellopodia, (B) filopodia, (C) blebs, (D) lobopodia. Adapted from [Bodor et al., 2020].

1.4.2.3 Polarity of organelle positioning

In addition to protein activity and the cytoskeleton, a lot of other cell components are polarized during cell migration. The most conserved is the positioning between the nucleus and the microtubule organizing center, that is often defined as the cell polarity axis [Llense and Etienne-Manneville, 2015]. The microtubule network will also be remodeled, leading to reorganization of the organelle positioning, which rely on the microtubule and actomyosin network for their transport [Barlan and Gelfand, 2017, van Bergeijk et al., 2016].

1.4.3 Single cell migration modes

There is a variety of modes of single cell migration depending on the nature of the adhesions of the cell to the substrate, the nature of the protrusions formed by the cell, the cell type, and its environment. These modes of migration are often divided into two main categories. Mesenchymal migration requires focal adhesions to the substrate and exhibits a traction mechanism. In contrast, amoeboid migration is independent of focal adhesions, interacts weakly with the substrate, and is based on propulsive forces (Figure 1.24). Originally thought to be cell-dependent, it is now well known that most cells can display both behaviors upon changes in environmental conditions [Liu et al., 2015], a property called plasticity.

1.4.3.1 Mesenchymal cell migration

Cell motility was first observed on 2D surfaces with fibroblasts, which are of the mesenchymal cell type, and gave the name to this migration type. It was first methodically described by Abercrombie in 1970s in a series of papers describing different aspects of cell movement [Abercrombie et al., 1970]. Mesenchymal cells migrate at speeds of 0.1-5µm/min [Bodor et al., 2020]. For a crawling cell to move forward, it needs to go through a protrusion-adhesion-retraction cycle [Vicente-Manzanares et al., 2005, Reig et al., 2014], as described in Figure 1.25.

Protrusion: protrusions are actin-driven, often filopodia or lamellipodia as de-

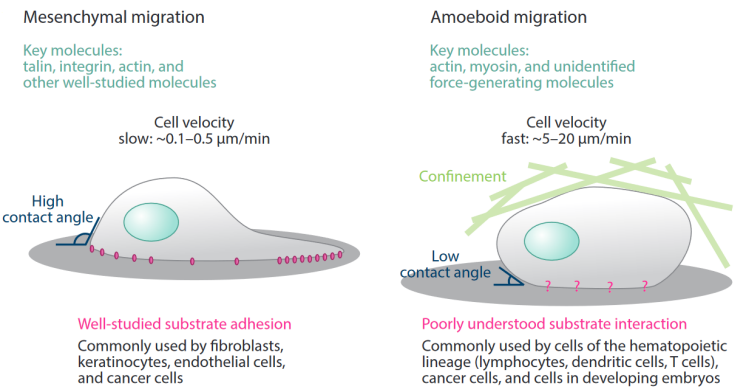

Figure 1.24: Overview of mesenchymal and amoeboid migration. Key molecules required for migration, cell velocities, and typical cell shapes are highlighted. (a) Mesenchymal migration can be achieved on a flat 2D surface. Cells typically display a flat, spread-out morphology due to substrate anchoring (pink dots), resulting in a high contact angle between the cell and the substrate. (b) Amoeboid migration often requires 3D confinement. Cells are round and do not adhere or adhere only weakly to their substrate via unknown molecules, resulting in low contact angles between the cell and the substrate. Taken from [Paluch et al., 2016].

scribed in 1.4.2.2. When no adhesion is formed, actin pushed against the membrane will flow backward and produce an actin retrograde flow [Cramer, 1997].
Adhesion: when an adhesion is formed that is linked to the actomyosin network, actin polymerization can be translated into forces that lead to the formation of membrane protrusion [Vicente-Manzanares and Horwitz, 2011].
Retraction: the rear of the cell must detach and be pulled forward. This will be done by the forces exerted along actin fibers by the myosin, and thanks to actin depolymerization.

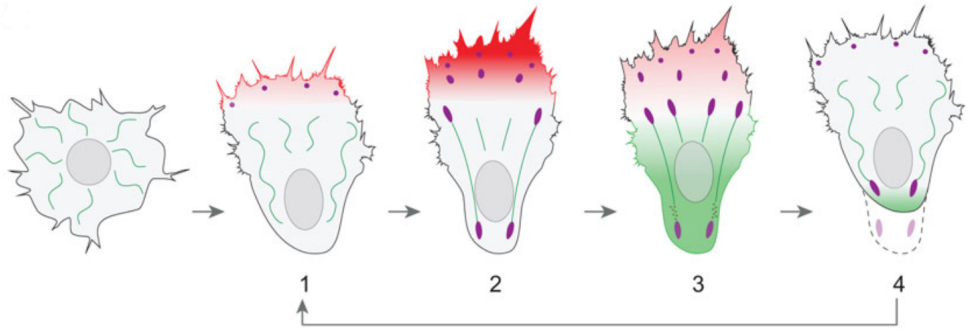

Figure 1.25: A current view of Abercrombie's cell migration cycle, highlighting actin polymerization-dependent processes (red), cell-substrate adhesive structures (purple) and myosin II-dependent events (green). Cells moving on 2D surfaces undergo repeated steps of: (1) extension of the leading edge and formation of immature cell-substrate adhesions; (2) maturation of cell-substrate adhesions; (3) forward translocation of the cell body; and (4) disassembly of focal adhesions coupled to retraction of the rear edge. Taken from [Reig et al., 2014].

Although mesenchymal migration has been originally studied on 2D substrates, it has now been observed in many 3D environments, where other processes must occur such as extracellular matrix degradation [Yamada and Sixt, 2019].

1.4.3.2 Amoeboid cell migration

In contrast with mesenchymal migration that relies on strong and specific adhesions to the substrate, increasing evidence indicate that many cells migrating in 3D environment rely on weak adhesion or no adhesion at all [Paluch et al., 2016]. This mode of migration, called amoeboid, relies on friction forces rather than traction forces.

In this mode of migration, cells do not spread because of the absence of specific adhesions to the substrate. They usually have to be in a confined environment in order to keep contact with the substrate, adopt a rounded morphology and are highly deformable. Amoeboid cells are much faster than mesenchymal cells (5-20µm/min), probably due to the absence of focal adhesion formation and disassembly.

In amoeboid migration, cells are propelled by actin flows that can be spontaneously generated, or come from chemical cues. Forces are transmitted to the substrate either through nonspecific interactions, or using environmental topography [Reversat et al., 2020]. It always requires high contractility, both to squeeze the cell and to propel the nucleus through narrow spaces [Lämmermann et al., 2008, Lomakin et al., 2020]. This contractility can be intrinsic to the cell type or triggered by extracellular cues.

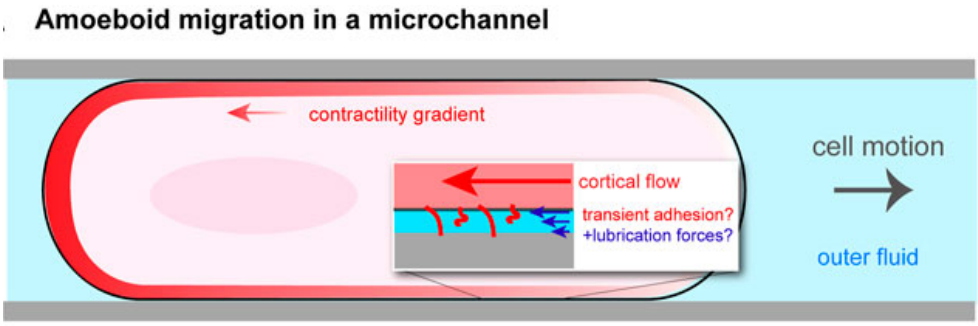

Figure 1.26: Amoeboid migration in a channel. Migration in a non-adherent microchannel (grey lines) relies on a contractility gradient (in red) that creates a cortical flow. Forces are transmitted to the substrate probably thanks to transient adhesions or lubrifications forces (rectangular box). Taken from [Callan-Jones, 2022].

1.4.3.3 Plasticity of cell migration

An important aspect of these two modes of migration is that they are not cell-specific. Most cells are plastic, in the sense that they can switch from one mode of migration to the other depending on the environment. This change in migration mode depends on three main control parameters - confinement, adhesion and contractility [Liu et al., 2015, Ruprecht et al., 2015]. As shown on Figure 1.27, both increasing confinement and decreasing adhesion lead to a switch from mesenchymal to amoeboid migration, in a number of cell types. This switch occurs through an increase in cell contractility, which is required for fast amoeboid migration.

This plastic behavior, especially in confined area, is particularly relevant during cancer invasion, when cells from the primary tumor have to cross a broad variety of environments with different types of constraints [Friedl and Alexander, 2011, Zanotelli et al., 2021].

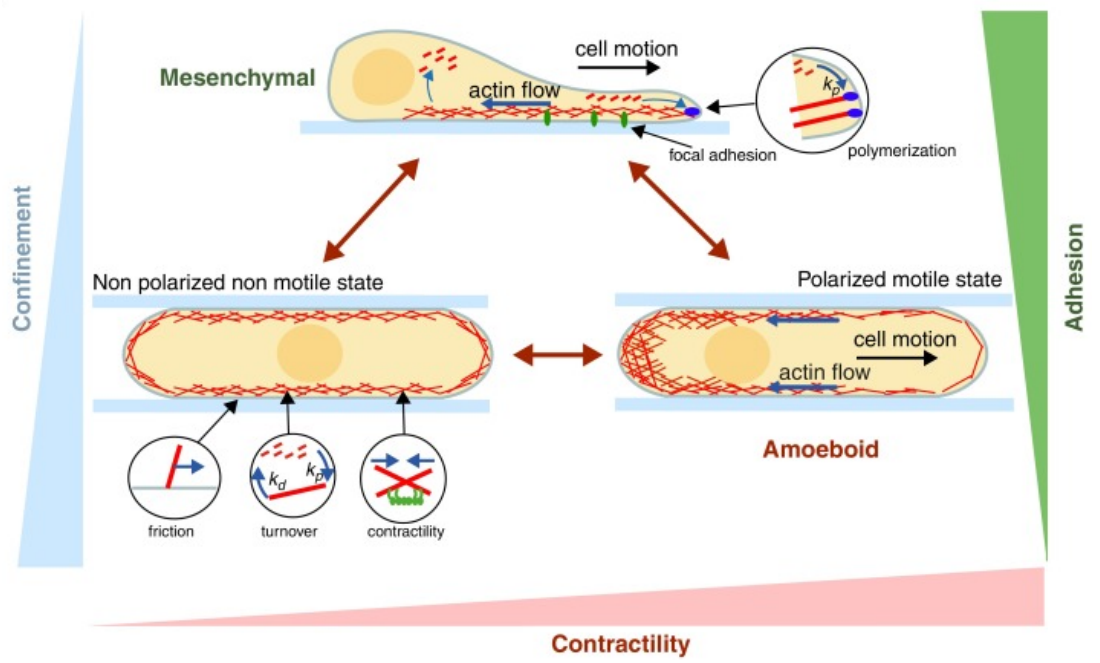

Figure 1.27: Plasticity of migration modes. Mesenchymal migration can be characterized by specific adhesion complexes (focal adhesions), and polymerization induced actin flows. By lowering adhesion and increasing confinement, cells can switch to an amoeboid mode characterized by cortical actin flows driven by actin/myosin contractility. Taken from [Callan-Jones and Voituriez, 2016].

1.4.4 Collective cell migration

Collective cell migration is required in many developmental and pathological processes, most commonly used examples being morphogenesis, wound healing and cancer metastases [Friedl and Gilmour, 2009, Mayor and Etienne-Manneville, 2016]. A lot of different classifications have been done, revealing the diversity of collective migration depending on the context [Scarpa and Mayor, 2016, Weijer, 2009, Friedl and Gilmour, 2009, Mayor and Etienne-Manneville, 2016]. When can we consider cells migrating together as collective migration? A nice review by Shellard and Mayor has classified all types of migration depending on their degree of collectiveness [Shellard and Mayor, 2019], and defined again what collectiveness, coordination and cooperation would mean for cell migration. As shown on figure 1.28, all nuances can be found in nature.

For Shellard and Mayor, coordination starts as soon as there is a common direction, and doesn't require cooperation if the direction is set by an external cue. Collective migration only refers to cells that are in contact but do not show necessarily any supracellular behavior. As an example, recent studies on epithelial trains of cells showed that polarity could be established at the single cell level, without large-scale transmission of signal [Jain et al., 2020]. However, a lot of *in vivo* studies reveal that collective cell migration can be coordinated at a higher level, which is why Shellard and Mayor added a new term, supracellular migration.

Supracellular migration refers to a type of collective migration that is better considered at the level of the group of cells than at the level of the individuals [Shellard and Mayor, 2019]. It usually requires supracellular structures (like supracellular actin cables, or microtubules), and division of functions (leaders and followers for example). This will lead to structures that can resemble the one of single cells as shown on Figure

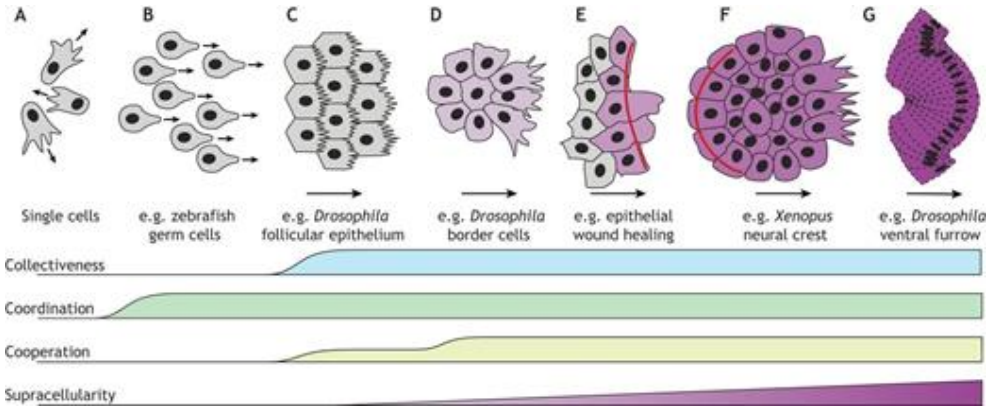

Figure 1.28: Varying degrees of supracellularity in cell migration.(A) Single cells migrating in random directions. (B) Mass movements of individually migrating cells, such as zebrafish primordial germ cells illustrated here, are coordinated by their response to SDF1. However, they do not move as a collective, nor cooperate with each other. (C) Collectively migrating cell populations such as the follicular epithelium begin to show cooperation and supracellular features, such as microtubule alignment. (D,E) Moderate supracellular features are more evident in migrating groups that have a free edge, such as Drosophila border cells (D), or cells involved in wound healing (E) Here, supracellular structures, such as an actomyosin cable (shown in red) and supracellular forces are at play. (F) High levels of supracellularity are exhibited by mesenchymal groups such as the neural crest; here, supracellular flow is a consequence of supracellular forces. (G) Full supracellularity has been demonstrated in the Drosophila ventral furrow, whose collective behaviour can be reproduced in acellular embryos (represented by dashed lines), thereby demonstrating that tissue movement is a not a consequence of individual cell movement. Taken from [Shellard and Mayor, 2019].

1.29.

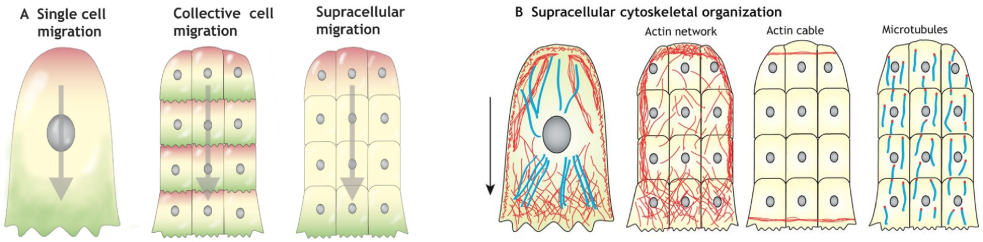

Figure 1.29: Supracellular migration. (A) In collective cell migration, cells can be all individually polarized without supracellular polarity, whereas in supracellular migration, cells behave as one cell, with supracellular polarity. (B) Cytoskeletal organization. Cells within supracellular entities show a highly organized supracellular cytoskeleton resembling single cells. This can include an actin meshwork that is associated with the edge of the entire group (red mesh), a bundle of supracellular actin fibers (thick red lines), or an alignment of microtubules according to their polarity (blue, with tip ends red). Adapted from [Shellard and Mayor, 2019].

In most of the cases presented above, collective migration happens on adherent substrates, in a mesenchymal-like way. There are usually leaders that display actin rich protrusions at the front and followers behind, with a higher contractility at the rear [Mayor and Etienne-Manneville, 2016], which resembles single cell mesenchymal migration. As in single cells, traction forces are transmitted to the substrate through focal adhesions, mostly at the leading edge of migrating epithelial sheets [Du Roure et al., 2005].

The second part of my results (see chapter 3) is part of a collaboration that describes

and explains a new type of collective migration without adhesion to the substrate. This study suggests a plasticity of collective cell migration that could resemble the one described previously on single cells [Pagès et al., 2022].

1.5 RhoA regulation in space and time

RhoA, as described before in 1.4.2.1, is one of the three main Rho-GTPases, and has been a key signalling protein that links both projects of my PhD (chapter 3 and 4). This current chapter will dive into the complex regulation of RhoA in space and time, and is almost fully taken from the review we wrote with Mathieu Coppey, inspired by the work of Josephine Gatin [de Seze et al., 2023].

While the functional roles of Cdc42 and Rac1 are relatively clear despite being multifunctional [Schwartz, 2004, Yamao et al., 2015], the functional roles of RhoA (presented in Figure 1.30) remain a matter of debate, especially in the context of cell migration. Some works have reported that RhoA is mainly active in contracting regions of the cell [Worthylake et al., 2001] (Figure 1.30.A), while others show strong RhoA activity in protruding regions of the cell [Kurokawa and Matsuda, 2005, Pertz et al., 2006] (Figure 1.30.B). The causal role of RhoA in cell contraction is coherent with the main pathways activated by RhoA. Indeed, RhoA is thought to be the driver of actomyosin contractility and thus rear retraction in cell migration, through its dual activation of the ROCK kinase and of the formin mDIA [Narumiya et al., 2009]. The kinase ROCK phosphorylates and activates non-muscle Myosin light chain, while mDIA polymerizes actin in form of bundles which provide a substrate for Myosin II to bind. The combination of actin polymerization and myosin activity leads to the contraction of the actin network. However, the causal role of RhoA in protrusion is less clear. At the leading front of mesenchymal migrating cells, cycles of protrusion and retraction of the lamellipodia propel the cell forward. Retraction events would suggest transient RhoA activation, but surprisingly RhoA activity was shown to peak with the initiation of protrusion [MacHacek et al., 2009], suggesting that protrusion events could be triggered by RhoA. Along this line, it was shown that mDIA activation and recruitment by RhoA could trigger lamellipodia and ruffles, in coordination with Arp2/3 [Isogai et al., 2015].

This apparent contradictory functional role calls for a finer understanding of RhoA regulation in space and time, which needs to be distinguished from the ones of Rac1 and Cdc42. Where and when is RhoA active? Where is RhoA within the cell and how does its localization influence its activity? How is its activity regulated? In this chapter, we will address these different questions by highlighting some of the work achieved in the last 30 years, which provide insights into the complexity of RhoA regulation.

We will first do a brief summary of the classical view of RhoA regulation by GEFs, GAPs and GDIs. We will then stress out the diverging pictures provided by live cell biosensors of active RhoA, which seem not sufficient to understand RhoA activity. We will therefore turn to RhoA itself, which dynamic localization in space and time departs from the other GTPases like Rac1 and Cdc42. Further on, we will point out other layers of regulation that need to be considered to understand RhoA activity, as RhoA is engaged in well-described positive and negative feedback loops that support complex patterns of RhoA activity in various biological systems. We will then review the different optogenetic approaches that were used in the literature to control RhoA signalling, as they teach us interesting aspects of RhoA activity, and could be used to

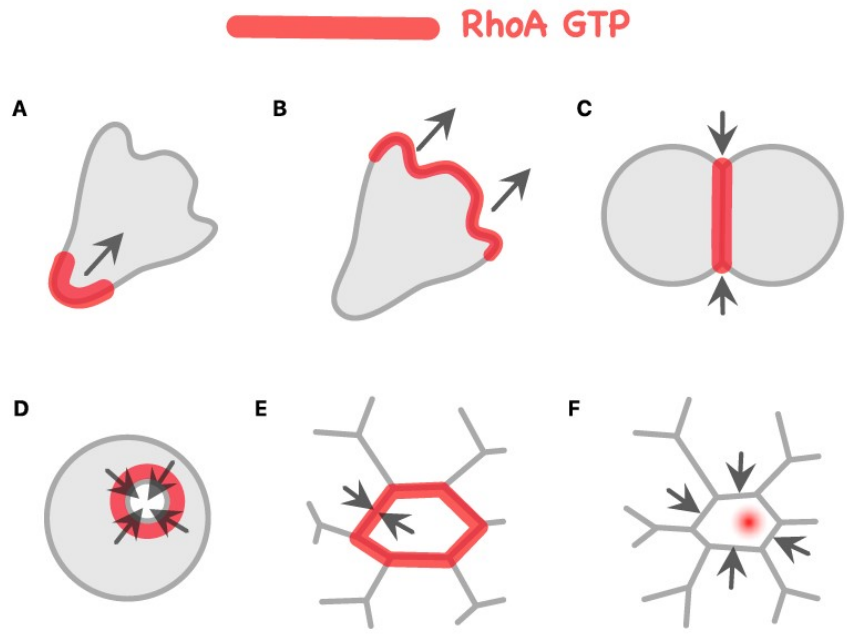

Figure 1.30: RhoA activities and functions. RhoA activity: (A) At the contracting rear of cells in mesenchymal [Worthylake et al., 2001] or amoeboid cell migration [Lä et al., 2009]. (B) At the protruding front in mesenchymal cell migration [Kurokawa and Matsuda, 2005, Pertz et al., 2006]. (C) At the contractile ring and furrow ingression during cytokinesis [Yüce et al., 2005]. (D) At the edge of a closing wound [Golding et al., 2019]. (E) At cell–cell junctions [Terry et al., 2011]. (F) Within contracting patches at the surface of pulsatile contracting cells [Koride et al., 2014, Michaux et al., 2018, Rauzi et al., 2010].

tackle the unanswered questions. We will finally propose and discuss a new cartoon depicting RhoA signalling, hopefully conveying the core teachings of this chapter.

1.5.1 Classical picture of RhoA regulation

As described in 1.4.2.1, RhoGTPases are mainly regulated by three protein families : GEFs that trigger the exchange from GDP-bound state to GTP-bound state (they "activate" the GTPase), GAPs that promote the opposite, and GDIs that hide the lipid moiety to sequester the Rho-GTPases in the cytosol.

For RhoA, multiple GEFs have been discovered, and structures are now well described [Aittaleb et al., 2010]. In [Müller et al., 2020], all known GEFs and GAPs have been tested for their ability to activate RhoA. 26 out of 75 GEFs have been identified that can increase RhoA activity when overexpressed in HEK293T cells, while 27 out of the 66 GAPs can inhibit it. It revealed the complexity of the GEFs and GAPs network, with a wide range of different localization and numerous crosstalks.

GEFs belong to two different protein families depending on their structure -DOCK family and Dbl family. The most studied GEFs of RhoA belong to the Dbl family, which signature is the Dbl homology (DH) domain, a catalytic domain consisting of around 200 residues. In the majority of Dbl family proteins, the catalytic DH domain is followed by a pleckstrin homology (PH) domain of around 100 residues [Jaiswal et al., 2013]. In Figure 1.31,five most known GEFs of RhoA are shown with their different domains. Despite their differences, they all have this DH domain followed by a PH domain. The PH domain is known for having a role of amplification of the signal [Chen et al., 2010, Medina et al., 2013], which is part of a positive feedback loop

discussed in 1.5.4. It has an affinity for phosphatidylinositol lipids within biological membranes [Wang and Shaw, 1995].

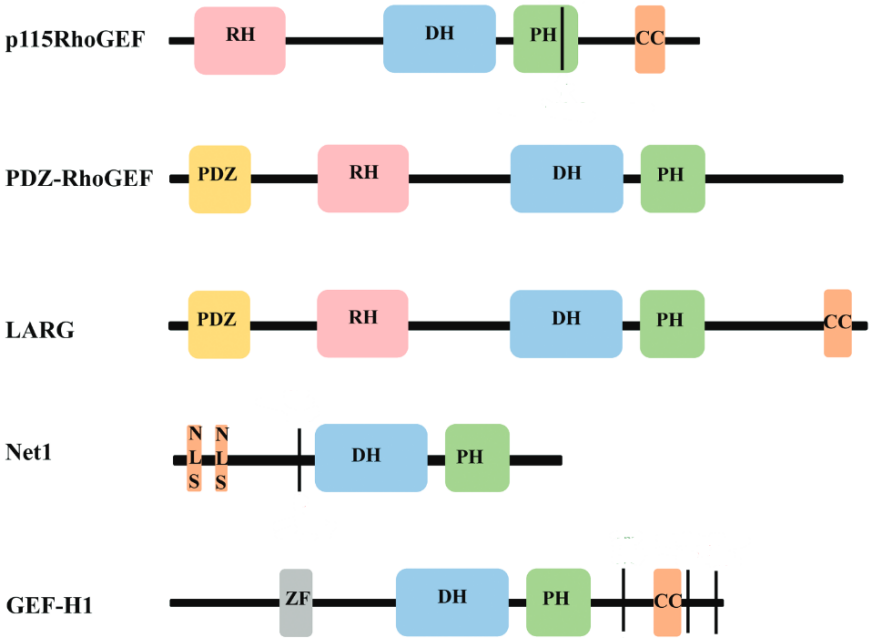

Figure 1.31: Schematic diagram of the domain structure of five most known RhoGEFs. C, coiled-coil; DH, Dbl homology; LR, leucine rich; NLS, nuclear localization signal; PDZ, post-synaptic density 95; disk large, zona occludens-1; PBM, PDZ binding motif; PH, Pleckstrin homology; RH, RGS homology; and ZF, Zinc finger-like binding domain. Adapted from [Patel and Karginov, 2014].

This classical picture of RhoA regulation by GEFs, GAPs and GDIs often leads to the idea that RhoA is a passive 'transmitter' of the signal coming from its regulator. In the following sections, I will challenge this point of view, by looking in more details at the specific dynamic of activity of RhoA, as described by the literature.

1.5.2 Where is RhoA active?

Biosensors of active RhoA report different patterns of activity

Like all other GTPases, RhoA is active in its GTP-state, which triggers the opening of its switch regions, leading to its binding to the effectors (Figure 1.32). Before the development of live fluorescent probes, RhoA activity was mainly measured with antibodies targeting its active form through pulldown assays, and its localization was looked at in fixed cells with fluorescent markers [Adamson et al., 1992]. Several live biosensors have since been designed to report RhoA activity in space and time, that is, the concentration of RhoA present in a GTP-state in one part of the cell. Among all these designs, two main strategies have been used. Surprisingly, it appears that these two strategies gave rise to different results when looking at the activity of RhoA in cell migration.

The first strategy is based on a binding domain specific to RhoA-GTP (RBD for Rho Biding Domain), fused to a fluorescent probe, which relocalizes at the places where RhoA is activated (Figure 1.32, (B) and (C)). Different binding domains have been used and published, with different fluorescent probes [Benink and Bement, 2005, Piekny and Glotzer, 2008]. They have all been tested and compared by Mahlandt et al. [Mahlandt et al., 2021], who designed a new probe with an enhanced affinity for active

RhoA. These probes have the huge advantage of looking at endogenous RhoA and being easy to use. However, they compete with the endogenous effectors and can thus have dominant-negative effects at high concentrations. They also cannot differentiate between RhoA, RhoB and RhoC, which can be implicated in different cellular processes. These RBD-based reporters tend to confirm what the canonical vision of RhoA was: The biosensors mainly relocalize to the zones of high contractility, mainly at cell–cell junctions, at the rear of migrating cells and at the division ring during cell division [Mahlandt et al., 2021, Wagner and Glotzer, 2016], the multivalent RBD biosensor (Figure 1.32 (C)) giving a better signal to background ratio than the monovalent one (Figure 1.32 (B)).

The second strategy takes advantage of fluorescence resonance energy transfer (FRET). For RhoA, to our knowledge, only single component FRET biosensors have been designed, where an exogenous RhoA is expressed fused to an RBD. Both RhoA and its RBD are flanked by a fluorescent protein: When RhoA is activated, the fluorescent probes get closer, and FRET can happen (Figure 1.32, (D) and (E)). The development of FRET biosensors to monitor Rho GTPases activity started in 2000 [Kraynov et al., 2000] with Rac1 biosensors than mainly confirmed its role in the formation of ruffles and lamellipodia at the front of migrating cells. On the contrary, RhoA FRET biosensors showed an unexpected result: Instead of being restricted to the rear of the cell, RhoA activity was mostly present at the front of migrating fibroblasts [Kurokawa and Matsuda, 2005, Pertz et al., 2006]. Moreover, this activity was very well correlated with the onset of membrane protrusion, showing a potential role of RhoA activity in ruffle formation. This seemingly paradoxical result was confirmed and discussed multiple times in different works since then, without giving rise to a definitive answer concerning the way RhoA engages different effectors in different contexts [Bolado-Carrancio et al., 2020, Müller et al., 2020, O'Connor and Chen, 2013, Tkachenko et al., 2011].

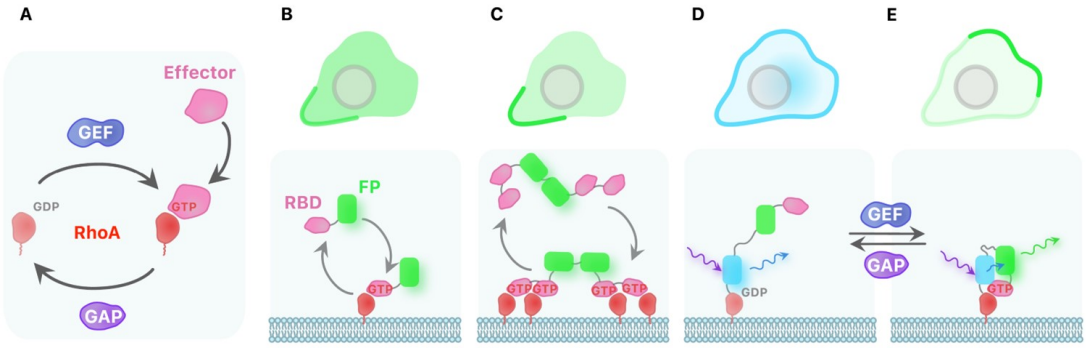

Figure 1.32: RhoA biosensors show two distinct activities. (A) RhoA binds effectors in its GTP-bound state that is promoted by GEFs and inhibited by GAPs. (B–E) For each figure, top: global cartoon of an optical section of a cell; bottom: molecular zoom on the plasma membrane and cytosol. (B) A cytosolic monovalent Rho binding domain (RBD) fused to a fluorescent protein (FP) binds to active RhoA and is thus enriched on the plasma membrane where RhoA is active. (C) A cytosolic multivalent RBD has a higher affinity than monovalent one, thus showing greater enrichment. (D, E) single chain FRET biosensor, constructed by a fusion between RhoA WT, a FRET pair of fluorescent proteins and an RBD. This biosensor is a sensor of local GEFs and GAPs activities. (D) In the GDP-bound inactive state, the biosensor localizes at the plasma membrane and appears thus insensitive to GDIs. (E) In the GTP-bound active state, RhoA binds to the RBD leading to FRET (excitation of the blue fluorophore that transmit energy to the green fluorophore) and reveals activity at the front of the cell.

To our knowledge, only works using these single-component FRET biosensors have reported high activity of RhoA correlated with protrusions in single cells, whereas binding domain reporters mainly showed the canonical contractile activity of RhoA at the rear of migrating cells (Figure 1.32). This observation could be linked to the difference in the spatiotemporal resolution of these biosensors, or to the difference in what they sense: While the RBD biosensor binds to RhoA WT and certifies its presence in an active state, the FRET biosensor avoids the dominant negative effect but is overexpressed and is not necessarily present at the places where endogenous RhoA is. Interestingly, FRET biosensors are more bound to the plasma membrane and more active than RhoA itself when overexpressed [Pertz et al., 2006, Fritz et al., 2013]. This difference between the localization of RhoA and the FRET biosensor was explained by the saturation of the guanosine dissociation inhibitors (GDIs) that interact in a one-to-one ratio with RhoA. However, this hypothesis does not hold, as overexpression of RhoA WT does not give the same membrane localization as the FRET biosensor, as we will see in the next section (Figure 1.33). This indicates another side effect of the FRET biosensor that may have a different pattern of localization and activity than RhoA, putatively because of the close proximity of the RBD.

Altogether, both biosensors give us interesting insights to understand RhoA signalling and activity. However, these complex and apparently contradictory behaviors are calling for a more complex picture of RhoA signalling, beyond the concept of RhoA simply being a local integrator of a given cocktail of GEFs, GAPs and GDIs present at one moment in one part of the cell [Pertz, 2010]. This new picture has to include the dynamic localization of RhoA in space and time, how this localization influences its activity, and the dynamic system in which RhoA autoregulates its own signal thanks to positive and negative feedback loops.

1.5.3 Where is RhoA itself?

RhoA is mostly cytosolic, even when overexpressed

As Cdc42 and Rac1, RhoA is post-translationally modified by the addition of a lipid moiety at its C-terminal CAAX motif which is supposed to target it to the plasma membrane [Hodge and Ridley, 2016]. This targeting is further enhanced by an additional polybasic domain next to its CAAX motif, the hypervariable region, which promotes its association with plasma membrane nanodomains enriched in negatively charged PIP2/PIP3 signalling lipids.

However, despite the similarities in their structure, the different Rho-GTPases are not targeted to the same compartments inside the cell. Michaelson et al. [Michaelson et al., 2001] looked precisely at the localization of RhoA, Rac1, Rac2, pCdc42, bCdc42, Rac2, H-Ras, K-Ras4B and RhoB. Contrarily to what is often said as a simplification, not all GTPases localize mostly at the plasma membrane (Figure 1.33, (B) and (F)). Particularly, RhoA appears mostly cytosolic and does not show any specific membrane localization except at cell–cell junctions and at the cleavage furrow during cytokinesis, which may be zones of high activity. Strikingly, this localization is not explained by the hypervariable region, known for being the targeting motif of most GTPases (Figure 1.33,(A) and (B)). Indeed, all overexpressed Rho-GTPases have the same localization than their hypervariable region expressed alone (Figure 1.33, (A) and (C)), except RhoA (Figure 1.33, (E) and (G)). This means that some information is contained in RhoA protein, apart from its hypervariable region, which maintains it in the cytosol when overexpressed (Figure 1.33 (G)). Michaelson et al. proved that this information is contained in the 73 amino-acid section of the NH2 terminal motif, which when removed leads to a localization of RhoA similar to its hypervariable region (Figure 1.33 (E)).

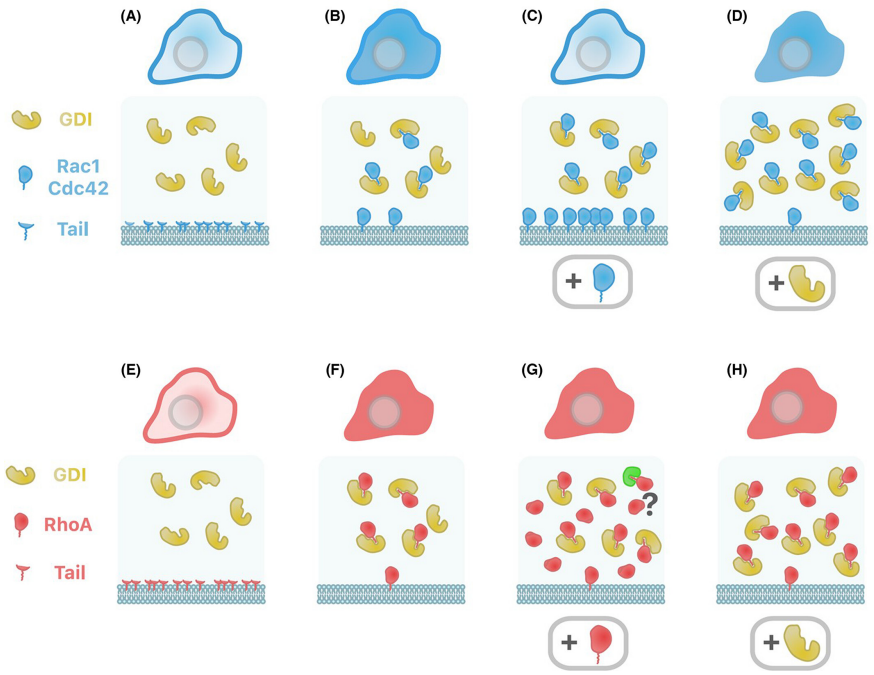

Figure 1.33: Localization of RhoGTPases and their tails, based on Michaelson et al. [Michaelson et al., 2001] (A) The polybasic/lipid modified tails of Rac1 and Cdc42 target them to the plasma membrane, yet (B) the full proteins at endogenous levels are partitioned between the cytosol and the plasma membrane thanks to the GDI that solubilize them. (C) When overexpressed, Rac1 and Cdc42 are more localized to the plasma membrane because of the saturation of GDIs. (D) The additional expression of GDIs counterbalances this titration effect and leads back to a cytosolic localization. (E) For RhoA, its polybasic/lipid modified tail is also targeted to the plasma membrane, but (F) the full protein at endogenous levels is cytosolic. (G) Overexpression of RhoA does not lead to membrane localization after GDI titration, either because an unknown factor (in green) binds RhoA and retains it in the cytosol or because a conformational state of RhoA allows the hindering of its lipid moiety. (H) Thus, additional expression of GDIs has no effect for RhoA.

The first suspect for the maintenance of RhoA inside the cytoplasm and lability of RhoA at the plasma membrane would be one of the GDIs, well known for hiding the hypervariable region of Rho-GTPases, thus keeping them solubilized in the cytosol. However, Michaelson et al. suggested that unlike for Rac1 or Cdc42, GDIs were not responsible for this localization of RhoA in the cytosol. Indeed, increasing by overexpression, the level of RhoA should lead to a saturation of GDIs, leading to an increase of the membrane-bound fraction of the protein, which was not the case for RhoA (Figure 1.33, (G) and (H)), contrary to Rac1 and Cdc42 (Figure 1.33, (C) and (D)). This led them to the conclusion that RhoA is maintained in the cytosol either through other protein interactions or by a different conformational state of the protein that would prevent the exposition of its lipid moiety (Figure 1.33 (E)). We can state three other hypotheses. The first possibility would be that RhoA upregulates GDIs expression, contrarily to Rac1 and Cdc42. The second explanation would be that overexpressed RhoA replaces endogenous RhoA, as suggested by Boulter et al. [Boulter et al., 2010]. The third hypothesis is that a subset of RhoA stays ungeranyl-geranylated but can still be recruited at places of high RhoA activity. Indeed, it seems that at least in some cell lines, 30% of the total amount of RhoA stays ungeranyl-geranylated. This pool of RhoA could then be able to participate in the dynamic localization of RhoA activity [Ohkawara et al., 2005].

One caution should be taken in interpreting the data of Michaelson et al. [Michaelson et al., 2001], since it was reported a few years after that tagging RhoA with a fluorescent protein in its N-terminus can affect its localization [Yüce et al., 2005, Yonemura et al., 2004]. Yonemura et al. [Yonemura et al., 2004] showed that GFP-tagged RhoA did not localize as the endogenous RhoA, the fusion protein being cytosolic without being able to report accumulation at the cleavage furrow or at cell–cell junctions. Interestingly, this effect seems to be restricted to the human RhoA, since Caenorhabditis elegans RhoA was able to report the right localization at the cleavage furrow [Yüce et al., 2005]. The mis-localization could be explained by the fact that tagged-RhoA has a higher affinity for GDIs [Tnimov et al., 2012]; however, the fact that overexpression of RhoA does not titrate out GDI still holds, which supports the cytosolic nature of RhoA, independently of possible artefacts coming from the fusion.

Localization of RhoA adds another layer of regulation

This maintenance of RhoA in the cytoplasm seems to be a key point in its regulation, as any small change in RhoA activity leads to its recruitment to the membrane. Indeed, constitutively active forms of RhoA (Q63L and G14V) are clearly more localized at the membrane, as well as the nucleotide-free form (T19N) [Michaelson et al., 2001]. Moreover, drug induction of RhoA activity leads to a rapid recruitment of RhoA at the plasma membrane, showing that RhoA localization also constitutes a layer of regulation [Yonemura et al., 2004]. This could lead to a simple picture of RhoA shuttling between an inactive form in the cytosol and an active form at the membrane [Graessl et al., 2017].

However, in their work of 2019 [Budnar et al., 2019], Budnar et al. showed that even in zones of contractility, an important proportion (more than 60%) of RhoA is very much labile at the plasma membrane. For this population, RhoA WT has a half-life at the membrane of 1-2s (Figure 1.34 (A)). This half-life is only slightly increased in the case of constitutively active RhoA Q63L, a mutant locked in the GTP-state and much less sensitive to GDIs [Longenecker et al., 2003] (Figure 1.34 (B)); this suggests that RhoA can exist in a GTP-state in the cytosol, either because of a lower but significant affinity for GDIs [Golding et al., 2019, Unen et al., 2015] or because of a

possible soluble state as mentioned in the previous section. This residence time at the membrane seems to be one order of magnitude smaller than for other Rho GTPases, such as Rac1 [Moissoglu et al., 2006]. This very interesting feature of RhoA modulates its ability to trigger actin polymerization as well as myosin activity. Indeed, different works have shown that RhoA needs to be localized at the plasma membrane to engage its downstream pathways [Budnar et al., 2019, Unen et al., 2015], especially through its two main effectors ROCK and mDia. In other words, it seems that RhoA can be in a GTP-state both in the cytosol and at the membrane, but its localization at the membrane is required for downstream signalling.

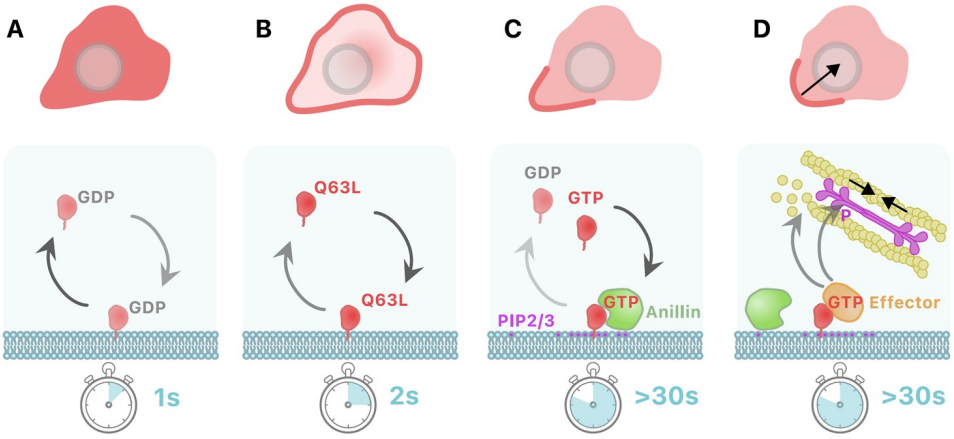

Figure 1.34: Stabilization of RhoA at the plasma membrane enhances its signalling activity. Exchange between membrane and cytosol happens at different timescale (shown by the watch, timescales are extracted from [Budnar et al., 2019]) for (A) RhoA-GDP, (B) constitutively active mutant of RhoA (RhoA-Q63L). (C) RhoA is stabilized at the membrane by anillin and PIP2/3, and once stabilized (D), RhoA binds to effectors and triggers actomyosin contractility.

Thus, the lability of RhoA as the membrane is an important part of its regulation, and Budnar et al. [Budnar et al., 2019] showed that RhoA dwell time at the membrane is regulated by effectors like anillin, which is found at zones of contraction, as well as negatively charged phospholipids like PIP2 and PIP3 (Figure 1.34 (C)). Importantly, anillin does not seem to have any effect on the proportion of RhoA in a GTP state, but it promotes its binding to effectors mDia or ROCK by increasing its residence time at the membrane (Figure 1.34 (D)).

This stabilization of RhoA at the plasma membrane by effectors and lipids adds a new layer to the classical regulation attributed to GEFs, GAPs and GDIs. Importantly, RhoA has also been shown to be integrated in shortly wired feedback loops that may fine tune or combine with active RhoA stabilization at the plasma membrane, which We will review in the next section.

1.5.4 How does RhoA regulate itself?

RhoA contractility waves reveal shortly wired positive and negative feedback loops

Apart from the GEFs, GAPs and GDIs, and its regulation through localization within the cell, RhoA has other very well-documented layers of regulation. Indeed, RhoA has been found to have a crucial role in the formation of waves of contractility that have been described in numerous model systems and contexts [Graessl et al., 2017, Bement et al., 2015] (Figure 1.35). These waves imply robust positive and negative

feedbacks that are directly linked to RhoA and its direct partners.

The first well-established feedback concerning RhoA is the positive feedback between RhoA and its GEFs. RhoA, when activated, can bind to the PH domain of its GEF from the Lbc family, triggering here an increase in GEF concentration leading to further activation of RhoA [Chen et al., 2010, Medina et al., 2013] (Figure 1.35.A). This direct positive feedback has been confirmed directly and more specifically for GEF-H1 in a series of publications [Graessl et al., 2017, Kamps et al., 2020, Kowalczyk et al., 2021], showing that active RhoA had a direct impact on the recruitment of GEF-H1 at the membrane and thus on its own activation.

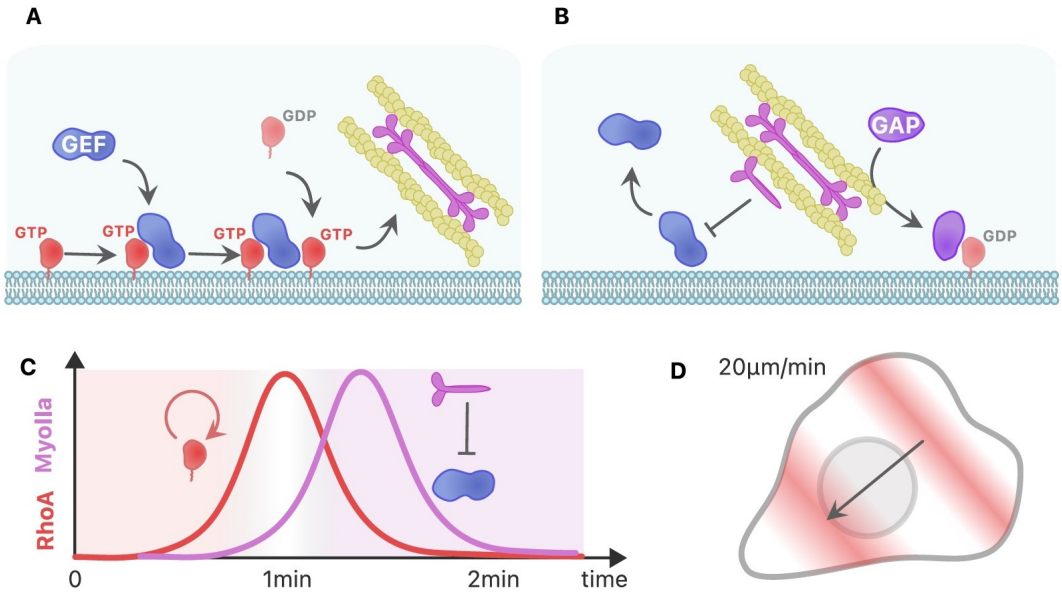

Figure 1.35: Positive and negative feedback loops. (A) Positive feedback loop between RhoA and its GEFs. (B) Two possible negative feedback loops involving the direct interaction of Myosin IIa with the GEFs or the recruitment of a GAP of RhoA by the actin. (C) Dynamic of RhoA pulses induced by these loops: Delay between positive and negative feedback loops lead to pulses of activity, which in 2D (D) can trigger waves of activity.

The robustness of waves of contractility has led to different hypotheses concerning the main negative feedback that is at play downstream of RhoA (Figure 1.35.B). They often imply Myo9b and p190RhoGAP as GAPs that are recruited on the actin and have a direct effect of inhibition of RhoA [Arthur and Burridge, 2001]. However, another direct negative feedback has been proposed [Kamps et al., 2020], which implies the interaction of Myosin II with the active domain of GEFs of RhoA, including GEF-H1, LARG and PDZ-RhoGEF [Lee et al., 2010]. This interaction seems to be very robust across cell lines [Kowalczyk et al., 2021] even if the direct molecular interaction has never been proven *in cellulo*.

Altogether, the shortly wired positive and negative feedbacks acting on RhoA allows the formation of pulses (Figure 1.35.C) and waves of activity (Figure 1.35.D), as soon as a delay is present between the two feedbacks. A pulse of RhoA activity is followed by a pulse of actomyosin and depending on transport/diffusion properties, these pulses can lead to either steady pulsatile activity or traveling waves. Such an excitability seems to be a central property of proteins regulating the cell cytoskeleton [Iglesias and Devreotes, 2011]. One question being to understand the determinants dictating whether RhoA activity is pulsatile/wave or stationary [Mori et al., 2008], such as at

the cleavage furrow [Goryachev et al., 2016].

1.5.5 Dissecting the layers of regulation through optogenetic approaches

The above sections revealed the complex dynamics of RhoA localization and activity in space and time, at very different timescales. These different layers of regulation call for techniques that enable precise spatiotemporal perturbations of RhoA signalling networks, combined with imaging and biosensors to monitor the different aspects of RhoA regulation. Optogenetic tools offer this versatility and spatiotemporal precision that are required in this process, as described in 1.3.3. We propose here to review briefly the different approaches described in the literature to control RhoA activity within the cell and describe what they teach us on RhoA signalling.

Direct recruitment of GEFs catalytic domains of RhoA to the plasma membrane has been a very successful strategy to activate RhoA [Wagner and Glotzer, 2016,Berlew et al., 2021,Valon et al., 2017] (Figure 1.36 (A), (B) and (D)), following the molecular principle that had been done before for Rac1 either with optogenetics [Levskaya et al., 2009] or even earlier with chemical approaches [Inoue et al., 2005]. In most cases, the whole GEF is not recruited but only the active region, the DH domain (Figure 1.36 (B)), sometimes associated with its auto amplification region, the PH domain (Figure 1.36 (A)). The GEF domain is fused to an optogenetic protein, the latter being then recruited to the plasma membrane, either through another part of a light-gated optogenetic dimerizer [Wagner and Glotzer, 2016,Valon et al., 2017] or thanks to a direct interaction with the plasma membrane [Berlew et al., 2021] (Figure 1.36 (D)). Different GEFs have been used, for instance, LARG [Wagner and Glotzer, 2016,O'Neill et al., 2018], PDZ-RhoGEF [Valon et al., 2017], P115-RhoGEF [Kelkar et al., 2022] or GEF-H1 [Kamps et al., 2020] and different optogenetic strategies (Figure 1.36 (A), (B) and (D)), but all lead to an increase in contractility at the place of activation. All those approaches show that the relocalization of a GEF domain to the plasma membrane is enough to trigger the activation of RhoA. Consequently, either RhoA is already present at the plasma membrane and is being activated there, or the GEF domain targets RhoA at the plasma membrane and stabilizes it in its active state, both hypotheses being compatible.

One of the first work presenting this optogenetic strategy described additionally an opposite tool relying on the sequestration of the cytosolic GEF domain to the membrane of mitochondria [Valon et al., 2017] (Figure 1.36 (C)). In this case, the authors saw a decrease in contractility due to this sequestration. This decrease was explained by an increased basal RhoA activity due to the presence of the GEF in the cytosol, which leads to a higher basal level of contractility, itself decreasing when the GEF is sequestered. This work shows that overexpression of a cytosolic GEF DH-PH domain leads to RhoA activation, possibly through elevated RhoA-GTP levels in the cytosol that are then targeted by themselves to the plasma membrane, since it was shown that over-expression of GEF cytosolic DH domain leads to a high FRET signal in the cytosol [Unen et al., 2015].

Interestingly, in the case of the single component optogenetic tool (Figure 1.36 (D)), the authors showed that the direct recruitment of RhoA WT itself at the plasma membrane is sufficient to activate it [Berlew et al., 2021]. The direct recruitment of RhoA WT was even more efficient than the recruitment of the GEF DH domain. In their optogenetic construct, RhoA lacks its CAAX tail (and thus lipid modification), which makes it less prone to interact with the plasma membrane and prevents it to interact with GDIs as well. Given that this tool works even if RhoA is initially

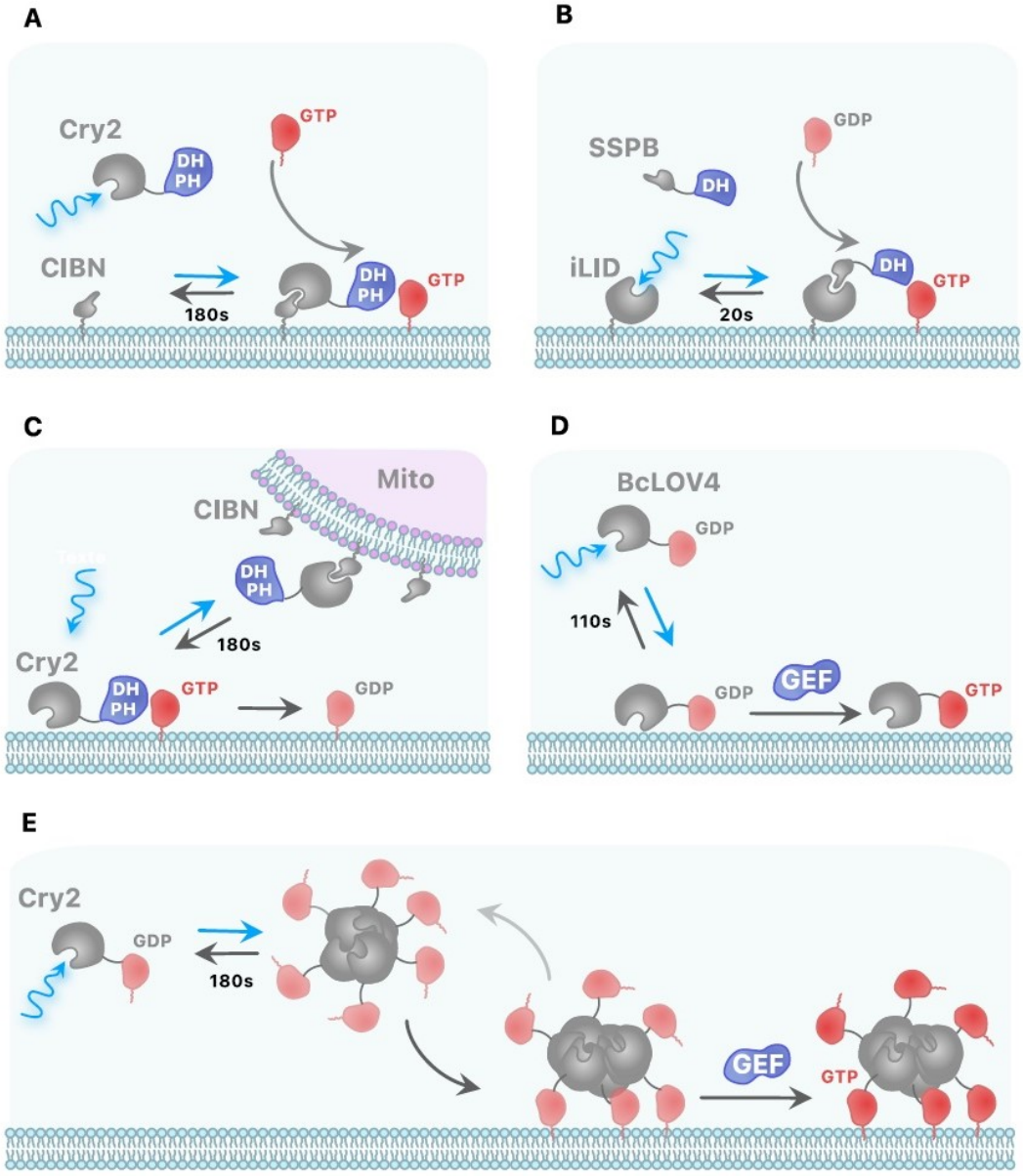

Figure 1.36: Optogenetic approaches to control RhoA activity. (A, B) Light-gated heterodimerization strategy to recruit active domain of GEFs of RhoA thanks to the optogenetic dimers: (A) CRY2-CIBN to recruit DH-PH domain and (B) SSPB-iLID to recruit DH domain. (C) Sequestration of GEFs to the mitochondria to decrease RhoA activity. (D) Direct recruitment of RhoA WT to the plasma membrane thanks to the BcLOV4 optogenetic tool. (E) Clustering of RhoA inside the cytosol thanks to the CRY2 optogenetic system induces its recruitment to the membrane and its activation. Black arrows with time show the dissociation time from the membrane.

in its inactive GDP state, it suggests that either membrane recruitment favors its activation by already membrane bound GEFs or that a fraction of this optoRhoA is already activated in the cytosol while not being engaged in downstream signalling. Additionally, the authors observed that the optoRhoA had a residence time on the plasma membrane higher than the lit state of BcLOV4, which suggests that other RhoA-dependent interactions stabilize RhoA at the plasma membrane.

Using a completely different strategy, Bugaj et al. relied on the clustering of RhoA to activate it [Bugaj et al., 2013]. They fused the full-length RhoA WT to the C terminus of CRY2, which is known to oligomerize upon blue light illumination. This optoRhoA showed an initial diffuse localization in the cytosol, as reported in 1.5.3 for RhoA WT [Michaelson et al., 2001, Yonemura et al., 2004], and upon blue illumination puncta appeared that were clearly targeted to the plasma membrane and that led to RhoA downstream activity (Figure 1.36 (E)). The mechanism by which this optogenetic strategy works is still unknown. One possibility is that the formation of a RhoA cluster increases its avidity to the plasma membrane, since weak multivalent interactions can lead to effective high affinity. Yet, it is not known whether the driving interactions are due to the polybasic tail of RhoA and the plasma membrane lipids or to the effector/protein interactors of RhoA that would be present at the plasma membrane in high local concentrations. As for the previous optoRhoA strategy, another open question is how RhoA gets activated by GEFs, either in the cytosol or at the plasma membrane.

Eventually, two other optogenetic strategies have been employed. The first relies on the sequestration of constitutively active RhoA at the mitochondria which is released by blue light [Wang et al., 2016]. The fact that constitutively active RhoA can be sequestered shows that its membrane targeting is indeed very labile and cannot outcompete the binding strength of Zdk1-LOV2, the optogenetic dimer. More recently, Ju et al. [Ju et al., 2022] proposed a strategy where the GEF DH-PH domain is anchored at the plasma membrane but is light-gated by the photodissociable dimeric Dronpa (pdDronpa). The advantage of this last technique is to offer a photo-switch without having to overexpress either an active GEF domain or the RhoA protein itself. Interestingly, the authors observed a variety of phenotypes upon optogenetic activation, including spikes and lamellipodia, even if the most abundant was the contractile phenotype which is observed with all the above strategies. Eventually, many other works have been using all those optogenetic constructs to probe RhoA activity in different contexts, and we refer to the excellent optobase.org website [Kolar et al., 2018] for readers to explore those works.

1.5.6 RhoA regulation in space and time - a new sketch?

What do we learn out of all these works? Can we draw a more realistic picture of RhoA regulation in space and time? We wanted this review [de Seze et al., 2023] to help people think about the role and dynamic of RhoA inside the cell, having a better cartoon in mind when looking at RhoA inside the complex signalling network. We were at first quite reluctant at the idea of having a sum-up cartoon that everyone could copy-paste in its slides: In some ways, it was contradictory with the goal of this review, which is underlying the exquisite complexity of RhoA regulation outside the scope of GEFs and GAPs and showing how little we know about some of the hidden layers of RhoA dynamics. However, we thought that certain key features of RhoA regulation exhibited here are poorly known and rarely cited, which lead us to add

(hopefully for the better) this small sum-up cartoon to the large number of already existing drawings that one can find in the literature and slides.

Let us comment it. First, RhoA is mostly cytosolic. Even more than the other GTPases Rac1 and Cdc42, even when overexpressed, which tells us that something retains RhoA in the cytoplasm, as discussed in 1.5.3. Second, it seems that RhoA can be in its GTP state both in the cytoplasm and at the membrane but binds to its effector mostly when it is at the membrane (Figure 1.37). Third, RhoA needs to be stabilized at the membrane to engage all the downstream pathways of contractility, and this stabilization is helped by effectors like anillin and by phospholipids like PIP2 (Figure 1.37). Fourth, the GEFs do not only have a role of activating RhoA, but they also promote its recruitment at the membrane, similarly to other GTPases such as Rabs and Arfs [Blümer et al., 2013]. This leads us to Figure 1.37, hopefully conveying those core principles.

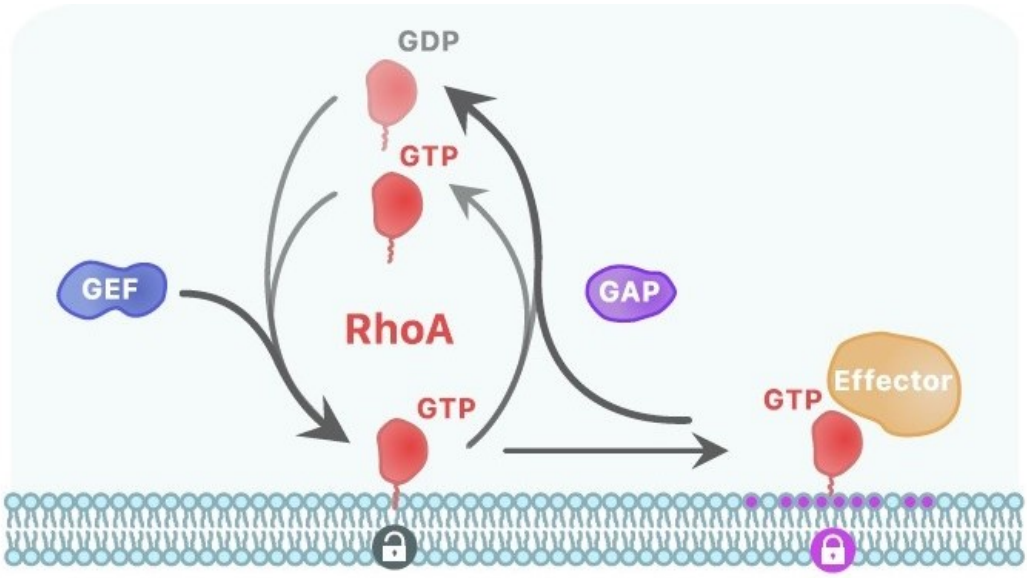

Figure 1.37: Revisited summary cartoon of RhoA activity. RhoA constantly shuttles between the plasma membrane and the cytosol both in its GDP and GTP-loaded states, with high turnover rates. Active GTP-bound RhoA preferentially binds to the plasma membrane. RhoA is activated and targeted to the plasma membrane by GEFs and is stabilized there thanks to interactions with effectors/scaffolds and negatively charged lipids. Once stabilized at the plasma membrane, RhoA-GTP has the highest potential to activate downstream pathways. GAP deactivates RhoA-GTP and thus tends to direct it to the cytosol.

These basic elements of RhoA regulation that we presented in this cartoon leave apart some very interesting features that are not all known and that may be important to understand the very specific roles of RhoA. First, we showed that active RhoA-GTP seems to be present in the cytosol, yet it does not seem to bind to effectors. Why does this pool of RhoA remain unable to trigger downstream pathways? One possibility could be that RhoA-GTP is either sequestered by a partner in the cytosol or in a specific conformational state that would prevent its binding to effectors. Another possibility is that RhoA effectors are mostly present at the plasma membrane. Second, we showed that FRET biosensors and RBD-based biosensors do not report the same activity pattern. Is it revealing a real dual role of RhoA? We suggested that the mislocalization of RhoA FRET biosensor could explain this difference, but it remains to be clarified.

Third, the optogenetic approaches showed that the recruitment of RhoA WT at the plasma membrane is sufficient to induce RhoA downstream activity. This could be simply due to the presence of GEFs at the membrane, but most of them are also present in the cytosol. Another possibility could be that the signalling activity of RhoA can be shifted just by increasing the dwell time of RhoA at the plasma membrane.

Fourth, an optogenetic strategy based on the oligomerization of RhoA-WT in the cytosol was surprisingly able to trigger RhoA activity. It is possible that the nanoscopic organization of RhoA at the plasma membrane adds another layer of regulation. Along this line, it was shown that Rac1 forms nanoclusters of a few dozens of molecules [Remorino et al., 2017], which are also enriched in Rho-GTPase interactors (GEFs, GAPs and effector) and in charged lipids (PIP2 and PIP3). It remains to be addressed if RhoA also forms such signalling nano-platform and whether this spatial organization plays a role in the stabilization of RhoA at the plasma membrane. Eventually, we highlighted the presence of shortly wired negative and positive feedbacks on RhoA activity. While we presented these additional layers of regulation independently of the previous ones, it would be interesting in the future to study the interplay of these feedbacks with the regulation of RhoA dwell-time at the plasma membrane.

Altogether, this chapter pinpoints the complexity of RhoA regulation and actions, and all the available tools can reveal us many aspects of it. Using live cell imaging techniques like biosensors and optogenetics will help us understand how RhoA is regulated and regulates opposite behaviors such as cell contractility and cellular protrusions, what is its precise role in contractility waves and how it coordinates its different roles within the cell. These approaches will be instrumental to understand, for example, how RhoA can engage different effectors and distinct downstream signalling pathways at two places within the same cell [Bolado-Carrancio et al., 2020]. RhoA is only one of the many hubs in cell signalling circuitry, but all the tools developed to study it make it a relevant protein model to understand how protein pleiotropy can be controlled and used by the cell in different contexts.

Chapter 2

PhD project, questions and approach

As stated in the introduction, cell biology tackles the question of life through the observation of cellular systems, either at the single or multicellular level, with the core idea that the cell is the key unit of life. Cellular life can be looked at from different points of view: centered on molecular/proteinic interactions, on the properties of the biochemical network, on molecular structures, on mechanics, on the interactions with the environment, on dynamics of activity of signalling pathways, on quantitative analysis of cell content, on regulatory networks, etc... all of these points of view being non mutually exclusive. During my PhD, I decided to study the impact of one specific pathway, the RhoA pathway, on the migration polarity of cells in a controlled environment.

I studied this impact in two different model systems, which correspond to the two chapters of the results (chapter 3 and 4) and are linked to very different research questions (detailed in 2.1 and 2.2). The first one deals with single cells migrating in a 2D environment, while the second one tackles the question of multicellular migration. How does RhoA pathway influence polarity in these two different types of migration? Can we understand the molecular mechanisms behind its role? How is RhoA pathway integrated in the complex molecular circuitry of the cell?

2.1 First project: how can one protein control antagonist migratory phenotypes?

The first project came out of an unexpected observation made at the beginning of my PhD. By optogenetically controlling the local recruitment of a GEF of RhoA at the membrane in RPE1 cells, I could observe two radically opposite migratory phenotypes. Some cells started to move in the direction of activation, creating a protrusion, whereas others escaped this area of activation and polarized in the other direction, revealing a retraction (see Figure 2.1).

This immediately raised an obvious question: how can one protein, recruited in the same way at the plasma membrane in the same cell line, lead to opposite phenotypes? What are the underlying pathways that trigger these phenotypes? Can we understand what differs in both cases that leads to these opposite cellular responses? If we understand this, can we control it?

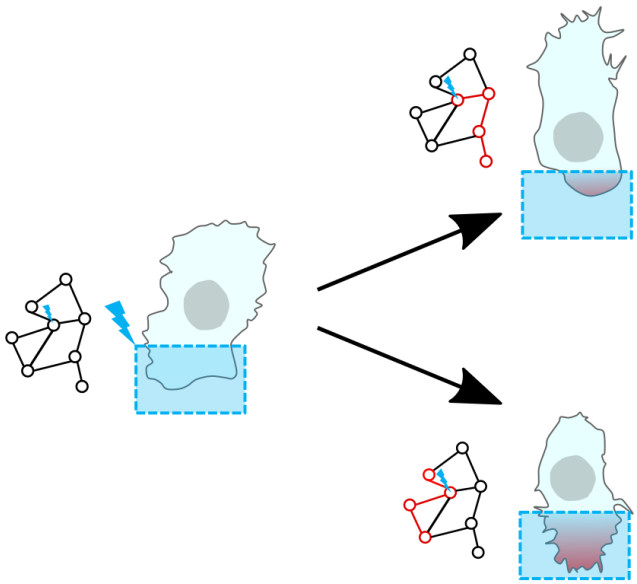

Figure 2.1: How can one protein control antagonist phenotypes? Scheme representing the main question. Local optogenetic control is represented on the cell by the blue square with lightning. This activation leads to two opposite phenotypes, protrusion or retraction. It means that the biochemical network is set in two different states, represented by the networks. Red colors are the activated nodes of the network. Dot with blue lightning is the node perturbated by optogenetics.

The ability of one protein to generate distinct cellular outcomes is a much-speculated mechanism; however, examples are scarce. Some well-studied examples involve protein hubs, such as Erk [Toettcher et al., 2013], PI3K [Tay et al., 2010] and NF-κB [Minas et al., 2020], which involve cellular responses at the transcriptional level. These examples happen at timescales of hours and different strategies have been described to multiplex such signals [Purvis and Lahav, 2013]. In our case, the difference in responses happened at the minutes timescale, which means that the transcription network is not involved, but only the protein protein interaction network. To our knowledge, there are only two examples of such a dual response at shorter timescales, both involving optogenetics ([Kerjouan et al., 2021] and [Ju et al., 2022]).

This example reveals the ability of proteins to multiplex. Through one channel (here, the GEF recruited to the membrane), different signals can be transmitted (here, protrusion or retraction). The goal of this project has been to decipher the physical and molecular mechanisms that enable this specific protein multiplexing ability, in order to reveal some key features of cell signalling complexity.

2.2 Second project: what drives collective amoeboid migration polarity?

The second project is part of a collaboration with Fanny Jaulin's lab at the Institut Gustave Roussy. They discovered a new mode of collective migration in colorectal cancer, which happened to be widely shared among different cell lines [Pagès et al., 2022]. This mode of migration does not require focal adhesions to the substrate and occurs in confined environments, reminiscent of amoeboid migration in single cells.

Single cell amoeboid migration relies on contractility for forces production, espe-

cially through RhoA pathway [Huang et al., 2014]. This led to the following main questions: is RhoA pathway and contractility also required in collective amoeboid migration? Is it responsible for force induction and/or collective polarization? How do these groups of cells polarize?

To tackle these questions I used optogenetic tools developed in our lab to precisely perturb RhoA activity during collective amoeboid migration (Figure 2.2). I could then measure the effects of changes in RhoA activity on collective migration speed and polarity. I launched also, together with a master 1 student, a project to get a better understanding of the onset of collective amoeboid migration, starting with smaller groups of cells.

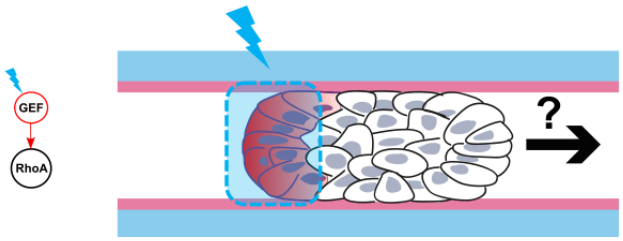

Figure 2.2: What is the role of contractility and RhoA pathway in collective amoeboid migration? A migrating cluster of cells is represented in a microfluidic channel. Perturbation is induced by light activation of RhoA (blue lightning, withing blue square), triggered by acting on one of its GEFs (scheme on the left).

Answering these questions was key to deciphering this new mode of collective migration, which is an important property of cancer metastasis formation in colorectal cancer, as well as in other cancer types [Pagès et al., 2022]. Understanding the different molecular and mechanical mechanisms responsible for this migration mode could be important for fighting cancer metastasis and reducing cancer lethality.

2.3 Approach: spatiotemporally controlled optogenetic inputs and quantitative imaging outputs

To tackle both of these projects, I used controlled environments with standard cell lines in order to minimize biological uncertainties and observe only the effect of the perturbation. Coated 2D glass coverslips were used for the first project, and microfluidic channels in the second.

As stressed in the last part of the introduction 1.5, RhoA exhibits very complex regulation patterns. This regulation takes into account interaction partners, such as GEFs, GAPs, or different effectors, as well as other layers of regulation, such as localization or specific positive and negative feedback loops. To be coherent with these dynamic features of RhoA, I performed in both projects live cell experiments with both inputs and outputs that could match the timescales and spatial scales at play in this pathway.

To this aim, I mainly worked with fluorescence microscopy and biosensors as outputs, as well as measurements of physical parameters (migration speed, direction, deformation,...). As inputs, I used optogenetic tools developed both in the lab or in other labs, and modified for the aim of the project. The strategy has been in both cases to look at the cell "state" for some time - cell state refering to the properties of the cell or the group of cells in terms of biosensors and physical parameters - and quantify the effects of optogenetic perturbations on this initial state (see Figure 2.3).

For both projects, I developed specific image analyses pipelines to extract the key measurable features describing the impact of optogenetic perturbations. A model was then built to explain as simply as possible the quantitative results: I developed it for the first project, while it was done by collaborators for the second one.

These models had some predictions that led us to go back to experiments and test them, confirming that they could be useful and taught us something about the two different cellular mechanisms studied in both of these project. A graphical summary of this approach can be seen on Figure 2.3.

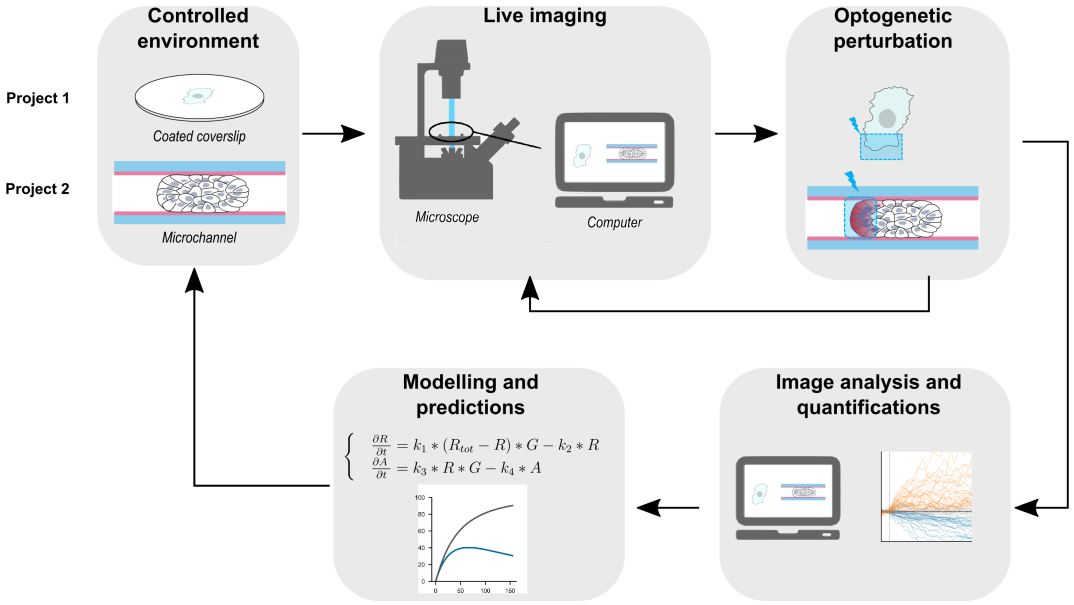

Figure 2.3: PhD approach. Experiments are done in controlled environment for both projects. Cells are imaged with fluorescence and bright field microscopy. Optogenetic perturbations are used as inputs and live imaging as output. Image are analysed and physical or biosensors parameters are quantified. A model is built to explain data, which leads to new predictions and questions that can be further answered by new experiments.

Chapter 3

Optogenetic control of protrusion and retraction with one GEF of RhoA

Cell migration is a fascinating process in which the cell must polarize itself by simultaneously controlling two seemingly opposite shape changes, protrusion at the front and retraction at the back. Normally, these two morphodynamic changes are thought to be spatially and temporally controlled by the segregation of protein activities within the cell space. Key controllers of these two processes are the small GTPases, in particular the three best known RhoA, Rac, and Cdc42 (see 1.4.2.1). Despite a canonical picture in which Rac and Cdc42 control protrusion and RhoA controls retraction, the complexity of signalling in space and time has led to much more complex networks describing crosstalks and interactions over the time course of cell migration, as described for the specific case of RhoA in 1.5.

In recent years, optogenetics has emerged as a very powerful tool to go beyond correlations and demonstrate causality in these questions [Vaidžiulytė et al., 2022, de Beco et al., 2018]. Working on optogenetic tools that bring GEFs of RhoA to the membrane for the project presented in chapter 4, I serendipitously found that some GEFs of RhoA can trigger both protrusion and retraction in the same cell type, polarizing the cell in opposite directions.

The fact that a protein can have different functions is not new, but examples that demonstrate a causal relationship between activation of a protein and opposite cellular responses exist mostly at the transcriptional level, on the timescale of hours [Toettcher et al., 2013]. To our knowledge, there are only two examples of such a dual response on shorter time scales, both involving optogenetics. In the first example [Kerjouan et al., 2021], two different acto-adhesive structures are formed in response to Src recruitment or clustering; the specificity is encoded here by the dynamics of Src nanoclusters at the adhesive sites. In the second example [Ju et al., 2022], RhoA activation by uncaging of a GEF of RhoA triggers focal adhesion growth via Src activation only at submaximal levels, revealing a selection of cellular response by signal amplitude.

During this project, I focused on one GEF of RhoA, PDZ-RhoGEF (PRG), also known as ARHGEF11, which was most efficient in eliciting both phenotypes. Interestingly, PRG is known for its role in cell migration, both at the rear [Iwanicki et al., 2008] and at the front [Nanda et al., 2023]. Moreover, PRG is known for being pro metastatic, is overexpressed in different cancers and favours migration and epithelial to mesenchymal transition [Ding et al., 2018, Du et al., 2020, Struckhoff et al., 2013].

I have been helped by Benoit Boulevard for different plasmid constructions, Maud Bongaerts for the Western Blots showing RhoA activities, and my supervisor Mathieu Coppey during the whole process.

3.1 Local optogenetic recruitment of DH-PH domain of PRG to the plasma membrane can lead to both protrusion and retraction in single cells

To understand the role of RhoA GEFs in migrating cells, we developed optogenetic tools based on the iLID-SspB dimerization system (see 1.3.3). Using a strategy already applied to other GTPases [Guntas et al., 2015, de Beco et al., 2018] and to RhoA itself (see 1.5.4), we anchored the iLID part of the dimer to the membrane thanks to a CAAX domain with mVenus fluorescent protein, and expressed the DH-PH domains of different GEFs of RhoA in the cytosol, linked to the SspB protein (Figure 3.1 (A)). We selected three of the most known GEFs of RhoA: LARG (ARHGEF12), GEF-H1 (ARHGEF2), and PDZ-RhoGEF (ARHGEF11) (Figure 3.1 (B)). The LARG DH domain was already used with the iLID system [O'Neill et al., 2018], the GEF-H1 DH domain had been recruited by optochemical methods [Kamps et al., 2020], and PRG was used with the CRY2-CIBN system [Valon et al., 2017]. All of these strategies have been shown to trigger cell contractility, either in single cells or in monolayers. We chose to retain the PH domain of the GEF because it is part of an autoamplification process [Chen et al., 2010] and sometimes appears to be required for GEF specificity [Ju et al., 2022]. We cloned these iLID-SspB dimers into a single plasmid separated by a P2A motif so that they were expressed at a one-to-one ratio [De Felipe et al., 2006].

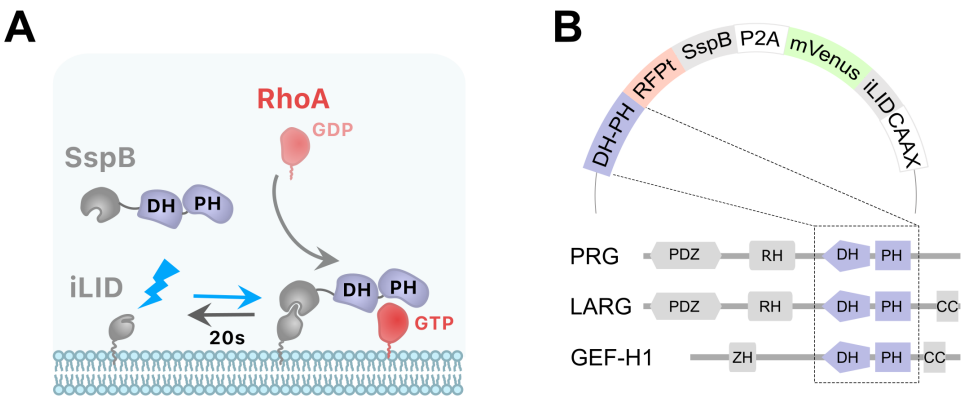

Figure 3.1: Optogenetic constructs to control RhoA signalling. (A) Scheme of the optogenetic tool. Optogenetic dimer (in gray) dimerizes upon blue light activation (blue arrow), and deassembles in the dark with an off rate of 20s (black arrow). DH-PH domain is fused to the SspB part (purple), which recruitment triggers RhoA activation, from GDP (light red) to GTP (dark red) state. (B) Transfected plasmids, with DH-PH domains (purple) shown in their wildtype position within the different RhoA GEF structures used here.

We then transiently transfected RPE1 cells with our optogenetic systems (henceforth called optoPRG, optoLARG, and optoGEF-H1) and examined the effects of local activation controlled thanks to a digital micromirror light source (see experimental timeline in Figure 3.2 and Material and Methods in chapter 6). We measured the variations in RFPt intensity in Hilo microscopy, which qunatifies the local recruitment. In

all cases, we saw a strong recruitment of the protein to the plasma membrane, between 3 and 10 fold, depending on the transfection intensity and the amount of light sent to the sample.

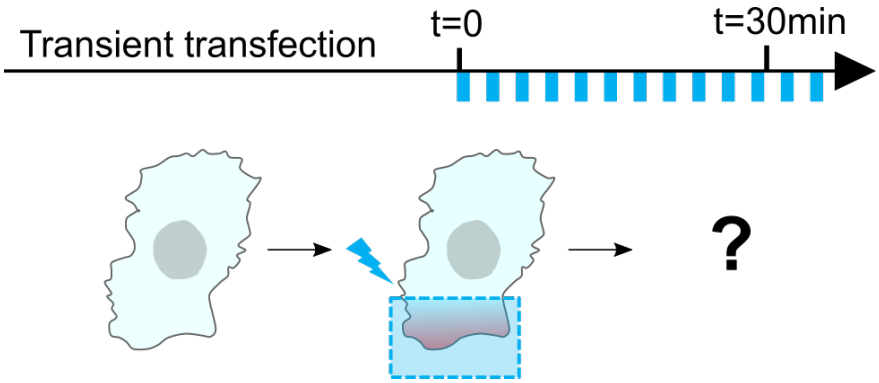

Figure 3.2: Experimental timeline. Transient transfection is done at least 30 hours before first local activation (blue squares). Activation is done by pulses (blue bars, top) at different frequencies, intensities and durations. Cells are observed for 30 to 60 minutes.

To our surprise, recruitment of these GEFs of RhoA to the membrane with the same experimental procedure, one pulse of light every 30 seconds, resulted in very different phenotypes (Figure 3.3). Whereas the recruitment of the DH-PH domain of LARG elicited only the expected retractile phenotype typical of RhoA pathway (Figure 3.3 (B)), GEF-H1 and PRG exhibited less predictable behavior (Figure 3.3 (C) and (D)). The retractile phenotype was observed in many cells, but a large proportion of cells showed a seemingly opposite response, namely a clear protruding phenotype with filopodia and ruffles.

For GEF-H1, the majority of the cells were very round after transfection and showed no response at all after optogenetic recruitment of the DH-PH domain to the membrane. Only a few cells (∼20%) showed distinct morphological changes after activation, most retracted, but some also showed distinct protruding phenotypes (Figure 3.3 (C)).

For the DH-PH domain of PRG, most cells showed a distinct phenotypic response upon blue light exposure (Figure 3.3 (A)). Almost 35% of the cells exhibited a distinct retracting phenotype leading to the formation of blebs or protrusions at the other side of the cell (Figure 3.3 (D), right). 40% exhibited a markedly protruding phenotype (Figure 3.3 (C), left) reminiscent of activation of a GEF of Cdc42 or Rac1 [de Beco et al., 2018], often leading to retraction of the other side of the cell. Some cells (∼10%) showed no clear response, and some showed what we called a mixed phenotype (remaining 25%): while we could see ruffles or filopodia forming at the site of activation, the cell did not move and appeared to contract at the same time, leading to blebs at the other pole of the cell.

We compared the evolution of the membrane area inside the activation square during the activation, with or without light (Figure 3.4 (E)). We could see the very clear impact of the recruitment of the DH-PH domain of PRG, that either triggers a diminution of membrane area - a retraction - or an increase in membrane area - a protrusion -, while control cells have much smaller membrane movements over the timecourse of the experiment.

To ensure that the cell's response was not due to an already set polarity, we repeated the activation at the other pole of the cell one hour after the first round of activation, when the cells had recovered from the first activation and were again in a resting state. Almost all cells retained the same phenotype: they protruded when they were already

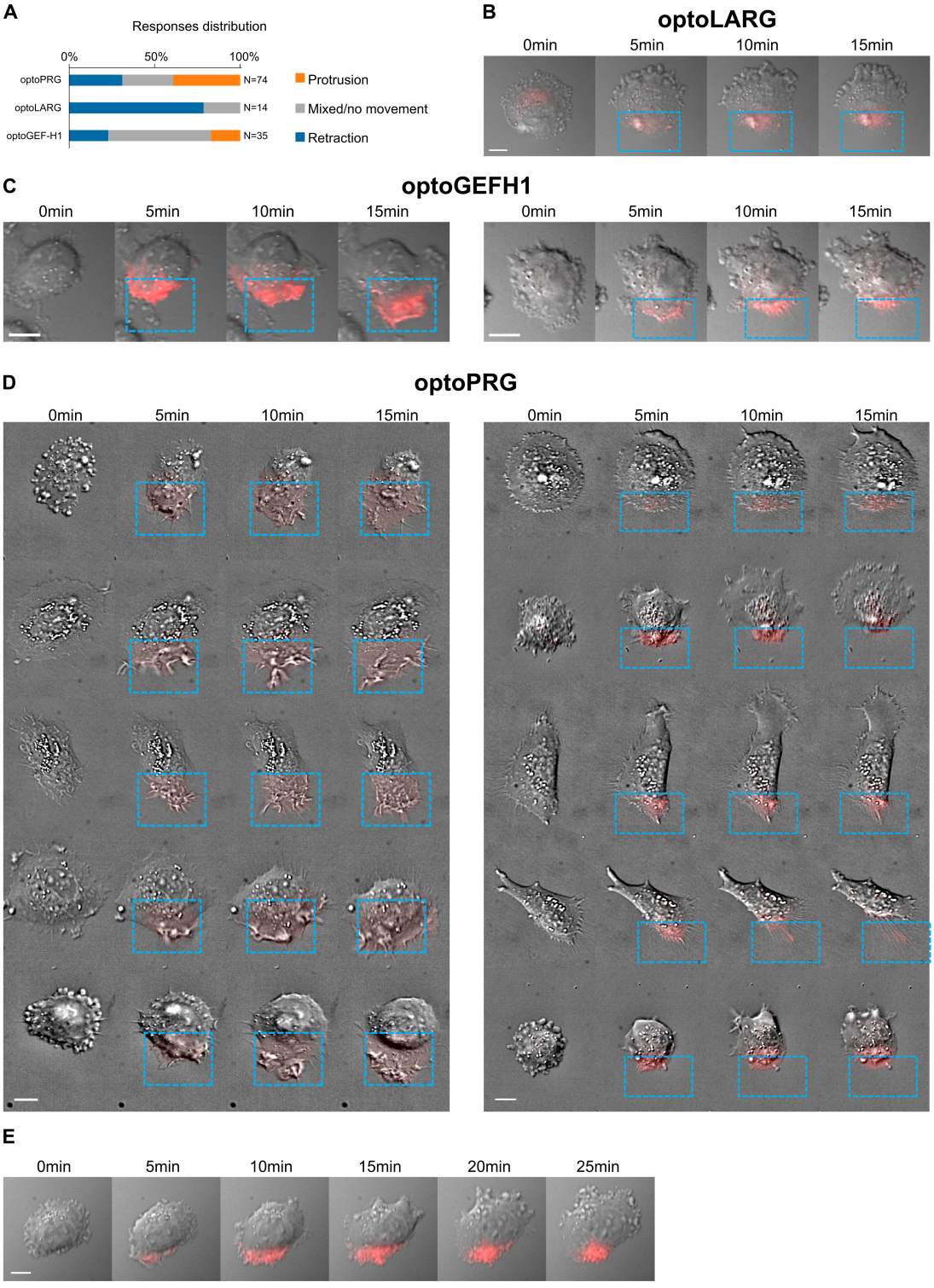

Figure 3.3: GEFs of RhoA can trigger opposite phenotypes. (A) Responses distribution for each optogenetic tool. (B) Representative retracting cell for optoLARG. (C) and (D) Representative protruding (left) and retracting (right) cells for optoGEF-H1 (C) and optoPRG (D). (E) Example of a mixed phenotype: here we see first protrusions (from 5 to 10 minutes) and then retraction with blebby structures forming at the opposite side of the cell. Blue squares: area of optogenetic activation. Red color: RFPt channel (optogenetic tool). Scale bars: 10 µm.

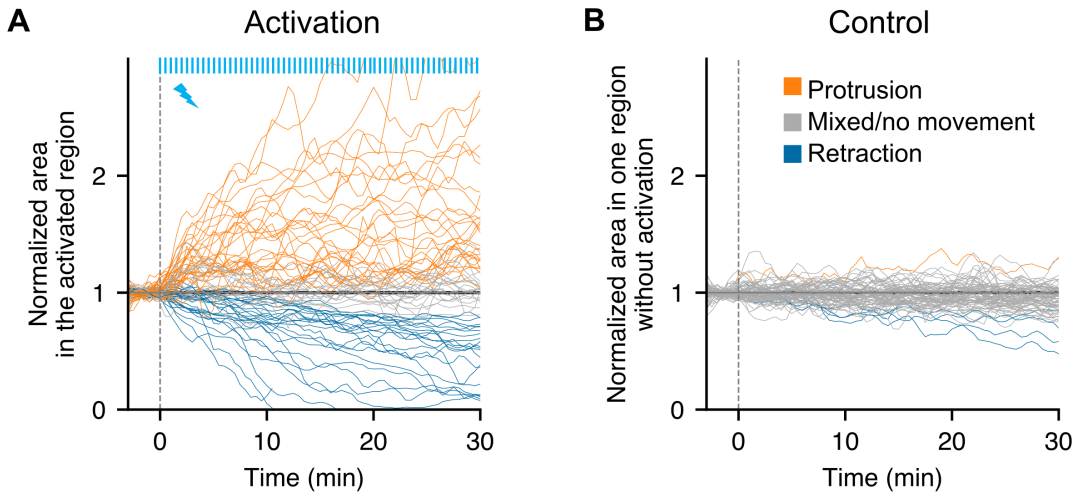

Figure 3.4: Evolution of membrane area in the activated region. Area of the cell in the activated region normalized by the mean area before activation, over time. t=0 is the starting point of the activation, each blue bar reprensenting one light impulse. Orange: protuding cells, blue: retracting cells, gray: non moving cells or mixed phenotype (labeled by hand).

protruding and retracted when they were already retracting (Figure 3.5). Only a few cells showed a mixed phenotype in the first or second round, whereas their phenotype was clear in the other round (Figure 3.5 (B)). Thus, we concluded that for one type of optogenetic activation (one frequency and one light intensity), the phenotype triggered by the recruitment of the DH-PH domain of PRG to the membrane was determined by the state of the cell and not by the cell section in which the optogenetic activation was performed.

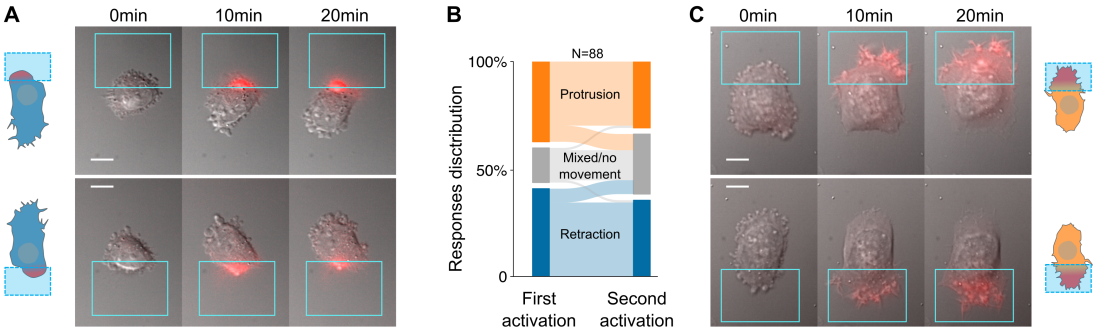

Figure 3.5: Activation on the two sides of transfected cells. (A) and (C), representative cells doing retraction (A) and protrusion (C) upon optogenetic activation. Scale bar: 10 µm. (B) Sankey diagram representing the proportion of cells doing a protrusion (orange), retraction (blue) or a mixed phenotype (gray) at one side (first activation) or the other (second activation).

To further verify that these opposite phenotypes were not cell line specific, we performed the experiment in Hela cells. The two phenotypes could be seen after transient transfection with optoPRG and activation with the same protocol, showing that these two opposites phenotypes are not restricted to RPE1 cells only (see Figure 3.6).

Thus, the DH-PH of PRG is able to induce both protrusion and retraction upon its recruitment in single cells. These opposite phenotypes occur in the same cell line, in the same biomechanical environment, and with the same dynamics of recruitment to

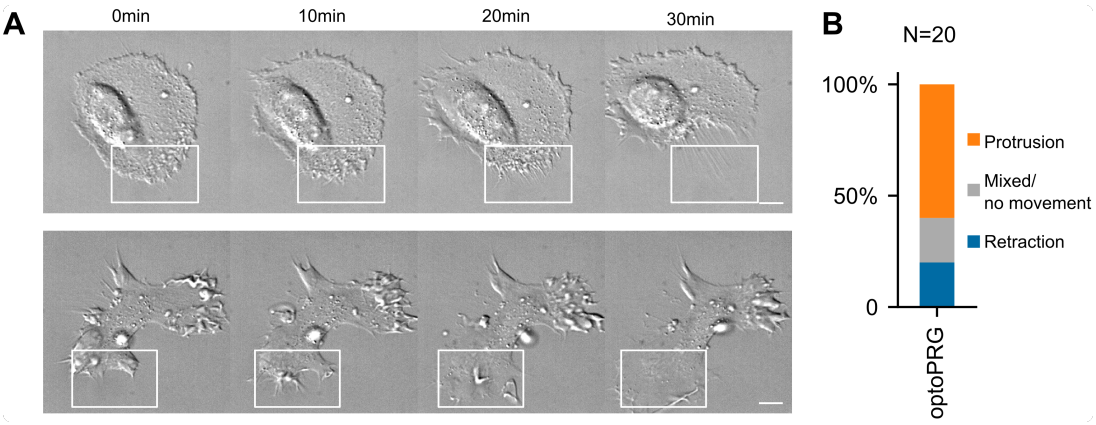

Figure 3.6: Transfection of Hela cells with optoPRG. (A) Representative cells doing retraction (on the top) and protrusion (on the bottom) upon optogenetic activation. Scale bar: 10 µm. (B) Proportion of cells doing a protrusion (orange), retraction (blue) or a mixed phenotype (gray) upon optogenetic activation. N=20 cells.

the membrane. This dual behavior is not cell-specific or exclusive to this GEF of RhoA, as it has also been observed with GEF-H1, although with much less efficiency. For our study, we focused on the optoPRG that elicits the strongest and most reproducible opposing phenotypes.

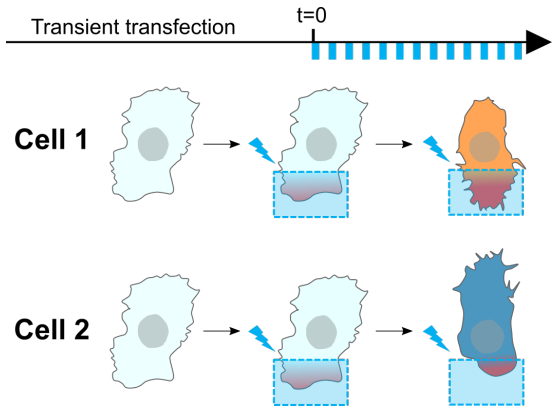

Figure 3.7: Graphical summary of the dual phenotype. Optogenetic recruitemnt of the DH-PH domain of PRG leads to two seemingly opposite responses that are dependent on the chosen activated cell.

3.2 Phenotype is dependent on basal concentration of exogenous DH-PH domain of PRG in the cytosol

What differs in the activated cells that leads to these opposite phenotypes? As all the experiments above are done by transiently transfecting the cells with the optogenetic tool, we end up in each experiment with a wide range of concentrations of optoPRG from one cell to the other (see Figure 3.8 for three reprensentative examples), that we can estimate by measuring the mean fluorescence intensity.

Looking at the area in the activated region after 5 minutes against the concentration of optoPRG before activation leads to a very clear result (Figure 3.9). Below a

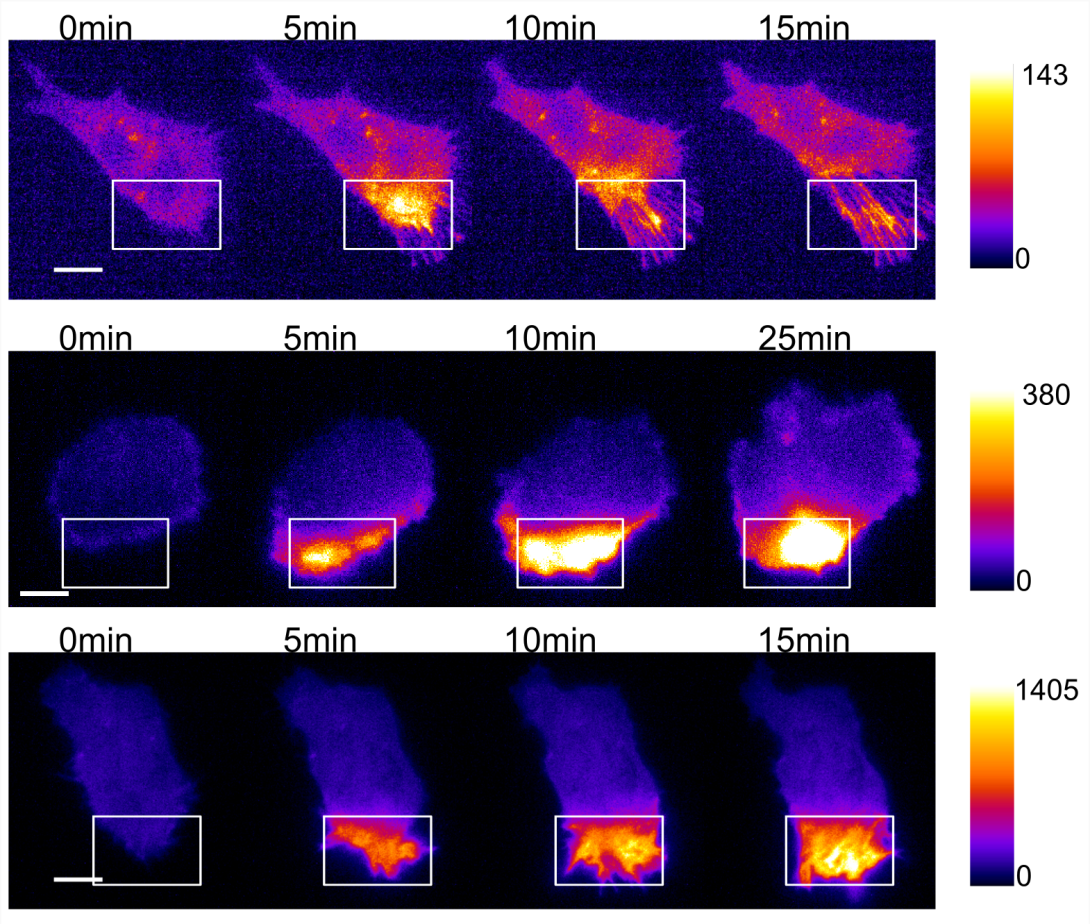

Figure 3.8: Three representative time lapse images of transiently infected cells, one retracting (top), one showing a mixed phenotype (middle), and one protruding (bottom). Intensities are very different, as seen with the colormaps presented on the right.

specific concentration threshold (∼40 a.u.), almost all the activated cells (∼95%) show a retraction of the membrane within the activation area (normalized area<1), while above this threshold, ∼85% of the cells extend their membrane (normalized area>1). This clearly demonstrates that the phenotype triggered by the activation of optoPRG can be predicted by its concentration within the cell before activation.

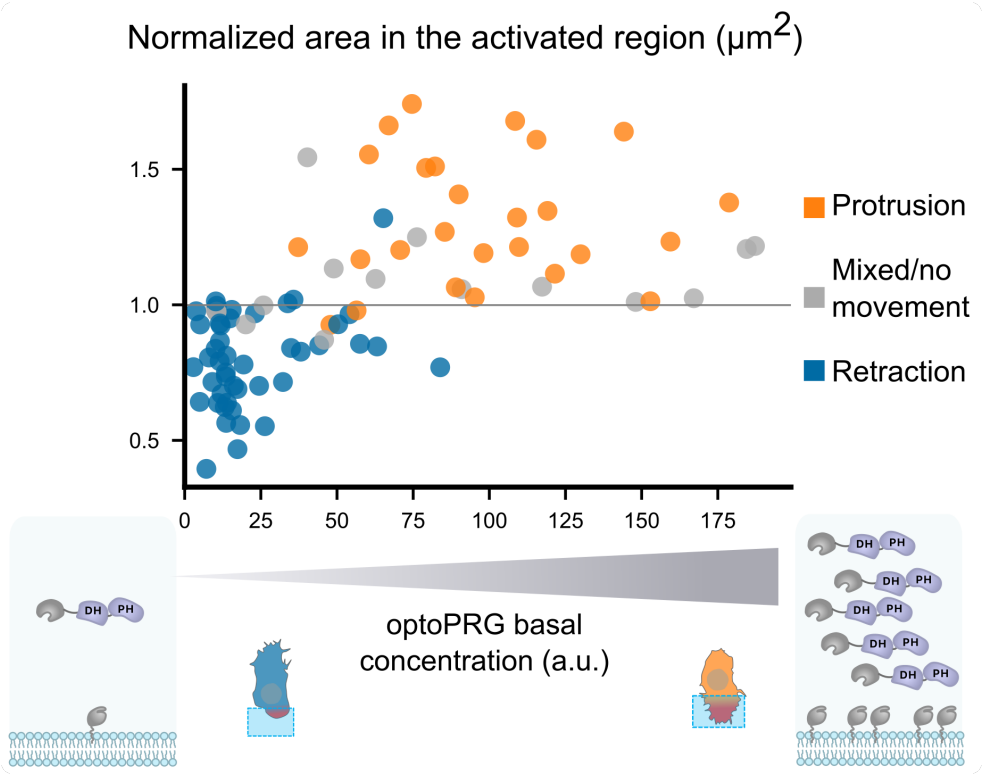

Figure 3.9: Phenotype dependence on global optoPRG concentration. Normalized area in the activated after 5 minutes. Color is labeled by hand. Schemes on the right and on the left represent high and low levels of expression (P2A plasmids implies approximately one-to-one ratio in iLID-SspB.

This leads to two hypotheses. Either the cell is responding to differences in the absolute recruitment of optoPRG to the membrane, or the cell is, before optogenetic activation, in a different state that leads to opposite reactions to optoPRG activation. To exclude one of these hypotheses, we first looked at the absolute recruitment to the membrane (Figure 3.10 (D)). Even if the absolute recruitment depends on the initial concentration, we saw many retracting cells reaching very high absolute optoPRG recruitments, which tends to rule out the first hypothesis. To further demonstrate it, we overexpressed in a different channel a non recruitable DH-PH of PRG, together with the optoPRG, in order to decouple global and recruited PRG concentration. We saw that overexpressing DH-PH domain of PRG strongly increased the number of protruding phenotypes in low expressing cells (from 0% to 45%). Moreover, it was clear that this switch in the phenotype also correlates with the initial concentration of overexpressed DH-PH of PRG, highly expressing cells being more and more prone to protrude (Figure 3.10 (E)).

We wanted to check whether we could measure this influence of the optoPRG on the cell state. We first measured the average cell area before activation in the two phenotypes, and saw a strong and significant difference, highly expressing cells being 1.5 times bigger than low expressing cells (Figure 3.11). We then looked at membrane

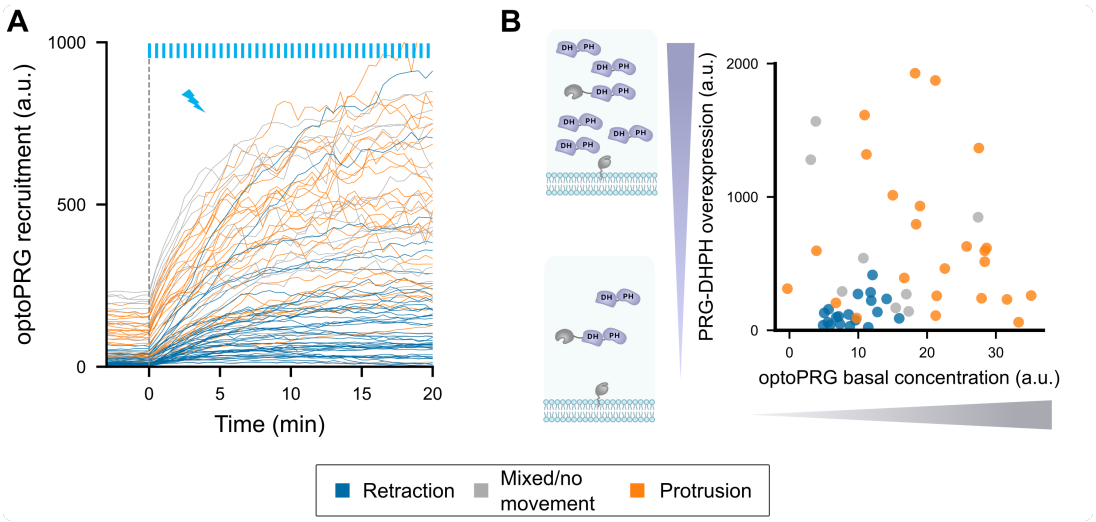

Figure 3.10: Global concentration before activation is responsible for phenotype choice. (A) Absolute fluorescence intensity of tagged recruited DH-PH domain, before (t<0) and after (t>0) activation. Blue bars: activation pulses. (B) Phenotype depending on both optoPRG concentration and PRG DH-PH overexpression, measured both by fluorescence intensity (a.u.). Increasing recruitable and non-recruitable DH-PH domain of PRG both lead to protruding phenotypes. Phenotypes are manually labelled.

ruffles without any optogenetic activation, by calculating the mean absolute speed of membrane displacement in one region. We showed that the difference was also significant, protruding cells having more (or stronger) membrane displacements, even before being activated.

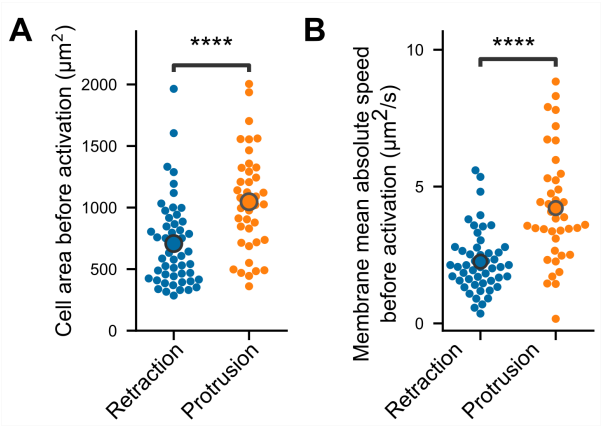

Figure 3.11: Two observables of the cell state are used here to compare protruding and retracting cells: Cell area before activation (A) and membrane mean absolute to measur membrane activity (B). **** P<0.0001 (Mann-Whitney)

These experiments led us to the conclusion that the main determining factor of the phenotype is the concentration of the DH-PH domain of PRG within the cell, before the optogenetic activation. This initial concentration changes the cell state, in a way that the recruitment of the DH-PH domain of PRG triggers opposite cellular responses.

3.3 Two distinct pathways seem to be triggered from the first activation timepoint

Very surprised by this ability of one protein to trigger opposite phenotypes, we sought to further characterize these responses by monitoring the activity of key proteins involved in RhoA pathway. We wanted to see how the differences in phenotypes was emerging from the different molecular activities. To this end, we initially investigated whether the variation in actin and myosin levels following optogenetic activation corresponded to the stereotypical dynamics of protrusions and retractions described in a previous study by Martin *et al.* [Martin et al., 2016]. We thus monitored Lifeact-iRFP and MRLC-iRFP (Myosin regulatory light chain) proteins during the optogenetic experiments. In the retraction phenotype, the first recruitment of optoPRG to the membrane is followed by an immediate polymerization of actin in the area of activation, as we quantified over multiple experiments (Figure 3.12 (A) top, (B), (C)). Myosin recruitment appeared to follow the one of the actin, leading to the retraction of the membrane in the minutes following the activation (Figure 3.12 (A), (B), (C)). In contrast, when cells were protruding, we observed a decrease in MRLC and Lifeact intensities following the first activation of our tool by light (Figure 3.12 (A) bottom, (B), (C)), like what was shown for protrusions triggered by PDGF in [Martin et al., 2016]. This first decrease is probably due to the depolymerization of stress fibers at the area of activation. It is followed by an increase in actin polymerization, most probably responsible for the net displacement of the membrane, while myosin stays lower that the initial state. This difference in actin and myosin dynamics following the recruitment of the same optoPRG to the membrane is visible within the 30 seconds after the first pulse of light (Figure 3.12 (C),(F)), even if the phenotypes can usually not be distinguished before one or two minutes by eye. This shows that the pathway triggered by this recruitment differs from the first tens of seconds after recruitment.

We then turned to RhoA, which is supposed to be upstream of actin and myosin, and just downstream of the PRG. As our optogenetic tool prevented us from using the previously developed FRET biosensors, we turned to the relocation biosensor designed by Mahlandt *et al.* [Mahlandt et al., 2021]. This very sensitive relocation biosensor is efficient with TdTomato, which overlaped the light frequency of the RFPt fluorophore used for quantifying optoPRG recruitment. We thus designed a new optoPRG with iRFP, which could trigger both phenotypes but was harder to transiently express, giving rise to a majority of retracting phenotype. Looking at the biosensor recruitment, we saw very different responses in both phenotypes (Figure 3.12 (G), (H), (I)). While retracting cells lead to strong and immediate activation of RhoA, protruding cells show a much smaller and delayed response. After the first minute of optogenetics activation, no significant change is seen in protruding cells (Figure 3.12 (I)). Either something is sequestering RhoA-GDP, or optoPRG preferentially binds to another partner (both hypotheses being non-mutuallly exclusive).

Altogether, these data demonstrate that cells exhibit very different responses to optoPRG activation, even at the level or RhoA activity itself. This has impacts on the polymerization of actin and myosin activity, which are responsible or at least contribute to the opposite phenotypes.

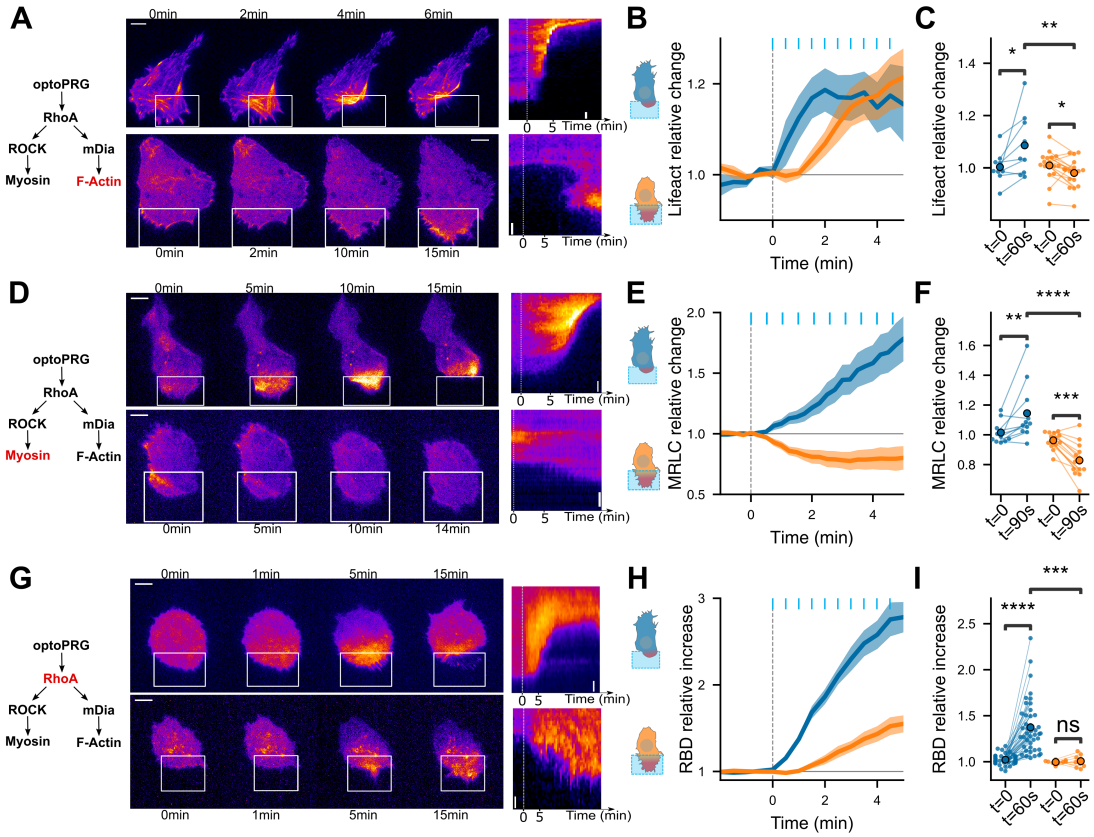

Figure 3.12: Distinct pathways are triggered from the first timepoint. Representative time-lapse images and kymographs (A),(D),(G) for representative cells labeled with Lifeact-iRFP (A), MRLC-iRFP(D), and RBD-2xTdTomato biosensor (G), activated with optoPRG starting at t=0min. White rectangles are areas of optogenetic activation. Scale bars are 10 µm. Corresponding mean normalized intensities are plotted along time (mean ± sem) (B), (E) and (H). *P<0.05 **P<0.01, ***P<0.001, **** P<0.0001 (Wilcoxon test to compare before/after, independent t-test otherwise)

3.4 PH domain of PRG is triggering inhibition of RhoA at high PRG concentration and is necessary but not sufficient for protruding phenotype.

As the phenotype triggered by optoPRG, revealed on a minute timescale, seems to be set by the reaction of the biochemical network after few tens of seconds, we turned to a much smaller time scale analysis of RhoA activity. Our first surprise came while looking at the response of the biosensor to a pulse of optoPRG activation. We show three representative examples of such responses (Figure 3.13). While at low optoPRG concentration (cell 1), RhoA activity follows the pulse of optoPRG with some delay, at higher concentrations (cell 2 and cell 3), RhoA activity would exhibit a very different behavior. It seems that, adding to the well-known activation of RhoA, DH-PH domain of PRG can also negatively regulate RhoA activity.

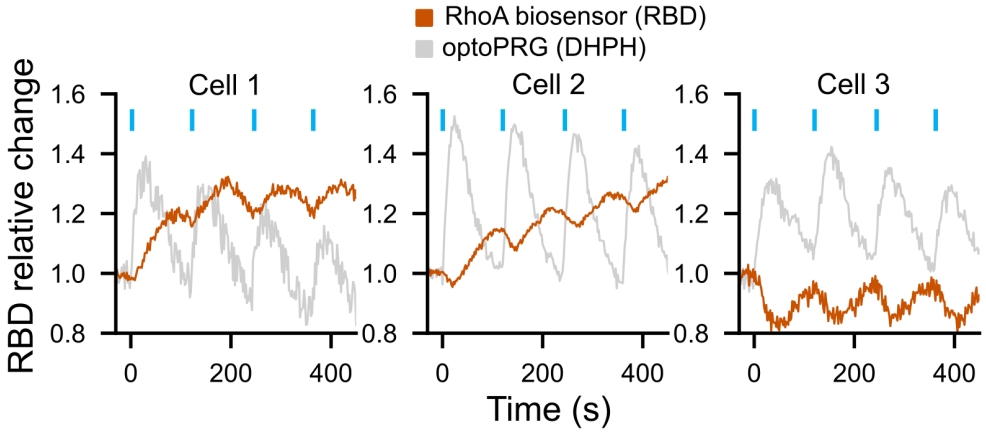

Figure 3.13: RhoA response to pulsatile activation. Three representative cells that show very different responses to optoPRG pulsatile activation. Cell 1 has a low optoPRG expression, while Cell 2 and Cell 3 have high concentration of optoPRG. Intensities are normalized by the mean intensity before the first activation (t=0).

Knowing that the PH domain of PRG triggers a positive feedback loop thanks to its binding to active RhoA [Chen et al., 2010], we hypothesised that this binding could sequester active RhoA, thus being responsible for its inhibition. To test our hypothesis, we designed a new optogenetic tool to recruit only the PH domain of PRG (called optoPH), while still looking at RhoA activity. In some cells, we could see a very clear decrease of the biosensor intensity following optoPH activation, very similar in terms of dynamic to the decrease observed in highly expressing cells (Figure 3.14(A) and (B)). This decrease was significant on the mean but not clearly visible in all cells (Figure 3.14(C)), which was expected at it should depend a lot on the basal RhoA activity. It confirmed that the PH domain or PRG alone is able to inhibit RhoA activity, probably through the direct binding proposed in [Chen et al., 2010] (Figure 3.14(D)).

We wondered whether this inhibition played a role in the protruding phenotype that we are seeing with the optoPRG. To check this, we mutated our optoPRG with a dual mutation (F1044A and I1046E) known for preventing the binding of the PH domain of PRG to RhoA-GTP [Chen et al., 2010]. This dual mutation had a strong impact on our tool, restricting the phenotypes to only the retracting ones, even at high enough basal concentrations (Figure 3.15 (A),(B)). This means that optoPRG

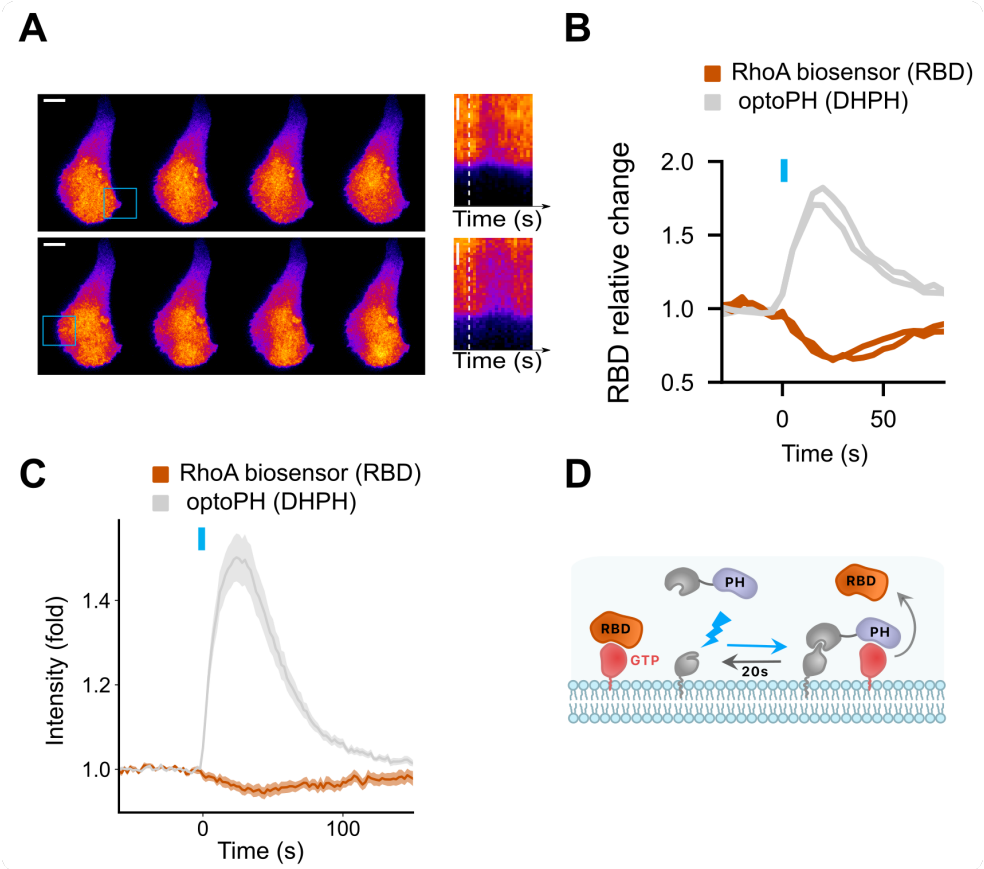

Figure 3.14: PH domain of PRG inhibits RhoA. (A) Representative image of an inhibition of RhoA by optogenetic recruitment of the PH domain of PRG (scheme of the optogenetic tool on the left). Scale bar: 10 µm. Region of activation is shown is the blue rectangle. On the right, kymograph taken within the activation region. White dotted line shows the starting point of the activation. (B) Quantification of the relative change in RBD biosensor after one pulse of optogenetic recruitment of the PH domain of PRG. In gray, optoPH recruitment, in red, RhoA biosensor. Light pulse is shown with the blue bar. (C) Mean ± sem of recruitment of optoPH and RBD biosensor evolution over 26 cells. Light pulse is shown with the blue bar. (D) Probable mechanism of PH domain dominant negative effect on RhoA.

needs to bind to RhoA-GTP, either before the activation to change the cell state, or during recruitment. To discriminate these hypotheses, we overexpressed the DH-PH domain in another fluorescent channel (iRFP), and recruited the mutated PH at the membrane. When doing so, we still had a large majority of retracting phenotype even in highly expressing cells (Figure 3.15 (C)), showing that the binding to RhoA-GTP is a key component of the protruding phenotype. We could still see some cells with very high PRG concentration displaying a small protruding phenotype, indicating that even if much less efficient, the mutated PH could still trigger protrusions.

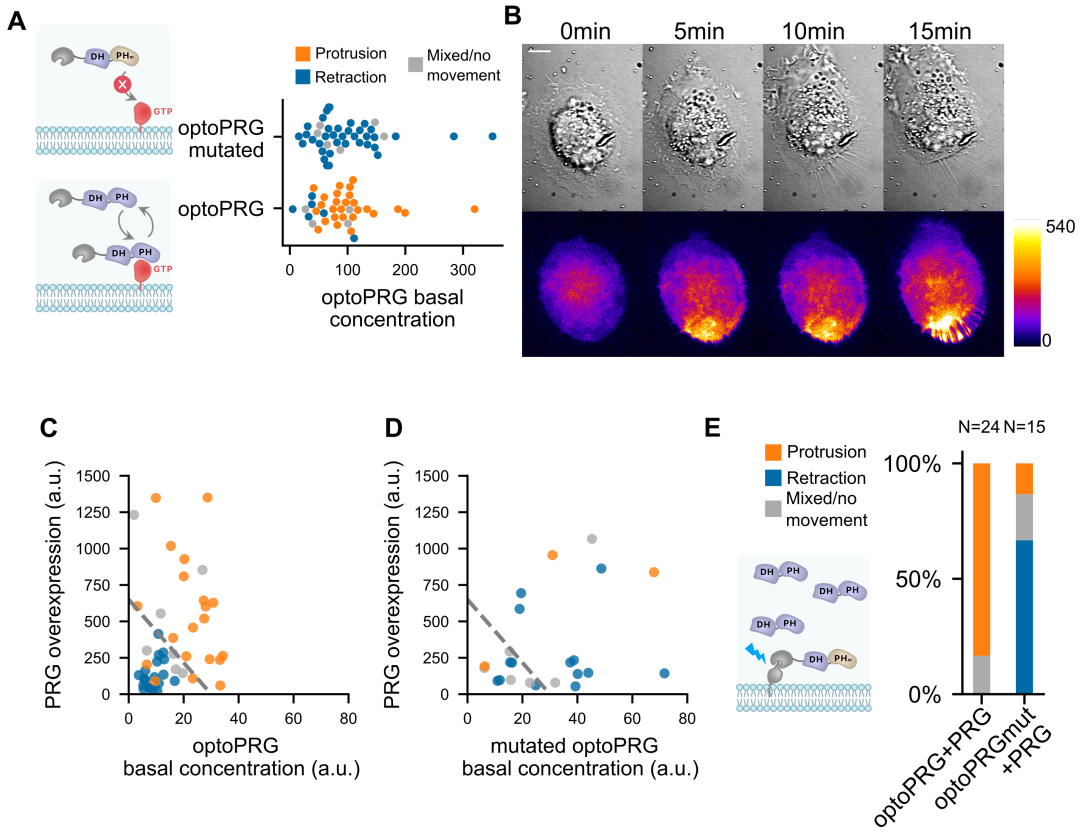

Figure 3.15: Binding of PH domain to RhoA-GTP is required for protrusions. (A) Phenotype after optogenetic activation for optoPRG (bottom) and optoPRG with the PH mutated for no binding to RhoA-GTP (top). On the left, schemes of the expected behavior of the corresponding proteins. (B) Representative image of a cell transfected with the optoPRG with mutated PH, doing a retraction despite the high optoPRG concentration. (C) (D) (E) Overexpression of the non recruitable PRG together with the optogenetic tools. (C) Control experiment with recruitment of optoPRG and overexpressed non recruitable PRG, and (D) same experiment with the mutated PH. Dashed line separates retracting and protruding phenotypes in control experiment. (E) Quantification of protruding and retracting phenotypes in highly expressing cells (above dashed gray line), with a scheme of the experiment on the left.

These experiments point towards a necessary role of PRG PH domain for protrusions, but is it sufficient? Indeed, decreasing contractility can be sufficient for protrusion formation, as has been shown with the use of the drug Y-27632 [Martin et al., 2016]. To check this, we looked at the phenotypic response of cells that overexpress PRG, where we would only recruit the PH domain. We couldn't see either clear protrusion or retraction happening following PH recruitment, as shown by membrane displacement on Figure 3.16. It revealed that the inhibitory function of the PH domain was not sufficient for triggering protrusion alone.

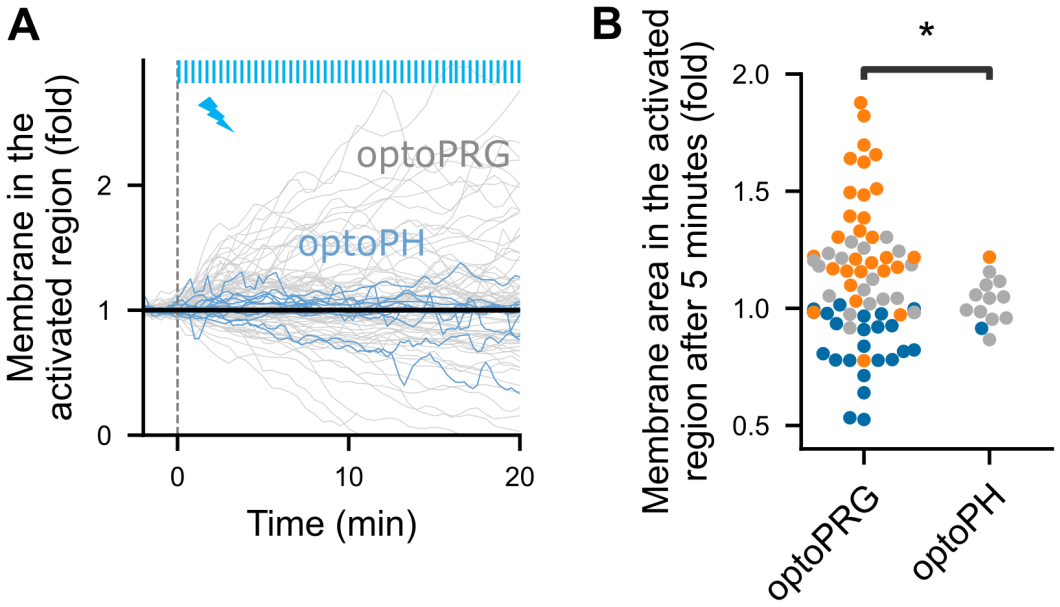

Figure 3.16: PH domain is not sufficient for protrusions. (A) Membrane displacement of optoPH cells (in blue) compared to optoPRG cells (in gray). No specific protrusion can be seen. (B) Normalized membrane area after 5 minutes in the activated for optoPRG and optoPH cells. Orange: protruding cells, gray: mixed phenotype or no movement, blue: retracting cells. *P<0.05 (Levene test)

Thus, we can conclude that the PH domain is required for efficiently triggering the protruding phenotype with optoPRG at the moment of activation, but is not sufficient. This points towards the activation of another effector, actively responsible for protrusion formation.

3.5 PRG activates Cdc42

To find the active process involved in the protruding phenotype, we turned to the two other most known GTPases, Rac and Cdc42, which are main drivers of cell protrusions. Indeed, a recent paper showed that the DH-PH domain of PRG was able to bind to Cdc42 and activate it, thanks to conformational change operated by GαS [Castillo-Kauil et al., 2020].

To look at the dynamic activity of Rac and Cdc42, we first used a PAK Binding Domain (PBD) linked to iRFP. PAK is known for being an effector of both Rac and Cdc42, but more sensitive as a biosensor to Cdc42 [Mahlandt et al., 2023]. After optogenetic activation, we saw an increase in PBD intensity in both the protruding and retracting phenotypes. After one minute, PBD intensity continuously increases for the protruding phenotype while it remains unchanged for the retracting phenotype (Figure 3.17 (A), (B), (C)). This suggested an immediate activation of Rac or Cdc42 after recruitment of optoPRG, that would be stopped after few minutes in the case of the retracting phenotype.

We then turned to recently published biosensors that are more specific to Rac and Cdc42 specifically [Nanda et al., 2023]. These biosensors enabled us to show that Cdc42 was the Rho-GTPase that was specifically activated immediately after optogenetic activation (Figure 3.17 (D), (E), (F)), Rac being activated afterwards and

only in the protruding phenotype (Figure 3.17 (G), (H), (I)), most probably due to the positive feedback between Cdc42 and Rac [de Beco et al., 2018]. It also confirmed that Cdc42 was activated in both phenotypes just after the optogenetic recruitment but kept being activated only in the case of the protruding phenotype, which suggests a probable inhibition in the retracting phenotype.

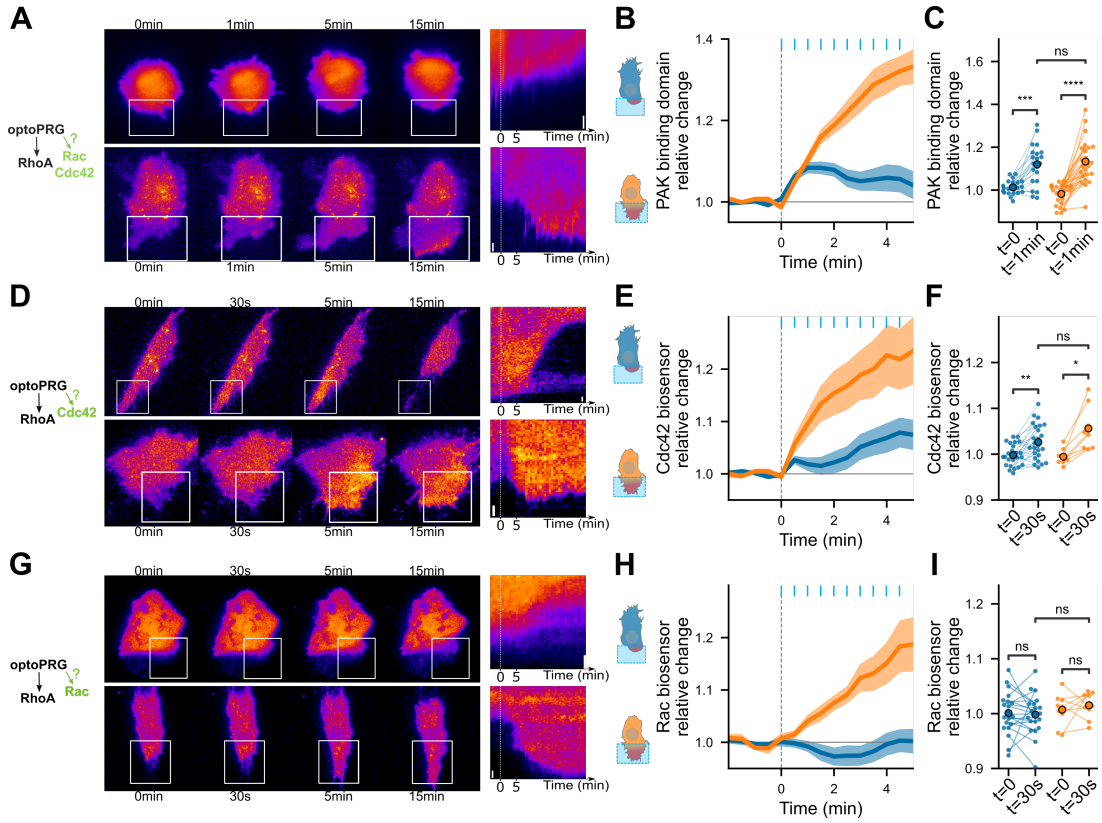

Figure 3.17: PRG activates Cdc42. Representative time-lapse images and kymographs (A),(D),(G) for representative cells labeled with PBD-iRFP (A), delCMV-mCherry-WaspGBD (D), and mCherry-3xp67Phox biosensor (G) (coming from [Nanda et al., 2023]), activated with optoPRG starting at t=0min. White rectangles are areas of optogenetic activation. Scale bars are 10 µm. Corresponding mean normalized intensities are plotted along time (mean ± sem) (B), (E) and (H). *P<0.05 **P<0.01, ***P<0.001, **** P<0.0001 (Wilcoxon test to compare before/after, independent t-test otherwise)

To confirm that it was indeed the activation of Cdc42 that was responsible for the protrusion, we performed an experiment with IPA3, a drug targeting PAK, one of the direct effector of Cdc42. We did a first optogenetic activation with a set of cells, in order to know their phenotypes, then incubated five minutes with 5 µM IPA3 and activated the cells again. A lot of cells rounded up, and none of them were able to protrude again, while retracting ones were often still able to retract (Figure 3.18 (A)). Some previously protruding cells were even able to change phenotype and retract after drug incubation (Figure 3.18 (B)). This confirmed us that activation of PAK through Cdc42 was required for the protruding phenotype to happen, but not for the retracting one.

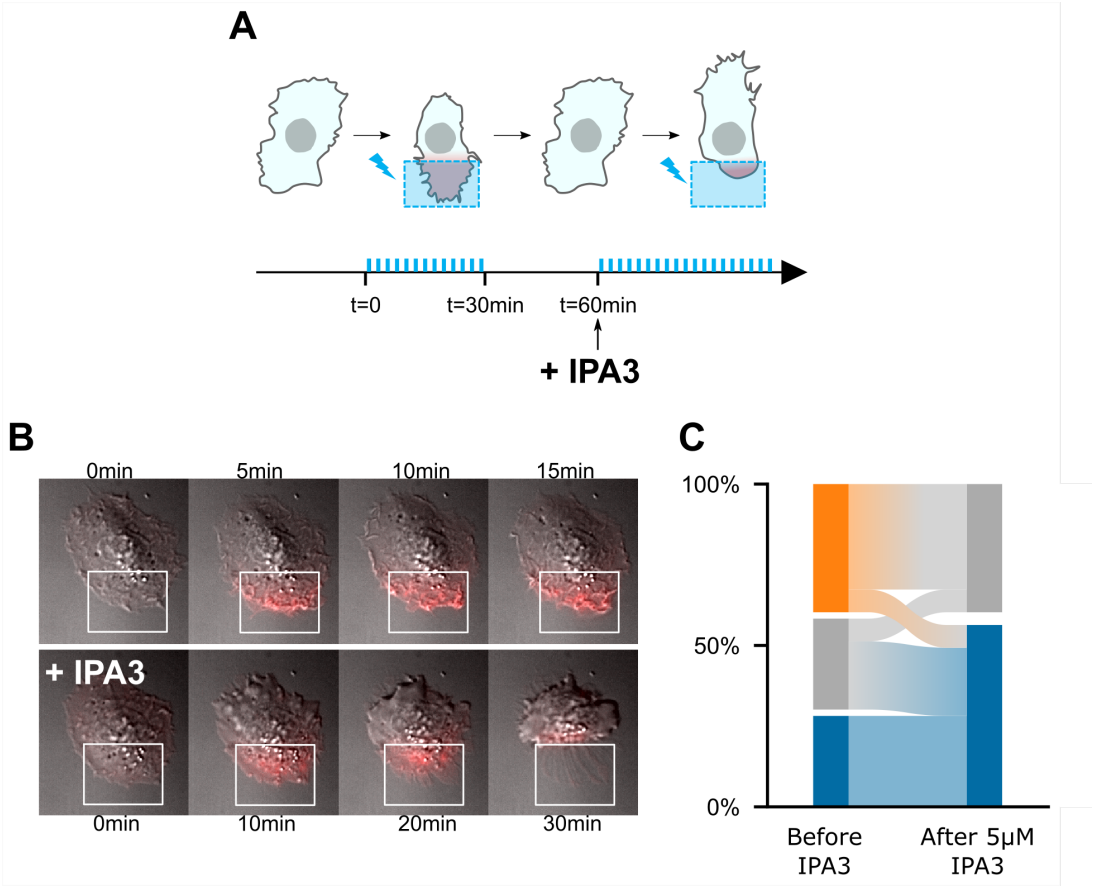

Figure 3.18: Inhibiting PAK triggers a phenotype switch. (A) Scheme describing the experimental timeline. Blue bars represent optogenetic pulses (every 30s). Half an hour after the first experiment, IPA3 is added at 5 µM. (B) Representative cell showing a protruding phenotype with ruffles (top), and a retracting phenotype after addition or IPA3 (bottom). (C) Quantification of phenotype switches for N=28 cells.

3.6 An effective model recapitulates reaction kinetics and enables a control of both phenotypes in the same cell

Given the complexity of all interactions happening, we sought for a minimal model that would capture the simple dependence of the phenotype with optoPRG concentration, as well as the biosensors dynamics.

Let us summarize the different facts that are essential to the model:

- Two opposite polarization phenotypes can be triggered by the recruitment of the same DH-PH domain of PRG at the membrane, in the same cell line, which means in the same biochemical environment.
- Phenotype can be predicted by the absolute concentration of the DH-PH domain of PRG before activation independently of the recruitment. This means that overexpression has an influence on cell state, defined as protein basal activities or concentrations before activation.
- RhoA, the direct effector of PRG, is activated in the retracting phenotype, but its activation is delayed in the protruding one.
- PH domain binding to RhoA-GTP is required for protruding phenotype but not sufficient, and it is acting as an inhibitor of RhoA activity.
- the DH-PH domain of PRG activates Cdc42, which is required for protruding phenotype.

To keep it as simple as possible, we considered that the resulting phenotype was the result of a competition between the relative amount of RhoA-GTP and Cdc42-GTP during the first 2 minutes, roughly the time when phenotypic changes start to be seen. Reaction are modeled as mass action kinetics happening at the area of activation - even for enzymatic reactions with the GEF. The latter is justified if the reaction is happening far from saturation and seems to be the case for GEFs or RhoA at least in another example [Kamps et al., 2020]. We considered the optogenetic recruitment as a variation of the total amount of PRG (noted G_{tot}) in this area, without modelling the complex interactions with the membrane. As described above, three interactions of PRG will be considered : the interaction with RhoA-GDP inducing a switch to RhoA-GTP, the interaction with Cdc42-GDP inducing a switch to Cdc42-GTP, and the interaction of the PH domain with RhoA-GTP. This last reaction gives rise to a complex (noted GR) that is inhibiting RhoA activity, but doesn't prevent GEF activity, as shown in [Chen et al., 2010].

This leads to three different reactions:

(a) $\mathrm{RhoA^{GDP}} \underset{\mathrm{k_2}}{\overset{\mathrm{k_1 \cdot G_{tot}}}{\rightleftharpoons}} \mathrm{RhoA^{GTP}}$, with typical concentration $K_a = \frac{k_2}{k_1}$

(b) $\mathrm{RhoA^{GTP}} + \mathrm{G} \underset{\mathrm{k_4}}{\overset{\mathrm{k_3}}{\rightleftharpoons}} \mathrm{GR}$, with typical concentration $K_b = \frac{k_4}{k_3}$

(c) $\mathrm{Cdc42^{GDP}} \underset{\mathrm{k_6}}{\overset{\mathrm{k_5 \cdot G_{tot}}}{\rightleftharpoons}} \mathrm{Cdc42^{GTP}}$, with typical concentration $K_c = \frac{k_6}{k_5}$

To which we can add three conservation equations for the concentrations :

- $R_{tot} = RhoA^{GDP} + RhoA^{GTP} + GR$

- $G_{tot} = G + GR$
- $Cdc42_{tot} = Cdc42^{GDP} + Cdc42^{GTP}$

which leads to the following system of equations, with R and C being respectively Rho^{GTP} and $\text{Cdc42}^{\text{GTP}}$ concentrations :

$$\begin{cases} \dfrac{dR}{dt} = k_1.G_{tot}(R_{tot} - R - GR) - k_2R - \dfrac{dGR}{dt} \\ \dfrac{dGR}{dt} = k_3R(G_{tot} - GR) - k_4GR \\ \dfrac{dC}{dt} = k_5G_{tot}(C_{tot} - C) - k_6C \end{cases} \tag{3.6.1}$$

We added few hypotheses, to reduce the number of unknown parameters:

- many GAPs are common to Cdc42 and RhoA ([Müller et al., 2020]), we considered the deactivation rates to be similar: $k_2 \approx k_6$.
- GTPases activated with strong stimuli -giving rise to strong phenotypic changes- lead to only 5% of the proteins in a GTP-state, both for RhoA and Cdc42 ([Pertz, 2010], [Benard et al., 1999], [Ren et al., 1999]. Therefore, we assumed that $Cdc42^{GTP} << Cdc42_{tot}$ and $RhoA^{GTP} << RhoA_{tot}$, even at high concentrations of optoPRG. We also considered that a few proportion of both optoPRG and RhoA^{GTP} were in complex, so that $GR << RhoA_{tot}$ and $GR << G_{tot}$.
- As we saw that the inhibition of RhoA by the PH domain or optoPRG was much faster than the activation of RhoA (see Figure 3.14), we considered that reaction (2) was constantly at equilibrium. Thus, the complex GR can be expressed as a function of G_{tot} and R (which will both evolve in time), as the following: $GR(t) = \dfrac{G_{tot}(t)R(t)}{K_b}$

With these hypotheses, before optogenetic activation, we have the following equilibria:

$$\begin{cases} R_{eq} = \dfrac{G_{eq}R_{tot}}{K_a} \\ GR_{eq} = \dfrac{G_{eq}R_{eq}}{K_b} \\ C_{eq} = \dfrac{G_{eq}C_{tot}}{K_c} \end{cases} \tag{3.6.2}$$

with $G_{tot}(t < 0) = G_{eq}$.

Introducing new variables $r = \frac{R}{R_{eq}}$, $c = \frac{C}{C_{eq}}$, $gr = \frac{GR}{GR_{eq}}$ and $g = \frac{G_{tot}}{G_{eq}}$ leads to the much simpler and independent equations :

$$\begin{cases} \dfrac{dr}{dt} = k_2(g - r) - \dfrac{GR_{eq}}{R_{eq}}.\dfrac{dgr}{dt} \\ \dfrac{dc}{dt} = k_2(g - c) \end{cases} \tag{3.6.3}$$

Equation describing RhoA dynamic

As gr is a product of two functions of t, r and g, $\frac{dgr}{dt}$ will be expressed as a function of r and $\frac{dr}{dt}$. Thus, we obtain, for the evolution of r, the following equation:

$$\frac{dr}{dt} = \frac{1}{1 + \frac{G_{eq} * g}{K_b}} \left(k_2(g - r) - \frac{G_{eq} * r}{K_b} \frac{dg}{dt} \right)$$

This gives for this equation only two unknown parameters : on the one side, k_2, and on the other side, $\frac{G_{eq}}{K_b}$ which will be the free parameter changing from one cell to the other, due to the difference in optoPRG transfection (see Figure 3.19).

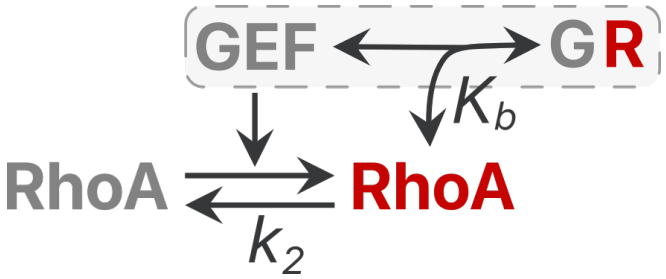

Figure 3.19: Interactions considered in the model. RhoA switches between an active (red) and inactive (grey) state, with a deactivation rate k_2 and an activation rate proportional to the total GEF concentration (GEF + GR). Active RhoA can also bind to the GEF, giving a complex GR, with a dissociation constant equal to K_b.

To evaluate k_2, we considered the measurements made with the biosensor of RhoA activity. This biosensor will have its intrinsic dynamic with a k_{on} and a k_{off}. Considering that only a small portion is bound to RhoA^{GTP} at any moment, the dynamic of the biosensor will follow the one of RhoA^{GTP} with a delay, given by k_{off} in the following equation :

$\frac{dbs}{dt} = k_{off}(r - bs)$ with bs the relative changes in the biosensor intensity.

k_2 and k_{off} can be estimated independently. When the PH domain is recruited alone, if we consider that the endogenous activities of GEFs and GAPs are slow compared to the binding of the PH to RhoA^{GTP}, we obtain $1 - rt \propto 1 - ph$ with ph the relative amount of PH domain. Thus, k_{off} can be fitted independently of the k_2 here. We can the see one of the fitted curve in Figure 3.20 (right), and calculate the mean fitted k_{off} over repetead experiments, which gives $k_{off} = 0.08 \pm 0.4 s^{-1}$

We can estimate k_2 by looking at cells with a very low concentration of optoPRG. In these cells, we expect the formation of the complex to be negligible compared to the activation of RhoA by the PH domain. Thus, the evolution of r will be given by the simple equation:

$\frac{dr}{dt} = k_2(g - r)$

Taking the mean value of the k_{off} found above, we can fit three different dynamics in three different cells with low concentration, as shown in 3.21, which gives a $k_2 = 0.014 \pm 0.003 s^{-1}$. As seen here, this very simple model seems to well represent the data that we get by inducing pulses of RhoA activity at low concentration (Figure 3.21, (B), (C) and (D)).

As stated above, this lets us with one free parameter for the equation describing the evolution of RhoA^{GTP}, G_{eq}/K_b, which will be the parameter changing from cell to

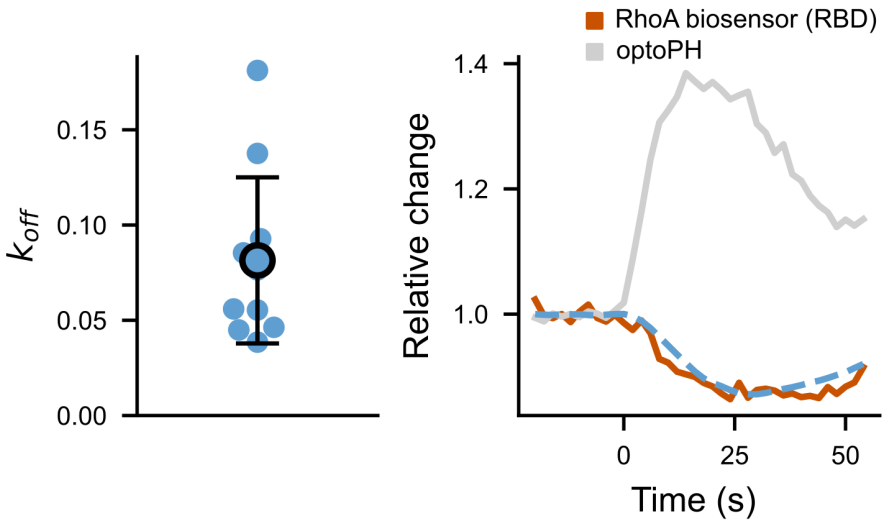

Figure 3.20: Fitting the k_{off} of the biosensor. On the left, the k_{off} as fitted for different cells (N=3 cells, with repeated measurements) gives a mean of $0.08s^{-1}$ and a standard deviation of $0.04s^{-1}$. On the right, an example of a fitted RBD curve (fit in blue, data in brown), plotted together with the normalized optoPH recruitment (gray curve)

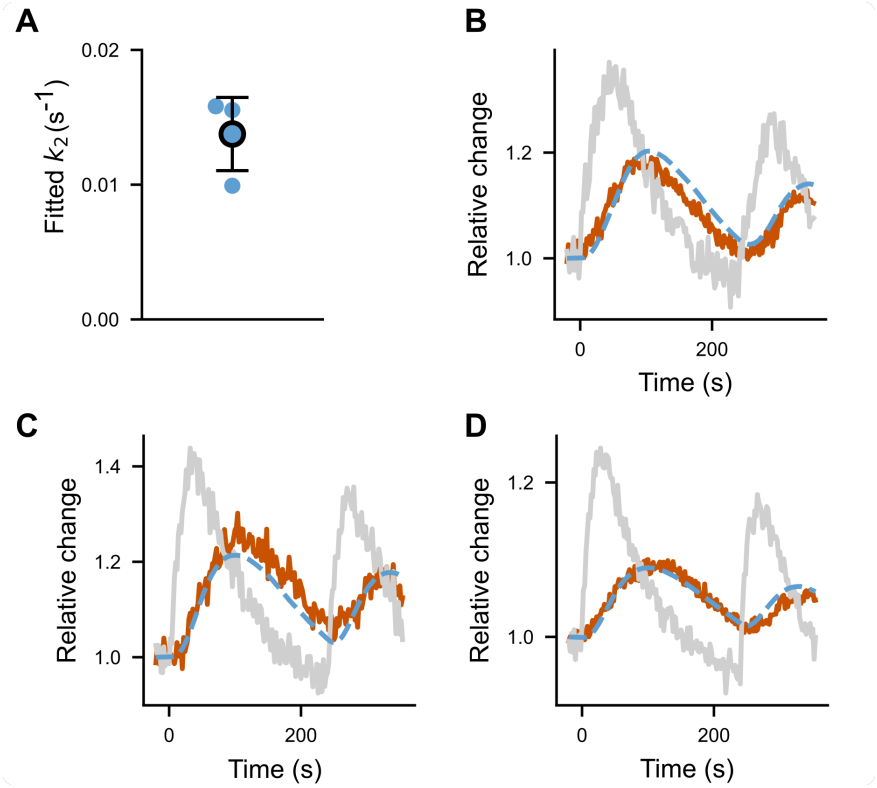

Figure 3.21: Fitting k_2 of the biosensor. (A) k_{off} as fitted for different cells (N=3 cells) gives a mean of $0.014s^{-1}$ and a standard deviation of $0.003s^{-1}$. (B), (C), (D) the three fitted curves (fit in dotted blue, data in brown), plotted together with the normalized optoPH recruitment (gray curve)

cell, due the different intensities of transfection. Can we recover the different behaviors of the biosensor seen in Figure 3.13 by moving this single parameter? Taking the two mean values of k_{off} and k_2 fitted above, we could, by changing only the ratio G_{eq}/K_b, recapitulate very different dynamics we had seen with the RBD biosensor, as shown on Figure 3.22 (A). Indeed, we recover the behavior of low transfected cells (low G_{eq}/K_b) where only the activation of RhoA is present, the behavior of highly transfected cells (high G_{eq}/K_b) where the recruitment of optoPRG leads to a inhibition of RhoA, and the behavior of cells with medium transfection, where complex dynamics with both inhibition and activation could be very well fitted.

As shown on Figure 3.22 (B), some dynamics could not be completely described with this model. These cells had a response in RhoA^{GTP} activity much stronger that the one expected from the model. This may mean the presence of an autoamplification process happening in some cases, which was not taken into account in the model.

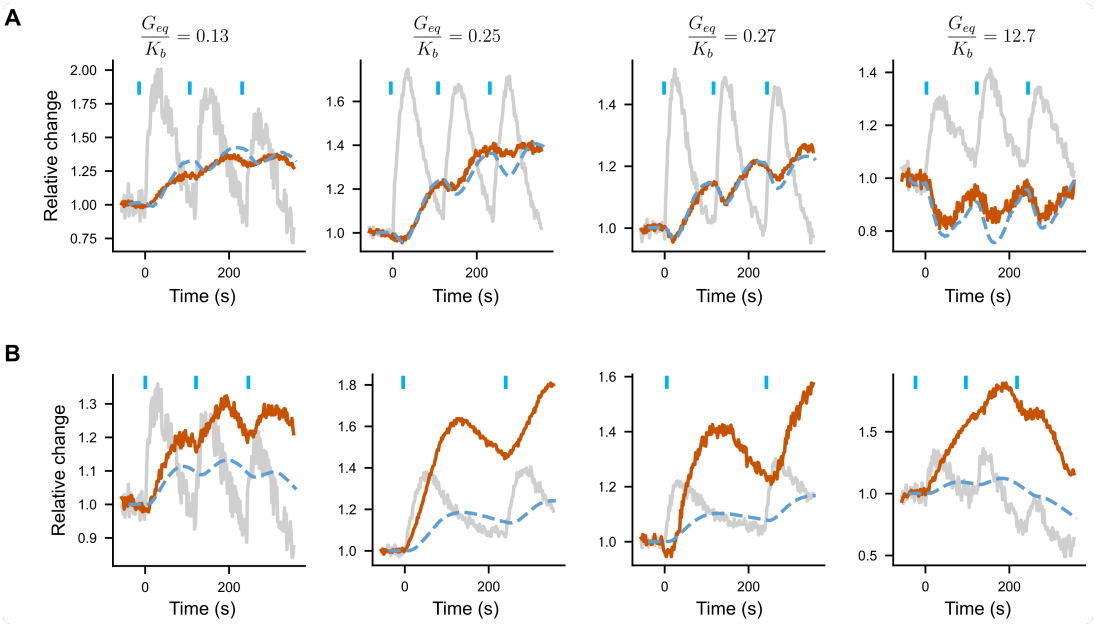

Figure 3.22: Fitting very different dynamics of RhoA activity with only one parameter. (A) Curves where the dynamic of RhoA activity is very well recapitulated by the model. (B) Curves where the dynamic of RhoA activity are less well recapitulated by the model; chosen value for G_{eq}/K_b is 0.001 for all these plots. For all plots, relative changes of optoPRG (in gray) and RhoA biosensor (in orange) are shown. Normalized by the mean intensity before the first activation, which corresponds to t=0.

Despite its limitation, we can consider the model describing RhoA response to optoPRG recruitment as a good representation of what is happening at both low and high concentrations of optoPRG.

Modeling the dual phenotype

Let us look now at RhoA and Cdc42 responses during five minutes with simulated optoPRG inputs comparable to the one of the experiments. For $\frac{G_{eq}}{K_{tot}}$, we choose values ranging between the extreme boundaries found in 3.22 (A). RhoA activity dynamic will vary depending on the value of $\frac{G_{eq}}{K_{tot}}$, while Cdc42 activity dynamic will stay the same 3.23.

As stated above, the activity of RhoA will be in competition with the activity of Cdc42, that is also activated by optoPRG. The resulting phenotype will be a retrac-

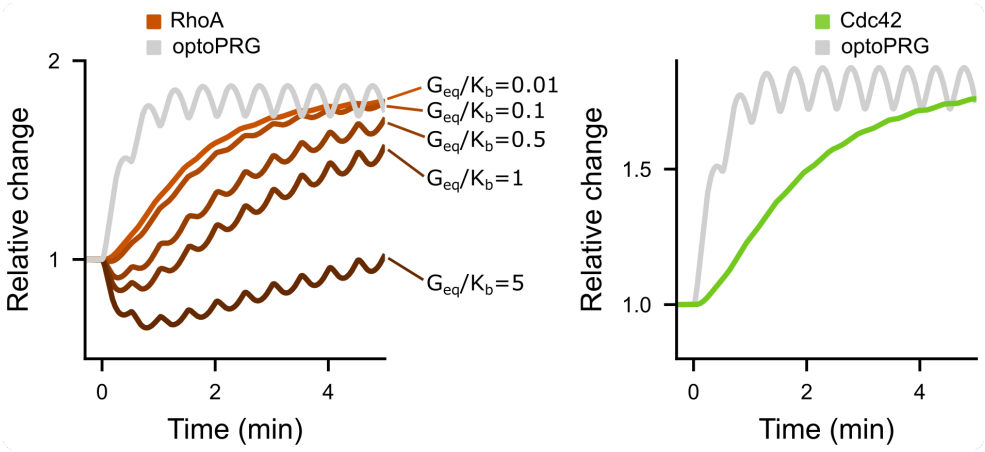

Figure 3.23: Activities of RhoA and Cdc42 depending on G_{eq}/K_b. On the left, activity of RhoA is plotted in red, for the given input function g(t) in grey. Values of G_{eq}/K_b are ranging from 0.01 to 1.

tion if the total increase of RhoA^{GTP} is superior to the total increase of $\text{Cdc42}^{\text{GTP}}$, with an unknown factor α that represents the efficiency of both GTPases to produce their specific phenotype. As we saw that the resulting phenotype was determined two minutes after the first activation, we choose this time point as the one where the other cellular processes and feedbacks take over. Thus, we compared the integrated activities of RhoA and Cdc42 during the two first minutes after activation. This gives the following conditions:

$$\begin{cases} \int_0^2 (R - R_{eq})dt > \alpha \int_0^2 (C - C_{eq})dt \implies retraction \\ \int_0^2 (R - R_{eq})dt < \alpha \int_0^2 (C - C_{eq})dt \implies protrusion \end{cases} \tag{3.6.4}$$

We can define $\alpha' = \alpha \frac{C_{tot} K_a}{R_{tot} K_c}$ to have the new condition :

$$\begin{cases} \gamma > 0 \implies retraction \\ \gamma < 0 \implies protrusion \end{cases} \tag{3.6.5}$$

with $\gamma = \int_0^2 (r - 1)dt - \alpha' \int_0^2 (c - 1)dt$

At low concentrations, r and c have the same dynamic, while the phenotype is always a retracting phenotype. Therefore, we expect α' to be lower than one.

For this type of activation, we saw that the switch between retracting and protruding phenotype was happening for $\frac{G_{eq}}{K_b} \approx 0.5$. Thus, we choose $\alpha' = 0.24$ so that $\gamma(\frac{G_{eq}}{K_b} = 0.5) = 0$. We also added a 'gray zone' around 0, where the cell would not do anything or do a mixed phenotype, because activity of RhoA and Cdc42 are equivalent. This gray zone will be materialized by an arbitrary constant value 3 a.u., such that $|\gamma| < 3 \implies mixed\ phenotype$.

We can now plot γ as a function of G_{eq}/K_b, which is shown on the Figure 3.24. γ is a simple decreasing function of G_{eq}/K_b, crossing 0 at $G_{eq}/K_b = 0.5$: the cell is retracting below this value, and it is protruding above.

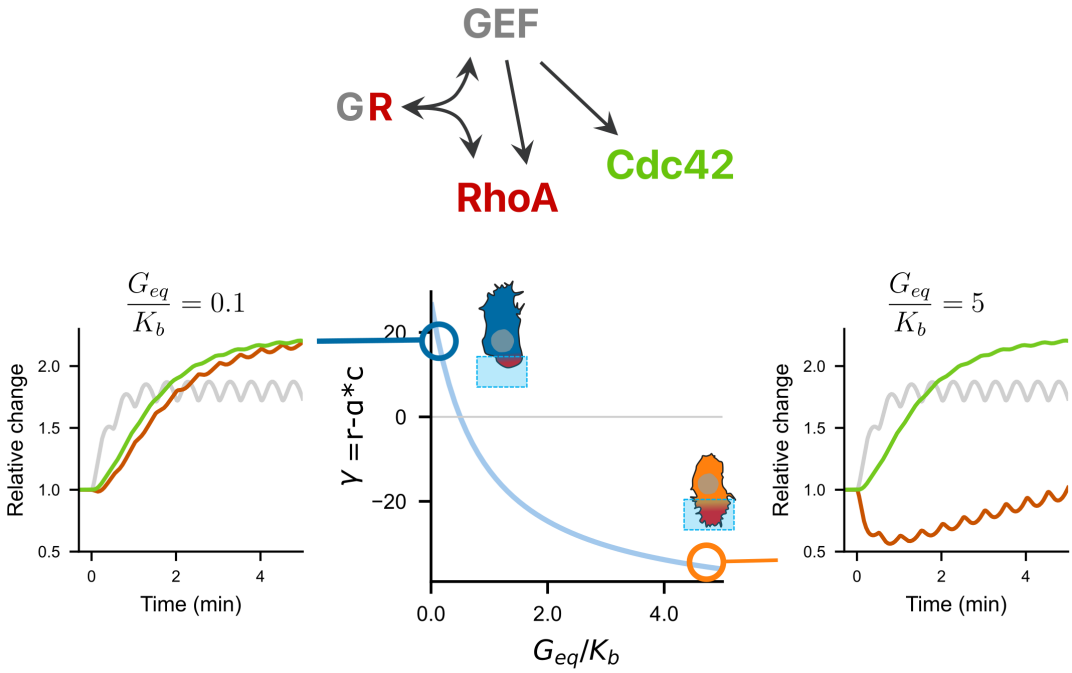

Figure 3.24: Model for antagonist phenotypes. Top, scheme of the found activities: the GEF PRG can activate both RhoA and Cdc42, but can also inhibit RhoA by directly binding to it. Bottom, center, γ, which corresponds to the difference between the activity of RhoA and Cdc42, is plotted in function of the free parameter G_{eq}/K_b. y=0 defines the limit between protruding (y<0) and retracting (y>0) cells. Two representative dynamics are shown on the right and on the left for the same input g(t), for a low and high G_{eq}/K_b.In grey, optoPRG recruitment to the membrane, in green, Cdc42 activity, in red, RhoA activity.

Predictions for changes in activation parameters

Now that we have an effective model of protrusion and retractions, we can start to change the patterns of activation, which is one of the main advantages of optogenetics. Indeed, two main parameters can be varied to control the input function $g(t)$. The first one is the frequency of the light pulses, the second one is the duration of the light pulse or intensity of the light, which will have an influence on the intensity of the recruitment. The dynamic range in which these parameters can vary depends on the optogenetic tool, on the optogenetic setup, and on time recruited protein. How will these two parameters influence the function γ?

We first looked at the impact of the duration of the pulse, which has an influence on the fold increase of the function g after one pulse of activation. With this imaging set-up -in HILO microscopy-, we could measure fold increases ranging from 1.1 (to be measurable) to 3 for one pulse of activation, depending on the cell. We can see the result of the variation of the phenotype depending on the intensity of the pulse and G_{eq}/K_b on Figure 3.25. In our model, no cell was able to switch from retracting to protruding or vice versa by only changing the intensity of the optogenetic pulse (changing x on the figure). It seems that increasing the light intensity can only increase the strength of the phenotype (going from a grey-blue zone to a blue zone for example), but not the type of the phenotype.

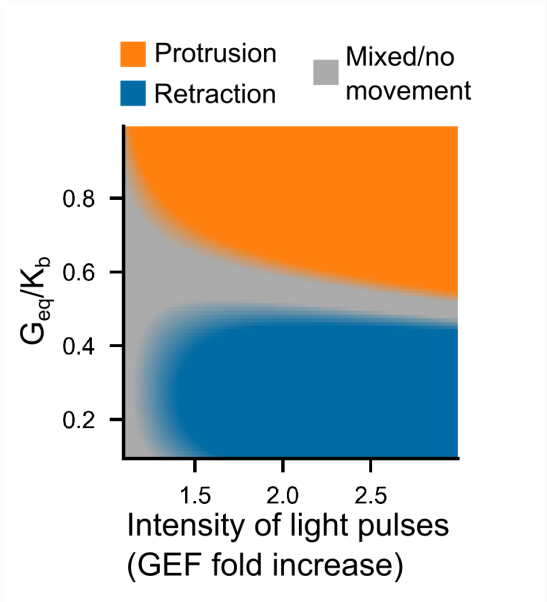

Figure 3.25: Phenotype in function of the pulses intensity and G_{eq}/K_b. Protruding (orange), retracting (blue) or mixed (grey) phenotypes are represented in function of the free parameter G_{eq}/K_b (y-axis) and the intensity of the optogenetic pulses, represented by the fold increase on the x axis.

Then, we looked at the influence of the frequency of the light pulses on the phenotype. We calculated the function γ for different input fuctions g(t) with different frequencies, normalized by the total recruited GEF for two minutes to have the frequency as the single varying parameter. We show on Figure 3.26 (A) how the frequency of the pulses alone influences the phenotype at different concentrations of G_{eq}/K_b. As can be seen on Figure 3.26 (A), few values of G_{eq}/K_b seem to be compatible with both phenotype by varying only the frequency, but much more than with the variation of intensity. These values are the one around 0.5, where the values of *gamma* tend to be

small, making the cell fall in the 'mixed phenotype' category. However, in these mixed cells, the model predicts that high frequency leads to more protruding phenotypes, while low frequencies lead to more retracting phenotype.

To confirm this prediction of cells where both phenotypes could be controlled by the frequency, we searched for cells with the following protocol. First, we looked for cells ranging from 15 to 35 in the arbitrary units of Figure 3.10, thanks to an automated cell finder (see 6.2.5). Second, we started with a strong activation every 60 seconds and checked the phenotype. We disgarded all cells that had a mixed phenotype or were too clearly protruding. Third, we activated every 30 seconds and checked the phenotype. When the cell was still retracting or had a mixed phenotype, we reduced again the duration between pulses and activated every 15s.

With this protocol, we confirmed two things. First, it seems that very few cells can really be controlled for the two phenotypes, at least with this optogenetic dimer. Indeed, out of $\approx$ 90 cells we preselected, only three two clearly different phenotypes, while a majority displayed a mixed phenotype similar to Figure 3.3 (E) when changing the frequencies of activation. Second, it is still possible to have these both phenotypes in the same cell, and decreasing the time between the pulses leads to more retraction. We show one example on Figure 3.26 (B).

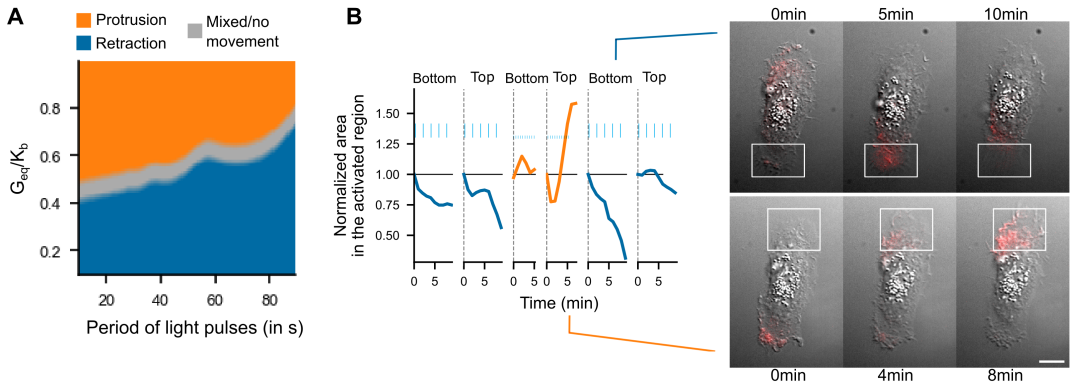

Figure 3.26: Controlling antagonist phenotypes by varying the frequency. (A) Protruding (orange), retracting (blue) or mixed (grey) phenotypes are represented in function of the free parameter G_{eq}/K_b (y-axis) and the duration time between two pulses (x axis). (B) One example of two phenotypes controlled in the same cell. On the left, first ten minutes of the cell trajectory for different frequencies of activation and intensities. Area activated is marked on the top, low frequency (blue bars more sparsed): every 30s, high frequency (blue bars close together): every 15s. On the right, two representative timelapse out of the six. Area of activation: white rectangle. Scale bar: 10µm.

3.7 Conclusion on the control of opposite phenotypes with one GEF of RhoA

To conclude, this model recapitulated the key features of the different observations and experimental results presented in this chapter. It did it with only two independently fitted parameter and one free parameter, as well as two effective constants comparing Cdc42 and Rho1 activity, and the link with the phenotype of the cell. It was sufficient to reproduce faithfully the complex dynamic of the RBD biosensor, and to understand the change of phenotype due to the concentration. It also predicted that

some cells could show both phenotype with changes in the frequency of optogenetic pulses.

The model can be summarized with the following figure (Figure 3.27(A)). At low concentration of the GEF, both RhoA and Cdc42 are activated by optogenetic recruitment of optoPRG, but RhoA takes over. At high GEF concentration, recruitment of optoPRG lead to both activation of Cdc42 and inhibition of already present activated RhoA, which pushes the balance towards Cdc42. In the end (Figure 3.27(B)), optogenetic modulation of PRG can be seen as moving the balance between RhoA and Cdc42 depending on the basal state (blue zone around the black curve in Figure 3.27(B)). This means that only the cells in good concentration range can use the same protein to control both antagonist responses.

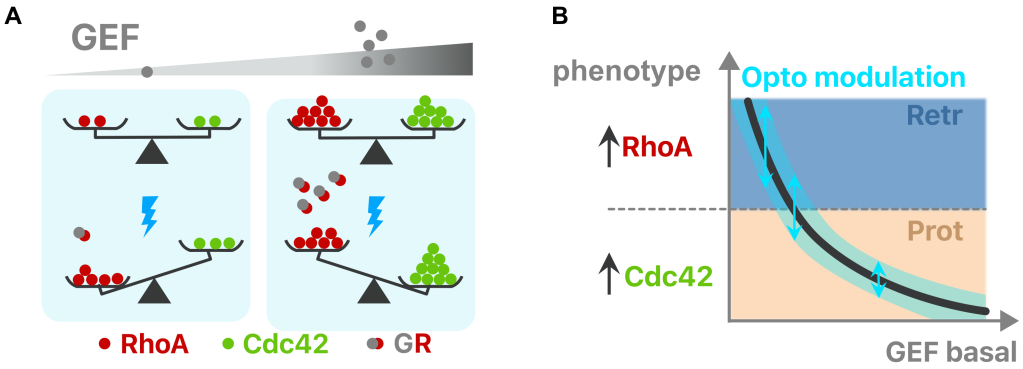

Figure 3.27: Graphical conclusion on the model. (A) Balance between RhoA and Cdc42 activity is represented in function of GEF basal concentration (grey gradient), both at the basal state (top) and after optogenetic activation (bottom, with blue lightning). At low concentrations RhoA takes over. At high concentration, optoPRG binds to active RhoA and inhibits it (complex GR), which enables Cdc42 to take over. (B) Curve showing the difference between RhoA and Cdc42 activity as a function of the basal intensity of the GEF. Phenotypes are marked with the colors (blue, retraction and orange, protrusion). Optogenetic modulation happens on vertical line, with the blue range, which limits the possibility of switching from one phenotype to the other.

Overall, this project has dissected in details a new type of pathway multiplexing. With one protein, here one part of a GEF of RhoA, we showed that we could control opposite phenotypes. We uncovered the molecular mechanisms behind these seemingly opposite responses and showed that a simple model with one free parameter could explain it. As the ability of one protein to multiplex is well known, it may be that this mechanism is a more general one. One could explain the changes in protein function in cancer with this simple example of changes in global concentration, a disscussion we will develop in the discussion chapter.

Chapter 4

Optogenetics to dissect collective amoeboid migration mechanism

The study presented in this chapter is part of a collaboration with the team "Collective invasion" of Fanny Jaulin in Institut Gustave Roussy, together with Mathieu Piel's team in Institut Curie and Raphael Voituriez's team in Laboratoire de physique théorique de la matière condensée. In the first section, I will introduce the work that has been mostly led by Diane-Laure Pagès and Emmanuel Dornier at Institut Gustave Roussy. I will present the physical model in the third section that has been developed by Ananyo Maitra and Raphael Voituriez. Both of these sections are fully published in [Pagès et al., 2022], as well as one part of my work presented in the second section. The experiments and analyses of the fourth section have been launched by me and further improved and analyzed by Romain Guignon during his internship under my supervision.

Fanny Jaulin's lab described few years ago groups of tumour cells able to perform collective invasion in 3D matrices, seemingly independent of focal adhesions and requiring contractility of the cell cluster [Zajac et al., 2018]. This suggested a collective amoeboid mode of migration, which had never really been described before, and motivated this strong interdisciplinary project between cell biology, microfluidics, and biophysical modelling.

4.1 Focal adhesions independent collective migration is driven by the contractility of the polarized cortex

Cancer cell clusters migrate in confined nonadhesive environments without requiring focal adhesions

To confirm the hypothesis of a focal-adhesion-independent mode of migration [Zajac et al., 2018], microchannels were designed and engineered at the appropriate size for cancer cell clusters to be multilayered but confined (Figure 4.1 (A)). These channels were coated with the anti-adhesive polymer polyethylene glycol (PEG) to avoid focal adhesion formation, and cell clusters with $\sim$ 50 to 100 cells were observed for 20 hours. A variety of cancer cells and cell lines were tested, revealing an ability of cell clusters to migrate with speeds up to 2mm/day (Figure 4.1 (B) and (C)). The cluster speed is in the order of magnitude of what has been reported *in vivo* for collective migration [Krndija et al., 2019]. As seen on the plotted trajectories in Figure 4.1,

moving clusters are persistent over hours, with a persistence of 0.75 ±0.01 over 20 hours.

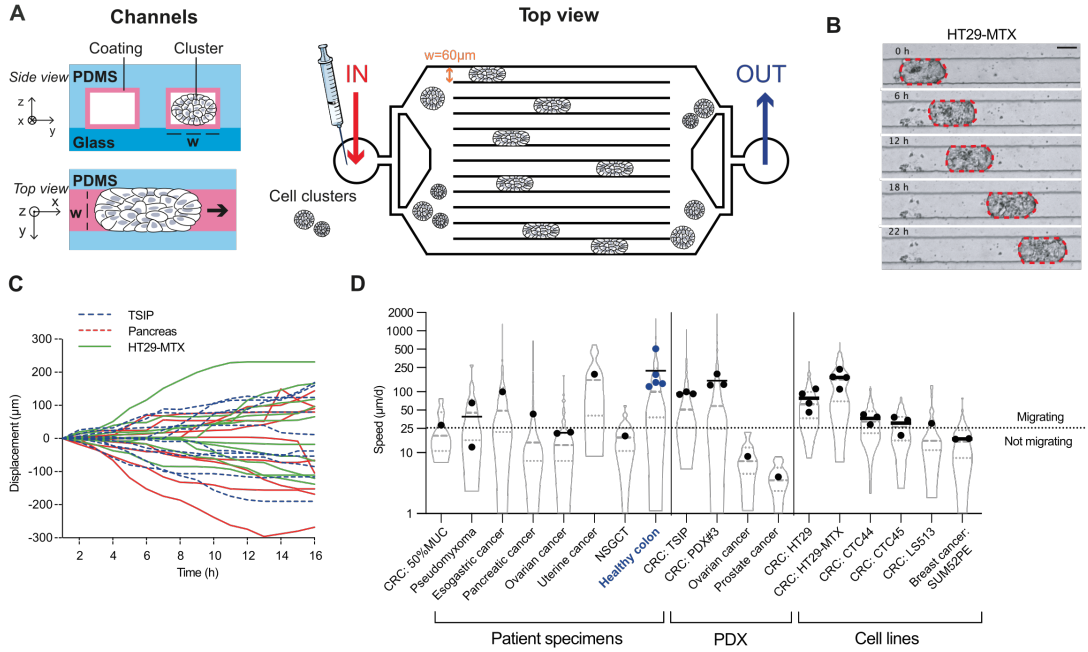

Figure 4.1: Cell clusters migrate in non adhesive microchannels. (A) Schematic representation of experimental setup. Taken from [Pagès et al., 2022]. (B) Representative tracks of clusters migrating in one direction (positive numbers) or the other (negative numbers). n=9 to 10 representative clusters of each cell type. Taken from [Pagès et al., 2022] (C) As an example, representative time-lapse sequences of the migration of HT29-MTX cell clusters. Scale bar, 50 µm. Taken from [Pagès et al., 2022]. (C) Mean instantaneous migration speed of diverse types of tumour clusters from patients (CRC: colorectal cancer, NSGCT: nonseminomatous germ cell tumour), Patient-derived Xenografts (PDXs) and cell lines (CTC: circulating tumour cells). Log10-scale. Dots are the mean speed over clusters for each independent experiment; lines are means over experiments. Taken from [Pagès, 2022].

For further mechanistic studies, HT29-MTX cell line (from colorectal cancer) was used. To check for focal adhesions, Turquoise–tagged paxillin has been expressed in HT29-MTX. Fluorescent paxillin was nearly absent in PEG-coated microchannels, compared with collagen-I-coated microchannels, and inhibition of two main regulators of focal adhesions, focal adhesion kinase and Src (with PF271 and SU6656, respectively, or saracatinib), did not slow down HT29-MTX clusters migrating in non adhesive microchannels. These results, among others, indicated that focal adhesions were not required for this mode of collective migration [Pagès et al., 2022].

Actomyosin cortex of migrating clusters is polarized and contractility is required for migration.

What forces drive migration in a non-adherent environment? In single-cell amoeboid migration, the actomyosin cortex has been shown to generate anterior-posterior flows, and transient interactions with the substrate transmit forces that allow cells to move (see 1.4.3.2). F-tractin and Turquoise-labeled myosin light chain (MLC) were imaged in HT29-MTX in Fanny Jaulin's lab. A distinct supracellular actomyosin cortex was evident in all clusters, which differed between non-moving and moving clusters (Figure 4.2 (A)). Whereas the cortex in static clusters were similar on both sides,

moving clusters showed a twofold accumulation toward the back during the migration period, with the front/back polarity correlated with the migration speed (Figure 4.2 (B) and (C)).

Pharmacological inhibition of Myosin-II activity by blebbistatin and ROCK activity by Y27632 further confirmed the role of actomyosin contractility in cluster migration. It significantly reduced the migration speed of cell clusters. This inhibition was accompanied by partial or complete abolition of myosin localization at the cortex in HT29-MTX clusters (Figure 4.2 (D), (E) and (F)).

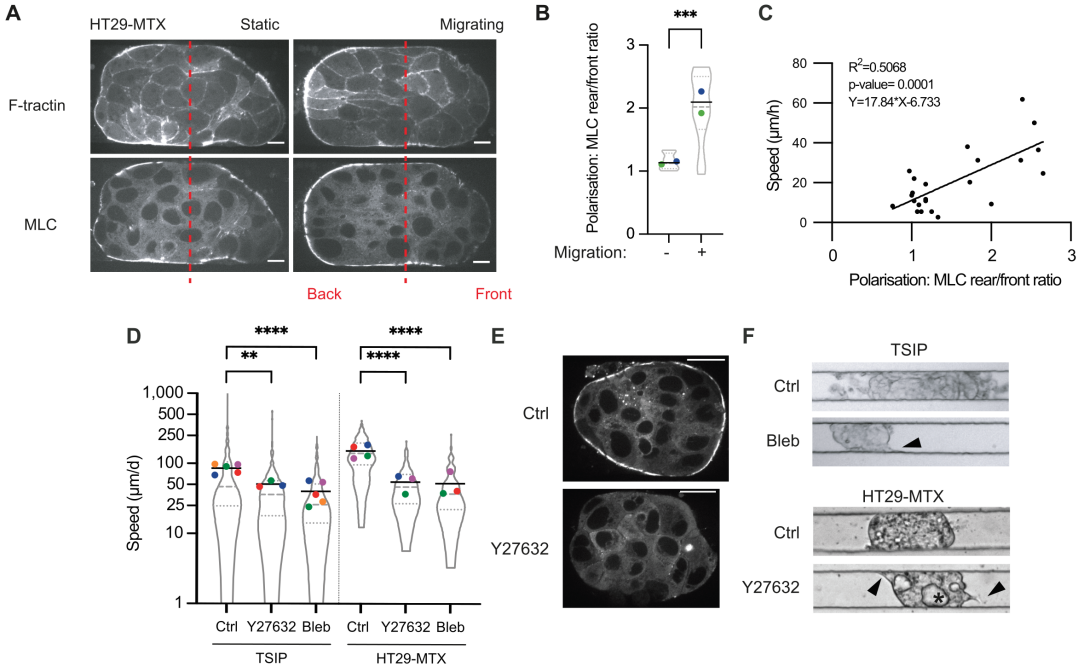

Figure 4.2: Actomyosin polarity of migrating cell clusters. (A) Median section of HT29-MTX stably expressing F-tractin-mRuby3 (top) and mTurquoise-MLC (bottom), in PEG-coated channels. Red dashed lines separate the front and back of clusters for quantification of ratio in b, Scale bar, 10 µm. b, Polarization of clusters as MLC (Myosin Light Chain) ratio between rear and front of the clusters migrating in PEG-coated microchannels. n=12 to 13 clusters. (C) Mean instantaneous speed and polarization of clusters, with linear regression. n=23 clusters from 3 independent experiments. (D) Mean instantaneous speed of clusters treated with Y27632, Blebbistatin (Bleb) or DMSO (Ctrl), log10-scale. n=106 to 205 clusters (one-way ANOVA), **P<0.01, ***P<0.001, **** P<0.0001. (E) Representative images of myosin cortex in mTurquoise-MLC-expressing HT29-MTX clusters in control condition or after Y27632 treatment. (F) Representative images of cluster shape after Blebbistatin or Y27632 treatments. Arrowheads: protrusions; star: cavity. Taken from Pagès, 2022.

This suggests that actomyosin contractility is necessary in this form of collective migration, which is independent of focal adhesion, as in amoeboid single-cell migration. It also suggests that the polarity of the actomyosin cortex is responsible for the polarization of the cluster, leading to efficient, sustained migration. To prove this further, we decided to use optogenetics as a means to control actomyosin polarity and test whether it is sufficient for cluster migration polarity.

4.2 Optogenetic control of cluster polarity with RhoA and Rac1

Optogenetic control of actomyosin polarity has been done in the literature at different level in signaling pathways, but the most common strategy has been to recruit GEFs, activators of the GTPases (see 1.4.2.1), to the membrane. This recruitment leads to activation of the GTPases at the membrane, and triggers their downstream effectors. As explained in the introduction(1.4.2.1), two GTPases are most known for setting single cell migration polarity: Rac1, known for triggering branched actin polymerization at the front of single migrating cells, and RhoA, responsible for actomyosin contractility. As seen in the first chapter of the results (chapter 3), this simple scheme can be complexified, but still holds in many circumstances.

The idea consisted in triggering locally (at a subcluster level) the activity of RhoA or Rac, and see how it impacts the migration of the whole cluster (Figure 4.3). We expected actomyosin to be polarized by the optogenetic activation of RhoA or Rac, and therefore bias cluster migration polarity or speed, either by speeding it up, or by slowing it down or reversing its migration.

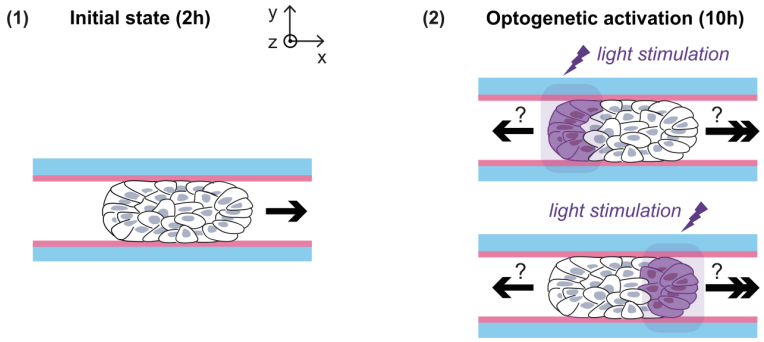

Figure 4.3: Scheme of the optogenetic experiments. Clusters are observed before optogenetic activation for 2 hours, and then activated at the front or the rear for 10 hours. Clusters are expected to change speed (double arrow) or direction (opposite arrow) upon optogenetic activation. Adapted from [Pagès et al., 2022].

As collective amoeboid migration is slow, experiments have to run for multiple hours. At the same time, optogenetic activation has to be local and take into account the cluster displacement. This leads to two experimental challenges:

- the first one is to maintain an optogenetic activation for hours without damaging the cells, and being still able to get multiple trajectories per experiment. This challenge was solved by using the optogenetic dimer CRY2-CIBN, which has a dimerization time of ~ 3 minutes, thus requiring a pulse of light every 2-3 minutes to maintain an activation.

- the second challenge comes from the cluster movement over a long period of time, and the need for local subcluster activation. To overcome it, I adapted a software previously developed in the lab, which performed microscopy stage displacement in order to follow single cells over a long period of time, associated with local optogenetic activation (see Materials and Methods 6.2.6 for more details).

With this in hand, I transduced HT29-MTX cells with the optogenetic dimer associated with different GEFs, creating stable cell lines. For RhoA, we used PDZ-RhoGEF

(also known as ARHGEF11) DH-PH domain that had been previously used to trigger actomyosin contractility [Valon et al., 2017] and LARG (also known as ARHGEF12) DH domain, that had been used also in other works with the iLid-Sspb dimer [O'Neill et al., 2018]. For Rac1, we used Tiam DH-PH domain that had been already used multiple times and proved to trigger Rac1 activation [de Beco et al., 2018]. As a control, tagged Cry2 alone was recruited to the plasma membrane, to take into account the effects of light exposure and recruitment of proteins to the membrane, as well as cell line selection. For all experiments, I looked at the migrating clusters for at least 1.5 hour before activating one side of the cluster, and compared the speed before and after activation.

4.2.1 RhoA activation can revert cluster polarity

Both cell lines with optoPRG (PDZ-RhoGEF DH-PH domain recruited to the membrane) and optoLARG (LARG DH domain recruited to the membrane) were selected by FACS (Fluorescence activated cell sorting) after transduction.

Results comparing the mean speed before and after activation can be summarized on the 2D graphs shown in Figure 4.4. If the optogenetic activation has no impact on the migration speed, dots lie on the y=x line. All clusters are activated on the left; thus, x<0 means that the cluster has been activated at the front, while x>0 means that the cluster has been activated at the rear. U-turns can be seen on top-left and bottom-right panes (respectively red and green). In the control, most of the clusters keep their migration direction and similar speed, there is little effect of the light alone on migration. On the contrary, activation of optoPRG has a strong effect on cluster migration. Most of the clusters activated at the front (x<0) reduce their speed, and a strong proportion will even completely change direction (red dots) (Figure 4.4 (A)).

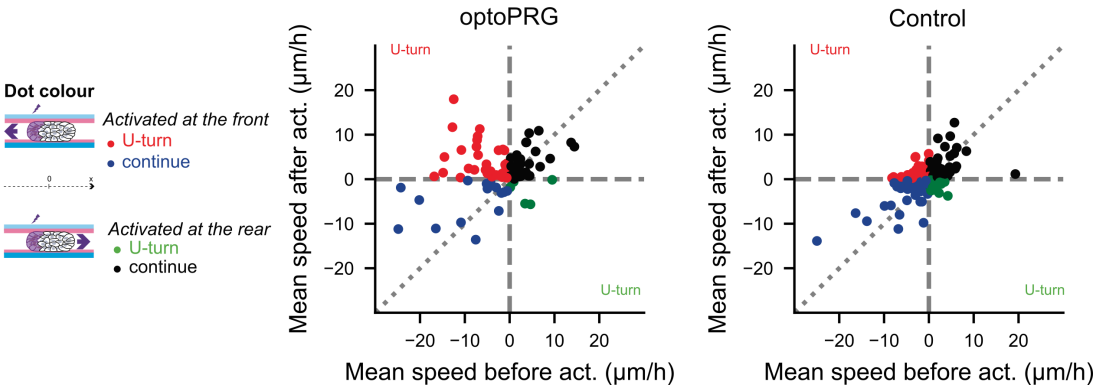

Figure 4.4: Mean velocity along the x-axis before (average over 1h30) and after (average over 10h) activation (act.) of optoControl and optoPRG clusters. n=119 (control), 88 (optoRhoA)

Looking at individual trajectories and time-lapse images of migrating clusters activated at the front, it was clear that optogenetic activation triggered strong U-turns, in two third of the clusters, that were almost never seen in optoControl cells (Figure 4.5). Visually, the optogenetic activation was immediately followed by a clear contraction of the clusters at the place of activation, revealing an increase in contractility.

To check that the optogenetic recruitment of PRG was associated with a change in the myosin polarization (thus, contractility), we transduced HT29-MTX optoPRG cell line with iRFP tagged MRLC (myosin regulatory light chain), allowing for simultaneous visualization during optogenetic activation. Looking at the evolution of the

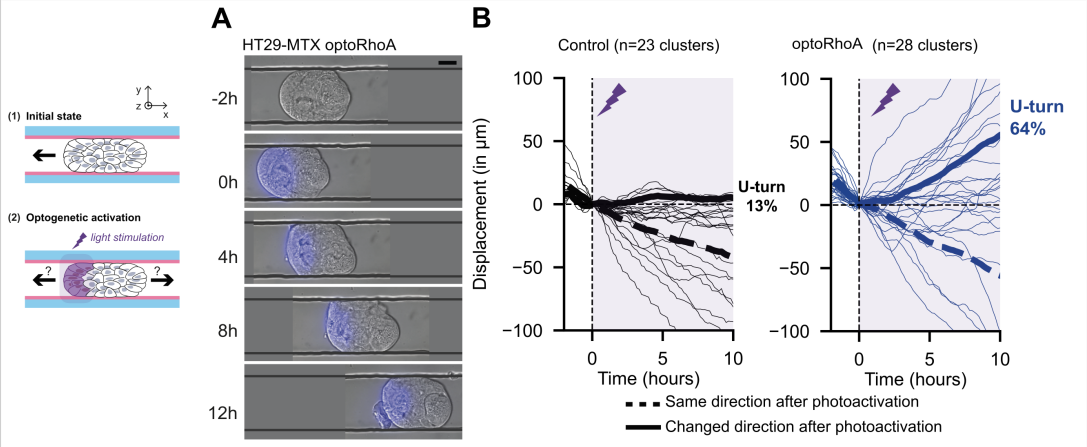

Figure 4.5: (A) Representative time-lapse sequences of a cluster making a U-turn upon activation (Scale bar, 20 µm). (B) Displacement of the clusters over time. Bold and dashed lines are means of trajectories changing direction or not, respectively. Purple zone: optogenetic activation. On the left, schematic of the experiment.

ratio between activated and not activated region of the cluster along time, we could confirm that the optogenetic activation was inducing a polarization of myosin activity toward the activated part, as expected (see Figure 4.6 (A) and (B)).

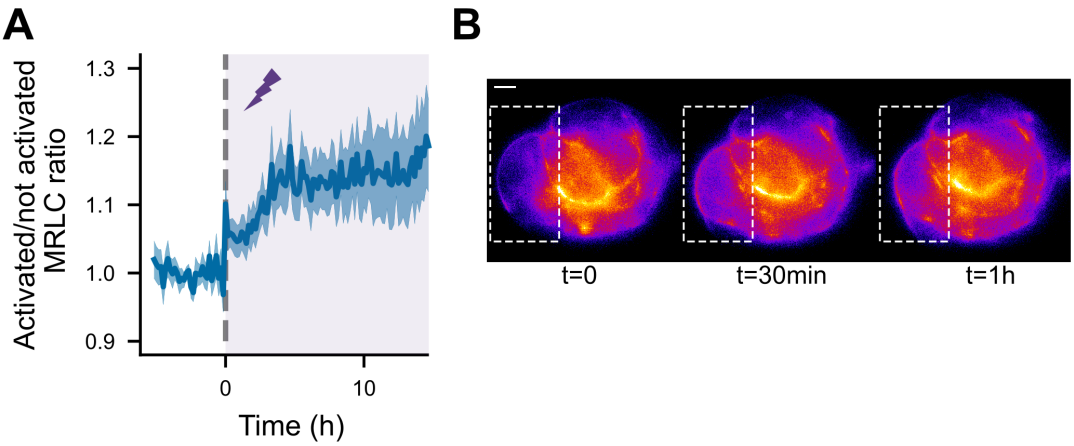

Figure 4.6: (A) Ratio between iRFP-tagged MRLC in the activated and not activated region of the cluster (mean ±sem). n=27.Purple zone: optogenetic activation. (B) Representative cluster shown at three different timepoints, before and after activation. Scalebar: 10µm, dashed rectangle: area of optogenetic activation

Clusters considered as static before the activation (moving less than 8µm for the two hours before) showed a clear bias after activation, with 81 % going in the opposite direction of the activation (Figure 4.7), compared to the control where no bias could be seen (52%, Figure 4.7). However, most of the clusters stayed in a very low migrating state compared to already migrating clusters - and comparable to the optoControl cells in term of speeds -, which indicates that optoPRG seems to be able to revert/orient an already existing migration, but not initiating it.

Surprisingly, experiments with optoLARG were much less convincing. The activation of optoLARG at one side had a strong contractile effect at the first point of activation. Indeed, a clear contraction could be seen, revealed by the little jump in

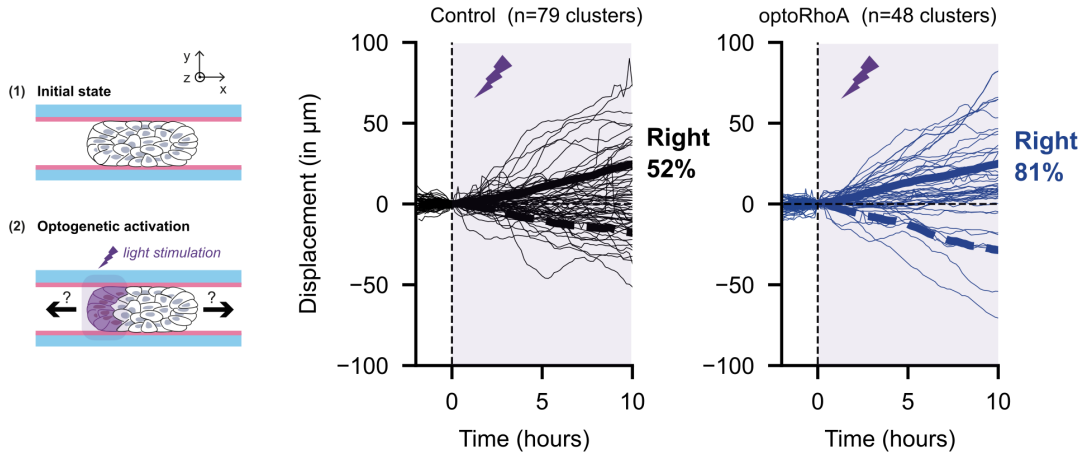

Figure 4.7: Reaction of static cluster to optogenetic activation. Displacement of the clusters over time. Bold and dashed lines are means of trajectories going to the right or to the left, respectively. Purple zone: optogenetic activation. On the left, schematic of the experiment.

most of the clusters right after activation, that we can see when looking at one cluster immediately after activation (see Figure 4.8 (A)). However, when comparing the speed after activation with the speed before, no particular effect of the activation could be seen (Figure 4.8 (C)), and only 26% of the clusters can be considered as doing a U-turn (Figure 4.8 (B)).

The reasons for this absence of influence of optoLARG can be multiple. First, as optoLARG has no PH domain, one amplification step is removed, and it could be that activation strength was not enough to trigger whole cluster polarization. Second, as optoPRG produces a high contractility basal state in the dark [Valon et al., 2017], it may be that this increase in contractility is important for being able to control polarity with RhoA. Third, it may be that signalling from optoLARG differs from the one of optoPRG, maybe by the effectors engaged.

Some experimental intricacies of these experiments are worth being mentioned here:

- for optoPRG, only approximately half of the cells were recruiting the dimer to the membrane upon blue light activation, despite very similar fluorescence intensities - which means very similar concentrations in both parts of the dimer. This seems hard to explain, as the non recruiting cells did not seem to have already membrane bound GEFs. One explanation could be a mutation in the CRY2 or CIBN that has been selected; however, repeating the transduction a second time with other cells gave the same proportion, as if some HT29-MTX had a way to block CRY2-CIBN dimerization upon blue light.

- for both optoLARG and optoPRG, I tried to have clonal cell lines. Coherent with the previous point, only half of the optoPRG cell lines were recruiting to the membrane. However, all the clonal cell lines were clearly impaired in their migration ability, leading to unexploitable results. Why is it so? As cluster movement relies on local fluctuations (see 4.3), it could be that heterogeneity favors these local fluctuations, which are removed when clusters are made out of clones.

- some of the experiments presented here have been performed with cells contaminated with mycoplasma -two out of the five experiments with optoPRG and two out of the four experiments with optoTiam. After having realized it, we

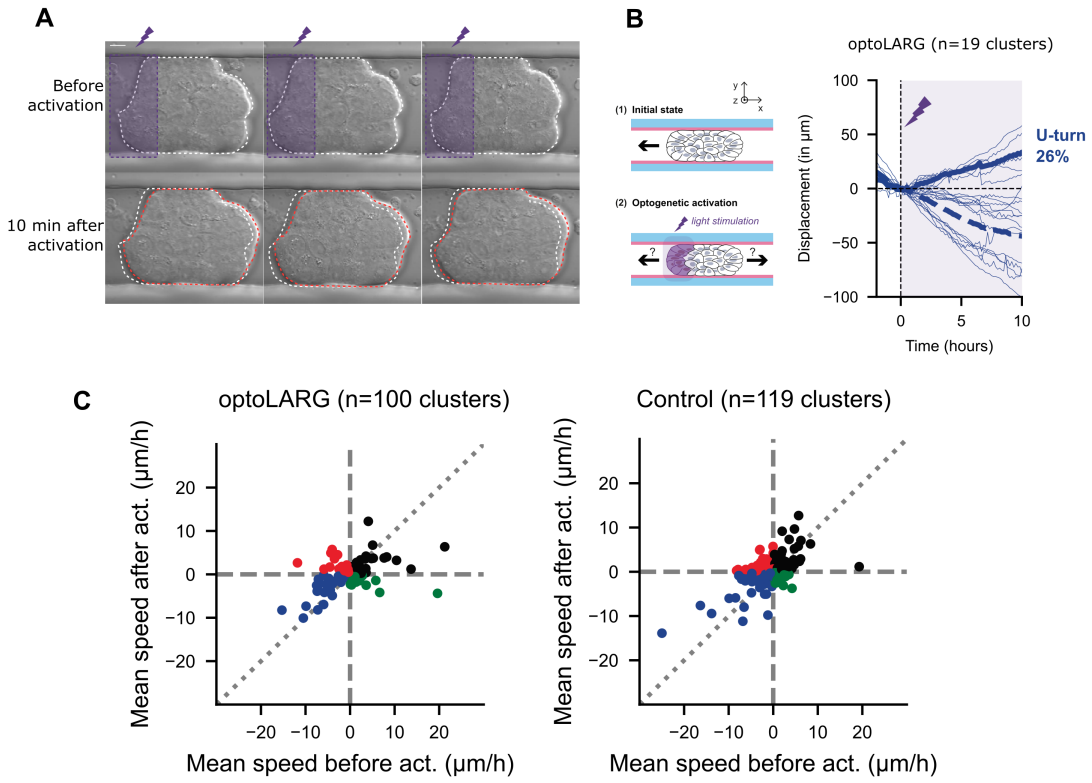

Figure 4.8: Reaction of optoLARG cluster to optogenetic activation. (A) Representative cluster activated at three different timepoints. Top, before activation. Bottom, 10 minutes after activation. Dashed line is the manual segmentation of the cluster before activation, to see the movement. Scale bar, 10µm. (B) Mean velocity along the x-axis before (average over 1h30) and after (average over 10h) activation (act.) of optoLARG and optoControl clusters. (C) Displacement of the clusters moving before activation and activated at the front. Bold and dashed lines are means of trajectories going to the right or to the left, respectively. Purple zone: optogenetic activation. On the left, scheme of the experiment.

checked that cell clusters were migrating with the same speed and with the same persistence than non contaminated cells. I also repeated all experiments at least twice. It seemed that mycoplasma had no effect on migration properties, so that all conclusions were holding.

4.2.2 Rac1 activation biases migration?

The cell line with optoTiam to control Rac activation showed very efficient cluster migration in the dark, with migration speeds that were above the ones of the controls (Figure 4.9). This suggests a leakage of the optogenetic tools, and tends to confirm that actin polymerization is key in this collective amoeboid mode migration.

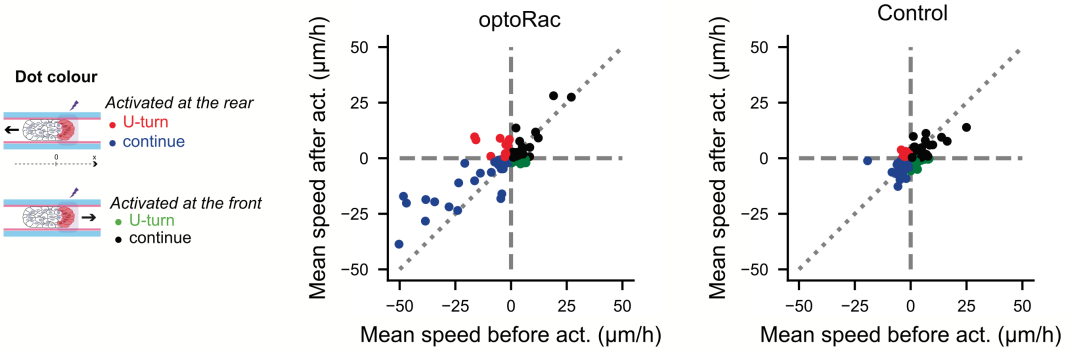

Figure 4.9: Mean velocity along the x-axis before (average over 1h30) and after (average over 10h) activation (act.) of optoControl and optoTiam clusters. n=119 (control), 89 (optoRac)

The effects of local optogenetic activation of Rac seem opposite to the ones of optoPRG. Indeed, clusters activated at the front (x>0 in Figure 4.9) did not show any specific change, while a majority of the clusters activated at the rear (x<0 in Figure 4.9) are at least slowed down by the optogenetic activation (above the y=x line on Figure 4.9). However, effects were much smaller than the ones of RhoA triggered by optoPRG, as very few changed direction (3 only out of 17, which is similar to the control). Moreover, it is hard to compare to the optoControl cells, as speeds before activation are radically different, which could explain the effect.

When looking at the individual trajectories (Figure 4.10 (A)), it is clear that the U-turns for the three clusters happen at the place of the optogenetic activation, which points toward a possible effect of Rac on cell cluster polarity, even if more data would be needed to confirm it. As for Rhoa, static cluster do show a clear bias after activation, going toward the activation of Rac1 (for 79% of them), but stay in a low migration state compared to other moving clusters (Figure 4.10 (B) and (C)).

All in all, optoTiam seems to have an opposite role compared to optoPRG, tending to define the activated part as a front (or as a less fast rear), but with a much smaller and less clear effect. These results would need more data and precise monitoring of the effect of optoTiam on the clusters at the level of Rac1 activity, as well as actin and myosin. It could be that the small effect we are seeing here is only the effect of inhibition of RhoA by Rac1, and that the bias in static clusters is due to some small protrusions happening because of Rac1 activation.

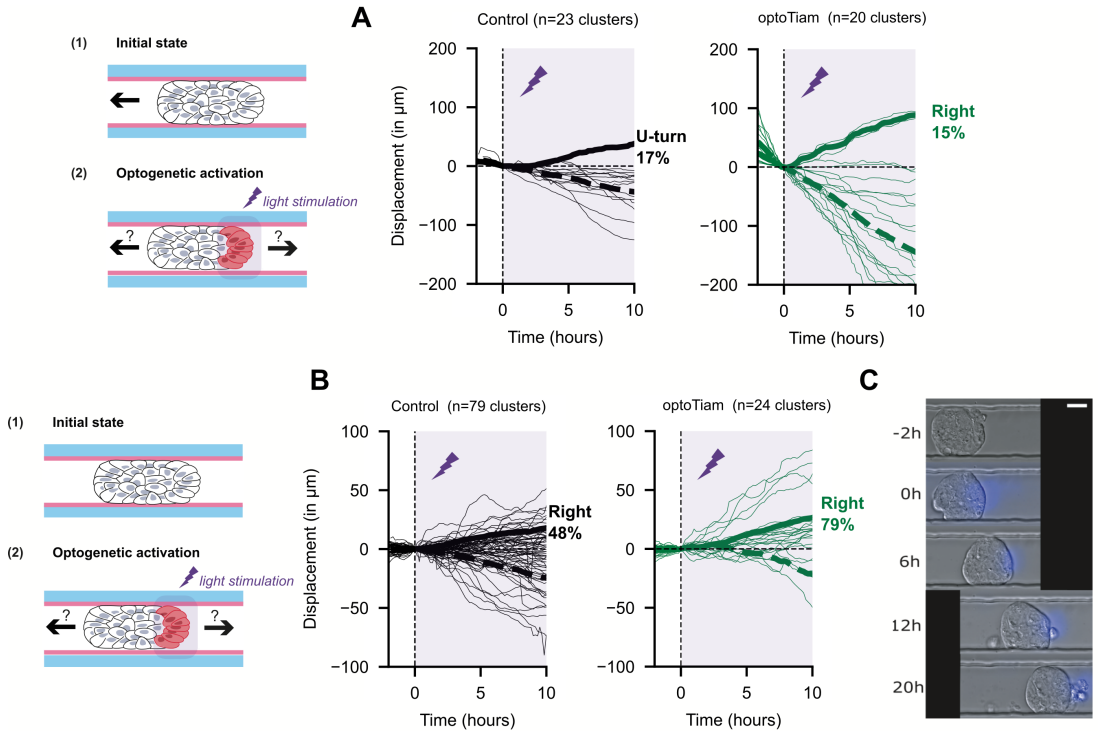

Figure 4.10: Individual trajectories for optoTiam activation of cell clusters. (A) Displacement of the clusters over time, for already moving clusters activated at the rear with optoTiam. (B) Displacement clusters over time, for static clusters activated with optoTiam. Bold and dashed lines are means of trajectories going to the right or to the left, respectively. Purple zone: optogenetic activation. On the left, schematic of the experiment. (C) Time-lapse sequences of a cluster starting to move upon activation (Scale bar, 20 µm).

4.3 Collective amoeboid migration could arise from polarized jiggling

Surprisingly, unlike in single cell amoeboid migration, no retrograde flow has been seen in the cell clusters that could explain forces generation. Indeed, neither persistent actomyosin retrograde flows, nor persistent cell flows could be observed in either plane of the cell cluster, as described in [Pagès et al., 2022].

Another mechanism had to be hypothesized to explain this very persistent focal-independent collective migration. When analyzing the myosin and nuclei fluctuations, at the periphery as well as in the whole cluster, it was clear that the amplitude of the fluctuations, or jiggling, was positively correlated with cluster migration speed: the more myosin/nuclei speeds fluctuate, the faster the cluster (Figure 4.12 (A) and (B)) Together with the gradient of contractility that is positively correlated with cluster speed and persistence (see 4.1), a minimal model was proposed to explain how these elements could power persistent collective migration. I will not go into the details of the model, which was developed by Ananyo Maitra and Raphael Voituriez, but explain its main principles.

The cluster is considered as an active elastic solid on a 1D axis. The two main ingredients of the model are the following :

- The myosin fluctuations described above are modeled as and active fluctuating contractile stress of magnitude ζ. This stress follows the local myosin activity,

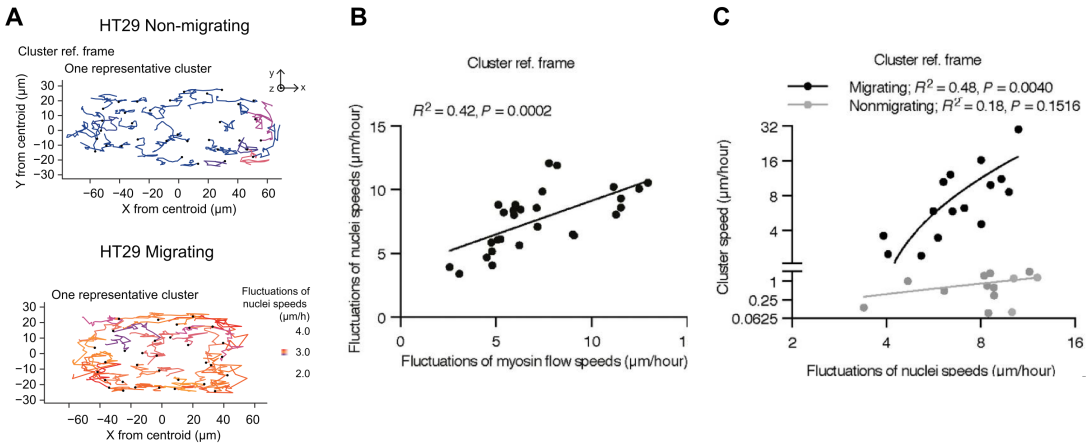

Figure 4.11: (A) Nuclei tracks in representative clusters, every 2 to 10 min over 8 to 11 hours in the cluster reference frame. (B) Amplitudes of myosin flows and nuclei speeds fluctuations. (C) Amplitudes of nuclei speeds fluctuations and cluster speeds (i.e., centroid direct displacement between first and last time point over total time, as migrating clusters do not change direction). Log scales. Lines, linear regressions; threshold between migrating/nonmigrating clusters, 2 µm/hour. n = 27 to 28 clusters (six independent experiments). Taken from Pagès et al., 2022

therefore shows a front-back gradient $\nabla\zeta$, which causes a gradient of fluctuating deformations.

- As described in 4.1, cluster seem to interact with the substrate via passive friction forces, which are generically nonlinear and assumed to be strain dependent. The force transmission will therefore be modeled as a function of the strain, which corresponds to the deformation.

These two ingredients lead to an asymmetry in the force transmission to the substrate, responsible for effective asymmetric movement. I refer to Pagès et al., 2022 for more details on the calculations that show that these are the minimum ingredients to induce cluster self-propulsion, with velocity $v \sim \nabla\zeta$, independently of any sustained retrograde flow of actomyosin or nuclei.

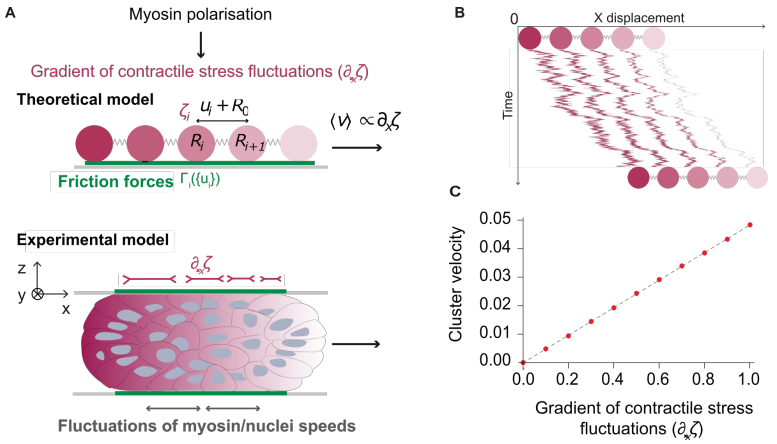

Figure 4.12: Model of collective amoeboid migration, driven by polarized jiggling. (A) Top: Discrete, one-dimensional model of the cell cluster obtained by averaging over the cluster along z-direction and discretizing along x-direction. The cluster is modelled as a series of beads, with average separation R0, connected by elastic elements modelled by gray springs. The active fluctuation of contractile stress on each bead is ζ_i which decreases from left to right and is represented by a color gradient. The friction experienced by each bead is γ_i which depends on the local strain u expressed as $u = R_{i+1} - R_i - R_0$. Bottom: schematic of the model of the cell cluster: fluctuations of cell displacements, friction forces γ with the microchannels (green plain line), gradient of contractile stress fluctuations $\partial x\zeta$ and cluster speed v. (B) A representative trajectory of a five-bead model with the strength of contractile fluctuations decreasing from left to right.

4.4 Going smaller - how many cells to be collective?

Compared to single-cell amoeboid migration, one of the major challenges of the study presented in the previous sections was the number of cells. These clusters were selected according to specific sizes comparable to those found *in vivo*. Typically, a 70µm filter was used before injection into the microchannels (see 6.2.2) and the observed cell clusters touched both walls: with these two criteria, most clusters had between 50 and 100 cells. This made it very difficult to assess the contribution of individual cells. For example, we could not determine whether some cells were more important for polarity or whether only a few cells contributed to force production.

This challenge came together with another question that arose from the experimental protocol. As can be seen in 4.1, the differences in velocity between clusters are very large. Some clusters are able to polarize and migrate as soon as they are in the microchannels, while others remain in a static state for several hours. It seems that the clusters were in different states before injection, that something happened in the Petri dish where they formed that we could not observe.

To address these two questions that I was very interested in, I started a project that aimed at seeing clusters formation and migration with very few cells - as few as possible -, to answer the following questions: how many cells are needed to start collective amoeboid migration? can we distinguish come specific cellular roles in the collective? Do the cells gain some ability by behaving as a collective?

This project was then taken over by Romain Guignon, a four-month master's intern in our lab. I was not able to spend as much time on this project as I would have liked, so this paragraph consists in preliminary - albeit promising - results, mostly coming and adapted from his internship report.

4.4.1 HT29-MTX cells assemble and migrate as small clusters in a confined non-adherent 2D environment

To study cluster formation from single cell, we designed new PDMS chips together with Li Wang from Piel's lab. We tested different designs and finally focused on microchannels of 9.5µm high, approximately the diameter of HT29-MTX single cells, and 500µm width to allow 2D motion (see Figure 4.13 for details). We introduced single HT29-MTX cells immediately after detachment with Trypsin, to have as many single cells as possible at the beginning of the experiment. We mostly performed experiments with a cell line developed in Jaulin's lab, with GFP-tagged MLC to see myosin and mCherry-tagged H2B to follow single nuclei, and looked at cells for 40 hours. This enabled the assessment of cluster speed as well as number of cells in each cluster, together with myosin distribution within these same clusters.

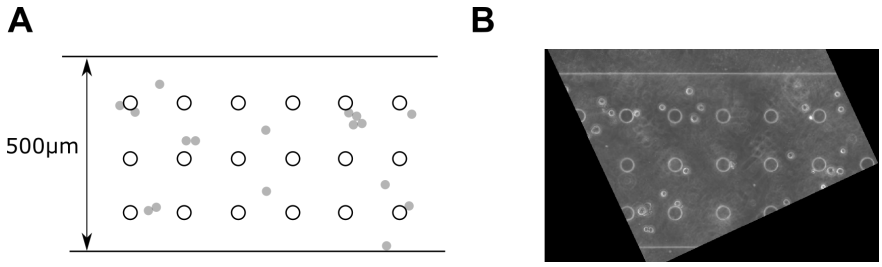

Figure 4.13: (A) Microchannel design for small clusters study. Circles are pillars to keep a constant height. Two designs were used, with 11.3 and 9.5µm height. (B) HT29-MTX cells imaged in phase contrast microscopy within microchannels.

Qualitatively, movement started half an hour after injection in the microchannels, in random directions. Most of the single cells do not seem to move, which was expected due to the height of the roof, comparable to cell size. Single cell did not show any protrusions that we could see, or blebs reminiscent of amoeboid migration: indeed, they were not confined enough for amoeboid migration (which starts with height of $\sim$ 5µm for this cell line), and PEG prevented focal adhesion formation.

When two cells are in close proximity, a fusion event happens: the two rounded cells form one round cluster (Figure 4.14 (1) and (2) as examples). Migration starts in this case, the cluster migrating as a whole (Figure 4.14 (1)). A cluster of two cells can also be formed after a cell division event (Figure 4.14 (4)). Clusters can merge when they encounter each other or merge with single cells, forming bigger clusters (Figure 4.14 (2),(3),(5)), reaching sometimes 20 to 30 cells migrating together. Very interestingly, this fusion event often leads to the formation of one supracellular myosin cortex (not shown here), not always easy to distinguish because of the differences in protein expression and the non confocal images. This is reminiscent of what was seen for the bigger clusters in 4.1. In phase contrast, cells are very hard to distinguish when fused, it seems that they behave as a whole (Figure 4.14 bottom). This suggests a supracellular behavior starting from a very small number of cells.

When looking at all cluster trajectories, no specific direction seems to be taken, (Figure 4.15), even if some patterns can be recognized because of the influence of the shape of the microchannel - cell sometimes stay around a pillar or on a border for a long time. Looking at the speed of the single cells and clusters over time reveals two different phases, present in all experiments (see Figure 4.15 (B), numbers 1 and 2). During the first phase of approximately $\sim$ 20 hours, the mean cluster speed is increasing, as all clusters start migrating at different timepoints. The number of cells

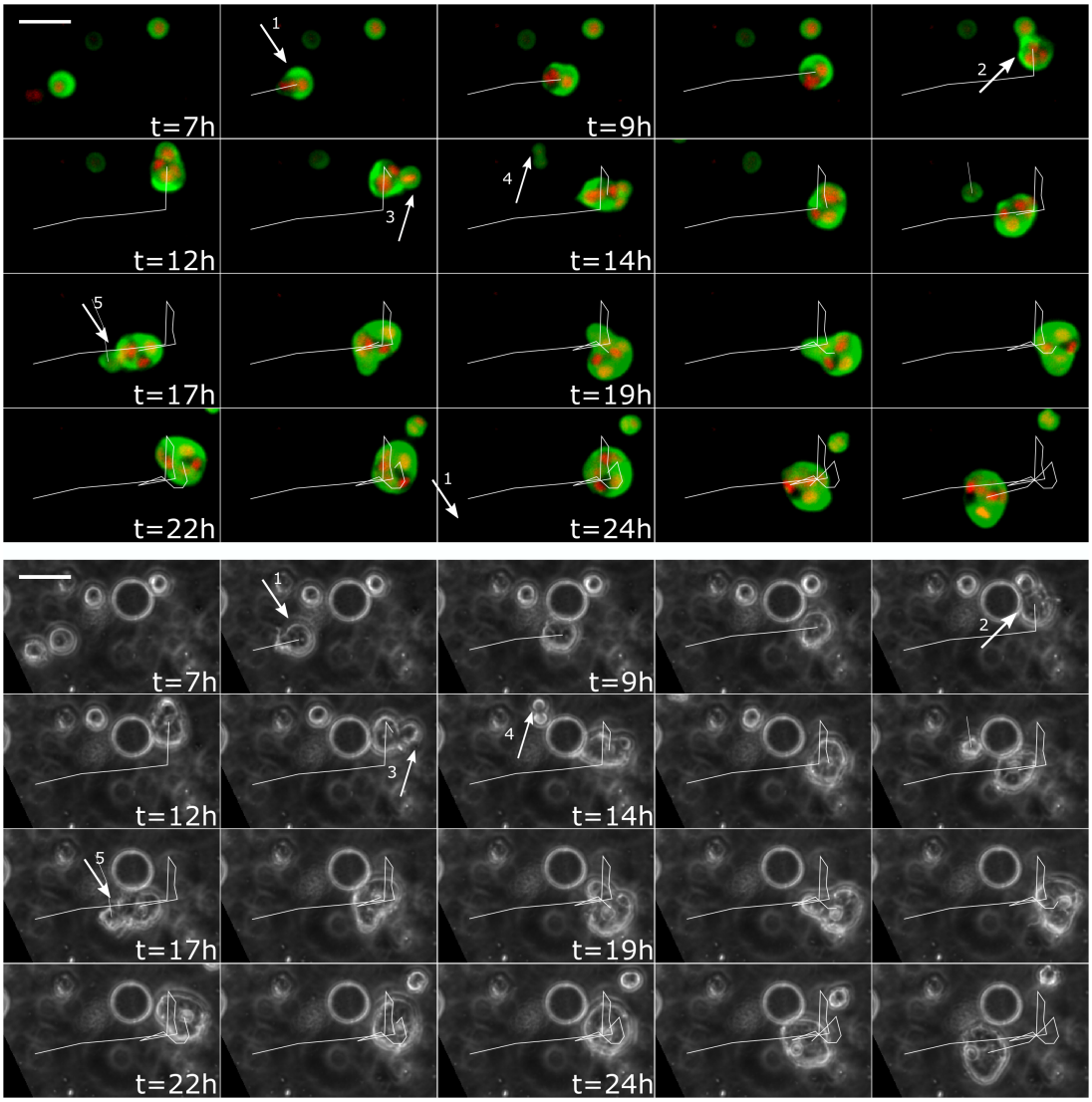

Figure 4.14: Representative timelapse of a cluster moving and growing in size. Top, merged image of MLC (in green) and H2B (in red). Bottom, phase contrast image. One image every hours, going from left to right and then top to bottom. Scale bar, 50µm. The white line is the past trajectory of the clusters. Events to look at are marked with an arrow and the number. (1) First fusion between the 2-cells moving cluster on the left that encounters a static single cell. (2) Second fusion. After having moved, the 3-cells cluster encounters a single cell and merges with it. (3) One cell pops out of the cluster to divide, and will then come back in the cluster, forming a 5-cells cluster. (4) A static single cell divides, it will then form one round two cells cluster. Only then, it will start moving. (5) The 2-cells cluster encounters the 5-cells cluster, forming a 7-cells cluster, that will further move away and grow bigger.

per clusters starts to grow, as the movement of the cells triggers new fusion events. After this time, there is a second phase of $\sim$ 20 hours where mean speed reaches a plateau. Fusion events still happen but do not have any impact on the mean speed.

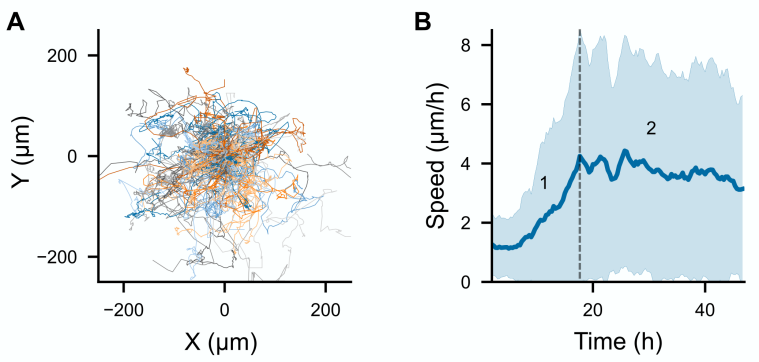

Figure 4.15: Trajectories and speed for small clusters. (A) All trajectories from one experiment plotted with a starting point at (0,0). (B) Mean speed for all clusters, mean ± std. vertical dashed line shows the limit between the two phases: (1) Phase of mean speed increase. (2) Phase of constant speed.

4.4.2 Cluster size influences migration speed

We looked at the details of migration properties depending on cluster size (in terms of number of cells). Very interestingly, in the plateau phase, cluster speed is increasing with the cell number, at least from one to 6 cells (Figure 4.16 (A) and (B)). This trend is significant on the experiment shown here, and was confirmed in a second experiment (data not shown). We confirmed that very few single cells do move, and those that do could be doublets where both nuclei are hard to distinguish by the segmentation algorithm (Figure 4.16 (B)). The directional persistence, calculated as the distance between first point and last point and the accumulated trajectory length can be plotted along time for the phase of constant speed (Figure 4.16 (C)). No clear effect of the size can be seen, but it surely requires more experiments.

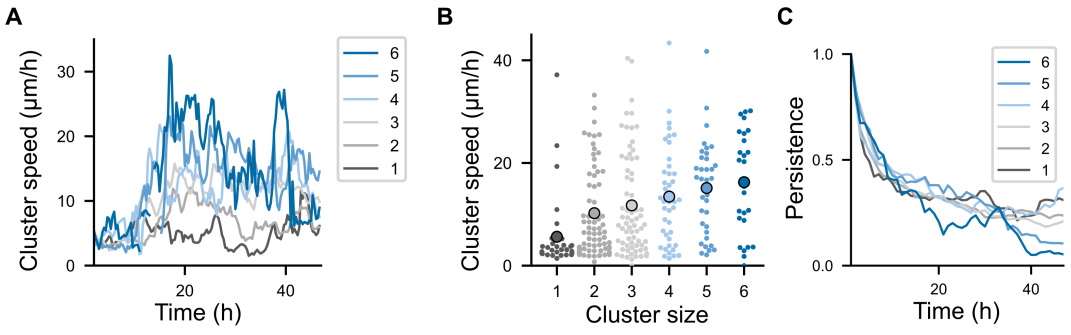

Figure 4.16: Speed and persistence of small clusters depending on their size. (one experiment) (A) Mean cluster speed in µm/h for each cluster size, from 1 (dark) to 6 (dark blue) cells per cluster. (B) Speed averaged over the plateau period (from 19 hours to 43 hours). One dot represents one track of one cluster of the specific size. (C) Mean directional persistence for each cluster size, from 1 (dark) to 6 (dark blue) cells per cluster, plotted only during phase (2) (constant mean speed)

The increase of the speed with size is confirming the similarity of small clusters to

single cell, with their rounded shape and supracellular myosin cortex. It means that cells are not acting as the sum of the individuals, but one way or another cooperate to improve their migration when they migrate together. It may well be that by having more contacts with both walls, friction powering movement increases, or that having more cells triggers more confinement, triggering more contractility and then more actomyosin movements. More data are surely needed, and further implications and perspectives will be discussed in the discussion 5.2.

4.5 Conclusion on collective amoeboid migration

This multidisciplinary project, of which I described some aspects here, clearly revealed a previously undescribed mode of collective migration, identified from patient explants, therefore most probably relevant in many cancers. It was named collective amoeboid because of its similarities with single cell amoeboid migration: no focal adhesions are required, and supracellular actomyosin cortex polarizes to generate propulsive friction forces (see Figure 4.17). The mechanism of forces generation and polarity is different as no supracellular flows can be observed, and led to a minimal model named polarized jiggling, where individual contractility fluctuations together with a supracellular gradient of contractility is enough to transmit persistent forces in one direction. This mode of migration could be extended to other biological systems, as very few elements are required, and resembles engineered biological robots made by Kriegman et al. [Kriegman et al., 2020].

My main contributions have been the optogenetic experiments, with all its experimental difficulties. Optogenetic activation of RhoA and Rac1 has revealed the ability of RhoA to control cluster polarity, but not migration initiation, whereas Rac1 had a smaller effect still to be deciphered.

Experiments with smaller clusters have showed the ability of HT29-MTX to fuse and make round clusters starting from two cells. These clusters have the ability to migrate as a whole in non-adhesive environment. They can even be faster and more persistent in the environmental conditions studied here, which points toward emergent properties gained by being multicellular. Many questions have been raised from all these experiments, that will be further discussed in the discussion chapter 5.2.

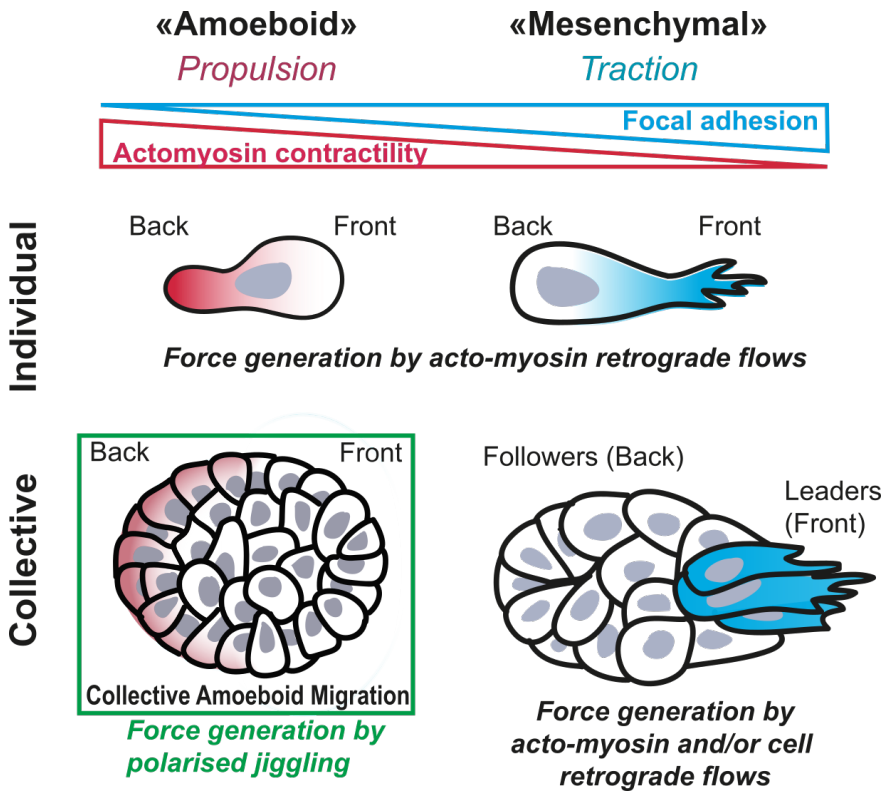

Figure 4.17: Schematic representation of the different modes of cell migration based on the ability of the cells to adhere to each other (individual versus collective migration) and to their environment (mesenchymal versus amoeboid). This results in traction- or propulsion-based locomotion. Single cell amoeboid migration and collective adhesion-based migration are driven by sustained acto-myosin or cell retrograde flows whereas collective amoeboid migration is driven by polarized jiggling. Taken from [Pagès, 2022]

Chapter 5

Discussion and Perspectives

These two projects differ greatly in the issues they address, leading to very different discussions and perspectives. What they have in common is the use of optogenetics in the context of migration and the specific perspective of Rho- GTPases, particularly RhoA. To address these differences, I will first discuss the issues and perspectives triggered by each of these projects (in 5.1 and 5.2). More general discussions on optogenetics for cell biology and research in life sciences will further developed in 5.3, as they pertain to both projects.

5.1 On the control of opposite phenotypes with one GEF of RhoA

The first project of my PhD thesis revealed a unique example of multiplexing in protein signaling pathways. In this project, the DH-PH domain of PRG has been used with an optogenetic tool to control its binding to the membrane. I have shown that local triggering of this recruitment to the membrane can result in two very different cellular responses: a protrusion in the activation region or a retraction in the same region. I was able to explain these opposite phenotypes by the differences in cellular concentration of PRG DH-PH before optogenetic activation: at low concentrations, recruitment triggers retraction, whereas high concentrations lead to protrusion.

In studying the signaling pathways responsible for these opposing phenotypes, I discovered the pleiotropy of the DH-PH domain of PRG . The known ability of the domain to activate RhoA was confirmed in the case of retraction phenotypes. However, in protruding phenotypes, it negatively regulated RhoA activity in the first minutes after optogenetic perturbations and simultaneously activated Cdc42.

These findings were summarized in a simple model that recapitulated the various experimental results. It predicted that some cells could show both phenotypes depending on the frequency of the pulses of light activation. I verified experimentally that this was the case, confirming that we had gained some understanding of the underlying biochemical network.

5.1.1 What are the direct interactions?

The use of optogenetics has revealed causal relationships between optoPRG recruitment to the membrane and two opposite phenotypes. The use of biosensors has

also shown causality between optoPRG recruitment and the activity of some proteins: in the case of retractions, optoPRG triggers the activity of RhoA, the polymerization of actin, and the recruitment of myosin in a few tens of seconds. In the case of protrusions, the same recruitment first inhibits RhoA activity, triggers Cdc42 activity, inhibits myosin activity, and then triggers actin polymerization.

This causality does not prove direct interactions experimentally, but we relied on the literature when making conclusions on our data:

- activation of RhoA by direct interaction with the DH-PH domain of PRG has been well studied: the structure of the complex is even known [Derewenda et al., 2004], and the ability of PRG DH-PH to greatly enhance RhoA-GDP switch to RhoA-GTP has been studied *in vitro* with purified proteins [Gasmi-Seabrook et al., 2010].

- The two main direct effectors of RhoA usually cited for contractility are mDia1, a formin that triggers actin polymerization, and ROCK kinase that promotes myosin activity. mDia1 and ROCK are known to cooperate as downstream effectors of RhoA for a long time and promote stress-fibre formation and contractility [Watanabe et al., 1999].

- inhibitory effect of DH-PH domain of PRG on RhoA activity comes out of one paper that showed the direct interaction of the PH domain with RhoA-GTP only (and not RhoA-GDP) [Chen et al., 2010]. In the same paper, overexpressing PH domain alone also reduced RhoA activity, which suggests a direct interaction preventing RhoA binding to effectors, as the binding happens on the same site.

- PRG DH-PH domain direct interaction with Cdc42-GDP and its ability to enhance the switch to Cdc42-GTP has been shown in one paper [Castillo-Kauil et al., 2020]. The linker region between the DH and the PH domain is required for effective interaction, as well as GαS activity.

- the ability of Cdc42 to promote actin polymerization and the whole protruding phenotype has been well studied, and shown causally by optogenetic recruitment of the more specific GEF ITSN [de Beco et al., 2018]. The inhibition of myosin activity and depolymerization of stress fibers have been shown for protrusions triggered by PDGF [Martin et al., 2016], but no biological pathway has been specifically proposed, to my knowledge.

To summarize, the two less studied interactions are the interactions of PRG with RhoA-GTP and the one with Cdc42. We could not check the direct interaction in our case, but the PH inhibition of RhoA activity and the fast activation of Cdc42 tend to confirm both of them.

Did we miss other interactions that might have a strong contribution to one of the two phenotypes? Recently, a negative feedback between myosin and the GEF of RhoA GEF-H1 has been shown in different papers [Kamps et al., 2020, Kowalczyk et al., 2022]. This negative feedback is supposed to come from a direct interaction of myosin head with DH domain of different GEFs of one family called the Dbl family -to which PRG,LARG and GEF-H1 belong-, described in [Lee et al., 2010]. Is this direct interaction playing a role in the inhibition of the myosin, and in the protruding phenotype? It could contribute to the effect but is probably not the main trigger, since we showed that DH domain alone was not enough to cause protrusions.

Another important interaction that could have been missed in this study is the organization at the plasma membrane. As RhoA needs to be stabilized at the plasma membrane to engage the effectors [Budnar et al., 2019], it could be that interactions with different phosphoinositides or membrane proteins plays a role in downstream signaling, enhancing the double phenotype effect. One experiment to tackle this question of membrane organization would be to look at RhoA and PRG with superresolution microscopy techniques. These have already uncovered some nanoscale structures of Rac1 at the plasma membrane [Remorino et al., 2017], and could certainly give insights on the organization of RhoA or PRG.

5.1.2 Is it true for other GEFs of RhoA?

In this study, DH-PH domain of PRG has been used to trigger opposite cellular responses. It has been shown that the protruding phenotype could be seen for DH-PH domain of GEF-H1 also, but very rarely (see Figure 3.3). Indeed, it seemed that transiently expressing optoGEF-H1 and optoLARG was much harder than for optoPRG, many cells dying or rounding up when positively transfected.

The interactions of the PH domain of GEF-H1 and LARG with RhoA-GTP are described in [Medina et al., 2013]: PH domain of GEF-H1 had almost the same inhibition ability as PH domain of PRG, while PH domain of LARG was less efficient. Moreover, it seems that DH-PH domain of LARG has no effect on Cdc42 [Castillo-Kauil et al., 2020], while I could no find any literature for DH-PH domain of GEF-H1. Full length overexpressed GEFs seem quite specific for RhoA, as PRG is [Müller et al., 2020], but recruitment to the membrane has not been specifically studied, to my knowledge.

What can we conclude out of this? It seems that the ability to trigger these clear antagonist phenotypes is not a common feature of the three GEFs mentioned here, but some similarities in their structure could lead to similar complex interactions and signalling. As an example, it is most probable that local increase in concentration of GEF-H1 and RhoA will lead to binding of PH domain to RhoA-GTP, which will in turn have an inhibitory effect on RhoA.

DH-PH domain of PRG is able to trigger protrusions thanks to three properties: it increases basal level of RhoA even when expressed in the cytosol, it can inhibit RhoA-GTP thanks to its PH, and it can activate Cdc42. These two less known features of PRG allow very high overexpression of the protein, thanks to two effects: first, the inhibition by the PH prevents too much overactivation of RhoA, as the PH titrates RhoA-GTP. Second, activation of Cdc42 probably prevents cell rounding by its competition with RhoA, which could also explain the increase in cell size for protruding cells. It may be that other GEFs share one or two of these features, without the others. We could design experiments to check this. As an example, we could express non recruitable PRG to increase basal level of RhoA-GTP, and see what are the effects of a recruitment of another GEF on RhoA activity. This kind of experiments could help us seeing the dynamic differences between RhoA GEFs in the cell, and get a better understanding of their role and interactions.

5.1.3 Is it true for other optogenetic tools?

One question coming out of this project is the specificity of this double phenotype for the optogenetic tool used in our experiments. Indeed, the recruitment of the DH-PH domain of PRG to the membrane has been used multiple times with CRY2/CIBN

dimer (see [Valon et al., 2017], [Andersen et al., 2023] and the second project in chapter 4), and no protruding phenotype has ever been described . Three reasons could explain this absence:

- First, in all these examples, the optogenetic tool was only used as a way to produce cell contractility. Thus, stable cell lines were created, with a selection depending on the ability of cells to actually contract upon optogenetic activation. It could be that protruding phenotypes were not taken into consideration, because they were not giving the desired contraction. However, in our hands, it was still very hard to obtain protruding phenotypes with CRY2/CIBN dimer (only one or two cells out of 50), which calls for further explanations.
- The second explanation could come out of the differences in dimer properties upon recruitment. CRY2 tends to oligomerize, and has a more stable interaction with CIBN than iLID with SspB (3 minutes versus 20 seconds, respectively). It may be that this difference in interaction tends to promote one effector over the other (RhoA over Cdc42 for example), selecting for only one possible phenotype.
- Third explanation is that the basal state of the cell is different with different optogenetic dimers. In our hands, it was harder to obtain high level of transfections for optoPRG with CRY2/CIBN than with iLID/SspB, as more cells were rounding and dying (data not shown). It may be that high level of optoPRG with CRY2/CIBN are more lethal, because of a positive feedback loop induced by the dimer.

Overall, it seems that iLID/SspB dimer is best suited for these two opposite phenotypes, and that specific dynamics are required for these opposite phenotypes to be observed. These protrusions and retractions were also observed recently with optogenetic activation of PRG, in [Ju et al., 2022], with a completely different optogenetic tool unlocking the GEF at the membrane. Some protrusions were described, confirming the present observation. However, no detailed explanation was given.

This specificity for only one kind of recruitment dynamic could be matter of further investigations. Indeed, it tells us how a seemingly similar cellular action, like recruiting a GEF to the membrane, can lead to different cellular responses. Therefore, it may reveal the underlying endogenous dynamic enabling a selection of a specific function by dynamics of recruitment. Experiments could be done to interrogate the impact of oligomerization on cellular responses and basal state of the cell, and other optogenetic tools could be used to understand what are the important dynamic parameters that drive the cell in one particular response.

5.1.4 Minimal model - could we improve it?

I presented in 3.6 a minimal model to recapitulate the different quantitative findings. One of the key goals of the model was to access the dynamics of the network in time and to understand how to better control it, using the flexibility of optogenetics.

There are obvious limitations to this model:

- only optoPRG is taken into account for RhoA activation, and not the other GEFs of RhoA. As it is overexpressed, it is probably overriding other GEFs, usually expressed at 10^{th} of nM, or 100^{th} for GEF-H1 [Kamps et al., 2020]. However, they certainly play a role in amplifying the signal at very low concentrations, which was not considered here.

- Rho-GTPases activation is proportional to both inactive Rho-GTPases and PRG concentrations, which doesn't take into account the possible Michael-Menten like kinetics. This was justified by one paper where RhoA total concentration was shown to be one order of magnitude below the Michaelis-Menten constant [Kamps et al., 2020]. However, the cell line was different (it was done in U2OS) and differences in concentrations can easily attain one order of magnitude. With Michaelis-Menten kinetics, we expect that with high optoPRG concentrations, RhoA activation happens at a rate less dependent on the GEF concentration. This means that recruitment of PRG to the membrane should trigger less activity of RhoA, facilitating the protruding phenotype.

- Total concentration of RhoA and Cdc42 were considered as in excess compared to the activated proteins. This hypothesis does not necessarily hold for high values of optoPRG, where saturation effects could happen.

- deactivation steps are considered to happen at fixed rates, which do not take into account the Michaelis-Menten kinetics induced by the binding of the GAPs to Rho-GTPases. The paper cited above [Kamps et al., 2020] confirmed this assumption in their case, which helped for the model's simplicity.

- other feedbacks, such as the negative feedback of active myosin on RhoA GEFs, are not taken into account. It can be justified by the fact that the phenotype is decided after one minute, and this negative feedback acts more at the few minutes timescale. However, it certainly plays a role at the timescale of the whole 20 to 30 minutes experiment.

Despite all these limitations, the model rendered well the experimental observations and hopefully helped understanding the dynamic of the system. Simplifications reduced drastically the number of parameters to be fitted, which prevented too much overfitting.

I think that complexifying the model would be useless without adding new quantifications. Two specific ones could be of interest: myosin negative feedback could be directly measured by using an optogenetic tool that directly activates myosin (or recruits activated myosin) and then monitoring the effects on RhoA activity at both low and high concentrations of optoPRG. Second quantification would be a more careful characterization of Cdc42 activation by optoPRG, by using pulses of activity, and ideally using FRET biosensors to have absolute quantifications. These quantifications would enable to add the myosin layer with actual measured parameters, and precise Cdc42 dynamic.

Another way to improve the model would be to add the spatial dimension, that was here neglected. Indeed, it is clear that different shapes of activation will lead to different efficiencies in the response [de Beco et al., 2018], and it is known that RhoA's role differs depending on its zone of activity within the cell [Pertz et al., 2006]. A model could ask the question of the feasibility of the dual phenotype by varying the area of activation instead of timing and amplitude, as most of diffusion coefficients could be quite easily measured by FRAP experiments.

5.1.5 RhoA in protrusions and retractions

One of the unsolved questions regarding the specific role of RhoA in cell migration is the seemingly opposite roles that it has at the two opposite sides of the cell. On

the one hand, RhoA is very active in retraction of the cell's rear, and optogenetic has confirmed that active RhoA clearly triggers stress fiber formation and retraction when active at the membrane [Berlew et al., 2021]. On the other hand, FRET measurements have shown that a pulse of RhoA activity is very well correlated with the onset of a protrusion in different cell types [Kurokawa and Matsuda, 2005, Pertz et al., 2006, MacHacek et al., 2009]. Does our study bring something to the debate?

I will be very speculative in this paragraph, based on unpublished data. To our knowledge, as stated in the introduction 1.5.1, all measurements of RhoA activity preceding protrusion were made in single component FRET biosensors. These biosensors do not directly sense endogenous RhoA activity but are biosensors of the local concentrations of GEFs and GAPs that act on RhoA, as well as GDIs for some of them. However, FRET biosensors do not have the same intracellular localization as RhoA, as it was already observed in [Pertz et al., 2006]. They are much more bound to the membrane, a fact we could confirm experimentally even with very recent versions of these biosensors (see the internship report of Josephine Gatin in A). Could it be that they sense potential RhoA activation, where no endogenous RhoA-GDP is present? As an example, we could imagine that local recruitment of PRG at the front endogenously triggers Cdc42 activity in migrating cells. However, when the FRET biosensor is present, it would show a pulse of RhoA activity because of a difference in localization. This could be true for any GEF that can activate two different Rho-GTPases.

One way to confirm or infirm this hypothesis would be to compare single component FRET biosensors of RhoA with relocation biosensors and compare recruitment of the optoPRG in both cases. It is a work that we started with Josephine Gatin during her internship, whose report is presented in the annex A. By monitoring both biosensors in the same cell, both in spontaneous migration and in PDGF (or another factor) induced migration, we could compare the dynamics and the specific patterns of activity rendered by these two very sensitive biosensors, and hopefully get a better understanding of these differences -if they indeed exist.

5.1.6 Is it biologically relevant?

It is without any doubt one of the most feared questions for physicists or cell biologists working in non-animal environments. Is what I am studying something that is happening *in vivo*? Is the process that I described a more general mechanism or only an artefact of the lab and experimental conditions I am working in?

These questions are legitimate and worth being asked, especially in this project. In the case of my study, nothing has proved that this double phenotype is indeed something that is used by the cell *in vivo*, and it could be that specific experimental conditions allow some sort of biological artefact. Studies looking at endogenous PRG in migrating cells, both in controlled environment and in model organisms or in cancer could tackle this question, to specifically look at the role of PRG in these contexts.

However, at least four important biological messages can be taken out of this project, and lead to further question:

- we show here a particular example of protein pleiotropy, and especially the importance of protein concentration in protein function. We showed that in the same cell line, changing the concentration of one single protein is enough to completely revert its function when being recruited to the membrane. Moreover, it is not necessarily a change of protein function at the transcriptional level but at the protein-protein interaction level. It is a known mechanism, but that was

never been shown so clearly for a concrete example, to my knowledge. We can speculate that this phenomenon is not unique and is an outcome of evolution that revised the same protein in different contexts.

- For this specific example, we even showed that the same protein could trigger antagonist functions in the same cell depending on the signal dynamics. Even if the context was quite specific (cells with a specific concentration), there are reasons to think that this kind of multiplexing is happening in vivo, where dynamics and local concentrations can highly vary in the cytoplasm and in different substructures. If the timescales governing the different interactions were more different (for example by having an optogenetic dimer that would be much faster), multiplexing within the same cell could happen much more easily. We are limited here by the optogenetic dimer, but it could well be that the cell has much more refined endogenous dynamics, which it uses for multiplexing.

- We highlighted a specific type of network that was able to have this multiplexing ability. DH-PH of PRG domain is a paradoxical component [Hart and Alon, 2013], in a double meaning: first, because it can both activate or inhibit RhoA with different affinities. Second, because it can both activate the contractility pathway via RhoA and the protruding pathway via Cdc42. As described in [Hart and Alon, 2013], these paradoxical components can have many interesting properties. One that is important in our case is that the cell can support very high concentrations, as the effector is inhibited at the same time. Indeed, this mechanism seems to prevent the overactivation of RhoA, which normally tends to round up the cells and is lethal (unpublished data with overexpressed constitutively active RhoA), a phenomenon we didn't observe with optoPRG. This kind of paradoxical component is quite common in biology [Hart and Alon, 2013], and the example we dissected here can help understand other similar network motifs.

- linked to this ability to be highly overexpressed and change its function, this study could have a particular relevance in cancer. Indeed, PRG is known for being overexpressed in different cancer and favors migration and epithelial to mesenchymal transition [Ding et al., 2018, Du et al., 2020, Struckhoff et al., 2013]. In all these cases it was studied as a promoter of RhoA activity. However, this project clearly suggests a possible switch in the role of PRG when overexpressed, acting more on Cdc42 activity. This kind of switch in function could be a mechanism happening for other GEFs or other proteins, and have to be really thought when designing therapies.

Altogether, even if the specific dual phenotype we are seeing in our experimental system may not be directly relevant in organisms or diseases, this study still opens very general biological questions. Through one example, it proves protein multiplexing ability, and reveals a specific network motif and structure to obtain it. It also shows the importance of precise dynamics in protein networks for proper functioning, a property that is surely not restricted to the system studied here.

5.2 On collective amoeboid migration

An extensive discussion on the different aspects of collective amoeboid migration has been led by Diane-Laure Pagès in her PhD manuscript [Pagès, 2022]. I refer to it

for the global perspective of collective amoeboid migration in the migration field, as well as all the links with cancer metastases. I will discuss here the results I obtained during my thesis (4.2 and 4.4), as well as some broader questions I think this project leads to.

5.2.1 Cluster powering and polarity

This study has revealed many things about force generation and polarity in collective migration. Powering requires actomyosin contractility, but does not need any focal adhesions and steady flows of actin or cells. Migration polarity is correlated with myosin polarity at a supracellular level. Thus, the model proposes that forces are transmitted to the substrate through transient interactions, a transmission that will depend on the position relative to the cluster because of the gradient of contractility. What triggers the supracellular actomyosin cable and its polarization?

Optogenetic experiments have shown that RhoA and Rac1 had an influence on cluster migration polarity. RhoA can invert the polarity of already migrating clusters, which means that it plays a role in collective amoeboid migration and is sufficient to dictate cluster polarity. However, it seems to be unable to actively trigger migration. Rac1 cannot invert cluster polarity as RhoA does, but is able to bias the onset of migration for immobile clusters, and optoRac clusters were moving much faster.

These findings confirm that the molecular determinants specifying the front and the rear -which are expected to exist as we can see a supracellular actomyosin polarity- are reminiscent of the ones in single cell migration. Indeed, in single cells, RhoA is often dictating the retractile rear while Rac1 triggers protrusions and actin polymerization at the front. However, unlike for single cell migration, these molecular cues are not sufficient for triggering collective amoeboid migration. Polarization does not necessarily come with force production, and molecular determinants responsible for these forces are not known. Actually, even in the much simpler system of single cell amoeboid migration, proteins responsible for force transmission to the substrate are still elusive. Integrins are one of the candidates, but the nature and the amplitude of these forces are still to be determined, and the exact nature of the friction is not known.

Overall, this second project revealed the main determinants of cluster polarity: actomyosin is polarized, with a polarized supracellular actomyosin cable, RhoA and Rac1 have an influence on polarity and RhoA is even sufficient to reverse it. For the forces, myosin fluctuations are correlated with migration speed, as well as nuclei fluctuations, and actomyosin contractility is required for movement.

Many questions are remaining, which we wanted to tackle with the experiments on small clusters: what triggers spontaneous supracellular movement? What triggers polarity? How many cells are required to create collective amoeboid movement? Are there some sorts of leader and follower cells?

5.2.2 Onset of collective amoeboid migration

With the project on small clusters (4.4), we made the following important observations. First, two cells can already group together, form a supracellular actomyosin cable and migrate as a whole in non adherent environment. This is also true for clusters with a higher number of cells, but two cells are enough. Second, it seems that fusion of the cells as one cluster precedes collective amoeboid migration. Third, in our

case where the height of the roof was fixed, we saw an increase in speed as the number of cells per cluster is increasing.

Importantly, cluster speed cannot increase indefinitely. Therefore, this last point means that there is certainly an optimal number of cell (or size) per cluster for efficient collective amoeboid migration in one configuration.

Even though we only have preliminary dat, we can give two hypotheses to explain this speed increase in small clusters migration:

- The first hypothesis is that cells fuse as a cluster but do not cooperate when they migrate. In this case, we are just seeing a "tug of war", where the most active cell takes over. Cluster speed is then only the mean speed of the cells in contact with the substrate. The only way to have an increasing speed by increasing the number of cells is to increase the cell's activity or forces transmission, which we could justify by the increase of the effective confinement.

- The second hypothesis is a form of cooperation. The easiest way to think of it would be a self-sorting process, where more active cells would be put in contact to the substrate, while less active would be more in the middle. In two- or three-cells clusters, sorting is not needed as there is an already set polarity. For clusters with more cells, this sorting would be actively needed. Such sorting that depends on interfacial tension, as an example, has been shown to happen in development [Canty et al., 2017]. We could imagine that this sorting is happening when cells group as clusters, or that it is triggered by confinement. In this case, we could have some kind of leader cells that would be the most active ones in contact to the substrate, and follower cells, less active, that are just passive in the cluster, but could replace leaders in some cases.

With the experimental set-up used in this project, a lot of these questions can be tackled. Unlike for bigger clusters, individual cells can be resolved if we look at higher magnifications. Fluxes of actin and myosin can certainly be observed at is the case in single cell amoeboid migration, and cell to cell variability can be measured. Actomyosin polarity and its onset can surely be measured with more precision, and optogenetic tools controlling contractility, actin polymerization, or other cellular properties can be used at the single cell level, which would enable to see how single cell activity and signaling relates to the group.

All in all, the study of small clusters amoeboid migration can certainly bring a lot of new knowledge about this new mode of migration, thanks to its simplicity compared to big clusters in microchannels.

5.2.3 A model system for emergence of multicellular behaviors?

One of the striking aspects of this new mode of migration is the ability of a cell cluster to act as a whole, with a supracellular behavior. The study on small clusters showed that by acting together, cells were gaining the ability to move faster in this specific environment. Moreover, it was shown that these cell clusters were more efficient in creating metastases than the same number of single cells [Zajac et al., 2018]. These cluster properties -that are not the sum of the individual properties of each cell- can be considered as emergent.

Emergence is a huge research topic in biology, as it concerns all living systems at very different scales. One key aspect of emergence is the transition from single cell

to multicellular behaviors. However, spontaneous transition from one to many cells is hard to study. In mammalian cell migration, experiment have been done with trains of cells [Jain et al., 2020], but the results showed no supracellular behavior, cells were still acting as individuals.

In our case, we know that cells fuse and start forming a supracellular actomyosin cable, already in a two-cell cluster. These cells are epithelial and are programed to cooperate, improve their speed when migrating together, but can still migrate alone. To my opinion, it can be a great system to look at emerging properties: how do each of the two cells change their structure, protein expression, activity, organization, when they are together? What do they "share" ? We know that they communicate as there is a supracellular actomyosin cable, but do they share other properties? How do they increase their speed, and do they also improve their ability to follow a gradient for example? Many questions can be asked with this experimental system, which will hopefully uncover some general properties of multicellular behaviors.

5.3 Broader perspectives

Both of these projects tackled specific questions related to cell biology, and call for further research in their own domains. However, my PhD has also raised more general questions and perspectives that I would like to develop here.

The first one concerns optogenetics, which has been the common denominator of both projects, together with the RhoA pathway. The second one refers to an important side project of my PhD related to the environmental impact of research, and some discussions about the future directions we could take.

5.3.1 Optogenetics to study cell signaling

Optogenetics, as described in the introduction, is a great tool in cell biology to demonstrate causality, notably because of its praised spatiotemporal precision. I have described some of the drawbacks and limitations in the introduction (see 1.3.3), but would like to come back on two of them, which were particularly revealed by my PhD experiments.

The first one is linked to the simplifications that are always introduced when speaking about optogenetic systems. As an example, recruitment of a GEF of RhoA to the membrane will be called opto-RhoA [Inaba et al., 2021] or even optoGEF-contract [Shellard et al., 2018]. This completely hides the complexity introduced by cell biologist for years, with dozens of activators of RhoA and a very complex function in different contexts. It seems that optogenetics has again reduced RhoA to one function, contraction, and that all GEFs are considered as equivalent, which is certainly not true. Simplifications are important to give a clear message, but I think that my PhD shows very clear examples of signaling complexity with optogenetics:

- the first project has revealed the differences between three GEFs of RhoA used with exact same recruiting tool, and has shown that one GEF could have very different effects depending on the context.

- this same project has shown that the expression of the optogenetic construct is key in understanding its function, as the tool can switch function by a change in concentration.

- the second project has confirmed the differences between two GEFs of RhoA, and the fact that optogenetic tools could have effects in the dark with the increasing speed of optoRac clusters.

How to avoid these oversimplifications? Few points include stopping describing optogenetics as on-off states, choosing names that more clearly refer to what the optogenetic tool is actually doing - what about "optorecruitLARG", as an example? -, and take into account the dynamics of the optogenetic tools in the analyses.

The second one is linked to the use of the optogenetic toolbox. This toolbox is increasing yearly, but has been going often in one direction: increasing the efficiency of the response. Researchers have been looking for stronger and faster recruitment, stronger and faster optogenetic responses, and stronger differences between dark and light states. However, this kind of strategies are most probably overriding the endogenous biological network. I saw it in my first project, where absolute concentrations of optoPRG are two orders of magnitude higher than the endogenous concentrations of PRG. It can teach us something about PRG interactions, but can we conclude something for how it works within a network?

Ideally, if possible, we would like optogenetic tools to perturb the protein network within its endogenous landscape. This requires much more careful measurements, dose-response curves of the optogenetics activation compared to endogenous range of activity, or design of specific tools that match as well as possible endogenous behaviors. Increasing data show how nanoscale spatial organization of proteins can greatly influence their activity: optogenetic tools now exist to play with these kinds of organization, thanks to oligomerizing variants of Cry2 for example, or the wide choice of affinity for optogenetic dimers.

5.3.2 Research in life science in a constrained world

This section comes out of work and reflections that followed my awareness concerning the climate, environmental and biodiversity crisis we are facing. It led me, together with Caroline Giuglaris, to compute the carbon footprint of our research lab, to propose a reduction plan, and launch a 20 people working group to halve our environmental impact by 2030. We presented this work multiple times and gathered it in a preprint added to the annex of my manuscript (see B). I deeply think that this crisis will have considerable impact on research in general, and more specifically on research in life science. Thus, I would like to discuss two points that seem to me important in this context.

First, research in life science is for the moment deeply dependent on fossil fuels, i.e., on carbon emissions. Its main emission factor comes from the purchases, followed by the travels (mainly emissions due to planes) and then electricity and heating. This seems to be a general trend for all biology labs, with differences coming from the type of experiments and the main sources of energy for electricity production in the country [De Paepe et al., 2023]. One way or another, this will have to be reduced, either because of higher prices, or because of regulations and constraints in the institutions and grants. Research will have to adapt, and the sooner, the better.

For our research unit, we proposed a trajectory of emission reduction aiming at halving emissions per capita from 2019 to 2030, a goal similar to the one proposed at the European Union level. We estimated the systemic reductions that come from our different suppliers, which have themselves taken pledges for carbon trajectory, and estimated the voluntary actions that have to be taken (see the first draft of the preprint

in B). We have to reduce emissions by 5% each year, and it is not an easy task; indeed, most decisions have an impact on our research. Most people agree on renovating a building or taking the train instead of the plane to go to Zurich from Paris, which are fairly transparent actions for research. However, few will accept to reduce the number of experiments, refuse to buy a new microscope or a new computer, participate in less conferences, or take more time to repair material or wash their own material instead of single use.

Mitigation strategies start to be proposed [De Paepe et al., 2023], but will require changes in mentality, or financial restrictions. Research in life sciences has grown in a world of energy abundance, which means that the changes required are systemic. Could I have done my PhD with a carbon budget divided by two? Yes, without doubt, with systemic changes combined with individual changes. It would have required more time (from me or from support teams) to repair what is broken, wash reusable glass dishes [Farley and Nicolet, 2022], build more efficient code to avoid buying a new computer, adapt new microscopes instead of buying a new one, etc... It would mean reducing the number of biological stocks in freezers, adapt air conditioning systems of the microscopy rooms, buy less drugs and consumables by more carefully planning experiments and sharing between the institute -which also requires time and careful stock management, as well as sharing systems. Lastly, it means not taking the plane in Europe, and allow one overseas conference during a PhD - which has been the case for me, also forced by Covid. Could I have done it with a carbon budget divided by ten? Certainly not in the actual world, which shows our dependencies on energy and modern society. How fast will we reach these new habits, and can it be done voluntarily without external laws or financial incentives? Can research then reach 'net zero' in 2050? Future will tell, but constraints will only grow, and the later, the harder the transformations will be.

In this first point, I tried to rapidly describe how we could adapt our habits, without changing research topics or the way we do science. However, research topics will also be impacted by the societal changes. Fundamental research is not working independently from the outer world, and it is always linked to interests of states and companies that fund it. The increasing existential threat of the ecological crisis will lead to changes in funding priorities - and has already started to do so -, which will certainly have profound impacts on the laboratory and research topics. Moreover, science, associated with technology, is often considered as partly responsible for the modern society we are living in, which is responsible for global destruction of life on the planet [Voulvoulis and Burgman, 2019]. As a result, science is also expected to change and find solutions to the different problems of the environmental crisis. More and more scientists are aware of the problem and are start to act, at their level or the level of their institute, but also by taking political actions [Capstick et al., 2022, Krawczyk et al., 2023]. This goes much beyond the reduction of the carbon footprint, which is necessary but not sufficient, to my opinion, for us to take part in the answer to this challenge. I expect that a lot of research subjects will have to be abandoned in front of the different economic and environmental impacts, and hope that scientists will be leaders in this transition, even if it comes with sacrifices.

To end with a more positive note, I would like to stress out the benefits that this crisis can have on research in life sciences. Indeed, it has really revealed our interdepedence with most living systems on Earth, both at the global and at the local scale. We understand everyday a bit better how life cannot be considered alone, but only with its environment and other living systems around. As a very concrete example, we see now how early life has shaped the atmospheric concentrations of the different

gases, and how we depend on it. We discover how water, plants and all living systems are interdependent, and research to understand those interdepedencies are increasing, at the local and global scale. To make a link with my introduction, we cannot limit the understanding of life to the understanding of the cell. One way or another, one has to take into account relationship between living systems, and how they shape each other. Let us continue uncovering the exquisite complexity of living systems and stay amazed in front of the fascinating mechanisms and interactions we have the chance to face and study.

Chapter 6

Materials and Methods

During my thesis, I used different techniques that perturb cellular processes in space and time in a controlled manner. These techniques include creation of stable cell lines, micropatterning, optogenetic activation, pharmacological and trafficking assays, live-cell imaging, and modelling. I employed image analysis and statistical techniques to extract the data from my experimental dataset.

6.1 Cells

6.1.1 Cell culture

hTERT RPE1 cells (CRL-4000 strain, ATCC, Manassas, VA) were cultured at 37 °C with 5% CO_2 in Dulbecco's modified Eagle's/F-12 medium supplemented with 10% fetal bovine serum, GlutaMAX (2 mM) and penicillin (100 U/mL)-streptomycin (0.1 mg/mL).

HT29-MTX-E12 cells were cultured at 37°C with 5% CO2 in Dulbecco's modified Eagle's medium, high glucose, GlutaMAX™, pyruvate(Thermo Fisher Scientific, Waltham, MA, ref #31966), supplemented with 10% fetal bovine serum, GlutaMAX (2mM) and penicillin (100 U/mL)-streptomycin (0.1 mg/mL).

Cells were passaged twice a week in a ratio of 1/10 by washing them with PBS (1X) solution and dissociating using TrypLE Express (Thermo Fisher Scientific, Waltham, MA) reagent for 3 to 5 minutes.

For cluster production, 1.5 million cells are plated in a Petri dish (non culture coated) with 10ml of culture medium for 3-5 days.

6.1.2 Plasmids

dTomato-2xrGBD (Plasmid #129625) (RhoA biosensor), pLL7:Venus-iLID-CAAX (#60411), 2XPDZ-mCherry-Larg(DH) (Plasmid #80407) plasmids were bought from Addgene (Watertown, MA).

pLVX: MRLC-iRFP, pLVX: Lifeact-iRFP pLVX: PBD-iRFP (PAK biosensor) plasmids were made by Simon de Beco (Institut Curie, France).

PRG(DHPH)-CRY2-mCherry and Tiam(DHPH)-CRY2-mCherry made by from Leo Valon (Institut Curie, France). pLL7:PRG(DHPH)-iRFP, pLL7:LARG(DH)-LARG-CRY2-RFPt, were subcloned in the lab, from PRG(DHPH)-CRY2-mCherry, and 2XPDZ-mCherry-Larg(DH) respectively.

pCMV:PRG(DHPH)-RFPt-SspB-P2A-mVenus-iLID-CAAX is a gift from Alessandra Casano (EMBL).

pLL7:PRG(DHPH)-iRFP-SspB-P2A-mVenus-iLID-CAAX was subcloned by Maud Bongaerts (Institut Curie, France) from PRG(DHPH)-CRY2-mCherry and pLL7:Venus-iLID-CAAX.

pCMV:PRG(PH)-iRFP-SspB-P2A-mVenus-iLID-CAAX was subcloned by Benoit Boulevard (Institut Curie, France) from pCMV:PRG(DHPH)-RFPt-SspB-P2A-mVenus-iLID-CAAX.

pCMV:PRG(PH)-RFPt-SspB-P2A-mVenus-iLID-CAAX was designed in the lab and synthesized by Twist Bioscience (Twist Bioscience, San Francisco).

Rac and Cdc42 biosensors, delCMV-mCherry-3xp67Phox and delCMV-mCherry-WaspGBD respectively, described in [Nanda et al., 2023], were gifts from Leif Dehmelt (Dortmund and Max Planck Institute of Molecular Physiology).

6.1.3 Transfection

Transfections were performed using jetPRIME®versatile DNA/siRNA transfection reagent according to the manufacturer's protocol. Different ratio of plasmid DNA were used depending on the constructs for cotransfections, and a ratio of 2:1 of transfection reagent and DNA was always used. Experiments were performed at least 30 hours after DNA transfection, and 48 hours after siRNA transfection.

6.1.4 Stable cell lines

Stable cell lines were generated using lentiviral infection. For lentivirus production, packaging cell line HEK 293T were cotransfected with pMD2g (envelope), psPAX2 (packaging) and lentiviral (transfer) plasmids in a 1:3:4 ratio, respectively. Lentivirus was harvested 48h after transfection and filtered from the supernatant of cell culture by passing it through 0.45µm filter. Next, the target cell line was transduced for 24h with media containing lentiviral particles. Cells were then selected by Fluorescence-activated Cell Sorting (FACS) according to the fluorescence level of transduced protein, with multiple rounds of selection if needed. For the HT29-MTX cell line recruiting DH-PH domain of PDZ-RhoGEF, cells have been transduced twice for the CRY2 part.

6.1.5 Drug assays

For all drugs assays, 25 to 50 cells were first selected and optogenetically activated for 30 to 40 minutes. Ten minutes after the end of the first activation, the medium was replaced by the drug diluted in complete DMEM/F-12 medium at specified concentrations and for the specific duration (see each figure for precision on concentration and duration). The drugs used are : Y-27632 dihydrochloride (selective ROCK inhibitor, TOCRIS bioscience, #1254, SMIFH2 (Formin FH2 Domain Inihibitor, CAS 340316-62-3, Calbiochem), Rho Inhibitor I (Cytoskeleton, Inc.), IPA-3 (p21-Activated Kinas Inhibitor III, CAS 42521-82-4, Calbiochem).

6.1.6 Optogenetics

For the design of the optogenetic dimers used during the PhD, we relied on two different optogenetic dimers: iLID-SspB described in [Guntas et al., 2015] and Cry2-CIBN described [Kennedy et al., 2010] for the collective amoeboid project. The cytosolic part (CRY2 or SspB) is attached to a part of the desired GEF, and a fluorescent protein (red or infrared). The other part of the dimer (CIBN or iLID) is attached to the plasma membrane via CAAX doamin, and also attached to a fluorescent protein(GFP or mVenus). CRY2 and iLID change conformation upon illumination with blue light

(below 510 nm, with a peak around 450nm for iLID [M. Salomon et al., 2000] and 360nm and 450nm for CRY2 [Liu et al., 2008]). After the conformational change, the binding affinity of the two parts of the dimer increases, which leads to the recruitment of the cytosolic part to the membrane. (Figure 6.1).

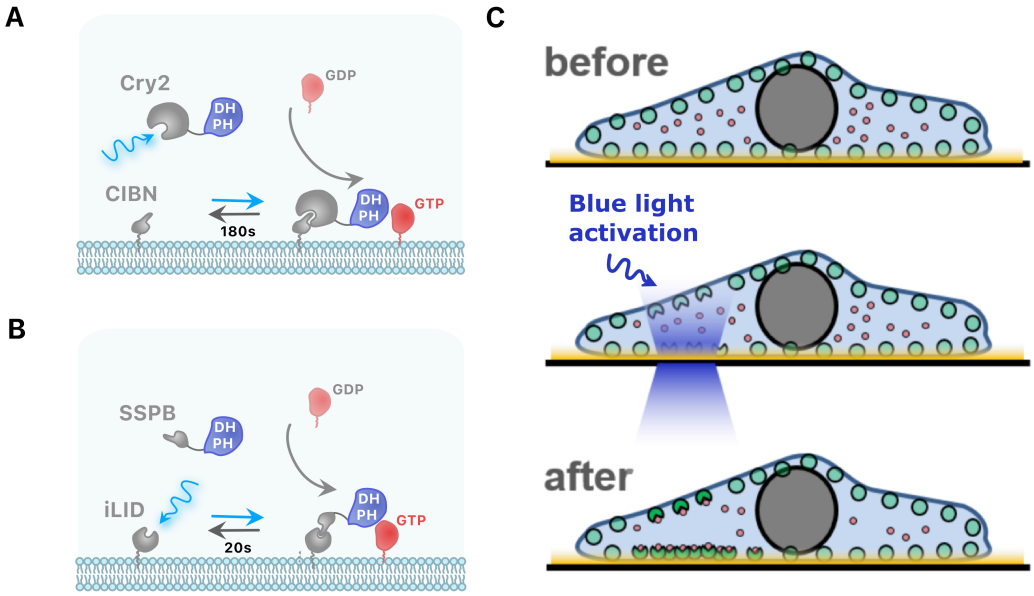

Figure 6.1: Optogenetic systems used during the thesis. Cartoon depicting recruitment of DH-PH domain thanks to CRY2-CIBN dimer (A) or iLID-SspB dimer (B). (C) Side view of optogenetic recruiment in a cell attached on a 2D substrate. Membrane part of the dimer is in green and cytosolic part in red. After blue light activation (creating a cone because it is focused on the bottom plane), there is a change in conformation in one of the dimer (here the one at the membrane), leading to binding of the cytosolic part. Adapted from [Valon et al., 2015].

HT29-MTX cells used in the collective amoeboid project were engineered to stably express the optogenetic dimer and selected for average-high fluorescence level by FACS. RPE1 and Hela cells used in the main project were always transiently transfected with the different plasmids and selected for different levels of intensity (6.1.2).

6.2 Imaging

6.2.1 Live-cell imaging

Imaging was performed at 37 °C in 5% CO_2. Two different microscopes have been used: an IX83 and an IX71 (Olympus, Melville, NY) both with inverted fluorescence and Differential Interference Contrast (DIC) and controlled with MetaMorph software (Molecular Devices, Eugene, OR). Both microscopes were equipped with a 60x objective (NA=1.45), motorized stage and filter wheel with SmartShutter Lambda 10-3 control system (Sutter Instrument Company, Novato, CA), a stage-top incubation chamber with temperature and CO_2 control (Pecon, Meyer Instruments, Houston, TX), a laser control system with azimuthal TIRF configuration (iLas2, Roper Scientific, Tucson, AZ).

The IX71 was equipped with an ORCA-Flash5.0 V3 Digital CMOS camera (Hamamatsu Photonics K.K., Japan), a z-axis guiding piezo motor (PI, Karlsruhe, Germany),

a CRISP autofocus system (ASI, Eugene, OR), and a DMD pattern projection device (DLP Light Crafter, Texas instruments, Dalas, TX), illuminated with a SPECTRA Light Engine (Lumencor, Beaverton, OR) at 440±10 nm.

The IX83 has a built in z-piezo and autofocus, and was equipped with a Evolve EMCCD camera (Photometrics, Tucson, AZ) and a FRAP configuration (iLas2, Roper Scientific, Tucson, AZ).

6.2.2 Imaging environment: coating and microchannels

Coverslip coating with fibronectin. Coverslips for live-cell imaging were prepared by cleaning round glass coverslips (d=25 mm, 0.17 mm thickness) (Menzel Gläser, Thermo Fisher Scientific, Waltham, MA) for 1 min in O2 plasma and incubating them with fibronectin (2 µg/mL) (Merck, Darmstadt, Germany) in 100 mM NaHCO3 (pH 8.5) for 1 h in room temperature. Coverslips were washed with PBS (1x) three times and stored in +4°C in PBS (1x). Before imaging, cells were dissociated using TrypLE Express (Thermo Fisher Scientific, Waltham, MA) reagent and seeded for adhesion on the coverslips, waiting at least three hours before imaging.

Microchannels preparation and drug incubation. Chips are made of a polydimethylsiloxane mixture (PDMS, RTV615, Neyco) 10:1 ratio with crosslinker. The mixture is poured on the epoxy mold and polymerised at room temperature for at least 48h. Loading ports are made with a 1mm hole puncher. Chips are sterilized with 70% ethanol for a few minutes, dried and activated for 1 min in a plasma cleaner together with a glass substrate (40mm or 25mm glass coverslip). PDMS chips are stuck to the activated glass and directly coated for at least 30 min with 0.1mg/ml pLL-g-PEG (pLL(20)-g[3.5]-PEG(2) from SuSoS). Chips are washed once in full DMEM and then submerged with medium for 1h to overnight.

Big clusters loading. Clusters are filtered on a 70µm strainer (Corning 431751), pelleted by a 400g pulse centrifugation and resuspended at 250 clusters/µl in full DMEM. Clusters are loaded using a 25µl syringe (Hamilton, 702SNR 22/51mm/pst3).

Small clusters loading. Cells are filtered on a 40µm strainer (Corning 431750) immediatly after detachment with Trypsin, centrifuged and resuspended in full DMEM. They are then loaded using the 25µl syringe (Hamilton, 702SNR 22/51mm/pst3).

6.2.3 TIRF and HILO microscopy.

Total Internal Reflection Microscopy (TIRF) (also known as evanescent wave microscopy) is a widefield microscopy technique, which uses properties of evanescent wave of light, that appear happening at the interface of two media with different refractive indices (usually, a specimen and a glass coverslip) when the laser is totally reflected (Figure 6.2). This evanescent wave of light decays exponentially and propagates ∼100-200 nm into the specimen. Only the fluorophores in this area are then excited and emit photons. This technique is mainly used to explore processes happening close to the membrane of live adherent cells [Mattheyses et al., 2010].

Our setups are equipped with azimuthal TIRF. Instead of projecting at a single angle, the laser spins at the backfocal plane of the objective. It generates homogeneous illumination and, like this, avoids fringe interferences and imaging artefacts.

With our TIRF system set-up, we could also easily switch to a Highly inclined and laminated optical sheet (HILO) microscopy, just by reducing the tilt of the laser. In this case, the laser goes through the sample at a sharp angle, and instead of illuminating the full volume as in wide-field epifluorescent imaging, it illuminates a fraction of it

with a thin inclined beam (Figure 6.2). This increases the signal-to-noise ratio of the image [Tokunaga et al., 2008].

We used TIRF microscopy for the biosensors of Rac and Cdc42 presented in Figure 3.17. For all other measurements with the first project presented in chapter 3, we used HILO microscopy, as well as for the second project presented in chapter 4.

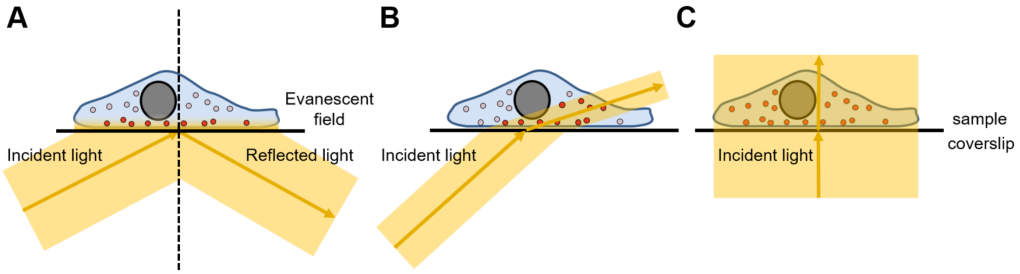

Figure 6.2: TIRF, HILO and wide-field epifluorescence microscopy. Comparison of fluorescent molecule activation when imaging with different microscopy techniques (adapted from [Tokunaga et al., 2008] and [Mattheyses et al., 2010]).

6.2.4 DMD projection device for patterned illumination

A Digital Micromirror Device (DMD) is an array of microscopic mirrors (10 µm x 10 µm), that can individually tilt [Davis, 2013], which make the light be reflected in two different directions. One of these directions is set in the light path ('on' state), when the other reflects the light elsewhere ('off' state). The DMD then acts as a projection device, which image can be coupled to the imaging plane. The DMD used in the experiments was a DLP4500 with a LC4500 controller from Keynote Photonics (Keynotes Photonics, Allen, TX). The chip has a dimension of 1140 x 912 micromirrors (6161.4µm x 9855µm), able to generate 8-bit grayscale patterns. We generated custom illumination patterns using the DMD and a blue LED illumination source (SPECTRA Light Engine (Lumencor, Beaverton, OR). For a scheme of our set-up, see Figure 6.3. Two strategies were used to create these patterns.:

- **projection through HDMI (High-definition multimedia interface) and "video mode"**: the DMD is used as a projector (a second screen). A custom made software was developed previously by the team in MATLAB allows to draw any pattern, and send it in full screen on the the DMD. This was the mode used for the imaging routine described in the section 6.2.5, therefore for all the experiments dealing with the cell clusters over long period of time.

- **projection through USB interface and static pattern**: I realized that the DLP4500 had an artifact in video mode: the dark pixels sent in video mode were not completely dark, they were still flipping 'on' from time to time, increasing the residual light in the non illuminated parts of the cells (this was not the case in the previous chipset we had, the DLP3000, which broke at the beginning of my PhD and that we could not get again). To solve this issue, I developed a Python-based software to send patterns through the ethernet command, through which all pixels can be controlled individually. The software is available on Github (https://github.com/jdeseze/DMD).

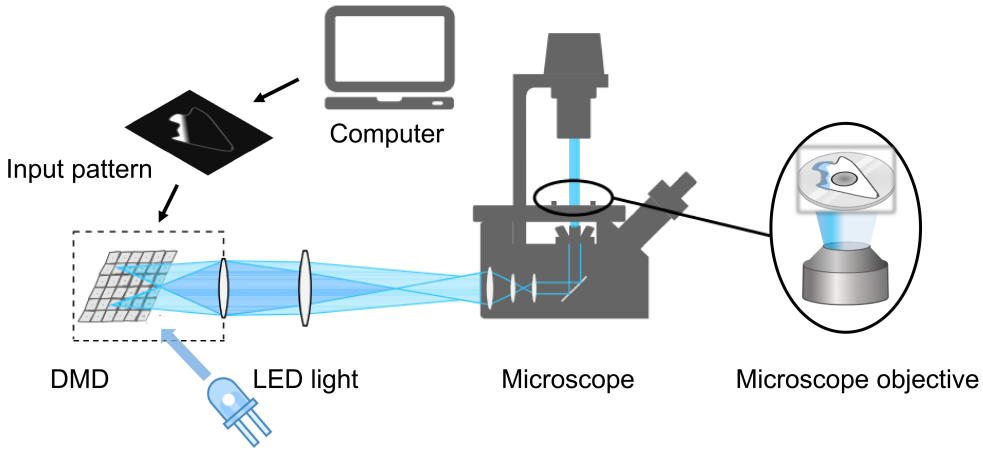

Figure 6.3: Light activation with DMD projection device. Taken from [Vaidziulyte-Simutiene, 2021], adapted from [Rullan et al., 2018].

6.2.5 Cell finder

The first project of my PhD required identifying transfected cells on coverslips with a wide range of fluorescence intensities, working with single cells. This prompted me to develop a small Python software (Python Software Foundation. Python Language Reference, version 3.9.5.), which I named **Cell finder**, that greatly facilitates the search for transfected cells. This software, available on Github (https://github.com/jdeseze/cellfinder), scans the entire available area, finds any fluorescent object larger than a predefined size (with a threshold to define what is fluorescent), and produces the resulting list of locations in customized format for the Metamorph imaging software. If the number of cells found is too important, I created a Python-based GUI interface to select only the desired positions based on the image acquired during the search trajectory. It allows seeding cells at low density to scatter them, and still have dozens of transfecting cells within one 25mm-coverslip for the experiments.

6.2.6 Imaging routine to follow migrating clusters

Imaging routine to follow migrating clusters was adapted from the software developed previously in the lab to follow and activate single cells [Vaidžiulytė et al., 2022]. The acquisition is running on MATLAB, with a graphical user interface (GUI) to define the different parameters of acquisition (Figure 6.5). Commands to control the displacement of the microscope stage are sent to the Metamorph imaging software. The patterns of illuminations are sent to the DMD as an image through the HDMI connection.

Improvements to the already existing software include: having an autofocus at each timestep (instead of each position) and correct all positions accordingly, reduce memory usage and image computations in order to increase the number of positions for one experiment (from 17 positions in 2.5 minutes to 35), adding a possibility to import directly all positions from metamorph generated positions, and modify the segmentation algorithm to match clusters specificity. I also adapted this improved software to other microscopy platforms in Institut Gustave Roussy, to be able to follow clusters of cells at high resolution for multiple hours.

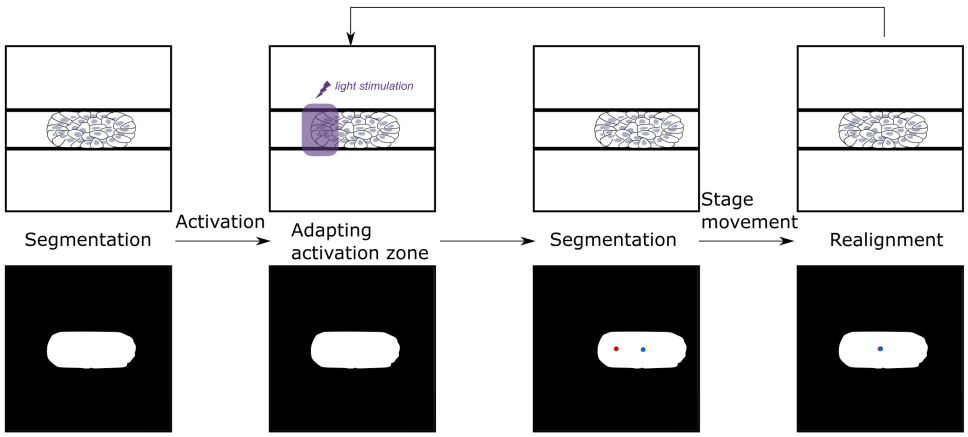

Figure 6.4: Description of the feedback routine. The cluster is automatically segmented and activated on the right or on the left, at one predifinite position. when the cluster moves, the center of the cluster (blue dot) is compared to the center of the field (red dot) and the stage is moved so that the two match. This is done at each time step, so that the stage and the activation follows the cluster in its movement. Adapted from [Vaidžiulytė et al., 2022].

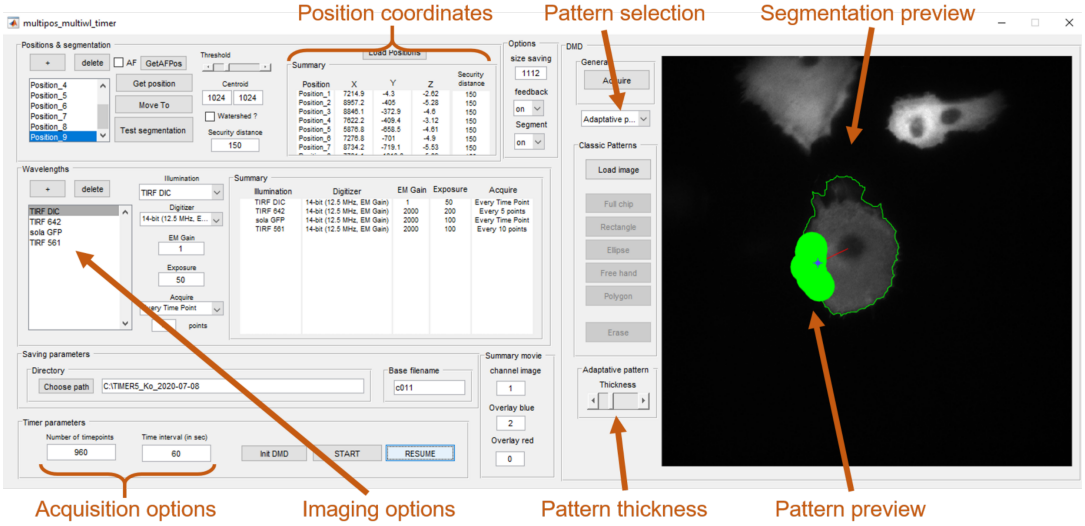

Figure 6.5: Feedback routine GUI to follow any fluorescent cell or cluster. Here a fluorescent single cell is shown on the right, with the corresponding segmentation in green, and the decided pattern of activation (wide green area), decided by an angle taken from the center of the cell. The GUI communicates with Metamorph Imaging software that is doing the interface with the different microscope components. Taken from [Vaidziulyte-Simutiene, 2021].

6.3 Image analysis

All image analyses have been done with homemade scripts, using Fiji software [Schindelin et al., 2012] and MATLAB (MATLAB version: 9.13.0 (R2022b), Natick, Massachusetts: The MathWorks Inc.; 2022.) for the collective amoeboid project, and Python (Python Software Foundation. Python Language Reference, version 3.9.5.) through the napari interface [Chiu and Clack, 2022] for the optogenetic control of antagonist functions. All movies were created with Fiji, as well as picture montages. The kymographs have been done thanks to the *Reslice* function in Fiji, with different linewidths depending on the with of the cell.

6.3.1 Pipeline analysis for membrane displacement and fluorescent quantifications

For all the experiments on single cells, quantification have been done thanks to custom plugins for napari imaging software [Chiu and Clack, 2022] that I developed during my thesis and available on github (https://github.com/jdeseze/napari-intensity-measurements). It comprises the following steps (see Figure 6.6):

- an experiment reader that reads Metamorph metadata (".nd" file) and directly select the good timepoints, and channels to display on the napari interface. (1)
- a croper, to select specific area when the cell is not alone on the field of view. (2)
- two different segmentation algorithms can be chosen. The first simply uses any fluorescent channels, performs a gaussian filter and has a tunable threshold (3). It was used for quantifying fluorescence when one fluorescent channel was very stable. The second uses the DIC channel and was used for quantification of membrane displacement. It uses optical flow Farneback algorithm in a similar way than in [Robitaille et al., 2022], using the function from openCV library, and thresholding it. The user has few tunable parameters, including the threshold and the number of iterations (which is a parameter of the optical flow algorithm).(4) It had the advantage of being completely independent of the fluorescence intensity which could be varying. Howevern, it required more tuning and could only be used if the cell is single.
- a calculation section, which saves all the desired quantities: intensity in the chosen channels, type of phenotypes, comments, as well as intensity a the drawn area (usually the area of activation). (5)

All the data are saved in custom python object, in Panda dataframes as well as in text files that can be read, to enable an easy data handling and further analyses.

6.3.2 Pipeline analysis for clusters movement

Analyses of cluster displacement was performed with the following steps:

- appropriate stiching of the movies taking into account the displacement of the xy stage due to feedback routine, done in MATLAB.
- automatic segmentation in Fiji, with one filtering step (*Gaussian Blur*), one automatic thresholding step (*Threshold>MaxEntropy*), one dilation step (*Dilate*), one step for filling holes (*Fill Holes*), and one eroding step (*Erode*).

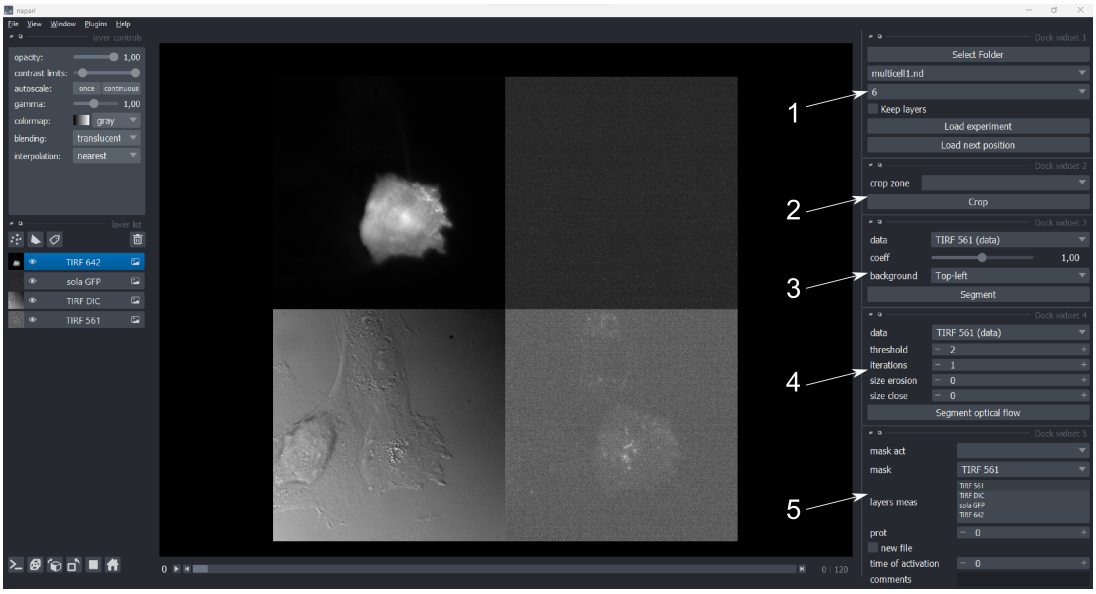

Figure 6.6: Image analysis with napari. Different independent napari plugins have been developed for image analysis. (1) the experiment reader comprises a folder picker and two dropdown list to select the experiment and cell number, according to the metadata that have been read. (2) the croper that crops all the different channels according to the area selected. (3) and (4) two different cell segmenter, one with a simple threshold (slidebar, (3)) for fluorescent data, and one that segments thanks to the optical flow method, that comprises four different parameter choices ('threshold', 'iterations', 'size erosion' and ' size close', (4)). The segmented area will appear as a contour on another binary channel. (5) the section to perform the analyses, where the area of activation is selected (dropdown list 'mask_act', that chooses along all shapes layers), the mask ('mask' dropdown list, to be selected among binary layers), the layers where the measurements have to be performed (layers meas multiselection). The user can decide what is the phenotype of the cell thanks to the 'prot' parameter, in my case 0 (retracting phenotype), 1 (protruding phenotype) or 2 (mixed or not moving phenotype). The frame of the first optogenetic activation can be reported in the time of activation section, and comments can be added.

- center of the cluster is found with MATLAB, giving access to the coordinates of the cluster along time, which enable the different plots.

For small clusters tracking, Trackmate7 [Ershov et al., 2022] was used in the channel of both MLC-GFP and H2B-mCherry through Fiji, and tracks extracted were further processed in python.

6.3.3 Data processing

Surface displacement : Surface displacement is the area of the intersection between the activated area and cell segmentation.

Normalization : Biosensors intensities are calculated the following way. First, background is substracted. Second, mean intensity in the intersection between activated area and cell segmentation is calculated. Third, this intensity is divided by the mean intensity in the non activated part of the cell. Fourth the intensity is normalized by the intensity before the optogenetic activation.

Dotplots of intensities : the normalized curved at the specific timepoints specified in each figures are plotted as swarmplots, with the means.

Images and movies : for DIC images, raw image are divided by the gaussian-filtered image with a large diameter, from 30 to 50 pixels, to correct for uneven illumination.

Sankey diagrams : sankey diagrams were done by modifying a python library called pySankey (https://pypi.org/project/pySankey/).

Persistence : persistence was calculated as the ratio between the actual distance from the initial point and the sum of the absolute value of all displacements.

Myosin ratio : clusters were cut it in half along the x-axis, and the ratio between left (activated) and right (non-activated) part was measured.

6.4 Modelling

The modelling was performed with Python software (Python Software Foundation. Python Language Reference, version 3.9.5.). The differential equations were integrated thanks to the *odeint* function from scipy.integrate package, and all the fitted parameters were found by the least squares method, using *fmin_powell* function from scipy.optimize for minimization, which uses Powell minimization's method.

Appendices

Appendix A

Spatio-temporal dynamic of small GTPase RhoA - Internship Report of Josephine Gatin

Spatio-temporal dynamic of small GTPase RhoA

Avril – Juillet 2022

Joséphine Gatin

institut Curie

ÉCOLE POLYTECHNIQUE

INSTITUT POLYTECHNIQUE DE PARIS

CONTENTS

ABSTRACT

Cell migration is an important biological process controlled by a fine balance between contraction and extension cell cytoskeleton, mainly regulated by the Rho-GTPases family of proteins. They have an active state (GTP-bound state) and an inactive. Among them, RhoA has been shown to be involved in actomyosin contractility by its regulating activity on several effectors including ROCK and mDIA. To have a better understanding of RhoA regulation in space and time, we looked at RhoA's localisation inside the cell. Confocal microscopy confirmed that RhoA was to a large extent in the cytosol. FRAP experiments showed that RhoA is very labile at the membrane and is stabilized at the membrane when in its GTP-bound state. Optogenetic activation of RhoA activators at the plasma membrane is triggering both contractile and protrusive phenotype and can lead to the local recruitment of RhoA at the plasma membrane. Therefore, RhoA can not be seen only as a switch. It is at the membrane with a turnover rate that depends on its activity state and its potential to bind to effectors and activators.

La migration cellulaire est un processus biologique important contrôlé par un équilibre entre la contraction et l'extension du cytosquelette cellulaire. Ce processus est notamment régulé par une famille de petites protéines : les Rho-GTPases qui ont un état actif (lié à GTP) et un état inactif. Parmi elles, RhoA est impliqué dans la régulation de la contractilité liée à l'actomyosine par son activité sur plusieurs effecteurs en aval dont ROCK et mDIA. Pour mieux comprendre la régulation de RhoA dans l'espace et dans le temps, nous avons étudié la localisation de RhoA à l'intérieur de la cellule. La microscopie confocale a confirmé que RhoA se trouvait en grande partie dans le cytoplasme. Des expériences de FRAP ont montré que RhoA est très labile à la membrane et est stabilisée à la membrane lorsqu'elle dans sa conformation GTP. L'activation optogénétique des activateurs de RhoA à la membrane plasmique peut provoquer deux phénotypes opposés dans les zones activées chez des cellules humaine : de la contraction ou de la protrusion. Cette activation peut conduire au recrutement rapide et local de RhoA à la membrane plasmique dans la zone activée. Par conséquent, RhoA ne peut pas être seulement considérée comme un interrupteur passif. Elle est présente à la membrane de manière dynamique avec une période de renouvellement qui dépend à la fois de son activité et de ses interraction avec ses effecteurs et ses activateurs.

ACKNOWLEDGMENTS

First, I would like to thank Jean De Seze for his daily communicative joy. I have to admit that this first research experience was fantastic thanks to his kind guidance and his enthusiasm. Thanks for the good advice, the shared code, the explanations, the help in designing the report. I still owe him some chocolate bars!

A big thank to Mathieu Coppey for welcoming me in the team. Always available to solve a microscope problem or to discuss a result, despite a busy schedule, his energy and good mood were of great help. Thanks for the time spent at the right moment so that I can continue to move forward. I realized that his interest in each and every one of the team member is invaluable.

I would like to thank my office mates Iris and Benjamin with whom I had a great time. I will keep beautiful memories, Toulouse, Hanabi and so on! Thanks for putting up with my idle questions, for the re-reading of the report, the advice and the beers after work.

I also would like to thank Romain, for this internship that we spent together, the help for the assembly of the filters, the Codex, the good jokes, the lunches,...

I would like to thank Maud, Lorena, Mirna and Benoît who helped with laboratory techniques and equipment.

I also have to thank a lot the LOCCO team, for the great team dynamic you have, that accompanied me during these 4 months and that was really nice and helpful.

I would like to thank Laurence Vaselin without whom we would not have experienced this superb team retreat in Oudans.

I want to thank Christophe Grolleau for all the help with the utilization of the Software MetaMorph.

I want to thank Caroline Giuglaris and Mathilde Lacroix for the Climate Fresk and their investment in the unity to design a more sustainable future for the lab.

INTRODUCTION

Cell migration is an important process in many physiological events such as embryonic development, wound healing and has also an important role in cancer development, particularly in the formation of metastases. Single cell migration is controlled by a fine balance between contraction and extension of its cytoskeleton, especially through actin and myosin dynamics. This cellular cytoskeleton is mainly regulated by master regulator proteins that share common features, the Rho-GTPases.

The three canonical Rho-GTPases, Rac1, Cdc42, and RhoA, are a set of small proteins which control a large number of intracellular processes such as the cytoskeleton's dynamics, cell-cell adhesion and apoptosis [1, 2, 3, 4]. These small proteins are hubs in signalling pathways, integrating both extracellular and intracellular signals. They regulate the activity of many effectors proteins in both space and time . Rho-GTPases continually switch between a GDP-bound inactive state and GTP-bound active state. The switch is possible thanks to the enzymatic activity of Guanine Exchange Factors (GEFs) and GTPase-activating proteins (GAPs) that respectively activate and inactivate the GTPases. In their active state, Rho-GTPases can recruit and activate a wide range of effectors, and thus trigger several signalling pathways. RhoA has been shown to be involved in actomyosin contractility, especially during rear retraction in mesenchymal cell migration. RhoA regulates both the activation of ROCK and the activation of the formin mDIA [5]. The kinase ROCK activates non-muscle Myosin II by phosphorylation and mDIA polymerizes actin in the form of bundles which provide a substrate for Myosin II to bind. Additionally, the sequestration of Rho GTPases by Guanine nucleotide Dissociation Inhibitor (GDIs) can modulate the level of active Rho GTPases (Figure 1).

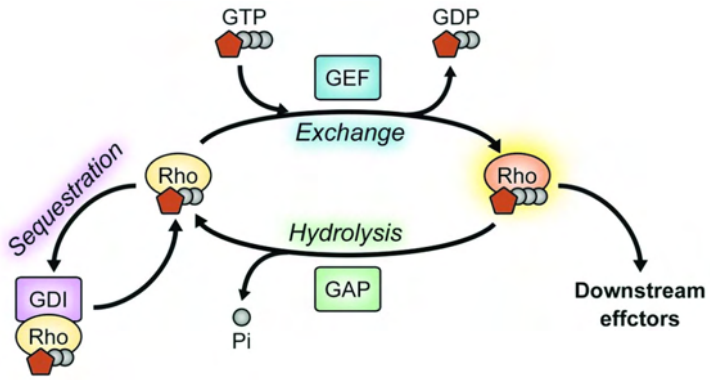

Figure 1: Overview of Rho GTPase regulation from [6]

Rho-GTPases are commonly described as plasma-membrane bound proteins. They are post-translationally modified through their C-terminal CAAX motif which leads to the addition of

a lipid moiety. This CAAX motif thus targets them to the plasma membrane [7]. This is why Rho-GTPases are classically viewed as 'passive' switches, waiting at the plasma membrane to be activated by GEFs and inactivated by GAPs. However, this simple vision of Rho-GTPases seems to be rather limited. Indeed, Rho-GTPases have been observed both in the cytosol and at the plasma membrane. In particular, RhoA is clearly mostly cytosolic while it is not the case of Rac1 and Cdc42 that are found equally at the plasma membrane and in the cytosol [8].

In addition, the functional role of RhoA is still debated, especially in the context of cell migration [9]. According to different works, RhoA's activity has been reported in both contracting and protruding regions of cell. The role of RhoA in cell contraction is coherent with the known pathways activated by RhoA, whereas the role of RhoA in protrusion is less clear [10].

To tackle the question of the functional role of RhoA, Jean de Seze (Mathieu Coppey's team, Institut Curie, Paris) uses optogenetics. Optogenetics allow the control of cellular processes using light sensitive proteins and specific illumination patterns (over space and time). Jean observed (unpublished work) that the activation of RhoA could lead to two opposite phenotypes, either a protrusion or a contraction.

During this internship project, we wanted to address the following question : How can RhoA activation lead to two opposite effects in the cell, and how are they regulated ?

The objective of my internship was thus to have a better understanding of RhoA regulation in space and time. To gain insights into these questions, I first wanted to look at RhoA's localisation inside the cell and how it was partitioned between the membrane and the cytosol depending on its activity. Using Confocal and Total Internal Reflection Fluorescence (TIRF) microscopy, I looked at transiently transfected cell lines and saw that RhoA is largely located in the cytosol. However, I will have to investigate more to compare precisely the proportion of RhoA at the membrane versus in the cytosol. Then I looked at the temporal dynamic of RhoA protein at the membrane with the technique of Fluorescence Recovery After Photobleaching (FRAP). I could show that RhoA has a temporal dynamic similar to a cytosolic protein suggesting that RhoA is very labile at the membrane. Finally, I looked at RhoA activity, and how it was linked to its localisation, using Fluorescence Resonance Energy Transfer (FRET) biosensors. This last part gave preliminary results that would need further investigation but showed that RhoA is not only been seen as staying active or inactive at the membrane, but is actively shuttling in and out of the plasma membrane with a turnover rate that depends on its activity state and its potential to bind to effectors.

1
SPATIO-TEMPORAL LOCALIZATION OF RHOA

RhoA was supposed to be located at the plasma membrane. The addition of a lipid moiety after translation and the fact that both its actuators and effectors are at the membrane, were evidences further supporting this fact.

Yet, the spatio-temporal localization of RhoA has not been very well studied, partially due to the assumption that RhoA is only at the plasma membrane, as a passive switch. However spatio-temporal localisation of signaling molecules could play a crucial role in the regulation of pathways. The interaction with both activators and effectors over space and time plays an important part in the processing of the signal.

Here, we considered RhoA as a dynamic protein in space and in time in order to better characterize its behavior. Our first approach was to observe the binding-unbinding reactions between RhoA and the plasma membrane. It allowed us to describe the different parameters involved in the dynamic of this protein. The kinetic of binding and unbinding are given by the rate constants associated to those two reactions. For instance, if we consider the binding of RhoA to the membrane, we have the following equation:

$$RhoA_{cytoplasm} \underset{k_{off}}{\overset{k_{on}}{\rightleftharpoons}} RhoA_{membrane} \qquad \text{with } K_d = \frac{k_{off}}{k_{on}} \tag{1}$$

with k_{on} the binding constant and k_{off} the unbinding constant. K_d is the dissociation rate of RhoA.

We can see that the dynamic reaction at the membrane depends on rates which characterize the stability of RhoA at the plasma membrane. Those rates also give us an idea of how much RhoA is retained at the surface of the membrane by intrinsic components or external actors such as its interaction partners. These rates may vary in space and in time. The equilibrium also depends on RhoA concentrations in the cytosol (or at least in the layer surrounding the plasma membrane) and in the membrane : the localization of RhoA is as important as the binding kinetics. Thus diffusion of RhoA in the cell is another parameter that must be taken in account to describe the spatio-temporal localization of RhoA. Indeed, diffusion is the ability of a molecule to passively move thanks to thermal agitation. The diffusion can be at the plasma membrane or in the cytosol. The diffusion processes are characterized by D_m and D_c, which are the diffusion cœfficients in the plasma membrane and in the cytosol respectively, given by

the equation of diffusion in the cytosol or in the plasma membrane :

$$\frac{\partial C_{m/c}}{\partial t} = D_{m/c} \nabla C_{m/c} \tag{2}$$

with $C_{m/c}$ the concentration of RhoA at the membrane or in the cytosol.

While these equations and parameters describe a theoretical behavior of RhoA at the membrane, different microscopy techniques have been developed in the last few decades in order to observe the spatio-temporal localization of proteins in living cells [11]. The basis of those techniques relies on fluorescent proteins that are fused to a protein of interest. To make those proteins expressed by cells, the coding sequence of the fused protein is inserted in a DNA plasmid containing a eucaryote and a procaryote origin of replication and a gene of resistance to an antibiotic (used to amplify the plasmid in bacterias and rapid selection of the positive colonies for purification). The construct is finally expressed in the cells in a transient manner. These techniques include Single-Particle Tracking (SPT), Fluorescence Correlation Spectroscopy (FCS) and Fluorescence Recovery After Photo-bleaching (FRAP).

It is also interesting to look at RhoA's active and inactive mutants to better understand the behavior of the wild type (WT) protein. Here we considered two principal mutants of the RhoA :
– the constitutively active RhoA Q63L : (glutamine to leucine substitution at residue 63) the GTPase is always in its active (GTP-bound) state because the mutation prevents its endogenous and GAP-stimulated activity. A similar mutation in Ras (Ras(Q61L)) behaves as an oncogenic mutation ;
– the constitutively inactive RhoA T19N : (threonine to asparagine substitution at residue 19) the mutation prevents the GTPase's affinity for GTP and reduces its affinity for GDP. The protein is always in its nucletiode free state or in its inactive (GDP-bound) state. Therefore it binds strongly to the GEFs (activators) and so it inhibits the activation of the wild type proteins by these GEFs (dominant negative).[12]

We first wanted to characterize the spatial and temporal localization of RhoA WT and its two mutants. To do so, we used different microscopy techniques implemented in the lab to measure the different kinetic parameters regulating RhoA dynamics as well as the proportion of RhoA at the membrane and in the cytosol.

1.1 Spatial localization of RhoA

A previous study proposed that RhoA was mainly localized in the cytosol [13] while others studies supported the fact that RhoA was at the membrane ([3]). To go further and better understand RhoA localization, we first tried to quantify the proportion of RhoA at the membrane using confocal microscopy as it had been previously done [13]. We also had the idea to use TIRF Microscopy in order to better characterize the proportion of RhoA at the membrane.

To observe the localization of RhoA we used confocal microscopy imaging (protocol in Annex 2.2). To compare the amount of RhoA at the membrane vs in the cytosol, we took picture for different values of z which allows to to consider different focal planes.

Cells expressing the constitutive active mutant of RhoA (Q63L) were much more contractile than the cells expressing RhoA WT. While we can observe by eye that, for both the WT and the Q63L cells, there is a large population of protein in the cytosol, we were not able to quantify the precise ratio of fluorescence between the membrane and the cytosol. This is mainly due to the fact that the determination of what was at the membrane was not so evident.(Figure 2)

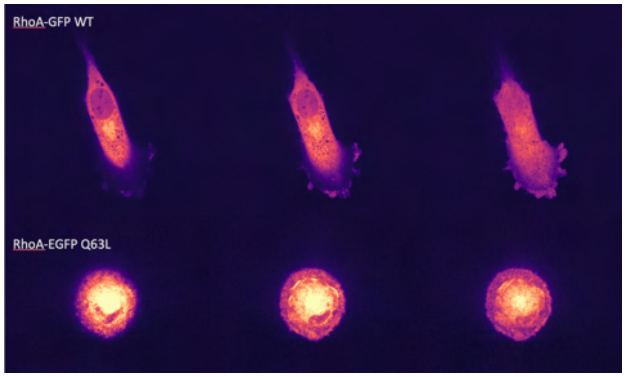

Figure 2: Confocal microscopy images at different z for 2 RPE1 cells transiently expressing RhoA-GFP WT or RhoA-EGFP Q63L. Left: mid-sagital plane, right: bottom plasma membrane, center: plane in between.

One way to solve this issue would be to co-express the RhoA reporters with a fluorescent membrane protein to be able to better localize RhoA proteins that are at the membrane.

While we were not able to test this idea, we did try an other way to localize RhoA. We used TIRF microscopy to determine the ratio of RhoA at the plasma membrane vs in the cytosol (data not shown).

• TIRF Microscopy experiment

TIRF (Total Internal Reflection Fluorescence) is an optical technique which allows us to only excite the fluorescent proteins within a few hundreds nm of the surface of the cover slips [14]. This method is based on the principle of total internal reflection of the excitation light in the transparent cover-slip. At the interface between the glass and the culture medium, an electromagnetic field -also called evanescent wave- is generated in the liquid. This evanescent wave has the same frequency as the excitation light and its intensity decreases exponentially with the distance from the interface, with an spatial extent of roughly 150nm. Thus, only the fluorescent molecules within a few hundred nanometers of the surface of the cover-slip are efficiently excited. Since the penetration depth of the evanescent wave depends on the angle used for reflection, it may be possible to discriminate between observation done at the membrane only vs at the membrane and the cytosol. Comparing the fluorescence intensities obtained for different angles of TIRF would allow us to deduce a ratio of protein at the membrane vs in the cytosol.

We performed some tests using RPE1 cells expressing a membrane protein (CAAX fused with the fluorescent protein mCherry) and a cytosolic protein (ilvX fused with the fluorescent

protein mScarlett) as control. In both cases, we used the same configuration of TIRF. As we had a lot of variation from one cell to the other, we normalized the curves. (Figure 3)

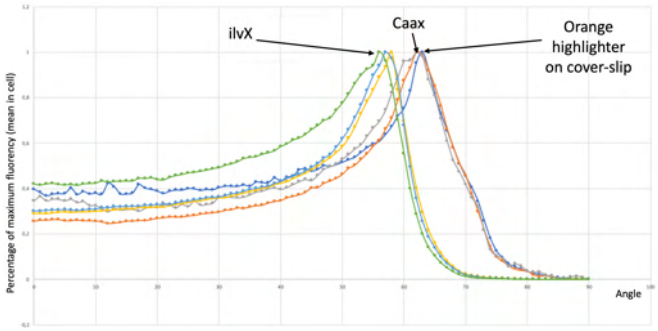

Figure 3: Fluorence obserbed in cells as a function of the angle of TIRF used (from epifluorescence to high TIRF) for cells expressing ilvX and Caax plasmids

To be able to characterize the spatial localization of RhoA, I decided to expressed several different plasmids so I could compare them : the membrane protein CAAX-mCherry, the cytosolic protein ilvX-mScarlett, RhoA-GFP WT, RhoA-EGFP Q63L, RhoA-EGFP T19N (already available in the lab) but also others plasmids including a RhoA biosensor and the protein RhoA fused with the fluorescent protein mCherry. We ordered this commercial plasmid. So I amplified it in bacterias and I made the mutants Q63L and T19N plasmids by microbiology (protocol developped in the Annexes 2.2). RPE1 cells were transiently transfected in 6 wells plates (between 60% and 80% of confluency) using the same protocol as used for the confocal microscopy experiment (see Annex 2.2).

After 24h, we observed the transfected cells on the TIRF setup. The illumination was controlled by the iLas2 system which allows TIRF and FRAP control. Unfortunately, we did not have the time to analyse the collected data. To go further, it would also be interesting to propose a model of RhoA behavior corresponding to our quantification.

Confocal experiment showed that RhoA is highly cytosolic but we were not able to determine a precise ratio of protein at the membrane vs in the cytosol. Thus, we switch to another microscopy setup, the TIRF setup. However, we did not have the time to correctly analyse the data obtained. Thus, further work is needed to characterise the precise partitioning of RhoA between the cytosol and the plasma membrane.

1.2 Temporal dynamics of RhoA

To characterize the temporal dynamics of RhoA and assess the parameters characterizing its shuttling at the membrane (k_{on} (binding), k_{off} (unbinding)), and its mobility (D_m and D_c), we decided to perform FRAP experiments. Indeed, Fluorescence Recovery after Photo-bleaching

(FRAP) is a technique that is commonly used to observe the dynamic of biological system such as the diffusion of membrane proteins or vesicles. It can be performed on living cells.

Principle of FRAP Microscopy A small region surface containing mobile fluorescent molecules is exposed to a brief intense pulse of light causing irreversible photo-chemical bleaching of the fluorescent protein in that region called 'region of interest' (ROI).[15]

This bleaching is supposed to only changes the state of the fluorophore that is linked to the protein we want to study, without perturbing the system, especially the protein's dynamics and interactions. However, it is good to keep in mind that the fusion of the protein with a fluorophore could change its conformation, folding or its direct environment (steric constraints), thus impacting its activity.

The recovery of fluorescence in the bleached ROI compared with a zone that was not photobleached is due to :

– the unbinding of bleached fluorescent protein replaced by cytosolic unbleached proteins, the timescale is given by the association / dissociation reaction and the cœfficients k_{on} and k_{off},
– the diffusion of fluorescent protein from outside the ROI, it can be cytosolic diffusion to allow fluorescent protein to bind to the membrane in the ROI (timescale of the second) but it can also be membrane diffusion (timescale of the minute).

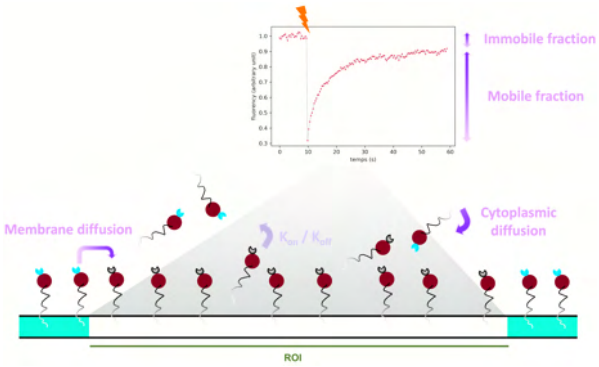

Figure 4: Principle of the FRAP technique

To determine those parameters for RhoA, we performed FRAP experiments as described in Annex 2.2 using the following plasmids :
– RhoA-GFP WT or Q63L
– RhoA-mCherry WT, Q63L or T19N (construction of mutants in Annexe 2.2)
– ilvX-mScarlett, a cytosolic protein from Escherichia coli (16 amino acids) which we use as control.

We then measured the intensity of the fluorescent reporters in the ROI after FRAP (recovery data in the bleached zone). Here is a typical example of raw data obtained (Figure 5)

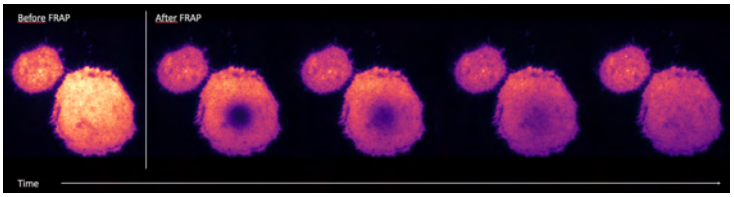

Figure 5: FRAP experimental datas

Data Analysis FRAP recovery data were extracted and analysed as follow :
– Cell segmentation and determination of a background zone for background correction
– Identification of the FRAP ROI using the Metamorph files and determination of a large area around the bleached zone (in order to extract zones in cells far from the ROI)
– Background subtraction in the entire image
– Normalisation the mean value of fluorescence before bleaching by the mean intensity in the zone far from the ROI (normal intensity in the cell). Indeed, we needed to normalized by the mean intensity in the cell far from the FRAP zone in order to correct for both photo-bleaching due to TIRF measurement and some additional bleaching at the moment of FRAP happening naturally in the cell(see Figure 6).

These normalized recovery data are then fitted to different models to extract the dynamic behavior. We used two different models :

- Simple exponential fit to compare the mobile fraction and the characteristic time of recovery.
$$Y + R_f(1 - exp(-\frac{t}{\tau}) \tag{3}$$
with Y the proportion of unbleached in the zone, R_f giving after normalization the mobile fraction of the bleached proteins and τ the characteristic time recovery of the bleached population

- Double exponential fit, assuming that possibly, there are at least 2 distinct population of RhoA (active or inactive) that could have different dynamics to extract different recovery characteristic times of recovery.
$$Y - A_{min}\, exp(-\frac{t}{\tau_{min}}) - A_{max}\, exp(-\frac{t}{\tau_{max}}) \tag{4}$$
with Y the mobile fraction of the bleached population, τ_{min} and τ_{max} the characteristic times recovery of the population that recovers the fastest and the slowest respectively, A_{min} and A_{max} counting for the proportion of those population with different recovery timescales

Recovery data are finally re-normalized by the values predicted by the model at t=0 to only consider the bleached population. This allows us to better superimpose different curves for comparison. The fitted parameters for some experiments were aberrant (negative cœfficients, mobile fraction far from the interval [0,1],...). We removed the aberrant values that were not not fitted well with our experimental data. Here are examples of this data analysis process (Figure

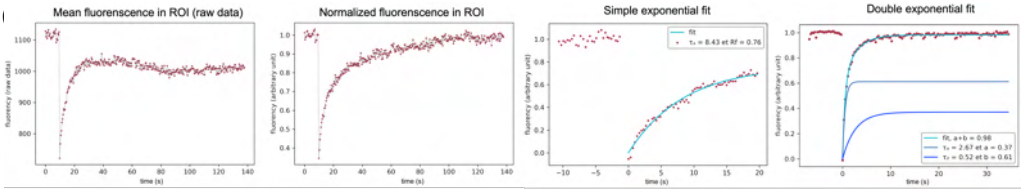

Figure 6: Extracted data in the bleached area (ROI) before and after normalization, example of fit for simple and double exponential

• Results

We plotted the 'mean curves', calculated by averaging all the curves obtained with different experiments on cells expressing each plasmid (Figure 7, plots of means and their standard deviation for between 5 and 20 curves for each plasmid). It gives us a good first idea of the timescales of recovery for each construct. We can see that the curves for the WT construct are similar to the recovery curve obtain for the cytosolic protein ilvX. We can also note that the two Q63L mutants have different behaviors. We performed this experiment with the RhoA-mCherry Q63L, the RhoA-mCherry T19N, the CaaX and the ilvX plasmids a long time after the other experiments. I used a different batch of cells and the setup configurations and calibration may have change a little. Since the ilvX behavior seems to be coherent with the profile of recovery of a cytosolic protein, those changes in setups may not have impact the profile of recovery. Possibly, there is an interaction between the fluorophore (mCherry or EGFP) and RhoA or its partners when it is in its active conformation.

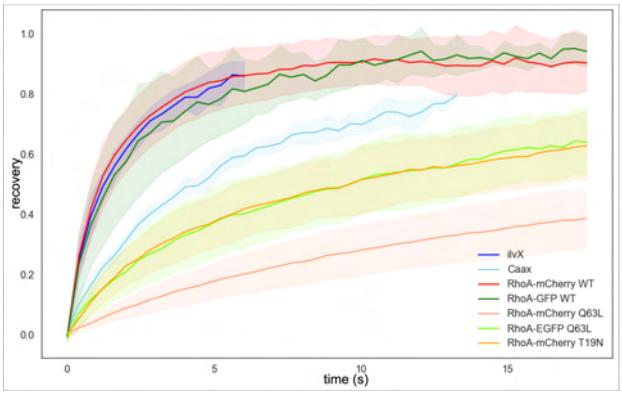

Figure 7: Mean curves of FRAP recovery

Simple exponential model We observed that the simple exponential data did not fit our experimental data very well (Figure 6). But it still gives us a good idea of the mobile fraction defined as the asymptote of the curve as well as the order of magnitude of the recovery.

We can notice some differences between experiments in the proportion of bleached proteins in the ROI (given by the parameter Y) (Figure 8). This could be explained by the fact that the experiments were not performed on the same days and other microscope users or vibrations (due to close works on the building) might have change the FRAP calibration.

Looking at the τ and mobile fractions on Figure 8, we can identify two different behaviors. WT mutants have a τ in the range the second (1.6s for ilvX, 2.4s for mCherry WT and 1.6s for GFP WT) and their mobile fraction is about 100% (91% for ilvX, 94% for mCherry WT and 97% for GFP

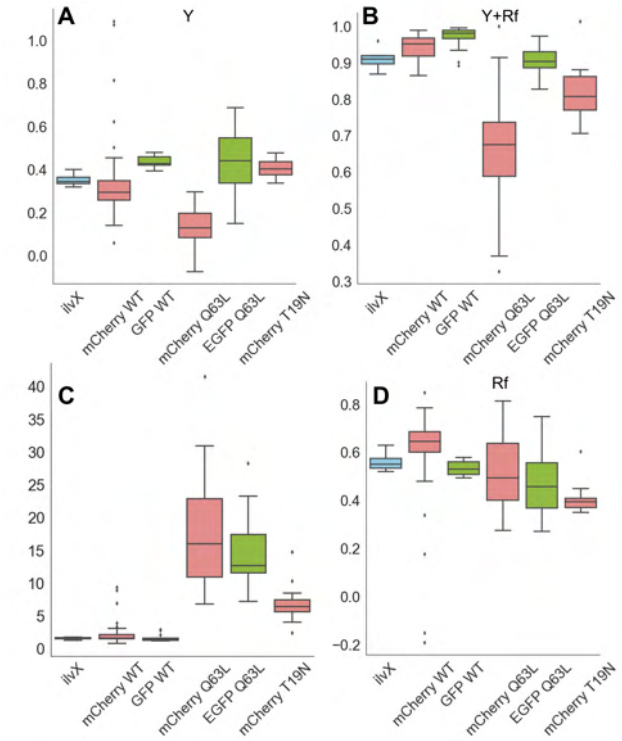

Figure 8: Parameters fitted with the simple exponential model. A: Y, normalized fluorescence at t=0, proportion of unbleached proteins ; B: $Y+R_f$, equivalent to the mobile fraction of the bleached population ; C: τ ; D: R_f

WT).The mutants (constitutive active Q63L and constitutive inactive T19N) have a greater τ (17.7s for mCHerry Q63L, 14.6s for EGFP Q63L and 6.8s for mCherry T19N) and a lower mobile fraction (67% for mCherry Q63L, 91% for EGFP Q63L and 81% for mCherry T19N). The difference between the WT and the mutants was always significant (p-value below 0.05 using a T-test).

From the literature, we know that the timescales of diffusion for a molecule of the considered radius ($2\mu m$) are on the timescale of the second for cytosolic diffusion and of the minute for membrane diffusion with the equation for a 2D circular region :

$$\tau \sim \frac{d^2}{16D} \tag{5}$$

with d the radius of circular region.

By comparing our experimental results with the theoretical values, we concluded that there are possibly two different and distinct RhoA populations. The first one is a population of unstable RhoA at the membrane and which recovers on a timescale comparable to the cytosolic diffusion. The other one seems to be stabilized at the membrane and so recovers on a longer timescale, on the order of 10's of seconds.

Supposing that there was possibly two different populations of RhoA, we decided to move to a double exponential model, that was indeed fitted our experimental data better than the mono-exponential one (Figure 6).

Double exponential model The double exponential model allowed us to observe the different timescales which correspond to the two potential population of RhoA (Figure 9).

- For WT proteins, we were able to extract one timescale τ_{min} around 0.6 second and one timescale τ_{max} around 4 seconds for mCherry and 5.2 second for GFP. Both τ are in the range of the timescale of cytosolic diffusion if we consider that we have a highly mobile population of RhoA unstable at the membrane. Indeed, those timescales were similar to those extracted for the cytosolic protein ilvX (τ_{min}=0.6 second and τ_{max}=2.6 seconds). A T-test allowed us to conclude that for both τ_{min} and τ_{max}, the two WT proteins were identical to ilvX (all p-values were greater than 0.1). In case of a very fast binding and unbinding reaction (unstable RhoA at the membrane), we only expect a recovery due to cytosolic diffusion (timescale of the second), as it is the limiting factor of fluorescence recovery.
- For Q63L mutants, when looking at Figure 9, we can see that the mobile fraction Y+Rf seems to be lower than the one of the WT proteins. We can also see an important

variability for the RhoA-mCherry mutant that we were not able to explain. The difference between WT and mutant is significant for the mCherry mutant (p-value lower than 0.05 when comparing mCherry WT and Q63L) but not for the EGFP mutant with the Student test (p-value=0.3). Similarly as for the WT, we extracted two different timescales for the mutants: a τ_{min} around 2.7seconds and a τ_{max} around 27 seconds. We can see that the τ_{min} has the same order of magnitude as the τ_{max} of the WT proteins (1 second). The τ_{max} has a greater timescale, about half a minute. In general, the Q63L mutants have greater τ than the WT proteins. This could suggest that the mutants are more stable at the membrane than the WT protein.

For the T19N inactive mutant we found that $\tau_{min} = 1.6s$ and that $\tau_{max} = 15.6$. Those τ are greater than those of the WT proteins. This could be explained by the fact that this mutant is inactive but binds to GEFs at the membrane, so that it is more 'stable' than the WT proteins at the plasma membrane.

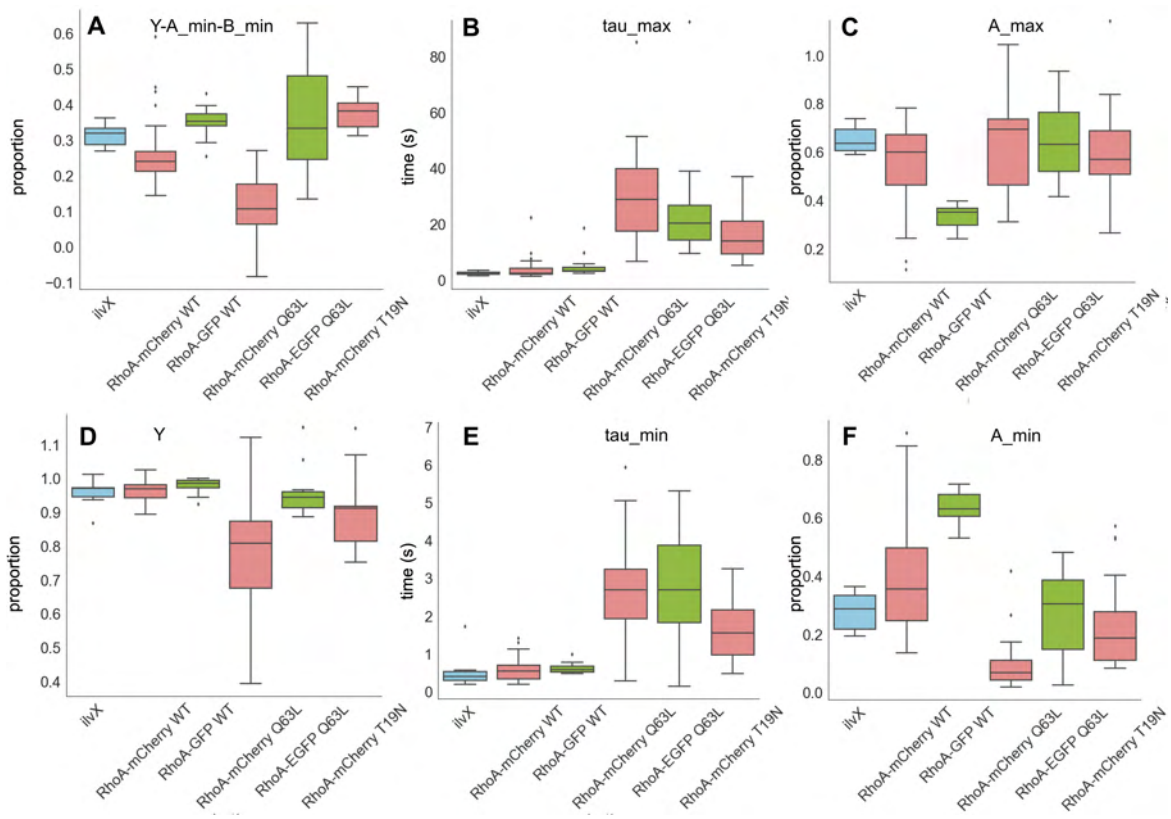

Figure 9: Parameters fitted with the double exponential model. A: $Y - A_{min} - B_{min}$,normalized fluorescence at t=0, proportion of unbleached proteins ; B: τ_{max} ; C: A_{max} normalized, propo0rtion of the bleached population that recovers with the timescale τ_{max} ;D: Y,mobile fraction of the bleached population ; E: τ_{min} ; F: A_{min} normalized, proportion of the bleached population that recovers with the timescale τ_{min}

Further investigations To test whether the timescale corresponds to the one of membrane diffusion, we realized experiments changing the size of the bleached area. We expected a difference in the recovery timescales if membrane diffusion is involved in the recovery. Indeed, pure membrane diffusion recovery timescale depends on the size of the region photo-bleached (equation 5).

When looking at our experimental recovery profile for this experiment, we observed a huge variability of recovery profiles for each construct, mainly depending on the cell but also on the region bleached (on the contrary, the experiments were very well reproducible using the same cell with the same ROI) (data showed in Annexe 2.2). Still, when looking at the mean curve obtained for the different experiments, we were able to see that the difference between the small and the large bleaching ROI is more important for the Q63L mutants than for the WT proteins (Figure 10). For further analysis, we should extract consistent timescales of recovery from large and small ROIs and compare their ratio.

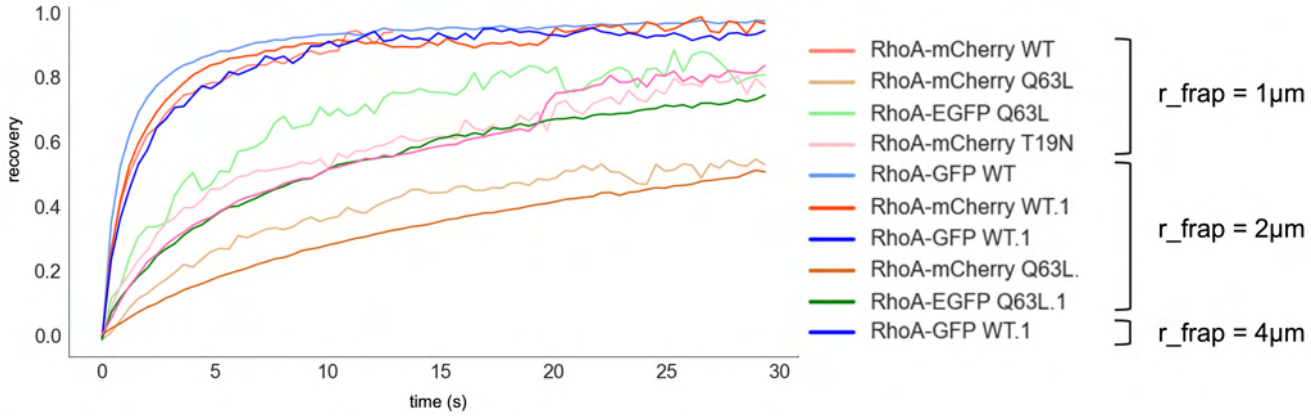

Figure 10: A: recovery for different cells in a large ROI (radius of $2\mu m$) or in a small one ($1\mu m$)

• Conclusion & Discussion

The timescales of FRAP recovery observed for RhoA WT were quite small (around a second) and comparable with timescales of recovery observed for the cytosolic ilvX protein. This suggests that RhoA is extremely labile at the plasma membrane. In addition, data shows a mobile fraction close to 100%.

However, the study of RhoA mutants showed that RhoA could be possibly stabilized at the membrane since timescales of FRAP recovery for active and inactive mutants are greater than the timescale of cytosolic diffusion. Interaction with binding partners could explain this slower dynamics and thus play an important role in the temporal dynamic localization of RhoA.

For further investigation, it would be really interesting to use a different model of FRAP recovery such as the Berkovitch model ([16]).

In this particular model, they take in account multiple variables in their FRAP recovery model such as diffusion cœfficients and binding kinetics constants. We tried to fit this model to our experimental data but we had some trouble to make the fitting algorithm converge (it has to fit 9 parameters). Yet, we did succeed to fit the data to one of experience (see Figure 11). Thus, more work could be done to determine a more consistent order of magnitude of diffusion cœfficients and k_{on} and k_{off} constants.

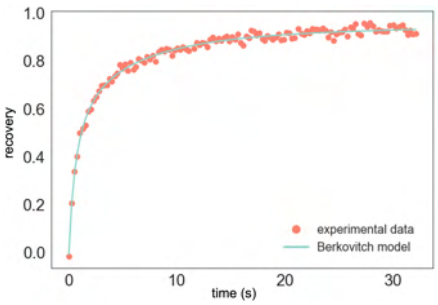

Figure 11: fit with Berkovitch model

Other aspects of FRAP experiments could be discussed as limitation to our current experimental set-up such as the possible dependence of timescales of recovery on the focus or the angle of TIRF. The smaller timescales that we determined and identified as corresponding to cytosolic diffusion may also come from the inevitable population of molecules bleached above the zone of FRAP, and possibly observed in TIRF.

Moreover, when we performed the experiments, we observed a lot of variation in the behavior of the recovery curves for cells expressing the same construct. It could be interesting to classify the cells (maybe by shape, plasmid level of expression or state of contractility) to see if there is a possible correlation between those different behaviors and a characteristic feature of cells. We also performed an experiment to test whether the recovery timescales depended on subcellular regions (middle of the membrane, contractile zone, protrusion). The preliminary results (not shown) were not really consistent and complex to analyse since geometrical factors can also impact the recovery timescales through diffusion.

We should also keep in mind that overexpressing the RhoA protein (as it is the case with our constructs) can unbalance the ratio between RhoA and its activators and effectors. Since RhoA's localization and stability seem to rely on the interactions between them, the observed spatio-temporal localization could be slightly different from the reality. Still, RhoA is a protein with high basal level of expression in cells so while an additional expression should be taken in account in the conclusion, it might have only a limited impact.

Finally, we saw that even if RhoA was often considered as a 'membrane protein', our confocal and FRAP experimental data showed that RhoA (WT) has more of a cytosolic behavior and seems to be naturally unstable at the membrane. Since RhoA is a GTPase and can have an activity, it is also key to understand how its spatio-temporal localization is correlated with its dynamic activity.

2
SPATIO-TEMPORAL ACTIVITY OF RHOA

Now that we have a better understanding of the dynamic localization of RhoA, we can investigate how the regulation of RhoA activity could be related to its localization. To do so, we need to monitor RhoA activity over space and time. Many biosensors have been developed to quantify the activity of Rho-GTPases, including dyes and FRET biosensors [17]. We are also interested in looking at the dynamic recruitment of RhoA by its activators. To do so, it could interesting to use optogenetic tools as they offer control on RhoA's activator with a precise spatio-temporal resolution using light. Thus, we used an optogenetic tool developed by Jean De Seze to recruit RhoA's activator (GEF catalytic domain) at the membrane. We also used a homemade FRET biosensor to observe the resulting dynamic activity and localization of RhoA. We had to design this biosensor so that it could be compatible with the activation and excitation lights used for the optogenetic tool.

2.1 Design of the FRET Biosensor

To observe RhoA's spatio-temporal activity, we used a FRET biosensor. Fluorescence Resonance Energy Transfer (FRET) is a physical process through which an excited fluorophore may transfer its energy to an acceptor fluorophore by non-radiative coupling. If the energy released by the donor has a wavelenght close to the excitation peak of the acceptor, it may excite it in a non-radiative way. [18] The efficiency of this transfer depends on the distance between the donor and the acceptor and is defined as proportional to $\frac{1}{d^6}$ with d the distance between donor and the acceptor. Thus, FRET is extremely sensitive to small changes in distance between the donor and acceptor (few nanometers).

By fusing donnor and acceptor fluorophores to different parts of a protein whose activity depends on its conformation, it becomes possible to look at the precise spatio-temporal activity of the protein of interest. In our biosensor design, when the protein is in its inactive state, the donnor and acceptor are far from each others. Using the excitation wavelenght of the donnor, only the donnor is excited and emit light. Upon activation, the biosensor changes conformation and brings the donnor and acceptor closer to one another. The energy emitted by the donor excites the acceptor which also starts emitting light. In our case we also wanted our FRET-biosensor to be compatible with the wavelenghts used for optogenetic recruitment of RhoA's

activators. Optognenetics experiments require blue light for activation (<530nm) so we decided to rely on red/far red FRET couple.

Therefore, we designed in collaboration with Nicolas Borghi a FRET-biosensor based on an existing RhoA FRET biosensor [19]. We used RhoA linked to 2 fluorophores mRuby2 (donnor) and mKate2 (acceptor), and a Rho Binding Domain (RBD) that is able to bind to RhoA-GTP only (see Figure 12). When RhoA is in its GDP state (inactive), only mRuby2 emits light. When RhoA is in its GTP state (active), the biosensor is folded, allowing FRET coupling between mRuby2 and mKate2.mKate2 will be the main provider of fluorescence signal.

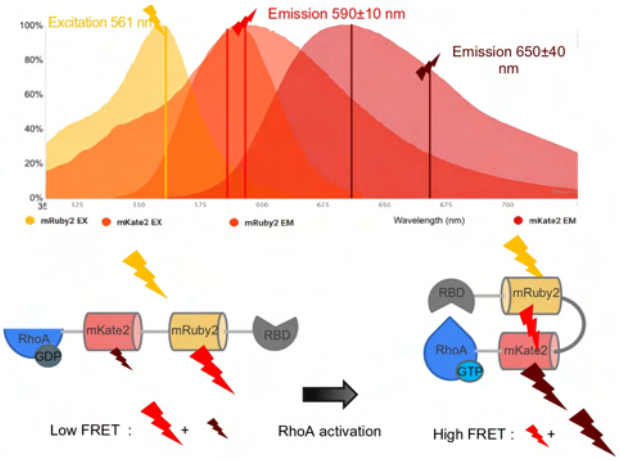

Figure 12: RhoA FRET biosensor design

To observe the activity of RhoA using this FRET-biosensor, we transiently transfected REP1 cells with same protocol described in 2.2 using the pTwist-lenti-RhoA-mRuby2-Kate2-RBD plasmid and the 2 mutant biosensors Q63L and T19N (see Annexes **??**). We then used TIRF microscopy in the same setup to excite mRuby2 at 561nm, and image the resulting fluorescence in two channels one by one at close intervals (200ms between the imaging of the two channels) :
– a 'FRET channel' with a bandpass filter 590±10nm to look at the emission peak of the donnor fluorophore mRuby2
– a 'mKate2 channel' with a bandpass filter 650±40nm to look at the emission peak of the acceptor fluorophore mKate2 (see 2.2)

In zones were RhoA is active, we should observe a decrease of intensity in the 'FRET channel' and an increase of intensity in the 'acceptor channel' so that in theory, the 'FRET ratio' of intensity $\frac{mKate2\ \ channel}{FRET\ \ channel}$ is higher in regions where RhoA is active compared with regions where RhoA is in its GDP state.

To check if the biosensor was well working, we did FRET experiments on the RPE1 cells transfected with the biosensor-RhoA WT, the biosensor-RhoA Q63L and the biosensor-RhoA T19N (we performed the mutations of the biosensor-RhoA WT as explained in the Annexe 2.2). The two mutants should give us the dynamics range of the biosensor, the Q63L giving the maximal expected value of FRET ratio and the T19N the minimal one.

We calculated this ratio for about 10 cells for each biosensors using the following method :
– registration of the two images (correction of possible small pixel shift between the two channels) and cell segmentation
– substraction of the background (mean intensity in a zone outside the cell) in both channels

- a 5 pixels median filter is applied
– calculation of the fluorescence ratio with the corrected intensities $\frac{mKate2\ \ channel}{FRET\ \ channel}$ for each pixel inside the cell and then calculation of the mean ratio inside the whole cell.

We took about 20 images for each cell (total time acquisition about 5 minutes) to see if there was a temporal variation of the FRET ratio. We could see that the FRET ratios corresponding to those sequences of images taken from the same cell were not varying over time: on the swarmplot (Figure 13), each cell corresponds to a cluster of dots (group of dots, or 'lines' of dots). Yet, the disparity of inter-cellular ratios was huge compared to the intra-cellular temporal variability. Indeed, the analysis of data shows a huge variability of FRET ratio for cells expressing the same construct with a ratio varying between 0.6 to 1.8 for a same construct.

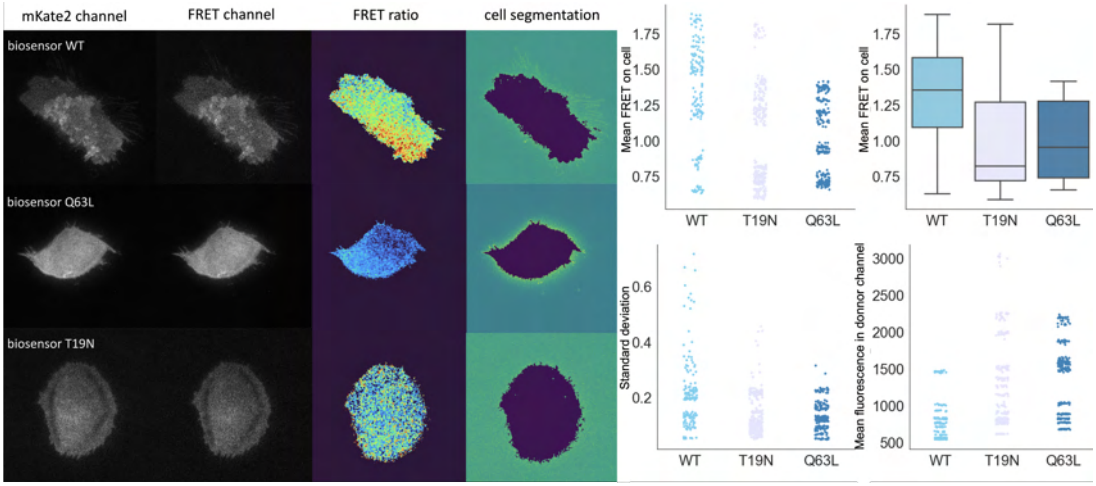

Figure 13: On the left, FRET experimental data : the acceptor and the donnor channels, the FRET calculation (the colorbar range is between 1 and 2) and the segmentation used to compute the FRET calculation ; on the right, FRET calculation analysis : mean FRET calculation (swarplot and boxplot), standard deviation of FRET value inside the cell, mean fluorenscence in the donnor channel inside the cell.

Were not able to observe significant difference between the FRET ratio found in RhoA WT, RhoA Q63L and RhoA T19N biosensors (Student test pvalues were all above 0.1). In theory, the constitutive active RhoAQ63L mutant is supposed to have the highest possible ratio since all the proteins RhoAQ63L-mRuby2-mKate2-RBD expressed in the cells have the folded 'FRET' conformation. On the contrary the RhoA T19N mutant is expected to present lower FRET ratio since the RBD is not supposed to bind to the GDP-bound conformation of RhoA (Figure 12). I first though that I may have photo-bleached differently the 2 fluorophores when looking for cells before imaging. Indeed, if the two fluorophores have not the same sensitivity to photo-bleaching, we may change the ratio by photo-bleaching cells before and during acquisition. Nevertheless, if photo-bleaching was significantly different for the 2 different fluorophores, I should have observed a change in the FRET ratio between the first frame of aquisition and the last, what was not the case : I was not able to see photo-bleaching in the two channels.
An other hypothesis was that there was a laser intensity variations but this was not consistent with intra-cellular FRET similar ratio and inter-cellular huge variability since I was doing

multiple position acquisitions.

The problem can come from the design of the biosensor itself. Since FRET technique is super sensitive to variations in distances, a too small or too long linker between mRuby2 and mKate2 can easily give unexpected results. However, it could also be that the setup used is not adapted to the FRET measurement. For further investigation, we should try to acquire data from a known biosensor to check if it is only the setup that causes the problem, or if it comes from the design of the biosensor itself.

I have to mention briefly that I performed some FRAP experiments on the RhoA WT -biosensor. The preleminary results showed FRAP curves and timescales for recovery more similar to the RhoA-EGFP Q63L mutants than to the RhoA WT studied in 1.2. The construct fused with the RhoA protein may impact its direct environment and so change its stability at the membrane. Furthers investigation should be done to understand how this probe designed to report the activity of RhoA could in fact have a direct impact this activity, through changes of dynamic parameters.

Finally, if we were not able to look at spatio-temporal activity of RhoA with the biosensor, it was still possible to look at the spatio-temporal localisation of RhoA after optogenetic activation.

2.2 Spatio-temporal regulation of RhoA after optogenetic activation

To determine dynamic features of the regulation of RhoA, we decided to use the optogenetic tool used by Jean De Seze. This optogenetic tool allows us to spatio-temporally recruit an activator of RhoA : the catalytic domain of the ARHGEF11.

For that, a photo-switchable dimer was used : the SspB-iLID light-gated dimerizer. When exposed to blue light, the affinity between the SSPB and the iLID domain is drastically enhanced leading to the binding of the two monomers to form a dimer. The SspB domain is bound to ARHGEF11 catalytic domain and the iLID domain is fused to a CAAX motif to localize it at the plasma membrane. When shining blue light, the dimerization occurs and the GEF is recruited to the membrane. When stopping the activation, the i LID gets naturally deactivated and the affinity between SspB and iLID will decrease in 20s, leading to a

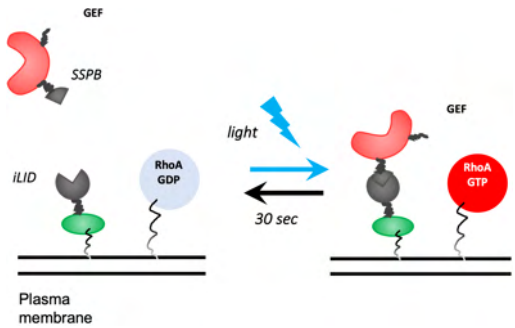

Figure 14: Optogenetic tool used to recruit RhoA'a activator, from Jean De Seze

re-localization of ARHGEF11-SspB in the cytosol (Figure 14). This allows us to have a precise temporal control of the recruitment of the GEF. The spatial control is done by illuminating only precise regions of the cell using a Digital Micromirror Device (DMD). The ARHGEF is also fused with an iRFP fluorescent protein photo-excitable at a far red wavelength so that we can monitor the recruitment of the GEF at the membrane.

The optogenetic tool is encoded in a single plasmid so that all the parts of the tool can be expressed at the same time.

To look at the spatio-temporal dynamic of RhoA following the recruitment of the ARHGEF11 at the plasma membrane, we coexpressed in the RPE1 cells both the optogenetic tool (optoRhoA) and the plasmid RhoA-mCherry WT. We activated the optogenetic tool by shining light on a subcellular region (20ms exposition of 491nm light every 30s). We then looked at the recruitment of the GEF in the activated region using TIRF microscopy at 638nm. We also looked at the recruitment of RhoA-mCherry at 561nm.

We were able to quantify the recruitment of ARHGEF11 in the activated region showing that the tool is working (Figure 15). We also observed a clear and rapid recruitment of RhoA at the plasma membrane in the activated zone since the recruitment of RhoA is already visible the first frame after activation (about 30s after the activation). Surprisingly, the level of RhoA decreases in the zone after 2 minutes even if the level of GEFs at the membrane was still increasing in the same area. This suggests that the recruitment of RhoA at the membrane is triggered by the recruitment of GEFs but seems to be also regulated by other inhibiting process in longer timescales, possibly through a delayed negative feedback loop.

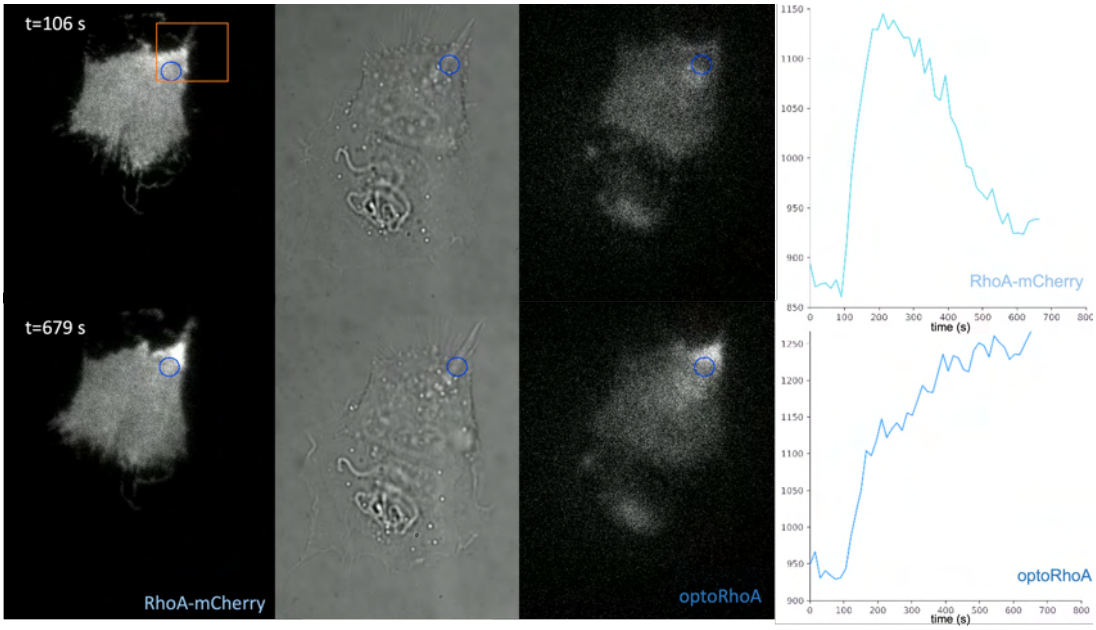

Figure 15: Recruitment of RhoA and ARHGEF11 in the zone of activation after the first activation (t=106s) and at the end of the experiment (t= 679). The cell contracts inside the activated zone (orange rectangle)

Further investigations still need to be performed since I did the experiment only for few cells and was not able to see the recruitment of RhoA for all the cells.

Furthermore, the recruitment of ARHGEF11 at the plasma membrane was mainly leading to contractile behaviors inside the activated zone, which was coherent with the phenotype already observed by Jean De Seze with the same tool (he usually uses the same tool with ARHGEF11 fused with mCherry instead of iRFP). However he was also able to observe protrusive phenotypes with the same cell type in the activated regions (see Figure 16). He showed that the protrusive behavior was correlated with a high basal level of ARHGEF11 expression.

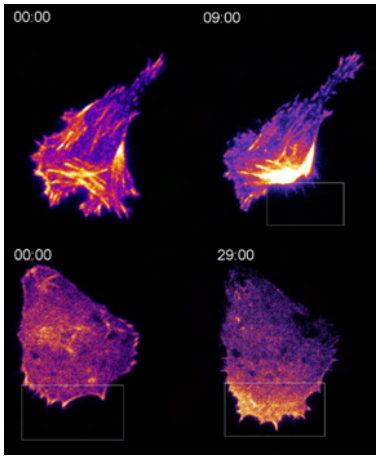

Figure 16: Examples of phenotype observed after activation by blue light for cells expressing optoRhoA. Up : contraction in the activated zone ; down : protrusion in the activated zone. *Images from Jean De Seze*

Then, I wanted to investigate why I was not able to see protrusion. It could be because of the level of expression of my plasmid but also because of a possible change in the balance between RhoA and its activators and effectors due to overexpression. Indeed, difference of concentrations have a role to play in the regulation of signaling pathway.

So I activated with same protocol (20ms of blue light every 30s) RPE1 cells expressing the optoRhoA construct alone or the optoRhoA and the RhoA-mCherry plasmid. I quantified the basal level of fluorescence inside each cell activated (after background substraction) and by eye, characterized the observed phenotype for each cell (Figure 17).

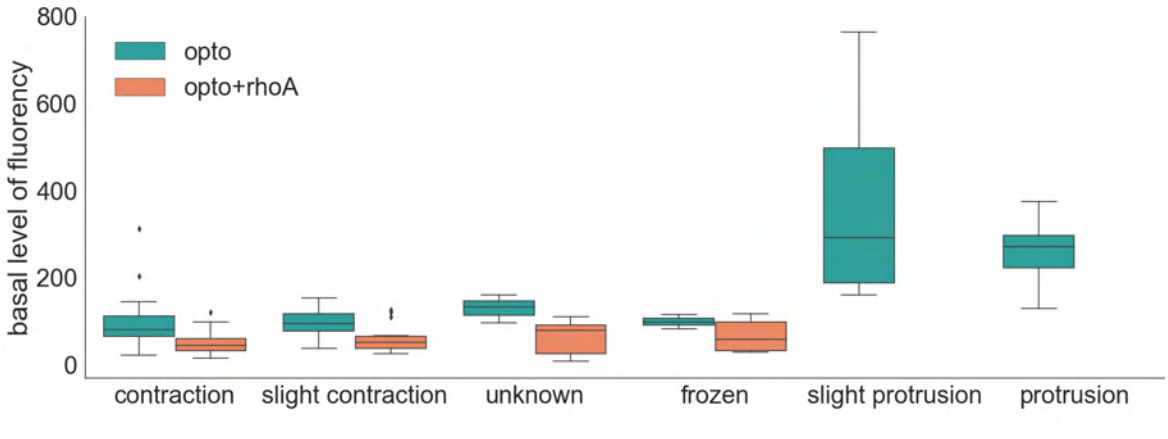

Figure 17: Basal cell expression of optoRhoA (normalized raw intensities using the same setup) in function of phenotype observed after activation with blue light (20ms exposition every 30s). In blue, cells expressing only optoRhoA ; in orange, cells coexpressing optoRhoA and RhoA-mCherry WT. Data for a hundred of activated cells are shown.

Since the level of fluorescence gives a good approximation of the level of expression of the

plasmid, I was able to reproduce the result of Jean De Seze : only cells with high level of expression of the optogenetic tools were doing protrusion. I also saw that when I coexpressed the opto tool with RhoA-mCherry, levels of expression of the tool were low enough such that they could explain the absence of the protrusive phenotype.

On possibility to reach higher level of expression while coexpressing the 2 plasmid is to change the ratio of DNA transfected, putting more optoRhoA plasmid than RhoA-mCherry. An other possibility is to change the promotor used to express the coding sequence and to replace it with a stronger promoter.

We should notice that the phenotype of some cells after activation was sometimes uncertain. Even if we could see the clear recruitment of GEFs, sometimes the cell is not reacting to the simulation (it freezes), sometimes, it is contracting and blebing at the same time.

Finally, we were able to see the recruitment of RhoA by following the optogenetic recruitment of its activators. This optogenetic activation leads to different phenotype on the activated zones : contractile or protrusive. More investigations need to be performed to characterize this recruitment and how it could be involved in the two mechanisms leading to the two different phenotypes. Coexpressing the optoRhoA tool and the FRET biosensor could give us a more accurate view of the mechanisms regulating its activity and its ability to trigger 2 phenotypes.

CONCLUSION

The objective of my internship was to have a better understanding of RhoA regulation in space and time. I first looked at RhoA's localisation inside the cell. Confocal microscopy confirmed that RhoA was to a large extent in the cytosol. We are trying to precisely characterize the ratio of RhoA at the membrane vs in the cytoplasm using TIRF microscopy.

Then I looked at the temporal dynamic of RhoA protein at the membrane with the technique of FRAP. I showed that RhoA has a temporal dynamic similar to a cytosolic protein suggesting that RhoA is very labile at the membrane. The analysis of the behavior of the constitutive active mutant showed that RhoA in its GTP-bound is more restrained at the membrane, probably stabilized at the membrane by other binding partners.

Finally, I tried to look at RhoA activity, using a new FRET biosensor. This tool seems to be not functional so further analysis is required to ensure it measures well the activity of RhoA. The optogenetic recruitment of GEFs in precise regions of cells led to both contractile and protrusive phenotype. We were able to see a rapid recruitment of RhoA in the activated zone suggesting that the localization of RhoA is highly correlated with its activity. Therefore, RhoA can not be seen anymore as a passive switch. It is at the membrane with a turnover rate that depends on its activity state and its potential to bind to effectors and activators.

ANNEX

Design process of single point mutated plasmids We created 4 different mutants based on 2 different mutations: Q63L and T19N. Maud Bongærts from the lab designed the strategy. We applied those 2 mutations to 2 different RhoA construct: RhoA fused to a fluorescent reporter (either mCherry or GFP) and RhoA fused to a FRET biosensor.

To create the plasmid for RhoA fused to a fluorescent reporter (here, mCherry), we used the pTwistlenti-RhoAWT-mCherry designed by Jean De Seze. The pTwistlenti-RhoAWT-mCherry was double digested with BamHI/SpeI restriction enzymes in Cutsmart® buffer.
Six different DNA fragments were amplified by PCR with high fidelity polymerase (Phusion®), using degenerated primers, designed for single point mutation insertion, and these two plasmids: pTwistlenti-FRETsensor(mRuby2-mKate2-rhoA WT) or pTwistlenti-RhoAWT-mCherry (see Figure 19).
After migration of all the products on agarose gel by electrophoresis, linearized pTwistlenti plasmid and fragments 1 to 6 were separated and extracted with Nucleospin Gel and PCR Cleanup® kit. PCR amplification of fragments and plasmid digestion gave the expected size. Concentrations were measured by spectrophotometric assay (Nanodrop®.)

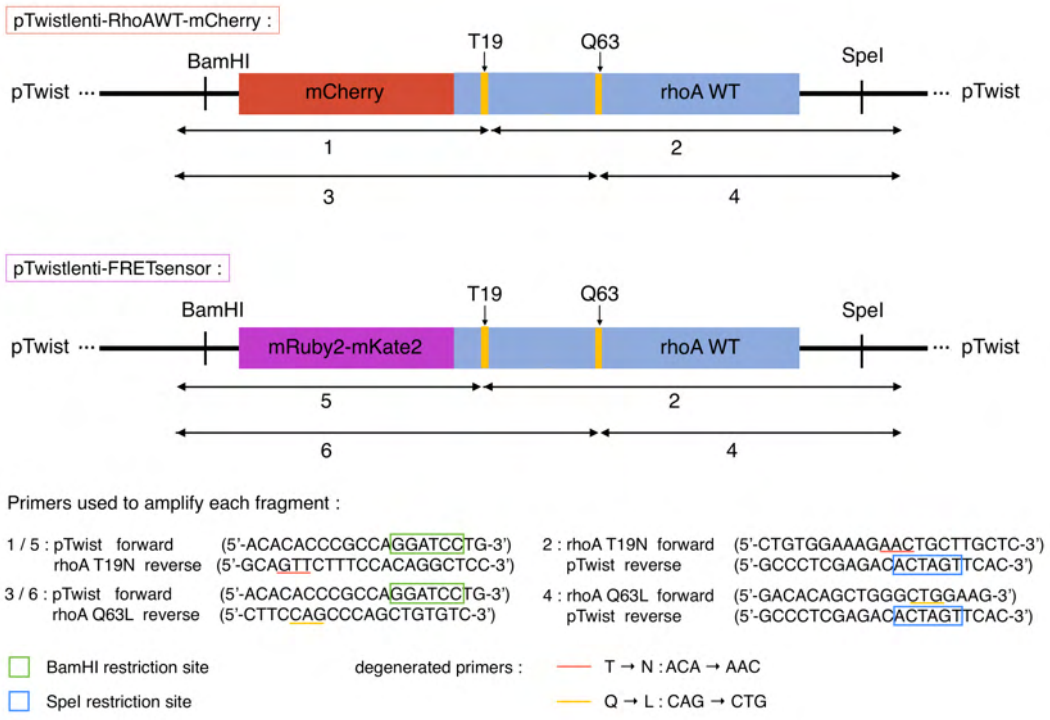

Figure 18: Cloning strategy for rhoA constitutive active (Q63L) and inactive (T19N) mutants

We then performed In Fusion® Reaction to ligate different combinations of fragments:

- rhoA mcherry T19N : fragments 1 and 2 + pTwistlenti linearized
- rhoA mCherry Q63L : fragments 3 and 4 + pTwistlenti linearized
- Biosensor T19N : fragments 5 and 2 + pTwistlenti linearized
- Biosensor Q63L : fragments 6 and 4 + pTwistlenti linearized

Competent E. coli bacteria (One Shot Top 10®) were then transformed with products of ligation and spread on selective plates supplemented with ampicillin. Bacteria clones were tested by PCR with pTwist primers and size of new fragments introduced in plasmids were checked after migration on agarose gel (1%).
The correct recombinant plasmids were then amplified from 2 colonies for each plasmid by growing an overnight culture supplemented with ampicillin.
Plasmids were then purified with the Nucleospin® Plasmid kit. The presence of single point mutations and gene integrity were confirmed by Sanger sequencing for the different clones.
One clone for each plasmid was finally re-amplified and recombinant plasmids containing the correct mutation were purified with XTra-MidiPlus® plasmid kit.

Microscopy set-ups We used two different microscope setups: a spinning disk confocal microscope and a TIRF (Total Internal Reflection Fluorescence) imaging setup.

– The confocal spinning disk microscope:
This microscope is composed of a Confocal Scanning Unit Motorized CSU-X1 from YOKOGAWA and Single-mode Laser Launch from Gataca system, attached to an Olympus Microscope IX71. The laser bench is equipped with the following lasers: 405 nm (120 mW), 488 nm (50 mW), 561 nm (50 mW) and 639nm (150 mW). The camera is a Photometrics BSI Express-Scientific CMOS Camera. The cells are placed in a STX stage top incubator from Tokai Hit which controls both the temperature and the CO_2 concentration. This set-up is controlled by MetaMorph. The confocal spinning disk is connected to a CCD camera.

– The TIRF imaging setup:
This microscope is composed of an Olympus IX83 inverted microscope. The illumination is controlled by the iLas2 system which allows TIRF and FRAP application. The camera is an electron multiplying Evolve EMCCD camera from Photometrics. The atmosphere in the cell incubator is controlled by the CO_2-Controller 2000 and the temperature controller TempControl 37-2 digital, both from Pecon. This microscope is fully automated and controlled by MetaMorph and the iLas2 software.

We mainly used a 100x objective from Olympus, N.A 1.49, oil, adapted for the TIRF imaging.

Confocal Microscopy experiments RPE1 cells (hTERT-immortalized retinal pigment epithelial cells) were grown in Dulbecco's Modified Eagle Medium supplemented with 10X FBS, 1X Glutamax and 1X Pen-Strep, at 37 °C, 5% CO_2.

The cells were plated in a fluorodish coated with fibronectin and were transiently transfected with a fluorescent reporter of RhoA. We waited for the cells to be between 60% and 80% of confluency and used jetPRIME® (200 µl of buffer, 2 µg of circular DNA (plasmid) and 4 µl of jetPRIME® transfection reagent). We used the 2 constructs: RhoA-GFP wildtype (WT) and RhoA-EGFP Q63L constitutive active mutant that were already available in the lab.

After 24h, cells were observed at 491nm with the confocal microscope.

FRAP experiments: RPE1 cells were grown as described in 2.2. Cells were transiently transfected as described in 1.1 with 2µg of circular DNA (plasmid)

We used the following plasmids :
– RhoA-GFP WT or Q63L
– RhoA-mCherry WT, Q63L or T19N (construction of mutants in Annexe 2.2)
– ilvX-mScarlett, a cytosolic protein from Escherichia coli (16 amino acids) which we use as control

After 24h, the cells were passed and plated onto 25-mm glass cover-slips coated with fibronectin. After 3 h, the plated cells and cover-slips were transferred onto a support and put in the microscopy chamber for observation.

Cells were observed in the TIRF setup described in 2.2. Fluorescence was observed by TIRF microscopy using the 491nm laser for the GFP plasmids and the 561nm laser for the other plasmids (mCherry and mScarlett fluorescent reporters).

We imaged the cells for several frames to observe the resting state of the molecules. Then FRAP was performed using 100% of intensity for the 491nm laser (Gaussian beam) in the bleached zone (ROI). ROIs are circular zone of radius from $1\mu m$ to $4\mu m$. The radius of the bleached area is $2\mu m$.

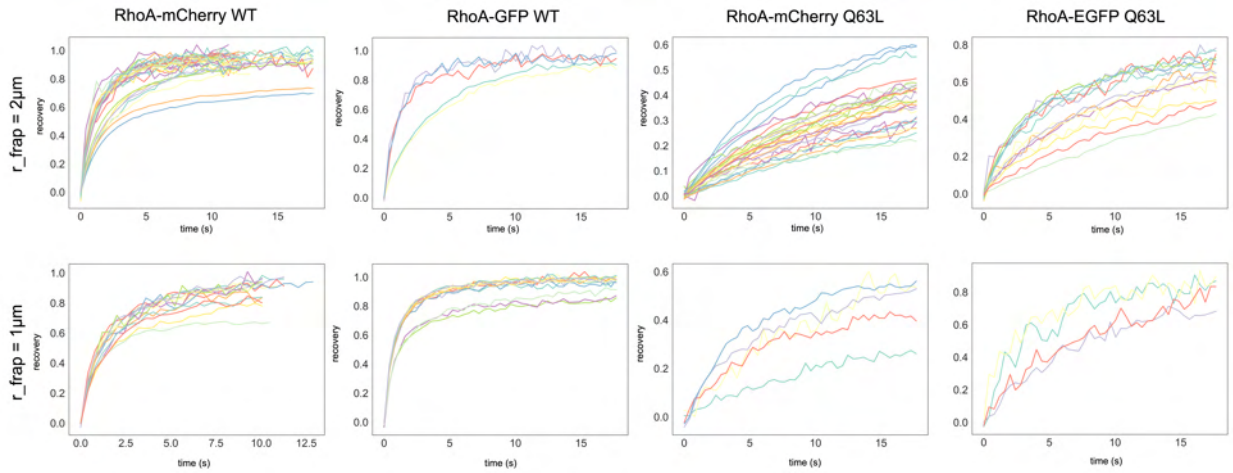

Figure 19: Recovery curves obtained for different size of a circular bleached area

Experimental FRAP curves τ fitted with the double exponential model

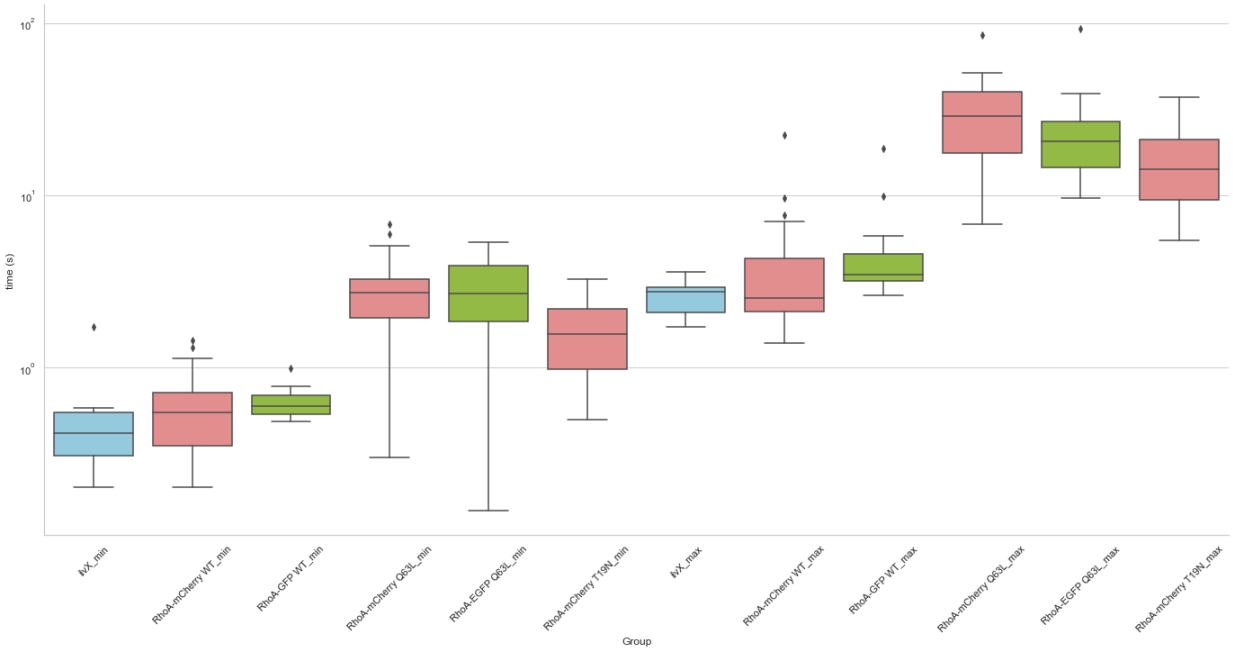

Figure 20: Timescales fitted with the double exponential model for the different constructs

REFERENCES

[1] A. Rev, C. Dev, B. Downloaded, A. B. Jaffe, and A. Hall, *Rho GTPases: Biochemistry and Biology*, Annual Review of Cell and Developmental Biology, pp. 247–272, 2005, doi: 10.1146/annurev.cellbio.21.020604.150721.

[2] A. Hall and C. D. Nobes, *Rho GTPases: molecular switches that control the organization and dynamics of the actin cytoskeleton*, Philos Trans R Soc Lond B Biol Sci, vol. 355, no. 1399, pp. 965–970, Jul. 2000, doi: 10.1098/rstb.2000.0632.

[3] S. Etienne-Manneville and A. Hall, *Rho GTPases in cell biology*, Nature, vol. 420, no. 6916, pp. 629–35, Dec. 2002, doi: 10.1038/nature01148.

[4] D. Spiering and L. Hodgson, *Dynamics of the Rho-family small GTPases in actin regulation and motility*, Cell Adhesion Migration, vol. 5, no. 2, p. 170, 2011, doi: 10.4161/CAM.5.2.14403.

[5] Narumiya, S., Tanji, M. Ishizaki, T. *Rho signaling, ROCK and mDia1, in transformation, metastasis and invasion*, Cancer Metastasis Rev 28, 65–76 (2009), doi: 10.1007/s10555-008-9170-7,

[6] Kim, K.; Lee, S.-A.; Park, D., *Emerging Roles of Ephexins in Physiology and Disease*, Cells 2019, 8, 87., doi : 10.3390/cells8020087.

[7] R. G. Hodge and A. J. Ridley, *Regulating Rho GTPases and their regulators*, Nature Reviews Molecular Cell Biology, vol. 17, no. 8, pp. 496–510, 2016, doi: 10.1038/nrm.2016.67.

[8] D. Michaelson, J. Silletti, G. Murphy, P. D'Eustachio, M. Rush, and M. R. Philips, *Differential localization of Rho GTPases in live cells: regulation by hypervariable regions and RhoGDI binding*, J Cell Biol, vol. 152, no. 1, pp. 111–26, Jan. 2001, [Online]. Available: http://www.pubmedcentral.nih.gov/articlerender.fcgi?artid=2193662tool=pmcentrezrendertype=ab

[9] M. MacHacek et al., *Coordination of Rho GTPase activities during cell protrusion*, Nature, vol. 461, no. 7260, pp. 99–103, 2009, doi: 10.1038/nature08242.

[10] O. Pertz, *Spatio-temporal Rho GTPase signaling - Where are we now?*, Journal of Cell Science, vol. 123, no. 11, pp. 1841–1850, 2010, doi: 10.1242/jcs.064345.

[11] Miyawaki A., *Proteins on the move: insights gained from fluorescent protein technologies*, Nat Rev Mol Cell Biol. 2011 Sep., doi: 10.1038/nrm3199.

[12] Cytoskeleton, *Rac1 protein: His tagged: human constitutively active* and Rac1 protein: GST tagged: human dominant negative, https://www.cytoskeleton.com.

[13] Michaelson D, Silletti J, Murphy G, D'Eustachio P, Rush M, Philips MR., *Differential localization of Rho GTPases in live cells: regulation by hypervariable regions and RhoGDI binding*, J Cell Biol, 2001 Jan., doi: 10.1083/jcb.152.1.111.

[14] Kenneth N. Fish, *Total Internal Reflection Fluorescence (TIRF) Microscopy*, 2009 Oct., doi: 10.1002/0471142956.cy1218s50.

[15] Axelrod D, Koppel DE, Schlessinger J, Elson E, Webb WW, *Mobility measurement by analysis of fluorescence photobleaching recovery kinetics*, Biophys J. 1976 Sep., doi: 10.1016/S0006-3495(76)85755-4.

[16] Berkovich R, Wolfenson H, Eisenberg S, Ehrlich M, Weiss M, Klafter J, Henis YI, Urbakh M., *Accurate quantification of diffusion and binding kinetics of non-integral membrane proteins by FRAP*, Traffic. 2011 Nov., doi: 10.1111/j.1600-0854.2011.01264.x.

[17] Hodgson L, Shen F, Hahn K., *Biosensors for characterizing the dynamics of rho family GTPases in living cells*, Curr Protoc Cell Biol. 2010 Mar;Chapter 14:Unit 14.11.1-26., doi: 10.1002/0471143030.cb1411s46.

[18] Sekar RB, Periasamy A., *Fluorescence resonance energy transfer (FRET) microscopy imaging of live cell protein localizations*, J Cell Biol. 2003 Mar 3;160(5):629-33, doi: 10.1083/jcb.200210140.

[19] Yoshizaki H, Ohba Y, Kurokawa K, Itoh RE, Nakamura T, Mochizuki N, Nagashima K, Matsuda M., *Activity of Rho-family GTPases during cell division as visualized with FRET-based probes*, J Cell Biol., 2003 Jul., doi: 10.1083/jcb.200212049.

[20] Berlew EE, Kuznetsov IA, Yamada K, Bugaj LJ, Boerckel JD, Chow BY., *Single-Component Optogenetic Tools for Inducible RhoA GTPase Signaling*, Adv Biol (Weinh). 2021 Sep;5(9):e2100810, doi: 10.1002/adbi.202100810.

Appendix B

Reducing the Carbon Footprint of Academic Research: A Case Study in a Biophysics Laboratory

Reducing the Carbon Footprint of Academic Research: A Case Study in a Biophysics Laboratory

Caroline Giuglaris[1], Jean de Seze[1]

[a]UMR 168 Laboratoire PhysicoChimie Curie, Institut Curie, PSL Research University, Sorbonne Université, CNRS, Paris, France

Abstract

Climate change is a scientifically proven phenomenon caused by anthropic activities, which requires urgent and significant reductions in greenhouse gas emissions. Despite the increasing vocalization of scientists advocating for political action, the issue of the environmental impact of academic research has been neglected for some time. Now, field-dependent initiatives have emerged, such as the non-profit organization My Green Lab, which delivers "green" certifications to biology and chemistry labs, and institute-dependent programs, such as the Max Planck Sustainability Network. In France, an independent collective was founded in 2019 to address the environmental footprint of academic research following the COP 15 Paris Agreement: Labos 1Point5. Building on their resources and methodology, we have quantified the overall carbon footprint of our biophysics laboratory, considering energy consumption, purchases and travel, for the years 2021. We investigate how this footprint would decrease by 2030 following systemic changes (change in the energy mix, suppliers' improvements...), and we propose scenarios based on additional voluntary initiatives to reach a final reduction of -50% compared to the 2021 baseline, following IPCC targets. We have now formed a group of more than 20 colleagues to achieve this goal, emphasizing the importance of collective action. Finally, we provide advices based on our own experience to assist others in addressing the environmental impact of academic research in their respective laboratories.

Keywords: carbon footprint, academia, decarbonization

1. Introduction

Fundamental research is and will be impacted by the energy [1, 2], climate and biodiversity crisis we currently face, in at least two different ways. First, modern research is highly dependent on public fundings, which start to set constraints to reduce the environmental impact of public expenses. Second, scientists depend on their suppliers for energy, travel, consumables and instruments, who are themselves facing environmental, energetic and legal constraints. Moreover, environmental awareness is more and more spread among researchers, who want to act and take part in transforming the society we live in.

To start reducing the environmental impact of current research, one has first to measure it, and then take decisions and actions to follow a given trajectory of reductions of emissions. The standard norm for measuring this impact is the quantification of the carbon footprint, which takes into account all the direct and indirect greenhouse gas emissions due to a specific activity. It reveals both how emission-intensive an activity is, as well as how dependent it is on emission-intensive industries.

Many initiatives have been taken around the world to start quantifying the carbon footprint of research laboratories [3, 4] and implement measures to reduce emissions [5–7]. In France, a collective of academics has put together a free online tool to compute the environmental impact of one's laboratory [8]. It allowed the measurement of the carbon footprint of 834 laboratories (as of July 2023) with a standardized protocol, and has led to several publications about the global picture of the carbon footprint of academia in France [9–11]. Now that the main emission sectors are known, laboratories have to define their strategies for aiming at a strong reduction of the carbon footprint of their research, and take concrete decisions to reach them.

Here, we provide a detailed example for such a carbon footprint trajectory, for a biophysics department in Institut Curie, Paris, France. Firstly, we present the detailed carbon footprint of the studied laboratory, which comprises both experimental and theory teams, and is composed of 160 people. Second, we propose a strategy to reduce emissions, aiming at a 50% reduction for 2030 compared to 2021, following the consensus of the IPCC (to be checked). To compute this trajectory, we take into account both the reductions that were pledged by our main suppliers, together with voluntary action that have to be taken within the lab to reach the target. We also discuss how the strategy is organized within this research department, with working groups tackling the most important emission sectors.

2. Results

2.1. Carbon footprint of Physico-Chimie Curie: a biophysics laboratory with experiments and theory

The specific research laboratory presented here is composed of 14 research teams, with approximately 160 full-time equivalent positions, including permanent and short-term scientists, engineers, technicians, and support staff. To compute the carbon footprint, we used the methodology and emission factors proposed by Labos 1Point5 [11]. We could not directly use the

online tool GES 1point5 to compute the emissions due to purchases. Indeed, it required a specific classification of the purchases, standardized by the CNRS (one of France national research institute), to which our laboratory is not affiliated. Thus, specific emission factors have been estimated for this laboratory, which details can be found in Material and Methods.

Figure 1 (a) presents the detailed estimated carbon footprint for the year 2021. It gives a global impact of 605 tCO_2 for this year, with a carbon footprint of 4 tCO_2/capita. Interestingly, it is very close to the average carbon footprint of French laboratories [12], and similar to what has been computed for another biophysics laboratory in Paris [13]. As for most research laboratories in France, purchases, including of consumables and equipments, represents the first sector of emissions, with approximately two third of the total. Indirect energy consumption (referred to as 'Scope 2'), in our case electricity and gas, comes as the second emission source (20%), and travel as the third (6%). Of note, 2021 has been a year of low international travel compared to 2019, because of the restrictions due to the COVID pandemic in many countries.

Purchases are the main source of emissions but also the most specific to the type of research. Our research unit is composed of both experimental and theory teams, with highly different research topics, there is a huge heterogeneity in the emission per capita in each team, as can be seen on **Figure 1 (c)**. It ranges from 7tCO_2/capita/year for experimental teams, to less than 1 tCO_2/capita/year for teams doing only theory.

For travels, we detailed in **Figure 1 (b)** the numbers of travels depending on the distance, and the cumulative distance. As already known and discussed multiple times [14], plane, taken mostly for conferences, is by far the main contributor to the impact of travel. As plane emissions are considered to be proportional to the distance travelled, few long distance travels contribute to most of the CO_2 emissions for travels.

Overall, the detailed carbon footprint presented here reveals the main sources of emission, as well as the heterogeneity of each of these sources, with some actions and types of research being responsible for a large majority of the emissions. It allows for prioritization of the actions and construction of a short and long term strategy for carbon footprint reduction.

2.2. Building a trajectory to reduce CO2 emissions

The carbon footprint of the laboratory revealed how much our research is dependent on the external suppliers, such as the companies to which we buy our material, our electricity supplier, or plane companies for travelling. As a consequence, the evolution of the carbon footprint of our research unit will be highly dependent on the evolution of the carbon footprint of our suppliers in the coming years. These suppliers have themselves taken pledges for emission reductions, that we need to take into account into our trajectory. Few companies have a clear and realistic trajectory beyond 2030. Thus, we have restricted ourselves to the 2021-2030 period, for both systemic and voluntary changes. As a target, we chose to aim at a 50% reduction for 2030 compared to 2021, in accordance with European Union commitments.

To estimate the emission reduction that would happen without any changes from our side - neither increasing nor decreasing our budget, purchases, travels, electricity or gas consumption - we have based our work on the commitments made by our major suppliers. Details can be found in the Methods sections, and have led us to an estimate of 23% reduction due to systemic changes. Most of it comes from the reduction in emission due to purchases (- ...%), electricity (- ...%) and planes (- %). We did not evaluate the feasibility of the commitments, but took the pledges as granted.

To reach a 50% reduction of 2030 compared to 2021, there is still a part that must be achieved through voluntary action - approximately 34%, which is equivalent to 5% each year. We have built a working scenario, with the reduction details for the major sources of carbon emission, presented in **Figure 2 (b)** . This scenario takes into account a mix between decisions at the level of Institut Curie (about 2000 scientists) and improvements in lab-level management. At the level of the institute, renovation of the building should be the measure with the most impact, but also the most costly (- 60% for a cost of at least 1 to 2 M€). At the level of the lab, we opted for a 30% reduction of the impact of purchases, 50% reduction of the emission due to travel, and 30% reduction of our electricity consumption.

In order to convert these goals into concrete actions and pathways, we organized into working groups, which focused on the main sub-targets that can be tackled at the level of the laboratory (**Figure 2 (c)**). They refine the computation of the carbon footprint, evaluate the impact of the different decisions that can be taken, and do a follow-up on their emission source. We added a communication team, absolutely required to raise awareness among researchers of the laboratory.

Some actions will be directly measurable, as the reductions of electricity or gas consumptions. Other, such as changes of consumptions habits, will be hardly visible at a constant budget, because of the use of factors of conversion between euros and CO_2. Thus, we decided to quantify these actions independently, and subtract them every year for a quantified estimate of our actions.

3. Discussion

We wanted to present here, as an example, the carbon footprint of a specific biophysics laboratory, mixing experimentalists and theoreticians, and a proposal to build a trajectory of reduction of the carbon footprint. We showed here that some part should be achieved by the systemic societal changes, but will not be enough to reach the ambitious target of 50% reduction proposed by the European Union. Reaching such a target will require both institutional and lab-level changes, which may have impacts on research efficiency and quality. These impacts are hard to evaluate, as they could come together with changes in terms of price of energy or purchases.

One point that we also wish to raise, is the goal that has to be taken for research. Should research do more, or less, than the rest of the society? We decided to set, as an arbitrary target, the goal of 50% reduction for 2030 compared to 2021, which follows the global aim at the scale of the European Union. One

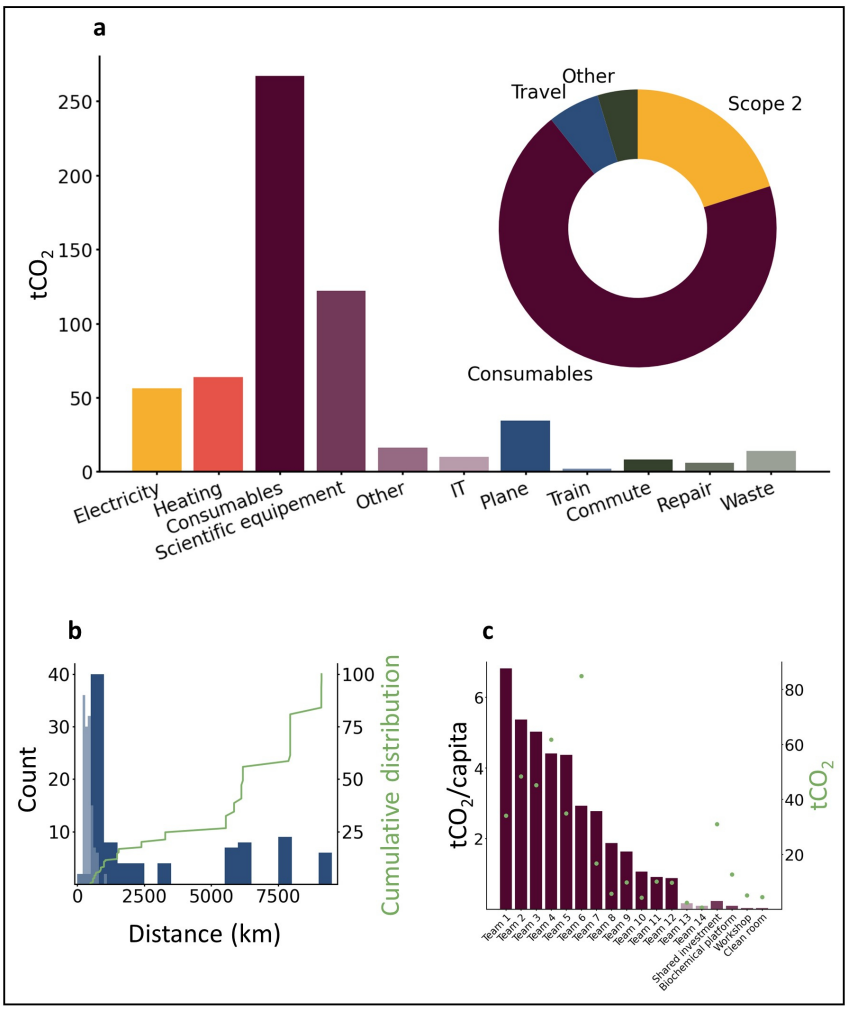

Figure 1: Carbon footprint for the year 2021. a. Carbon footprint of the laboratory with 160 people (in tCO_2 equivalent) for the main different emission sectors. Top right, donut chart grouping the purchases (in violet), electricity and heating (scope 2, in yellow), travels (in blue), and the other sectors (in green). b. Number of travels depending on the distance traveled for the train (light blue) and the plane (dark blue). In green, cumulative distribitution of total kilometers traveled. c. Emission per capita due to purchases for each team of the Department, in decreasing order. In green, total value of the emissions of purchases, right axis.

could argue that research should be exempted from these efforts. However, we personally think that research should do its part and will anyway have to adapt to the global changes, the sooner, the better. In any case, the strategy used here can be adapted to any target, taking into account systemic and voluntary changes for emission reduction trajectory.

As for all carbon footprints, most values taken here are subject to discussion. We chose the values given by Labos 1Point5, as a point of reference, because they are widely used in the French community. Compared to other laboratories in other countries, the emission factors will be most diverging for the impact of electricity, which is dependent on the electricity mix of the country. France's electricity mix is low-carbon compared to most countries (cite), and gives us a particularly low impact of electricity consumption. In other laboratories, electricity can be the first source of emission. Another impact negligible here compared to other laboratories is the commuting section. Indeed, the laboratory being situated at the heart of Paris, few people need to use their car on a daily basis, which considerably reduces the impact of commute.

We have good reasonable orders of magnitude, but are surely not exhaustive on our carbon footprint. One of the unknowns is the impact of external servers used for computation. We did not add any estimate, as most researchers were doing their computations locally - which is then taken into account in the electricity consumption - and we had no way to evaluate the amount and impact of this computation. We don't have any estimate for refrigerant gases either, which can be strong greenhouse gases, but are harder quantify.

Additionally, this study is focused on the carbon footprint of our laboratory, but we did not assess yet other environmental impacts of our research. Water usage (for material sterilization) and environmental pollutions (due to the incineration of bio-contaminated products) are expected to be high, and to have a

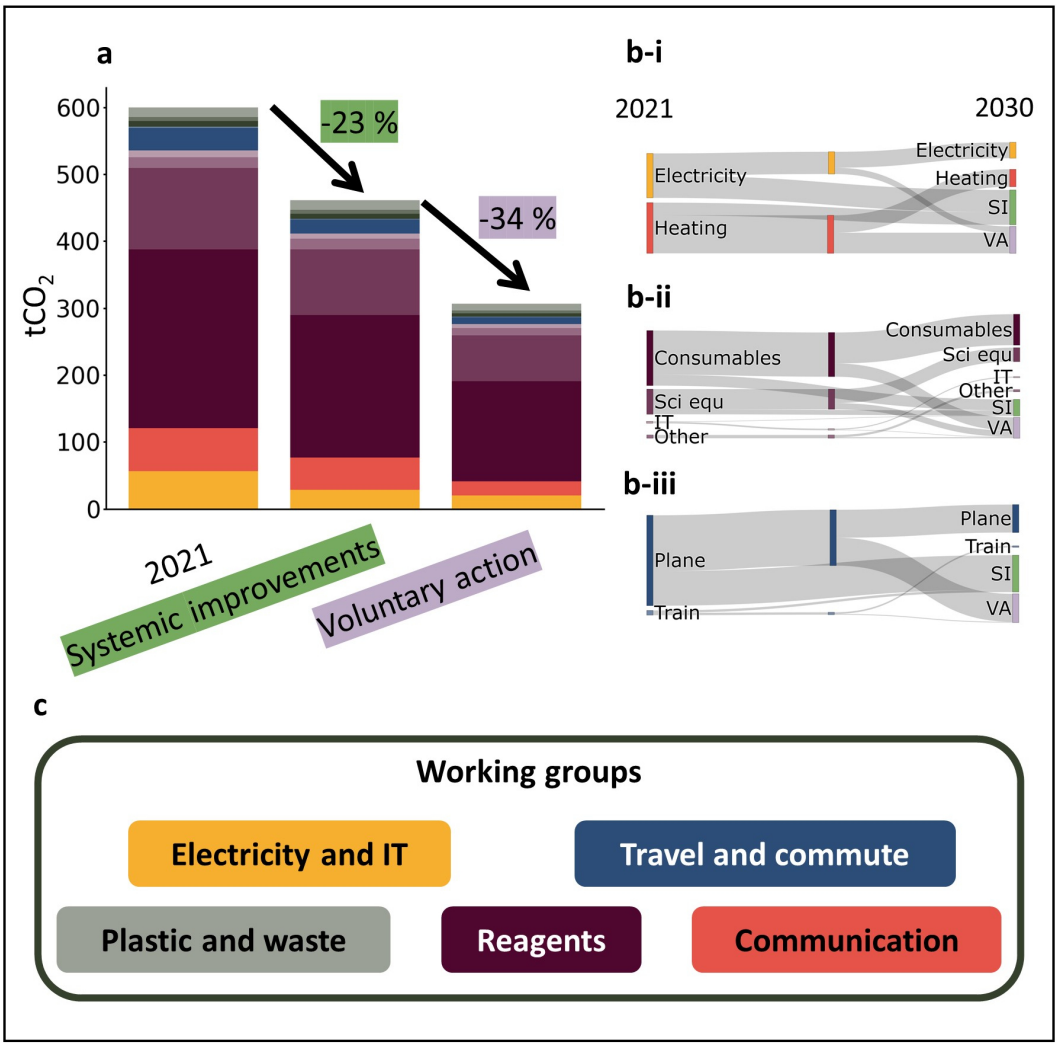

Figure 2: Proposed trajectory. a. Proposed trajectory of emission reduction. Taking 2021 as a reference (left bar), systemic improvements sue to suppliers will account for around 23% (middle bar), voluntary actions need to decrease emissions by 34% to reach a total of 50% reduction (right bar). Colors represent the different sectors presented in 1 b. Detailed reductions, due to systemic improvements (SI) or voluntary actions (VA) for electricity and heating (i), purchases (ii) and travels (iii) c. Working groups created in our department to tackle the different emission sectors.

negative impact on the biodiversity, air quality etc.

Overall, our study proposes an example of carbon footprint computation and building of a trajectory for emission reduction, which underlines the importance of quantification for targeting the most impactful emission sectors. We think that starting such a project in a laboratory also helps raise awareness among researchers, who can then be involved in their personal life, or even change their research subject to help our society facing the environmental crisis we are living in.

4. Methods

4.1. Data collection

4.2. Macro emission factors

4.3. Evaluation of systemic changes

Acknowledgements

References

1. Owens, B. Energy crisis squeezes science at CERN and other major facilities. en. *Nature* **610,** 431–432. ISSN: 0028-0836, 1476-4687. https://www.nature.com/articles/d41586-022-03257-8 (2023) (Oct. 2022).

2. Kwan, J. Europe's energy crisis hits science. en. *Science* **377,** 1244–1245. https://www.science.org/content/article/europe-s-energy-crisis-hits-science (2023) (Sept. 2022).

3. Martin, P. *et al.* A comprehensive assessment of the carbon footprint of an astronomical institute. en. *Nature Astronomy* **6,** 1219–1222. ISSN: 2397-3366. https://www.nature.com/articles/s41550-022-01771-3 (2023) (Nov. 2022).
4. Vidal Valero, M. How green is your research? These scientists are cutting their carbon footprints. en. *Nature* **616,** 16–17. ISSN: 0028-0836, 1476-4687. https://www.nature.com/articles/d41586-023-00837-0 (2023) (Apr. 2023).
5. Farley, M. How green is your science? The race to make laboratories sustainable. en. *Nature Reviews Molecular Cell Biology* **23,** 517–517. ISSN: 1471-0072, 1471-0080. https://www.nature.com/articles/s41580-022-00505-7 (2023) (Aug. 2022).
6. Bowler, J. How my lab went from 4,000 kg to 130 kg of waste a year. en. *Nature,* d41586–022–02092–1. ISSN: 0028-0836, 1476-4687. https://www.nature.com/articles/d41586-022-02092-1 (2023) (Aug. 2022).
7. Farley, M. & Nicolet, B. P. Re-use of laboratory utensils reduces CO2 equivalent footprint and running costs. en. *PLOS ONE* **18** (ed Jahanger, A.) e0283697. ISSN: 1932-6203. https://dx.plos.org/10.1371/journal.pone.0283697 (2023) (Apr. 2023).
8. Mariette, J. *et al.* An open-source tool to assess the carbon footprint of research. *Environmental Research: Infrastructure and Sustainability* **2,** 035008. ISSN: 2634-4505. https://iopscience.iop.org/article/10.1088/2634-4505/ac84a4 (2023) (Sept. 2022).
9. Blanchard, M., Bouchet-Valat, M., Cartron, D., Greffion, J. & Gros, J. Concerned yet polluting: A survey on French research personnel and climate change. en. *PLOS Climate* **1** (ed Fairbrother, M.) e0000070. ISSN: 2767-3200. https://dx.plos.org/10.1371/journal.pclm.0000070 (2023) (Sept. 2022).
10. Berné, O. *et al.* The carbon footprint of scientific visibility. *Environmental Research Letters* **17,** 124008. ISSN: 1748-9326. https://iopscience.iop.org/article/10.1088/1748-9326/ac9b51 (2023) (Dec. 2022).
11. De Paepe, M., Jeanneau, L., Mariette, J., Aumont, O. & Estevez-Torres, A. *Purchases dominate the carbon footprint of research laboratories* en. preprint. Apr. 2023. http://biorxiv.org/lookup/doi/10.1101/2023.04.04.535626 (2023).
12. *Transition bas carbone : un plan ambitieux pour le CNRS* French. Tech. rep. (CNRS, Nov. 2022). https://www.cnrs.fr/fr/cnrsinfo/transition-bas-carbone-un-plan-ambitieux-pour-le-cnrs.
13. Sarfa, G., Marrec, L., Loverdo, C. & Estevez-Torres, A. *Empreinte carbone du Laboratoire Jean Perrin* French. Tech. rep. (Sept. 2020). https://www.labojeanperrin.fr/?news69.
14. Ciers, J., Mandic, A., Toth, L. & Op 'T Veld, G. Carbon Footprint of Academic Air Travel: A Case Study in Switzerland. en. *Sustainability* **11,** 80. ISSN: 2071-1050. http://www.mdpi.com/2071-1050/11/1/80 (2023) (Dec. 2018).

Appendix A. Carbon footprint

Appendix A.1. Emission factors (table)

Appendix B. Scenario

Appendix B.1. Suppliers' claims (table)

Bibliography

[Abercrombie et al., 1970] Abercrombie, M., Heaysman, J. E., and Pegrum, S. M. (1970). The locomotion of fibroblasts in culture I. Movements of the leading edge. *Experimental Cell Research*, 59(3):393–398.

[Adamson et al., 1992] Adamson, P., Paterson, H. F., and Hall, A. (1992). Intracellular localization of the P21rho proteins. *Journal of Cell Biology*, 119(3):617–627.

[Aittaleb et al., 2010] Aittaleb, M., Boguth, C. A., and Tesmer, J. J. (2010). Structure and Function of Heterotrimeric G Protein-Regulated Rho Guanine Nucleotide Exchange Factors. *Molecular Pharmacology*, 77(2):111–125.

[Alon, 2020] Alon, U. (2020). An introduction to systems biology : design principles of biological circuits. page 324.

[Andersen et al., 2023] Andersen, T., Wörthmüller, D., Probst, D., Wang, I., Moreau, P., Fitzpatrick, V., Boudou, T., Schwarz, U. S., and Balland, M. (2023). Cell size and actin architecture determine force generation in optogenetically activated cells. *Biophysical journal*, 122(4):684–696.

[Arthur and Burridge, 2001] Arthur, W. T. and Burridge, K. (2001). RhoA Inactivation by p190RhoGAP Regulates Cell Spreading and Migration by Promoting Membrane Protrusion and Polarity.

[Avery et al., 1944] Avery, O. T., Macleod, C. M., and McCarty, M. (1944). STUDIES ON THE CHEMICAL NATURE OF THE SUBSTANCE INDUCING TRANSFORMATION OF PNEUMOCOCCAL TYPES : INDUCTION OF TRANSFORMATION BY A DESOXYRIBONUCLEIC ACID FRACTION ISOLATED FROM PNEUMOCOCCUS TYPE III. *The Journal of experimental medicine*, 79(2):137–158.

[Bansal et al., 2022] Bansal, A., Shikha, S., and Zhang, Y. (2022). Towards translational optogenetics. *Nature Biomedical Engineering*, 7(4):349–369.

[Bar-Even et al., 2011] Bar-Even, A., Noor, E., Savir, Y., Liebermeister, W., Davidi, D., Tawfik, D. S., and Milo, R. (2011). The moderately efficient enzyme: Evolutionary and physicochemical trends shaping enzyme parameters. *Biochemistry*, 50(21):4402–4410.

[Barlan and Gelfand, 2017] Barlan, K. and Gelfand, V. I. (2017). Microtubule-Based Transport and the Distribution, Tethering, and Organization of Organelles. *Cold Spring Harbor perspectives in biology*, 9(5).

[Beadle and Tatum, 1941] Beadle, G. W. and Tatum, E. L. (1941). Genetic Control of Biochemical Reactions in Neurospora. *Proceedings of the National Academy of Sciences*, 27(11):499–506.

[Belly et al., 2022] Belly, H. D., Yan, S., da Rocha, H. B., Ichbiah, S., Town, J. P., Turlier, H., Bustamante, C., and Weiner, O. D. (2022). Actin-driven protrusions generate rapid long-range membrane tension propagation in cells. *bioRxiv*, page 2022.09.07.507005.

[Bement et al., 2015] Bement, W. M., Leda, M., Moe, A. M., Kita, A. M., Larson, M. E., Golding, A. E., Pfeuti, C., Su, K. C., Miller, A. L., Goryachev, A. B., and Dassow, G. V. (2015). Activator-inhibitor coupling between Rho signaling and actin assembly make the cell cortex an excitable medium. *Nature cell biology*, 17(11):1471.

[Benard et al., 1999] Benard, V., Bohl, B. P., and Bokoch, G. M. (1999). Characterization of Rac and Cdc42 activation in chemoattractant- stimulated human neutrophils using a novel assay for active GTPases. *Journal of Biological Chemistry*, 274(19):13198–13204.

[Benink and Bement, 2005] Benink, H. A. and Bement, W. M. (2005). Concentric zones of active RhoA and Cdc42 around single cell wounds. *Journal of Cell Biology*, 168(3):429–439.

[Berlew et al., 2021] Berlew, E. E., Kuznetsov, I. A., Yamada, K., Bugaj, L. J., Boerckel, J. D., Chow, B. Y., Berlew, E. E., Kuznetsov, I. A., Bugaj, L. J., Boerckel, J. D., Chow, B. Y., and Yamada, K. (2021). 2100810 (1 of 8) Single-Component Optogenetic Tools for Inducible RhoA GTPase Signaling.

[Birnbaumer, 2007] Birnbaumer, L. (2007). The discovery of signal transduction by G proteins. A personal account and an overview of the initial findings and contributions that led to our present understanding. *Biochimica et biophysica acta*, 1768(4):756.

[Blümer et al., 2013] Blümer, J., Rey, J., Dehmelt, L., Maze, T., Wu, Y. W., Bastiaens, P., Goody, R. S., and Itzen, A. (2013). RabGEFs are a major determinant for specific Rab membrane targeting. *The Journal of cell biology*, 200(3):287–300.

[Bodor et al., 2020] Bodor, D. L., Pönisch, W., Endres, R. G., and Paluch, E. K. (2020). Of Cell Shapes and Motion: The Physical Basis of Animal Cell Migration. *Developmental Cell*, 52(5):550–562.

[Bolado-Carrancio et al., 2020] Bolado-Carrancio, A., Rukhlenko, O. S., Nikonova, E., Tsyganov, M. A., Wheeler, A., Garcia-Munoz, A., Kolch, W., von Kriegsheim, A., and Kholodenko, B. N. (2020). Periodic propagating waves coordinate rhogtpase network dynamics at the leading and trailing edges during cell migration. *eLife*, 9:1–34.

[Boulter et al., 2010] Boulter, E., Garcia-Mata, R., Guilluy, C., Dubash, A., Rossi, G., Brennwald, P. J., and Burridge, K. (2010). Regulation of Rho GTPase crosstalk, degradation and activity by RhoGDI1. *Nature Publishing Group*.

[Boyden et al., 2005] Boyden, E. S., Zhang, F., Bamberg, E., Nagel, G., and Deisseroth, K. (2005). Millisecond-timescale, genetically targeted optical control of neural activity. *Nature neuroscience*, 8(9):1263–1268.

[Bray, 1995] Bray, D. (1995). Protein molecules as computational elements in living cells. *Nature*, 376:307.

[Brenner et al., 1961] Brenner, S., Jacob, F., and Meselson, M. (1961). An unstable intermediate carrying information from genes to ribosomes for protein synthesis. *Nature*, 190(4776):576–581.

[Budnar et al., 2019] Budnar, S., Husain, K. B., Gomez, G. A., Naghibosadat, M., Varma, A., Verma, S., Hamilton, N. A., Morris, R. G., and Yap, A. S. (2019). Anillin Promotes Cell Contractility by Cyclic Resetting of RhoA Residence Kinetics. *Developmental Cell*, 49(6):894–906.e12.

[Bugaj et al., 2013] Bugaj, L. J., Choksi, A. T., Mesuda, C. K., Kane, R. S., and Schaffer, D. V. (2013). Optogenetic protein clustering and signaling activation in mammalian cells.

[Caliari et al., 2021] Caliari, A., Xu, J., and Yomo, T. (2021). The requirement of cellularity for abiogenesis. *Computational and Structural Biotechnology Journal*, 19:2202–2212.

[Callan-Jones, 2022] Callan-Jones, A. (2022). Self-organization in amoeboid motility. *Frontiers in Cell and Developmental Biology*, 10:1000071.

[Callan-Jones and Voituriez, 2016] Callan-Jones, A. C. and Voituriez, R. (2016). Actin flows in cell migration: from locomotion and polarity to trajectories. *Current Opinion in Cell Biology*, 38:12–17.

[Campellone and Welch, 2010] Campellone, K. G. and Welch, M. D. (2010). A nucleator arms race: cellular control of actin assembly. *Nature reviews. Molecular cell biology*, 11(4):237–251.

[Canty et al., 2017] Canty, L., Zarour, E., Kashkooli, L., François, P., and Fagotto, F. (2017). Sorting at embryonic boundaries requires high heterotypic interfacial tension. *Nature Communications*, 8(1).

[Capstick et al., 2022] Capstick, S., Thierry, A., Cox, E., Berglund, O., Westlake, S., and Steinberger, J. K. (2022). Civil disobedience by scientists helps press for urgent climate action. *Nature Climate Change 2022 12:9*, 12(9):773–774.

[Castillo-Kauil et al., 2020] Castillo-Kauil, A., García-Jiménez, I., Cervantes-Villagrana, R. D., Adame-García, S. R., Beltrán-Navarro, Y. M., Gutkind, J. S., Reyes-Cruz, G., and Vázquez-Prado, J. (2020). Gαs directly drives PDZ-RhoGEF signaling to Cdc42. *The Journal of Biological Chemistry*, 295(50):16920.

[Chen et al., 2010] Chen, Z., Medina, F., Liu, M. Y., Thomas, C., Sprang, S. R., and Sternweis, P. C. (2010). Activated RhoA binds to the Pleckstrin Homology (PH) domain of PDZ-RhoGEF, a potential site for autoregulation. *Journal of Biological Chemistry*, 285(27):21070–21081.

[Chiu and Clack, 2022] Chiu, C.-L. and Clack, N. (2022). napari: a Python Multi-Dimensional Image Viewer Platform for the Research Community. *MiMic*, 28(S1):1576–1577.

[Christie et al., 1999] Christie, J. M., Salomon, M., Nozue, K., Wada, M., and Briggs, W. R. (1999). LOV (light, oxygen, or voltage) domains of the blue-light photoreceptor phototropin (nph1): Binding sites for the chromophore flavin mononucleotide. *Proceedings of the National Academy of Sciences of the United States of America*, 96(15):8779–8783.

[Christie et al., 2002] Christie, J. M., Swartz, T. E., Bogomolni, R. A., and Briggs, W. R. (2002). Phototropin LOV domains exhibit distinct roles in regulating photoreceptor function. *Plant Journal*, 32(2):205–219.

[Cirit and Haugh, 2011] Cirit, M. and Haugh, J. M. (2011). Quantitative models of signal transduction networks: How detailed should they be? *Communicative & Integrative Biology*, 4(3):353.

[Cobb, 2017] Cobb, M. (2017). 60 years ago, Francis Crick changed the logic of biology. *PLOS Biology*, 15(9):e2003243.

[Cooper, 2000] Cooper, G. M. (2000). Structure of the Plasma Membrane.

[Corthell, 2014] Corthell, J. T. (2014). Immunoprecipitation. *Basic Molecular Protocols in Neuroscience: Tips, Tricks, and Pitfalls*, pages 77–81.

[Cramer, 1997] Cramer, L. P. (1997). Molecular mechanism of actin-dependent retrograde flow in lamellipodia of motile cells. *Frontiers in bioscience : a journal and virtual library*, 2.

[Cramer, 2013] Cramer, L. P. (2013). Mechanism of cell rear retraction in migrating cells. *Current Opinion in Cell Biology*, 25(5):591–599.

[Crick and Francis, 1970] Crick and Francis (1970). Central Dogma of Molecular Biology. *Natur*, 227(5258):561–563.

[CRICK, 1958] CRICK, F. H. (1958). On protein synthesis. *Symposia of the Society for Experimental Biology*, 12:138–163.

[Davis, 2013] Davis, W. O. (2013). Optical MEMS for displays in portable systems. *Handbook of Mems for Wireless and Mobile Applications*, pages 569–594.

[de Beco et al., 2018] de Beco, S., Vaidžiulytė, K., Manzi, J., Dalier, F., di Federico, F., Cornilleau, G., Dahan, M., and Coppey, M. (2018). Optogenetic dissection of Rac1 and Cdc42 gradient shaping. *Nature Communications*, 9(1).

[De Felipe et al., 2006] De Felipe, P., Luke, G. A., Hughes, L. E., Gani, D., Halpin, C., and Ryan, M. D. (2006). E unum pluribus: multiple proteins from a self-processing polyprotein. *Trends in biotechnology*, 24(2):68–75.

[de la Cova et al., 2017] de la Cova, C., Townley, R., Regot, S., and Greenwald, I. (2017). A Real-Time Biosensor for ERK Activity Reveals Signaling Dynamics during C. elegans Cell Fate Specification. *Developmental cell*, 42(5):542–553.e4.

[De Paepe et al., 2023] De Paepe, M., Jeanneau, L., Mariette, J., Aumont, O., Estevez-Torres, A., and Perrin, J. (2023). Purchases dominate the carbon footprint of research laboratories. *bioRxiv*, page 2023.04.04.535626.

[de Seze et al., 2023] de Seze, J., Gatin, J., and Coppey, M. (2023). RhoA regulation in space and time. *FEBS Letters*, 597(6):836–849.

[Dekel and Alon, 2005] Dekel, E. and Alon, U. (2005). Optimality and evolutionary tuning of the expression level of a protein. *Nature*, 436(7050):588–592.

[Dekel et al., 2005] Dekel, E., Mangan, S., and Alon, U. (2005). Environmental selection of the feed-forward loop circuit in gene-regulation networks. *Physical biology*, 2(2):81–88.

[Derewenda et al., 2004] Derewenda, U., Oleksy, A., Stevenson, A. S., Korczynska, J., Dauter, Z., Somlyo, A. P., Otlewski, J., Somlyo, A. V., and Derewenda, Z. S. (2004). The Crystal Structure of RhoA in Complex with the DH/PH Fragment of PDZRhoGEF, an Activator of the Ca2+ Sensitization Pathway in Smooth Muscle. *Structure*, 12(11):1955–1965.

[Ding et al., 2018] Ding, Z., Dhruv, H., Kwiatkowska-Piwowarczyk, A., Ruggieri, R., Kloss, J., Symons, M., Pirrotte, P., Eschbacher, J. M., Tran, N. L., and Loftus, J. C. (2018). PDZ-RhoGEF Is a Signaling Effector for TROY-Induced Glioblastoma Cell Invasion and Survival. *Neoplasia (New York, N.Y.)*, 20(10):1045–1058.

[Du et al., 2020] Du, J., Zhu, Z., Xu, L., Chen, X., Li, X., Lan, T., Li, W., Yuan, K., and Zeng, Y. (2020). ARHGEF11 promotes proliferation and epithelial-mesenchymal transition of hepatocellular carcinoma through activation of β-catenin pathway. *Aging (Albany NY)*, 12(20):20235.

[Du Roure et al., 2005] Du Roure, O., Saez, A., Buguin, A., Austin, R. H., Chavrier, P., Siberzan, P., and Ladoux, B. (2005). Force mapping in epithelial cell migration. *Proceedings of the National Academy of Sciences of the United States of America*, 102(7):2390–2395.

[Duan et al., 2017] Duan, L., Hope, J., Ong, Q., Lou, H. Y., Kim, N., McCarthy, C., Acero, V., Lin, M. Z., and Cui, B. (2017). Understanding CRY2 interactions for optical control of intracellular signaling. *Nature Communications*, 8(1):4–13.

[Dutrochet, 1824] Dutrochet, H. (1824). *Recherches anatomiques et physiologiques sur la structure intime des animaux et des végétaux et sur leur motilité*.

[Elosegui-Artola et al., 2018] Elosegui-Artola, A., Trepat, X., and Roca-Cusachs, P. (2018). Control of Mechanotransduction by Molecular Clutch Dynamics. *Trends in Cell Biology*, 28(5):356–367.

[Ender et al., 2022] Ender, P., Gagliardi, P. A., Dobrzyński, M., Frismantiene, A., Dessauges, C., Höhener, T., Jacques, M. A., Cohen, A. R., and Pertz, O. (2022). Spatiotemporal control of ERK pulse frequency coordinates fate decisions during mammary acinar morphogenesis. *Developmental cell*, 57(18):2153–2167.e6.

[Ershov et al., 2022] Ershov, D., Phan, M. S., Pylvänäinen, J. W., Rigaud, S. U., Le Blanc, L., Charles-Orszag, A., Conway, J. R., Laine, R. F., Roy, N. H., Bonazzi, D., Duménil, G., Jacquemet, G., and Tinevez, J. Y. (2022). TrackMate 7: integrating state-of-the-art segmentation algorithms into tracking pipelines. *Nature Methods 2022 19:7*, 19(7):829–832.

[Etienne-Manneville and Hall, 2002] Etienne-Manneville, S. and Hall, A. (2002). Rho GTPases in cell biology. *Nature*, 420(6916):629–635.

[Etoc et al., 2018] Etoc, F., Balloul, E., Vicario, C., Normanno, D., Liße, D., Sittner, A., Piehler, J., Dahan, M., and Coppey, M. (2018). Non-specific interactions govern cytosolic diffusion of nanosized objects in mammalian cells. *Nature materials*, 17(8):740–746.

[Farley and Nicolet, 2022] Farley, M. and Nicolet, B. P. (2022). Re-use of labware reduces CO2 equivalent footprint and running costs in laboratories. *bioRxiv*, page 2022.01.14.476337.

[Fischer, 1894] Fischer, E. (1894). Einfluss der Configuration auf die Wirkung der Enzyme. *Berichte der deutschen chemischen Gesellschaft*, 27(3):2985–2993.

[Fletcher and Mullins, 2010] Fletcher, D. A. and Mullins, R. D. (2010). Cell mechanics and the cytoskeleton. *Nature*, 463(7280):485.

[Friedl and Alexander, 2011] Friedl, P. and Alexander, S. (2011). Cancer invasion and the microenvironment: plasticity and reciprocity. *Cell*, 147(5):992–1009.

[Friedl and Gilmour, 2009] Friedl, P. and Gilmour, D. (2009). Collective cell migration in morphogenesis, regeneration and cancer. *Nature Reviews Molecular Cell Biology 2009 10:7*, 10(7):445–457.

[Fritz et al., 2013] Fritz, R. D., Letzelter, M., Reimann, A., Martin, K., Fusco, L., Ritsma, L., Ponsioen, B., Fluri, E., Schulte-Merker, S., Rheenen, J. V., and Pertz, O. (2013). A versatile toolkit to produce sensitive FRET biosensors to visualize signaling in time and space. *Science Signaling*, 6(285).

[Fuchs et al., 2014] Fuchs, G., Voichek, Y., Benjamin, S., Gilad, S., Amit, I., and Oren, M. (2014). 4sUDRB-seq: measuring genomewide transcriptional elongation rates and initiation frequencies within cells. *Genome biology*, 15(5):R69.

[Gahmberg et al., 2019] Gahmberg, C. G., Grönholm, M., Madhavan, S., Jahan, F., Mikkola, E., Viazmina, L., and Koivunen, E. (2019). Regulation of cell adhesion: a collaborative effort of integrins, their ligands, cytoplasmic actors, and phosphorylation. *Quarterly reviews of biophysics*, 52:e10.

[Gasmi-Seabrook et al., 2010] Gasmi-Seabrook, G. M., Marshall, C. B., Cheung, M., Kim, B., Wang, F., Jang, Y. J., Mak, T. W., Stambolic, V., and Ikura, M. (2010). Real-time NMR Study of Guanine Nucleotide Exchange and Activation of RhoA by PDZ-RhoGEF. *Journal of Biological Chemistry*, 285(8):5137–5145.

[Goglia and Toettcher, 2019] Goglia, A. G. and Toettcher, J. E. (2019). A bright future: optogenetics to dissect the spatiotemporal control of cell behavior. *Current Opinion in Chemical Biology*, 48:106–113.

[Goglia et al., 2020] Goglia, A. G., Wilson, M. Z., Jena, S. G., Silbert, J., Basta, L. P., Devenport, D., and Toettcher, J. E. (2020). A Live-Cell Screen for Altered Erk Dynamics Reveals Principles of Proliferative Control. *Cell systems*, 10(3):240–253.e6.

[Golding et al., 2019] Golding, A. E., Visco, I., Bieling, P., and Bement, W. M. (2019). Extraction of active RhoGTPases by RhoGDI regulates spatiotemporal patterning of RhoGTPases. *eLife*, 8.

[Goryachev et al., 2016] Goryachev, A. B., Leda, M., Miller, A. L., Dassow, G. V., and Bement, W. M. (2016). Small GTPases How to make a static cytokinetic furrow out of traveling excitable waves.

[Graessl et al., 2017] Graessl, M., Koch, J., Calderon, A., Kamps, D., Banerjee, S., Mazel, T., Schulze, N., Jungkurth, J. K., Patwardhan, R., Solouk, D., Hampe, N., Hoffmann, B., Dehmelt, L., and Nalbant, P. (2017). An excitable Rho GTPase signaling network generates dynamic subcellular contraction patterns. *The Journal of Cell Biology*, 216(12):4271.

[Grecco et al., 2011] Grecco, H. E., Schmick, M., and Bastiaens, P. I. (2011). Signaling from the Living Plasma Membrane. *Cell*, 144(6):897–909.

[Gros et al., 1961] Gros, F., Hiatt, H., Gilbert, W., Kurland, C. G., Risebrough, R. W., and Watson, J. D. (1961). Unstable Ribonucleic Acid Revealed by Pulse Labelling of Escherichia Coli. *Nature 1961 190:4776*, 190(4776):581–585.

[Guilluy et al., 2011] Guilluy, C., Garcia-Mata, R., and Burridge, K. (2011). Rho protein crosstalk: another social network? *Trends in Cell Biology*, 21(12):718–726.

[Guntas et al., 2015] Guntas, G., Hallett, R. A., Zimmerman, S. P., Williams, T., Yumerefendi, H., Bear, J. E., and Kuhlman, B. (2015). Engineering an improved light-induced dimer (iLID) for controlling the localization and activity of signaling proteins. *Proceedings of the National Academy of Sciences*, 112(1):112–117.

[Hahn et al., 2009] Hahn, A. T., Jones, J. T., and Meyer, T. (2009). Quantitative analysis of cell cycle phase durations and PC12 differentiation using fluorescent biosensors. *Cell cycle (Georgetown, Tex.)*, 8(7):1044.

[Hart and Alon, 2013] Hart, Y. and Alon, U. (2013). The Utility of Paradoxical Components in Biological Circuits. *Molecular Cell*, 49(2):213–221.

[Hetmanski et al., 2019] Hetmanski, J. H., de Belly, H., Busnelli, I., Waring, T., Nair, R. V., Sokleva, V., Dobre, O., Cameron, A., Gauthier, N., Lamaze, C., Swift, J., del Campo, A., Starborg, T., Zech, T., Goetz, J. G., Paluch, E. K., Schwartz, J. M., and Caswell, P. T. (2019). Membrane Tension Orchestrates Rear Retraction in Matrix-Directed Cell Migration. *Developmental Cell*, 51(4):460.

[Hino et al., 2020] Hino, N., Rossetti, L., Marín-Llauradó, A., Aoki, K., Trepat, X., Matsuda, M., and Hirashima, T. (2020). ERK-Mediated Mechanochemical Waves Direct Collective Cell Polarization. *Developmental Cell*, 53(6):646–660.e8.

[Hoang et al., 2013] Hoang, A. N., Jones, C. N., Dimisko, L., Hamza, B., Martel, J., Kojic, N., and Irimia, D. (2013). Measuring neutrophil speed and directionality during chemotaxis, directly from a droplet of whole blood. *TECHNOLOGY*, 01(01):49–57.

[Hodge and Ridley, 2016] Hodge, R. G. and Ridley, A. J. (2016). Regulating Rho GTPases and their regulators. *Nature Reviews Molecular Cell Biology*, 17(8):496–510.

[Hooke, 1665] Hooke, R. (1665). *Micrographia*. [[The Royal Society]].

[Huang et al., 2014] Huang, B., Lu, M., Jolly, M. K., Tsarfaty, I., Onuchic, J., and Ben-Jacob, E. (2014). The three-way switch operation of Rac1/RhoA GTPase-based circuit controlling amoeboid-hybrid-mesenchymal transition. *Scientific Reports 2014 4:1*, 4(1):1–11.

[Hunter, 2000] Hunter, T. (2000). Signaling - 2000 and beyond. *Cell*, 100(1):113–127.

[Huveneers and Danen, 2009] Huveneers, S. and Danen, E. H. (2009). Adhesion signaling - crosstalk between integrins, Src and Rho. *Journal of cell science*, 122(Pt 8):1059–1069.

[Iglesias and Devreotes, 2011] Iglesias, P. A. and Devreotes, P. N. (2011). Biased excitable networks: How cells direct motion in response to gradients.

[Iizuka et al., 2011] Iizuka, R., Yamagishi-Shirasaki, M., and Funatsu, T. (2011). Kinetic study of de novo chromophore maturation of fluorescent proteins. *Analytical biochemistry*, 414(2):173–178.

[Inaba et al., 2021] Inaba, H., Miao, Q., and Nakata, T. (2021). Optogenetic control of small GTPases reveals RhoA mediates intracellular calcium signaling. *The Journal of Biological Chemistry*, 296.

[Inoue et al., 2005] Inoue, T., Heo, W. D., Grimley, J. S., Wandless, T. J., and Meyer, T. (2005). An inducible translocation strategy to rapidly activate and inhibit small GTPase signaling pathways. *Nature Methods*, 2(6):415–418.

[Isogai et al., 2015] Isogai, T., van der Kammen, R., Leyton-Puig, D., Kedziora, K. M., Jalink, K., and Innocenti, M. (2015). Initiation of lamellipodia and ruffles involves cooperation between mDia1 and the Arp2/3 complex. *Journal of cell science*, 128(20):3796–3810.

[Iwanicki et al., 2008] Iwanicki, M. P., Vomastek, T., Tilghman, R. W., Martin, K. H., Banerjee, J., Wedegaertner, P. B., and Parsons, J. T. (2008). FAK, PDZ-RhoGEF and ROCKII cooperate to regulate adhesion movement and trailing-edge retraction in fibroblasts. *Journal of cell science*, 121(Pt 6):895–905.

[Jacob and Monod, 1961] Jacob, F. and Monod, J. (1961). Genetic regulatory mechanisms in the synthesis of proteins. *Journal of molecular biology*, 3(3):318–356.

[Jacobson et al., 1984] Jacobson, K., O'Dell, D., and August, J. T. (1984). Lateral diffusion of an 80,000-dalton glycoprotein in the plasma membrane of murine fibroblasts: Relationships to cell structure and function. *Journal of Cell Biology*, 99(5):1624–1633.

[Jain et al., 2020] Jain, S., Cachoux, V. M., Narayana, G. H., de Beco, S., D'Alessandro, J., Cellerin, V., Chen, T., Heuzé, M. L., Marcq, P., Mège, R. M., Kabla, A. J., Lim, C. T., and Ladoux, B. (2020). The role of single cell mechanical behavior and polarity in driving collective cell migration. *Nature physics*, 16(7):802.

[Jaiswal et al., 2013] Jaiswal, M., Dvorsky, R., and Ahmadian, M. R. (2013). Deciphering the molecular and functional basis of Dbl family proteins: A novel systematic approach toward classification of selective activation of the Rho family proteins. *Journal of Biological Chemistry*, 288(6):4486–4500.

[Janes and Yaffe, 2006] Janes, K. A. and Yaffe, M. B. (2006). Data-driven modelling of signal-transduction networks. *Nature Reviews Molecular Cell Biology 2006 7:11*, 7(11):820–828.

[Janiszewska et al., 2020] Janiszewska, M., Primi, M. C., and Izard, T. (2020). Cell adhesion in cancer: Beyond the migration of single cells. *The Journal of biological chemistry*, 295(8):2495–2505.

[Jarsch et al., 2016] Jarsch, I. K., Daste, F., and Gallop, J. L. (2016). Membrane curvature in cell biology: An integration of molecular mechanisms. *The Journal of Cell Biology*, 214(4):375.

[Ju et al., 2022] Ju, J., Lee, H. N., Ning, L., Ryu, H., Zhou, X. X., Chun, H., Lee, Y. W., Lee-Richerson, A. I., Jeong, C., Lin, M. Z., and Seong, J. (2022). Optical regulation of endogenous RhoA reveals selection of cellular responses by signal amplitude. *Cell Reports*, 40(2):111080.

[Kamps et al., 2020] Kamps, D., Koch, J., Juma, V. O., Campillo-Funollet, E., Graessl, M., Banerjee, S., Mazel, T., Chen, X., Wu, Y. W., Portet, S., Madzvamuse, A., Nalbant, P., and Dehmelt, L. (2020). Optogenetic Tuning Reveals Rho Amplification-Dependent Dynamics of a Cell Contraction Signal Network. *Cell Reports*, 33(9).

[Kelkar et al., 2022] Kelkar, M., Bohec, P., Smith, M., Sreenivasan, V., Lisica, A., Valon, L., Ferber, E., Baum, B., Salbreux, G., and Charras, G. (2022). Spindle reorientation in response to mechanical stress is an emergent property of the spindle positioning mechanisms. *bioRxiv*, page 2022.02.13.480269.

[Kennedy et al., 2010] Kennedy, M. J., Hughes, R. M., Peteya, L. A., Schwartz, J. W., Ehlers, M. D., and Tucker, C. L. (2010). Rapid blue-light-mediated induction of protein interactions in living cells. *Nature Methods*, 7(12):973–975.

[Kerjouan et al., 2021] Kerjouan, A., Boyault, C., Oddou, C., Hiriart-Bryant, E., Grichine, A., Kraut, A., Pezet, M., Balland, M., Faurobert, E., Bonnet, I., Coute, Y., Fourcade, B., Albiges-Rizo, C., and Destaing, O. (2021). Control of SRC molecular dynamics encodes distinct cytoskeletal responses by specifying signaling pathway usage. *Journal of Cell Science*, 134(2).

[Kestler et al., 2008] Kestler, H. A., Wawra, C., Kracher, B., and Kühl, M. (2008). Network modeling of signal transduction: establishing the global view. *BioEssays*, 30(11-12):1110–1125.

[Khammash, 2021] Khammash, M. H. (2021). Perfect adaptation in biology. *Cell systems*, 12(6):509–521.

[Kim et al., 2021] Kim, H., Ju, J., Lee, H. N., Chun, H., and Seong, J. (2021). Genetically Encoded Biosensors Based on Fluorescent Proteins. *Sensors (Basel, Switzerland)*, 21(3):1–18.

[Kim et al., 2016] Kim, N., Kim, J. M., and Heo, W. D. (2016). Optogenetic Control of Fibroblast Growth Factor Receptor Signaling. *Methods in molecular biology (Clifton, N.J.)*, 1408:345–362.

[Kolar et al., 2018] Kolar, K., Knobloch, C., Stork, H., Žnidarič, M., and Weber, W. (2018). OptoBase: A Web Platform for Molecular Optogenetics. *ACS Synthetic Biology*, 7(7):1825–1828.

[Kolch et al., 2015] Kolch, W., Halasz, M., Granovskaya, M., and Kholodenko, B. N. (2015). The dynamic control of signal transduction networks in cancer cells. *Nature Reviews Cancer*, 15(9):515–527.

[Koonin, 2012] Koonin, E. V. (2012). Does the central dogma still stand? *Biology Direct*, 7:27.

[Koride et al., 2014] Koride, S., He, L., Xiong, L. P., Lan, G., Montell, D. J., and Sun, S. X. (2014). Mechanochemical regulation of oscillatory follicle cell dynamics in the developing Drosophila egg chamber. *Molecular Biology of the Cell*, 25(22):3709–3716.

[Kowalczyk et al., 2021] Kowalczyk, M., Kamps, D., Wu, Y., Dehmelt, L., and Nalbant, P. (2021). Monitoring the Response of Multiple Signal Network Components to Acute Chemo-Optogenetic Perturbations in Living Cells.

[Kowalczyk et al., 2022] Kowalczyk, M., Kamps, D., Wu, Y., Dehmelt, L., and Nalbant, P. (2022). Monitoring the Response of Multiple Signal Network Components to Acute Chemo-Optogenetic Perturbations in Living Cells. *Chembiochem : a European journal of chemical biology*, 23(4).

[Krawczyk et al., 2023] Krawczyk, A., Jaguszewska, N., Ziółkiewicz, W., and Grodzińska-Jurczak, M. (2023). The ivory tower of academia in the era of climate change: European scientists' engagement in science popularization related to single-use plastics. *Environmental Science & Policy*, 146:185–202.

[Kraynov et al., 2000] Kraynov, V. S., Chamberlain, C., Bokoch, G. M., Schwartz, M. A., Slabaugh, S., and Hahn, K. M. (2000). Localized Rac Activation Dynamics Visualized in Living Cells. *Science*, 290(5490):333–337.

[Krebs and Beavo, 1979] Krebs, E. G. and Beavo, J. A. (1979). Phosphorylation-dephosphorylation of enzymes. *Annual review of biochemistry*, 48:923–959.

[Krebs and Fischer, 1956] Krebs, E. G. and Fischer, E. H. (1956). The phosphorylase b to a converting enzyme of rabbit skeletal muscle. *Biochimica et biophysica acta*, 20(1):150–157.

[Kriegman et al., 2020] Kriegman, S., Blackiston, D., Levin, M., and Bongard, J. (2020). A scalable pipeline for designing reconfigurable organisms. *Proceedings of the National Academy of Sciences of the United States of America*, 117(4):1853–1859.

[Krndija et al., 2019] Krndija, D., Marjou, F. E., Guirao, B., Richon, S., Leroy, O., Bellaiche, Y., Hannezo, E., and Vignjevic, D. M. (2019). Active cell migration is critical for steady-state epithelial turnover in the gut. *Science (New York, N.Y.)*, 365(6454):705–710.

[Krueger et al., 2019] Krueger, D., Izquierdo, E., Viswanathan, R., Hartmann, J., Cartes, C. P., and de Renzis, S. (2019). Principles and applications of optogenetics in developmental biology. *Development (Cambridge, England)*, 146(20).

[Kurokawa and Matsuda, 2005] Kurokawa, K. and Matsuda, M. (2005). Localized RhoA Activation as a Requirement for the Induction of Membrane Ruffling. *Molecular Biology of the Cell*, 16(9):4294.

[Lä et al., 2009] Lä, T., Sixt, M., Humphries, M., and Reynolds, A. (2009). Mechanical modes of 'amoeboid' cell migration This review comes from a themed issue on Cell-to-cell contact and extracellular matrix Edited by. *Current Opinion in Cell Biology*, 21:636–644.

[Lämmermann et al., 2008] Lämmermann, T., Bader, B. L., Monkley, S. J., Worbs, T., Wedlich-Söldner, R., Hirsch, K., Keller, M., Förster, R., Critchley, D. R., Fässler, R., and Sixt, M. (2008). Rapid leukocyte migration by integrin-independent flowing and squeezing. *Nature*, 453(7191):51–55.

[Lauffenburger and Horwitz, 1996] Lauffenburger, D. A. and Horwitz, A. F. (1996). Cell Migration: A Physically Integrated Molecular Process. *Cell*, 84(3):359–369.

[Lee et al., 2010] Lee, C. S., Choi, C. K., Shin, E. Y., Schwartz, M. A., and Kim, E. G. (2010). Myosin II directly binds and inhibits Dbl family guanine nucleotide exchange factors: a possible link to Rho family GTPases. *The Journal of cell biology*, 190(4):663–674.

[Leithner et al., 2016] Leithner, A., Eichner, A., Müller, J., Reversat, A., Brown, M., Schwarz, J., Merrin, J., De Gorter, D. J., Schur, F., Bayerl, J., De Vries, I., Wieser, S., Hauschild, R., Lai, F. P., Moser, M., Kerjaschki, D., Rottner, K., Small, J. V., Stradal, T. E., and Sixt, M. (2016). Diversified actin protrusions promote environmental exploration but are dispensable for locomotion of leukocytes. *Nature Cell Biology 2016 18:11*, 18(11):1253–1259.

[Lennon-Duménil and Moreau, 2021] Lennon-Duménil, A. M. and Moreau, H. D. (2021). Barotaxis: How cells live and move under pressure. *Current opinion in cell biology*, 72:131–136.

[Levskaya et al., 2009] Levskaya, A., Weiner, O. D., Lim, W. A., and Voigt, C. A. (2009). Spatiotemporal control of cell signalling using a light-switchable protein interaction. *Nature*, 461(7266):997–1001.

[Li and Gundersen, 2008] Li, R. and Gundersen, G. G. (2008). Beyond polymer polarity: how the cytoskeleton builds a polarized cell. *Nature reviews. Molecular cell biology*, 9(11):860–873.

[Li et al., 2011] Li, X., Wang, Q., Yu, X., Liu, H., Yang, H., Zhao, C., Liu, X., Tan, C., Klejnot, J., Zhong, D., and Lin, C. (2011). Arabidopsis cryptochrome 2 (CRY2) functions by the photoactivation mechanism distinct from the tryptophan (trp) triad-dependent photoreduction. *Proceedings of the National Academy of Sciences of the United States of America*, 108(51):20844–20849.

[Liu et al., 2008] Liu, H., Yu, X., Li, K., Klejnot, J., Yang, H., Lisiero, D., and Lin, C. (2008). Photoexcited CRY2 interacts with CIB1 to regulate transcription and floral initiation in Arabidopsis. *Science*, 322(5907):1535–1539.

[Liu et al., 2015] Liu, Y. J., Le Berre, M., Lautenschlaeger, F., Maiuri, P., Callan-Jones, A., Heuzé, M., Takaki, T., Voituriez, R., and Piel, M. (2015). Confinement and low adhesion induce fast amoeboid migration of slow mesenchymal cells. *Cell*, 160(4):659–672.

[Llense and Etienne-Manneville, 2015] Llense, F. and Etienne-Manneville, S. (2015). Front-to-rear polarity in migrating cells. *Cell Polarity 1: Biological Role and Basic Mechanisms*, pages 115–146.

[Lomakin et al., 2020] Lomakin, A. J., Cattin, C. J., Cuvelier, D., Alraies, Z., Molina, M., Nader, G. P., Srivastava, N., Saez, P. J., Garcia-Arcos, J. M., Zhitnyak, I. Y., Bhargava, A., Driscoll, M. K., Welf, E. S., Fiolka, R., Petrie, R. J., de Silva, N. S., González-Granado, J. M., Manel, N., Lennon-Duménil, A. M., Müller, D. J., and Piel, M. (2020). The nucleus acts as a ruler tailoring cell responses to spatial constraints. *Science (New York, N.Y.)*, 370(6514).

[Longenecker et al., 2003] Longenecker, K., Read, P., Lin, S. K., Somlyo, A. P., Nakamoto, R. K., and Derewenda, Z. S. (2003). Structure of a constitutively activated RhoA mutant (Q63L) at 1.55 Å resolution. *urn:issn:0907-4449*, 59(5):876–880.

[M. Salomon et al., 2000] M. Salomon, J. M. C., Elke Knieb, Ulrika Lempert, , and Briggs, W. R. (2000). Photochemical and Mutational Analysis of the FMN-Binding Domains of the Plant Blue Light Receptor, Phototropin.

[MacHacek et al., 2009] MacHacek, M., Hodgson, L., Welch, C., Elliott, H., Pertz, O., Nalbant, P., Abell, A., Johnson, G. L., Hahn, K. M., and Danuser, G. (2009). Coordination of Rho GTPase activities during cell protrusion. *Nature*, 461(7260):99–103.

[Mahdessian et al., 2021] Mahdessian, D., Cesnik, A. J., Gnann, C., Danielsson, F., Stenström, L., Arif, M., Zhang, C., Le, T., Johansson, F., Shutten, R., Bäckström, A., Axelsson, U., Thul, P., Cho, N. H., Carja, O., Uhlén, M., Mardinoglu, A., Stadler, C., Lindskog, C., Ayoglu, B., Leonetti, M. D., Pontén, F., Sullivan, D. P., and Lundberg, E. (2021). Spatiotemporal dissection of the cell cycle with single-cell proteogenomics. *Nature*, 590(7847):649–654.

[Mahlandt et al., 2021] Mahlandt, E. K., Arts, J. J., van der Meer, W. J., van der Linden, F. H., Tol, S., van Buul, J. D., Gadella, T. W., and Goedhart, J. (2021). Visualizing endogenous Rho activity with an improved localization-based, genetically encoded biosensor. *Journal of cell science*, 134(17).

[Mahlandt et al., 2023] Mahlandt, E. K., Kreider-Letterman, G., Chertkova, A. O., Garcia-Mata, R., and Goedhart, J. (2023). Cell-based optimization and characterization of genetically encoded location-based biosensors for Cdc42 or Rac activity. *Journal of cell science*, 136(10).

[Martin et al., 2016] Martin, K., Reimann, A., Fritz, R. D., Ryu, H., Jeon, N. L., and Pertz, O. (2016). Spatio-temporal co-ordination of RhoA, Rac1 and Cdc42 activation during prototypical edge protrusion and retraction dynamics. *Scientific reports*, 6.

[Martin, 2015] Martin, S. G. (2015). Spontaneous cell polarization: Feedback control of Cdc42 GTPase breaks cellular symmetry. *BioEssays*, 37(11):1193–1201.

[Mattheyses et al., 2010] Mattheyses, A. L., Simon, S. M., and Rappoport, J. Z. (2010). Imaging with total internal reflection fluorescence microscopy for the cell biologist. *Journal of cell science*, 123(Pt 21):3621–3628.

[Mayor and Etienne-Manneville, 2016] Mayor, R. and Etienne-Manneville, S. (2016). The front and rear of collective cell migration. *Nature Reviews Molecular Cell Biology 2016 17:2*, 17(2):97–109.

[Medina et al., 2013] Medina, F., Carter, A. M., Dada, O., Gutowski, S., Hadas, J., Chen, Z., and Sternweis, P. C. (2013). Activated RhoA Is a Positive Feedback Regulator of the Lbc Family of Rho Guanine Nucleotide Exchange Factor Proteins *. *Journal of Biological Chemistry*, 288(16):11325–11333.

[Mendel, 1865] Mendel, G. (1865). *Versuche über Pflanzenhybriden*. Vieweg+Teubner Verlag.

[Michaelson et al., 2001] Michaelson, D., Silletti, J., Murphy, G., D'Eustachio, P., Rush, M., and Philips, M. R. (2001). Differential localization of Rho GTPases in live cells: Regulation by hypervariable regions and RhoGDI binding. *Journal of Cell Biology*, 152(1):111–126.

[Michaux et al., 2018] Michaux, J. B., Robin, F. B., Mcfadden, W. M., and Munro, E. M. (2018). Excitable RhoA dynamics drive pulsed contractions in the early C. elegans embryo. *J. Cell Biol*, 217:4230–4252.

[Milo and Phillips, 2015] Milo, R. and Phillips, R. (2015). *Cell Biology by the Numbers*. Garland Science.

[Minas et al., 2020] Minas, G., Woodcock, D. J., Ashall, L., Harper, C. V., White, M. R., and Rand, D. A. (2020). Multiplexing information flow through dynamic signalling systems. *PLOS Computational Biology*, 16(8):e1008076.

[Mitchison and Cramer, 1996] Mitchison, T. J. and Cramer, L. P. (1996). Actin-based cell motility and cell locomotion. *Cell*, 84(3):371–379.

[Moissoglu et al., 2006] Moissoglu, K., Slepchenko, B. M., Meller, N., Horwitz, A. F., and Schwartz, M. A. (2006). In vivo dynamics of Rac-membrane interactions. *Molecular Biology of the Cell*, 17(6):2770–2779.

[Mori et al., 2008] Mori, Y., Jilkine, A., and Edelstein-Keshet, L. (2008). Wave-Pinning and Cell Polarity from a Bistable Reaction-Diffusion System. *Biophysical Journal*, 94(9):3684.

[Mulder, 1839] Mulder, G. J. (1839). *Ueber die Zusammensetzung einiger thierischen Substanzen*, volume 16. John Wiley & Sons, Ltd.

[Müller et al., 2020] Müller, P. M., Rademacher, J., Bagshaw, R. D., Wortmann, C., Barth, C., van Unen, J., Alp, K. M., Giudice, G., Eccles, R. L., Heinrich, L. E., Pascual-Vargas, P., Sanchez-Castro, M., Brandenburg, L., Mbamalu, G., Tucholska, M., Spatt, L., Czajkowski, M. T., Welke, R. W., Zhang, S., Nguyen, V., Rrustemi, T., Trnka, P., Freitag, K., Larsen, B., Popp, O., Mertins, P., Gingras, A. C., Roth, F. P., Colwill, K., Bakal, C., Pertz, O., Pawson, T., Petsalaki, E., and Rocks, O. (2020). Systems analysis of RhoGEF and RhoGAP regulatory proteins reveals spatially organized RAC1 signalling from integrin adhesions. *Nature Cell Biology 2020 22:4*, 22(4):498–511.

[Naganathan and Muñoz, 2005] Naganathan, A. N. and Muñoz, V. (2005). Scaling of folding times with protein size. *Journal of the American Chemical Society*, 127(2):480–481.

[Nair et al., 2019] Nair, A., Chauhan, P., Saha, B., and Kubatzky, K. F. (2019). Conceptual Evolution of Cell Signaling. *International Journal of Molecular Sciences*, 20(13).

[Nanda et al., 2023] Nanda, S., Calderon, A., Duong, T.-T., Koch, J., Sachan, A., Xin, X., Solouk, D., Wu, Y.-W., Nalbant, P., and Dehmelt, L. (2023). Crosstalk between Rac and Rho GTPase activity mediated by Arhgef11 and Arhgef12 coordinates cell protrusion-retraction cycles. *bioRxiv*, page 2023.02.20.529203.

[Narumiya et al., 2009] Narumiya, S., Tanji, M., and Ishizaki, T. (2009). Rho signaling, ROCK and mDia1, in transformation, metastasis and invasion. *Cancer and Metastasis Reviews*, 28(1-2):65–76.

[Ni et al., 1999] Ni, M., Tepperman, J. M., and Quail, P. H. (1999). Binding of phytochrome B to its nuclear signalling partner PIF3 is reversibly induced by light. *Nature*, 400(6746):781–784.

[Nobes and Hall, 1995] Nobes, C. D. and Hall, A. (1995). Rho, Rac, and Cdc42 GTPases regulate the assembly of multimolecular focal complexes associated with actin stress fibers, lamellipodia, and filopodia. *Cell*, 81(1):53–62.

[Noble, 2018] Noble, D. (2018). Central Dogma or Central Debate? *Physiology*, 33(4):246–249.

[O'Connor and Chen, 2013] O'Connor, K. L. and Chen, M. (2013). Dynamic functions of RhoA in tumor cell migration and invasion. *Small GTPases*, 4(3):141–147.

[Ohkawara et al., 2005] Ohkawara, H., Ishibashi, T., Sakamoto, T., Sugimoto, K., Nagata, K., Yokoyama, K., Sakamoto, N., Kamioka, M., Matsuoka, I., Fukuhara, S., Sugimoto, N., Takuwa, Y., and Maruyama, Y. (2005). Thrombin-induced Rapid Geranylgeranylation of RhoA as an Essential Process for RhoA Activation in Endothelial Cells. *Journal of Biological Chemistry*, 280(11):10182–10188.

[O'Neill et al., 2018] O'Neill, P. R., Castillo-Badillo, J. A., Meshik, X., Kalyanaraman, V., Melgarejo, K., and Gautam, N. (2018). Membrane Flow Drives an Adhesion-Independent Amoeboid Cell Migration Mode. *Developmental Cell*, 46(1):9–22.e4.

[Oron et al., 2012] Oron, D., Papagiakoumou, E., Anselmi, F., and Emiliani, V. (2012). Two-photon optogenetics. *Progress in Brain Research*, 196:119–143.

[Pagès, 2022] Pagès, D. L. (2022). *Cellular mechanisms of cancer collective invasion and response to treatments*. PhD thesis.

[Pagès et al., 2022] Pagès, D. L., Dornier, E., de Seze, J., Gontran, E., Maitra, A., Maciejewski, A., Wang, L., Luan, R., Cartry, J., Charlotte, C. J., Raingeaud, J., Lemahieu, G., Lebel, M., Ducreux, M., Gelli, M., Scoazec, J. Y., Coppey, M., Voituriez, R., Piel, M., and Jaulin, F. (2022). Cell clusters adopt a collective amoeboid mode of migration in confined nonadhesive environments. *Science advances*, 8(39).

[Paluch et al., 2016] Paluch, E. K., Aspalter, I. M., and Sixt, M. (2016). Focal Adhesion-Independent Cell Migration. *Annual review of cell and developmental biology*, 32:469–490.

[Paluch and Raz, 2013] Paluch, E. K. and Raz, E. (2013). The role and regulation of blebs in cell migration. *Current opinion in cell biology*, 25(5):582–590.

[Park et al., 2017] Park, H., Kim, N. Y., Lee, S., Kim, N., Kim, J., and Heo, W. D. (2017). Optogenetic protein clustering through fluorescent protein tagging and extension of CRY2. *Nature communications*, 8(1).

[Parnes, 2000] Parnes, O. (2000). The envisioning of cells. *Science in context*, 13(1):71–92.

[Parri and Chiarugi, 2010] Parri, M. and Chiarugi, P. (2010). Rac and Rho GTPases in cancer cell motility control. *Cell Communication and Signaling 2010 8:1*, 8(1):1–14.

[Patel and Karginov, 2014] Patel, M. and Karginov, A. V. (2014). Phosphorylation-mediated regulation of GEFs for RhoA. *Cell Adhesion and Migration*, 8(1):11–18.

[Peglion and Goehring, 2019] Peglion, F. and Goehring, N. W. (2019). Switching states: dynamic remodelling of polarity complexes as a toolkit for cell polarization. *Current Opinion in Cell Biology*, 60:121–130.

[Pendin et al., 2017] Pendin, D., Greotti, E., Lefkimmiatis, K., and Pozzan, T. (2017). Exploring cells with targeted biosensors. *Journal of General Physiology*, 149(1):1–36.

[Perry and Maddox, 2019] Perry, J. A. and Maddox, A. S. (2019). Uncovering the secret life of Rho GTPases. *eLife*, 8.

[Pertz, 2010] Pertz, O. (2010). Spatio-temporal Rho GTPase signaling - where are we now? *Journal of cell science*, 123(Pt 11):1841–1850.

[Pertz et al., 2006] Pertz, O., Hodgson, L., Klemke, R. L., and Hahn, K. M. (2006). Spatiotemporal dynamics of RhoA activity in migrating cells. *Nature*, 440(7087):1069–1072.

[Piekny and Glotzer, 2008] Piekny, A. J. and Glotzer, M. (2008). Anillin Is a Scaffold Protein That Links RhoA, Actin, and Myosin during Cytokinesis. *Current Biology*, 18(1):30–36.

[Poelwijk et al., 2011] Poelwijk, F. J., De Vos, M. G., and Tans, S. J. (2011). Tradeoffs and optimality in the evolution of gene regulation. *Cell*, 146(3):462–470.

[Pollard, 1986] Pollard, T. D. (1986). Rate constants for the reactions of ATP- and ADP-actin with the ends of actin filaments. *The Journal of Cell Biology*, 103(6):2747.

[Prasher et al., 1992] Prasher, D. C., Eckenrode, V. K., Ward, W. W., Prendergast, F. G., and Cormier, M. J. (1992). Primary structure of the Aequorea victoria green-fluorescent protein. *Gene*, 111(2):229–233.

[Purcell, 1977] Purcell, E. M. (1977). Life at low Reynolds number. *American Journal of Physics*, 45(1):3–11.

[Purvis and Lahav, 2013] Purvis, J. E. and Lahav, G. (2013). Encoding and decoding cellular information through signaling dynamics. *Cell*, 152(5):945–956.

[Raftopoulou and Hall, 2004] Raftopoulou, M. and Hall, A. (2004). Cell migration : Rho GTPases lead the way. *Developmental Biology*, 265:23–32.

[Rauzi et al., 2010] Rauzi, M., Lenne, P.-F., and Lecuit, T. (2010). Planar polarized actomyosin contractile flows control epithelial junction remodelling. *Nature*, 468.

[Reig et al., 2014] Reig, G., Pulgar, E., and Concha, M. L. (2014). Cell migration: From tissue culture to embryos.

[Remorino et al., 2017] Remorino, A., De Beco, S., Cayrac, F., Di Federico, F., Cornilleau, G., Gautreau, A., Parrini, M. C., Masson, J.-B., Dahan, M., and Coppey, M. (2017). Gradients of Rac1 Nanoclusters Support Spatial Patterns of Rac1 Signaling. *Cell Reports*, 21(7):1922–1935.

[Ren et al., 1999] Ren, X.-D., Kiosses, W. B., and Schwartz, M. A. (1999). Regulation of the small GTP-binding protein Rho by cell adhesion and the cytoskeleton. *The EMBO Journal*, 18(3):578–585.

[Reversat et al., 2020] Reversat, A., Gaertner, F., Merrin, J., Stopp, J., Tasciyan, S., Aguilera, J., de Vries, I., Hauschild, R., Hons, M., Piel, M., Callan-Jones, A., Voituriez, R., and Sixt, M. (2020). Cellular locomotion using environmental topography. *Nature*, 582(7813):582–585.

[Ridley, 2015] Ridley, A. J. (2015). Rho GTPase signalling in cell migration. *Current Opinion in Cell Biology*, 36:103.

[Ridley and Hall, 1992] Ridley, A. J. and Hall, A. (1992). The small GTP-binding protein rho regulates the assembly of focal adhesions and actin stress fibers in response to growth factors. *Cell*, 70(3):389–399.

[Ridley et al., 1992] Ridley, A. J., Paterson, H. F., Johnston, C. L., Diekmann, D., and Hall, A. (1992). The small GTP-binding protein rac regulates growth factor-induced membrane ruffling. *Cell*, 70(3):401–410.

[Robitaille et al., 2022] Robitaille, M. C., Byers, J. M., Christodoulides, J. A., and Raphael, M. P. (2022). Robust optical flow algorithm for general single cell segmentation. *PLoS ONE*, 17(1).

[Rodbell, 1970] Rodbell, M. (1970). Colloquium on the Role of Adenyl Cyclase... - Google Scholar.

[Rottner and Schaks, 2019] Rottner, K. and Schaks, M. (2019). Assembling actin filaments for protrusion. *Current opinion in cell biology*, 56:53–63.

[Royes et al., 2020] Royes, J., Biou, V., Dautin, N., Tribet, C., and Miroux, B. (2020). Inducible intracellular membranes: Molecular aspects and emerging applications. *Microbial Cell Factories*, 19(1).

[Rullan et al., 2018] Rullan, M., Benzinger, D., Schmidt, G. W., Milias-Argeitis, A., and Khammash, M. (2018). An Optogenetic Platform for Real-Time, Single-Cell Interrogation of Stochastic Transcriptional Regulation. *Molecular cell*, 70(4):745–756.e6.

[Ruprecht et al., 2015] Ruprecht, V., Wieser, S., Callan-Jones, A., Smutny, M., Morita, H., Sako, K., Barone, V., Ritsch-Marte, M., Sixt, M., Voituriez, R., and Heisenberg, C. P. (2015). Cortical Contractility Triggers a Stochastic Switch to Fast Amoeboid Cell Motility. *Cell*, 160(4):673–685.

[Rzadzinska et al., 2004] Rzadzinska, A. K., Schneider, M. E., Davies, C., Riordan, G. P., and Kachar, B. (2004). An actin molecular treadmill and myosins maintain stereocilia functional architecture and self-renewal. *The Journal of Cell Biology*, 164(6):887.

[Sapp, 2003] Sapp, J. (2003). Genesis: the evolution of biology.

[Scarpa and Mayor, 2016] Scarpa, E. and Mayor, R. (2016). Collective cell migration in development. *Journal of Cell Biology*, 212(2):143–155.

[Schindelin et al., 2012] Schindelin, J., Arganda-Carreras, I., Frise, E., Kaynig, V., Longair, M., Pietzsch, T., Preibisch, S., Rueden, C., Saalfeld, S., Schmid, B., Tinevez, J. Y., White, D. J., Hartenstein, V., Eliceiri, K., Tomancak, P., and Cardona, A. (2012). Fiji: an open-source platform for biological-image analysis. *Nature Methods 2012 9:7*, 9(7):676–682.

[Schleiden, 1838] Schleiden, M. J. (1838). Beiträge zur Phytogenesis.

[Schwann, 1839] Schwann, T. (1839). *Mikroskopische Untersuchungen über die Uebereinstimmung in der Struktur und dem Wachsthum der Thiere und Pflanzen*. Sander, Berlin, 1. auflage edition.

[Schwartz, 2004] Schwartz, M. (2004). Rho signalling at a glance. *Journal of Cell Science*, 117(23):5457–5458.

[SenGupta et al., 2021] SenGupta, S., Parent, C. A., and Bear, J. E. (2021). The principles of directed cell migration. *Nature reviews. Molecular cell biology*, 22(8):529–547.

[Sever and Brugge, 2015] Sever, R. and Brugge, J. S. (2015). Signal Transduction in Cancer. *Cold Spring Harbor Perspectives in Medicine*, 5(4).

[Shellard and Mayor, 2019] Shellard, A. and Mayor, R. (2019). Supracellular migration - beyond collective cell migration. *Journal of cell science*, 132(8).

[Shellard et al., 2018] Shellard, A., Szabó, A., Trepat, X., and Mayor, R. (2018). Supracellular contraction at the rear of neural crest cell groups drives collective chemotaxis. *Science (New York, N.Y.)*, 362(6412):339.

[Shin et al., 2017] Shin, Y., Berry, J., Pannucci, N., Haataja, M. P., Toettcher, J. E., and Brangwynne, C. P. (2017). Spatiotemporal Control of Intracellular Phase Transitions Using Light-Activated optoDroplets. *Cell*, 168(1-2):159–171.e14.

[Shrestha et al., 2015] Shrestha, D., Jenei, A., Nagy, P., Vereb, G., and Szöllősi, J. (2015). Understanding FRET as a Research Tool for Cellular Studies. *International Journal of Molecular Sciences*, 16(4):6718.

[Singh and Padgett, 2009] Singh, J. and Padgett, R. A. (2009). Rates of in situ transcription and splicing in large human genes. *Nature structural & molecular biology*, 16(11):1128–1133.

[Siwiak and Zielenkiewicz, 2013] Siwiak, M. and Zielenkiewicz, P. (2013). Transimulation - Protein Biosynthesis Web Service. *PLoS ONE*, 8(9):73943.

[Snapp, 2009] Snapp, E. L. (2009). Fluorescent proteins: a cell biologist's user guide. *Trends in Cell Biology*, 19(11):649–655.

[Struckhoff et al., 2013] Struckhoff, A. P., Rana, M. K., Kher, S. S., Burow, M. E., Hagan, J. L., Del Valle, L., and Worthylake, R. A. (2013). PDZ-RhoGEF is essential for CXCR4-driven breast tumor cell motility through spatial regulation of RhoA. *Journal of cell science*, 126(Pt 19):4514–4526.

[Sumner, 1926] Sumner, J. B. (1926). THE ISOLATION AND CRYSTALLIZATION OF THE ENZYME UREASE: PRELIMINARY PAPER. *Journal of Biological Chemistry*, 69(2):435–441.

[Sung et al., 2021] Sung, H., Ferlay, J., Siegel, R. L., Laversanne, M., Soerjomataram, I., Jemal, A., and Bray, F. (2021). Global Cancer Statistics 2020: GLOBOCAN Estimates of Incidence and Mortality Worldwide for 36 Cancers in 185 Countries. *CA: a cancer journal for clinicians*, 71(3):209–249.

[Sutherland and Rall, 1957] Sutherland, E. W. and Rall, T. W. (1957). The properties of an adenine ribonucleotide produced with cellular particles, ATP, Mg++, and epinephrine or glucagon. *Journal of the American Chemical Society*, 79(13):3608.

[Tay et al., 2010] Tay, S., Hughey, J. J., Lee, T. K., Lipniacki, T., Quake, S. R., and Covert, M. W. (2010). Single-cell NF-κB dynamics reveal digital activation and analogue information processing. *Nature 2010 466:7303*, 466(7303):267–271.

[Terry et al., 2011] Terry, S. J., Zihni, C., Elbediwy, A., Vitiello, E., Leefa, I. V., San, C., Balda, M. S., and Matter, K. (2011). Spatially restricted activation of RhoA signalling at epithelial junctions by p114RhoGEF drives junction formation and morphogenesis. *Nature Publishing Group*, 13.

[Tkachenko et al., 2011] Tkachenko, E., Sabouri-Ghomi, M., Pertz, O., Kim, C., Gutierrez, E., MacHacek, M., Groisman, A., Danuser, G., and Ginsberg, M. H. (2011). Protein Kinase A Governs a RhoA-RhoGDI Protrusion-Retraction Pacemaker in Migrating Cells. *Nature cell biology*, 13(6):660.

[Tnimov et al., 2012] Tnimov, Z., Guo, Z., Gambin, Y., Nguyen, U. T. T., Wu, Y. W., Abankwa, D., Stigter, A., Collins, B. M., Waldmann, H., Goody, R. S., and Alexandrov, K. (2012). Quantitative Analysis of Prenylated RhoA Interaction with Its Chaperone, RhoGDI. *The Journal of Biological Chemistry*, 287(32):26549.

[Toettcher et al., 2013] Toettcher, J. E., Weiner, O. D., and Lim, W. A. (2013). Using Optogenetics to Interrogate the Dynamic Control of Signal Transmission by the Ras/Erk Module. *Cell*, 155(6):1422–1434.

[Tokunaga et al., 2008] Tokunaga, M., Imamoto, N., and Sakata-Sogawa, K. (2008). Highly inclined thin illumination enables clear single-molecule imaging in cells. *Nature methods*, 5(2):159–161.

[Towbin et al., 2017] Towbin, B. D., Korem, Y., Bren, A., Doron, S., Sorek, R., and Alon, U. (2017). Optimality and sub-optimality in a bacterial growth law. *Nature Communications 2017 8:1*, 8(1):1–8.

[Tsai et al., 2019] Tsai, T. Y., Collins, S. R., Chan, C. K., Hadjitheodorou, A., Lam, P. Y., Lou, S. S., Yang, H. W., Jorgensen, J., Ellett, F., Irimia, D., Davidson, M. W., Fischer, R. S., Huttenlocher, A., Meyer, T., Ferrell, J. E., and Theriot, J. A. (2019). Efficient Front-Rear Coupling in Neutrophil Chemotaxis by Dynamic Myosin II Localization. *Developmental cell*, 49(2):189–205.e6.

[Unen et al., 2015] Unen, J. V., Reinhard, N. R., Yin, T., Wu, Y. I., Postma, M., Gadella, T. W. J., and Goedhart, J. (2015). Plasma membrane restricted RhoGEF activity is sufficient for RhoA-mediated actin polymerization. *Scientific Reports 2015 5:1*, 5(1):1–16.

[Vaidžiulyte et al., 2019] Vaidžiulyte, K., Coppey, M., and Schauer, K. (2019). Intracellular organization in cell polarity – placing organelles into the polarity loop. *Journal of Cell Science*, 132(24).

[Vaidziulyte-Simutiene, 2021] Vaidziulyte-Simutiene, K. (2021). Understanding internal cell coordination during migration. Technical report.

[Vaidžiulytė et al., 2022] Vaidžiulytė, K., Macé, A. S., Battistella, A., Beng, W., Schauer, K., and Coppey, M. (2022). Persistent cell migration emerges from a coupling between protrusion dynamics and polarized trafficking. *eLife*, 11.

[Valon et al., 2015] Valon, L., Etoc, F., Remorino, A., Di Pietro, F., Morin, X., Dahan, M., and Coppey, M. (2015). Predictive Spatiotemporal Manipulation of Signaling Perturbations Using Optogenetics. *Biophysical journal*, 109(9):1785–1797.

[Valon et al., 2017] Valon, L., Marín-Llauradó, A., Wyatt, T., Charras, G., and Trepat, X. (2017). Optogenetic control of cellular forces and mechanotransduction. *Nature Communications 2017 8:1*, 8(1):1–10.

[van Bergeijk et al., 2016] van Bergeijk, P., Hoogenraad, C. C., and Kapitein, L. C. (2016). Right Time, Right Place: Probing the Functions of Organelle Positioning. *Trends in cell biology*, 26(2):121–134.

[Vicente-Manzanares and Horwitz, 2011] Vicente-Manzanares, M. and Horwitz, A. R. (2011). Cell migration: an overview. *Methods in molecular biology (Clifton, N.J.)*, 769:1–24.

[Vicente-Manzanares et al., 2009] Vicente-Manzanares, M., Ma, X., Adelstein, R. S., and Horwitz, A. R. (2009). Non-muscle myosin II takes centre stage in cell adhesion and migration. *Nature Reviews Molecular Cell Biology 2009 10:11*, 10(11):778–790.

[Vicente-Manzanares et al., 2005] Vicente-Manzanares, M., Webb, D. J., and Horwitz, A. R. (2005). Cell migration at a glance. *Journal of cell science*, 118(Pt 21):4917–4919.

[Vignais, 2001] Vignais, P. (2001). *La biologie, des origines à nos jours*. EDP Sciences.

[Virchow, 1855] Virchow, R. (1855). *Archiv für pathologische Anatomie und Physiologie und für klinische Medicin. Band 114*.

[Voulvoulis and Burgman, 2019] Voulvoulis, N. and Burgman, M. A. (2019). The contrasting roles of science and technology in environmental challenges. *https://doi.org/10.1080/10643389.2019.1565519*, 49(12):1079–1106.

[Wagner and Glotzer, 2016] Wagner, E. and Glotzer, M. (2016). Local RhoA activation induces cytokinetic furrows independent of spindle position and cell cycle stage. *The Journal of cell biology*, 213(6):641–649.

[Wang and Shaw, 1995] Wang, D. S. and Shaw, G. (1995). The Association of the C-Terminal Region of β1ΣII Spectrin to Brain Membranes Is Mediated by a pH Domain, Does Not Require Membrane Proteins, and Coincides with a Inositol-1,4,5 Trisphosphate Binding Site. *Biochemical and Biophysical Research Communications*, 217(2):608–615.

[Wang et al., 2016] Wang, H., Vilela, M., Winkler, A., Tarnawski, M., Schlichting, I., Yumerefendi, H., Kuhlman, B., Liu, R., Danuser, G., and Hahn, K. M. (2016). LOVTRAP: An optogenetic system for photoinduced protein dissociation. *Nature Methods*, 13(9):755–758.

[Watanabe et al., 1999] Watanabe, N., Kato, T., Fujita, A., Ishizaki, T., and Narumiya, S. (1999). Cooperation between mDia1 and ROCK in Rho-induced actin reorganization. *Nature cell biology*, 1(3):136–143.

[Weijer, 2009] Weijer, C. J. (2009). Collective cell migration in development. *Journal of Cell Science*, 122(18):3215–3223.

[Welch et al., 2011] Welch, C. M., Elliott, H., Danuser, G., and Hahn, K. M. (2011). Imaging the coordination of multiple signalling activities in living cells. *Nature Reviews Molecular Cell Biology 2011 12:11*, 12(11):749–756.

[Welf et al., 2020] Welf, E. S., Miles, C. E., Huh, J., Sapoznik, E., Chi, J., Driscoll, M. K., Isogai, T., Noh, J., Weems, A. D., Pohlkamp, T., Dean, K., Fiolka, R., Mogilner, A., and Danuser, G. (2020). Actin-Membrane Release Initiates Cell Protrusions. *Developmental Cell*, 55(6):723–736.e8.

[Wennerberg et al., 2005] Wennerberg, K., Rossman, K. L., and Der, C. J. (2005). The Ras superfamily at a glance. *Journal of cell science*, 118(Pt 5):843–846.

[Wittmann et al., 2020] Wittmann, T., Dema, A., and van Haren, J. (2020). Lights, cytoskeleton, action: Optogenetic control of cell dynamics. *Current opinion in cell biology*, 66:1.

[Worthylake et al., 2001] Worthylake, R. A., Lemoine, S., Watson, J. M., and Burridge, K. (2001). RhoA is required for monocyte tail retraction during transendothelial migration. *The Journal of Cell Biology*, 154(1):147.

[Wu, 2005] Wu, D. (2005). Signaling mechanisms for regulation of chemotaxis. *Cell Research 2005 15:1*, 15(1):52–56.

[Yamada and Sixt, 2019] Yamada, K. M. and Sixt, M. (2019). Mechanisms of 3D cell migration. *Nature reviews. Molecular cell biology*, 20(12):738–752.

[Yamao et al., 2015] Yamao, M., Naoki, H., Kunida, K., Aoki, K., Matsuda, M., and Ishii, S. (2015). Distinct predictive performance of Rac1 and Cdc42 in cell migration. *Scientific Reports 2015 5:1*, 5(1):1–14.

[Yang et al., 2021] Yang, J. M., Chi, W. Y., Liang, J., Takayanagi, S., Iglesias, P. A., and Huang, C. H. (2021). Deciphering cell signaling networks with massively multiplexed biosensor barcoding. *Cell*, 184(25):6193–6206.e14.

[Yonemura et al., 2004] Yonemura, S., Hirao-Minakuchi, K., and Nishimura, Y. (2004). Rho localization in cells and tissues. *Experimental Cell Research*, 295(2):300–314.

[Yüce et al., 2005] Yüce, Ö., Piekny, A., and Glotzer, M. (2005). An ECT2–centralspindlin complex regulates the localization and function of RhoA. *The Journal of Cell Biology*, 170(4):571.

[Zajac et al., 2018] Zajac, O., Raingeaud, J., Libanje, F., Lefebvre, C., Sabino, D., Martins, I., Roy, P., Benatar, C., Canet-Jourdan, C., Azorin, P., Polrot, M., Gonin, P., Benbarche, S., Souquere, S., Pierron, G., Nowak, D., Bigot, L., Ducreux, M., Malka, D., Lobry, C., Scoazec, J. Y., Eveno, C., Pocard, M., Perfettini, J. L., Elias, D., Dartigues, P., Goéré, D., and Jaulin, F. (2018). Tumour spheres with inverted polarity drive the formation of peritoneal metastases in patients with hypermethylated colorectal carcinomas. *Nature Cell Biology*, 20(3):296–306.

[Zanotelli et al., 2021] Zanotelli, M. R., Zhang, J., and Reinhart-King, C. A. (2021). Mechanoresponsive metabolism in cancer cell migration and metastasis. *Cell metabolism*, 33(7):1307.

[Zhou et al., 2012] Zhou, X. X., Chung, H. K., Lam, A. J., and Lin, M. Z. (2012). Optical control of protein activity by fluorescent protein domains. *Science*, 338(6108):810–814.

[Zimmerman et al., 2016] Zimmerman, S. P., Hallett, R. A., Bourke, A. M., Bear, J. E., Kennedy, M. J., and Kuhlman, B. (2016). Tuning the Binding Affinities and Reversion Kinetics of a Light Inducible Dimer Allows Control of Transmembrane Protein Localization. *Biochemistry*, 55(37):5264.

RÉSUMÉ

Les cellules perçoivent des signaux chimiques ou physiques externes, les interprètent à l'aide de leur réseau de protéines et modifient leur comportement en conséquence. Mieux comprendre les systèmes vivants passe par le décryptage des signaux biochimiques à l'intérieur de la cellule, qui sont responsables de réponses phénotypiques spécifiques. Parmi tous les processus cellulaires, la migration cellulaire est fascinante car elle révèle la capacité des cellules à agir comme des unités individuelles ou collectives, qui se polarisent par elles-mêmes et ont leur propre indépendance.
Les Rho-GTPases jouent un rôle clé dans la migration des cellules de mammifères : ce sont des protéines souvent considérées comme des contrôleurs du cytosquelette cellulaire, et donc responsables des changements morphologiques provoqués par les filaments et les moteurs tels que l'actine et la myosine. Pour sonder le réseau de protéines et étudier les liens de cause à effet sur le comportement cellulaire ou multicellulaire, l'optogénétique est un outil formidable qui permet un contrôle spatio-temporel précis de l'activité des Rho-GTPases.
Ce manuscrit aborde la question du contrôle de la migration cellulaire et multicellulaire par les Rho-GTPases à travers deux systèmes modèles différents, grâce à l'optogénétique.
Le premier projet porte sur la migration et la polarisation de cellules individuelles après le recrutement membranaire d'un activateur de la protéine RhoA (un domaine GEF). En utilisant l'optogénétique, j'ai découvert qu'un domaine GEF est capable de déclencher deux réponses phénotypiques opposées dans la même lignée cellulaire : une protrusion ou une rétraction. La caractérisation des phénotypes a permis de montrer que le choix est dicté par la concentration de l'activateur optogénétique présent dans la cellule avant l'activation. J'ai décrit la conséquence de ce changement de concentration sur les voies de signalisation impliquées et j'ai développé un modèle qui récapitule les principaux résultats avec peu de paramètres. Grâce à lui, j'ai pu contrôler les deux effets opposés de cette protéine dans la même cellule. Ce projet révèle et explique un exemple clair de multiplexage des signaux cellulaires, à savoir la capacité d'une voie de signalisation à avoir plusieurs fonctions, ici dans le même contexte cellulaire et à l'échelle de la minute.
Le second projet a été réalisé en collaboration avec l'équipe de Fanny Jaulin de l'Institut Gustave Roussy. Il visait à comprendre un nouveau mode de migration collective découvert par eux dans l'initiation des métastases du cancer colorectal. Cette migration d'amas épithéliaux de dizaines à centaines de cellules repose sur des propriétés uniques : absence d'adhésions focales sur le substrat, environnement confiné, et forte contractilité. Ce mode de migration collective rappelle la migration amiboïde d'une seule cellule. En utilisant des outils optogénétiques développés dans notre laboratoire et des canaux microfluidiques, j'ai conçu et réalisé des expériences pour comprendre le rôle des Rho-GTPases dans la polarité et la migration de ces sphères multicellulaires. Mon principal résultat est qu'un déséquilibre de contractilité déclenché par la protéine RhoA est suffisant pour contrôler la polarité et le mouvement du groupe de cellules.
Dans l'ensemble, mon doctorat a permis de comprendre comment la voie de signalisation RhoA agit pour établir une polarité dans la migration cellulaire : je l'ai examinée au niveau de la cellule unique, révélant un exemple unique de multifonctionnalité d'une protéine, ainsi qu'au niveau collectif, disséquant un nouveau mode de migration collective des cellules cancéreuses.

MOTS CLÉS

optogénétique, migration cellulaire, RhoA, invasion, contractilité, protrusion

ABSTRACT

Cells sense external chemical or physical signals, interpret them using their protein network and modify their behavior accordingly. A better understanding of living systems involves deciphering how biochemical signals are transmitted within the cell, leading to specific phenotypic responses. Among all cellular processes, cell migration is fascinating because it reveals the ability of cells to act as individual or collective units, which polarize by themselves and have their own independence.

Rho-GTPases play a key role in mammalian cell migration: they are proteins often regarded as controllers of the cellular cytoskeleton, and therefore responsible for morphological changes caused by filaments and motors such as actin and myosin. To probe the protein network and study causal links on cellular or multicellular behavior, optogenetics is a great tool that enables precise spatio-temporal control of Rho-GTPase activity.

This PhD manuscript addresses the question of the control of single and multicellular migration by Rho-GTPases, using optogenetics in two different model systems.

The first project focuses on the migration and polarization of single cells following membrane recruitment of a RhoA activator (a GEF domain). Using optogenetics, I discovered that a GEF domain is capable of triggering two opposite phenotypic responses in the same cell line: protrusion or retraction. Characterization of the phenotypes showed that the choice is dictated by the concentration of optogenetic activator present in the cell prior to activation. I described the consequences of this change in concentration on the signalling pathways involved, and developed a model that summarizes the main results with few parameters. Thanks to it, I was able to control the two opposite effects of this protein in the same cell. This project reveals and explains a clear example of cellular signal multiplexing, i.e. the ability of a signaling pathway to have multiple functions, here in the same cellular context and on a minute scale.

The second project was carried out in collaboration with Fanny Jaulin's team at the Institut Gustave Roussy. It aimed to understand a new mode of collective migration discovered by them in the initiation of colorectal cancer metastases. This migration of epithelial clusters of tens to hundreds of cells relies on unique properties: absence of focal adhesions to the substrate, confined environment, and high contractility. This mode of collective migration is reminiscent of single cell amoeboid migration. Using optogenetic tools developed in our laboratory and microfluidic channels, I designed and carried out experiments to understand the role of Rho-GTPases in the polarity and migration of these multicellular spheres. My main finding is that a contractility imbalance triggered by the RhoA protein is sufficient to control the polarity and movement of the cell group.

Overall, my PhD has provided insight into how the RhoA signaling pathway acts to establish polarity in cell migration: I examined it at the single-cell level, revealing a unique example of multifunctionality of a protein, as well as at the collective level, dissecting a novel mode of collective cancer cell migration.

KEYWORDS

optogenetic, cell migration, RhoA, invasion, contractility, protrusion